WARWICK
THE UNIVERSITY OF WARWICK

A Thesis Submitted for the Degree of PhD at the University of Warwick

Permanent WRAP URL:

http://wrap.warwick.ac.uk/153546

Copyright and reuse:
This thesis is made available online and is protected by original copyright.
Please scroll down to view the document itself.
Please refer to the repository record for this item for information to help you to cite it.
Our policy information is available from the repository home page.

For more information, please contact the WRAP Team at: wrap@warwick.ac.uk

warwick.ac.uk/lib-publications

MONASH WARWICK ALLIANCE

MONASH University

WARWICK
THE UNIVERSITY OF WARWICK

Understanding the Structure, Toxicity and Inhibition of IAPP at the Nanoscale

Emily Helen Pilkington
BSc (1) Hons.

A thesis submitted for the degree of Doctor of Philosophy at
Monash University and the University of Warwick in 2019

Monash Institute of Pharmaceutical Sciences
381 Royal Parade
Parkville, VIC 3052
Australia

Faculty of Chemistry
University of Warwick
Gibbet Hill, Coventry CV4 7EQ
United Kingdom

Copyright notice

© The author, 2019.

I certify that I have made all reasonable efforts to secure copyright permissions for third-party content included in this thesis and have not knowingly added copyright content to my work without the owner's permission.

Abstract

The aggregation of peptides or proteins to form amyloid fibrils and plaques is associated with the pathologies of a range of neurological disorders and metabolic diseases, including Alzheimer's disease (AD), Parkinson's disease (PD) and type II diabetes mellitus (T2D). Human islet amyloid polypeptide (IAPP), specifically, contributes to glycemic control but also mediates the dysfunction of insulin-producing pancreatic β-cells in T2D. Furthermore, IAPP in circulation is capable of cross-seeding amyloid-beta and alpha-synuclein, associated with AD and PD respectively. Given no current anti-amyloid treatment is currently commercially available, fundamental understanding of amyloidosis within the complex cellular environment is required against amyloid diseases.

In this thesis, conditions to slow down the rapid fibrillization of IAPP to reduce or eliminate intermediate toxic aggregates have been identified *in vitro*. IAPP intermediate species were characterized and a novel 'biannular' morphology identified, with two distinct fibrillating populations then eliciting differential cytotoxicity to mature amyloids in primary cells *in vitro*. The behavior of fibrillating and fibrillar amyloid species in the presence of model proteins, lipids and ultrasmall lipid membranes was investigated, with regards to their effects on amyloid fibrillization, morphology and associated cytotoxicity *in vitro*, progressing then towards an in-depth study into the 'protein corona' formation of amyloid fibrils within complex biological media. Proteomic analysis identified amyloid-enriched proteins that are known to play significant roles in mediating cellular machinery and processing, potentially leading to pathological outcomes and therapeutic targets. Finally, a biocompatible star polymer ('PHEA') was synthesized to mimic the anti-amyloidosis properties of natural polyphenols and effectively rescue IAPP toxicity in mouse islets. Surprisingly, the relatively rigid and amphiphilic PHEA stars induced the formation of novel amyloid morphologies through promoting fibrillization, and accelerated amyloidogenesis to eliminate toxic intermediates in a fashion reminiscent of melanin production. This thesis outlines a logical progression towards the development of effective anti-amyloid strategies: whereby through first gaining insight into amyloidosis, this knowledge can be then applied to ameliorate amyloid pathologies.

Publications during enrolment*

**Journal articles written and published during candidature wherein experimentation was completed prior to start date are not included here.*

(1) Pilkington, E. H.; Lai, M.; X. Ge, Stanley, W. J.; Wang, B.; Wang, M.; Kakinen, A.; Sani, M-A.; Whittaker, M. R.; Gurzov, E. N.; Ding, F.; Quinn, J. F.; Davis, T. P.; Ke, P. C., Star Polymers Reduce Islet Amyloid Polypeptide Toxicity via Accelerated Amyloid Aggregation, *Biomacromolecules* **2017,** *18,* 4249-4260.

(2) Pilkington, E. H.; Xing, Y.; Wang, B.; Käkinen, A.; Wang, M.; Davis, T. P.; Ding, F.; Ke, P. C., Effects of Protein Corona on IAPP Amyloid Aggregation, Fibril Remodelling, and Cytotoxicity. *Sci. Rep.* **2017,** *7*, 2455.

(3) Wang, B.; Pilkington, E. H.; Sun, Y.; Davis, T. P.; Ke, P. C.; Ding, F., Modulating protein amyloid aggregation with nanomaterials, *Environ. Sci. Nano* **2017**, *4,* 1772-1783.

(4) Xing, Y.; Pilkington, E. H.; Wang, M.; Nowell, C. J.; Käkinen, A.; Sun, Y.; Wang, B.; Davis, T. P.; Ding, F.; Ke, P. C., Lysophosphatidylcholine modulates the aggregation of human islet amyloid polypeptide. *Phys. Chem. Chem. Phys.* **2017,** *19*, 30627-30635.

(5) Wang, M.; Käkinen, A.; Pilkington, E. H.; Davis, T. P.; Ke, P. C., Differential Effects of Silver and Iron Oxide Nanoparticles on IAPP Aggregation and Toxicity. *Biomater. Sci.* **2017,** *5*, 485-493.

(6) Javed, I.; Sun, Y.; Adamcik, J.; Wang, B.; Käkinen, A.; Pilkington, E. H.; Ding, F.; Mezzenga, R.; Davis, T. P.; Ke, P. C., Cofibrillization of Pathogenic and Functional Amyloid Proteins with Gold Nanoparticles against Amyloidogenesis. *Biomacromolecules* **2017,** *18*, 4316-4322.

(7) Wang, M.; Gustafsson, O. J. R.; Pilkington, E. H.; Kakinen, A.; Javed, I.; Faridi, A.; Davis, T. P.; Ke, P. C., Nanoparticle-proteome *in vitro* and *in vivo*, *J. Mat. Chem. B* **2018,** *6,* 6026-6041.

(8) Tanaka, J.; Tani, S.; Peltier, R.; Pilkington, E. H.; Kerr, A.; Davis, T. P.; Wilson, P., Synthesis, aggregation and responsivity of block copolymers containing organic arsenicals, *Polym. Chem.* **2018,** *9,* 1551-1556.

(9) Pilkington, E. H.; Gustaffson, O. J. R.; Xing, Y.; Hernandez-Fernaud, J.; Zampronio, C.; Kakinen, A.; Faridi, A.; Ding, F.; Wilson, P.; Ke, P. C.; Davis, T. P., Profiling the Serum Protein Corona of Fibrillar Human Islet Amyloid Polypeptide, *ACS Nano* **2018**, *12,* 6066-6078.

(10) Sun, Y.; Käkinen, A.; Xing, Y.; Pilkington, E. H.; Davis, T. P.; Ke, P. C.; Ding, F., Nucleation of β-rich oligomers and β-barrels in the early aggregation of human islet amyloid polypeptide. *Biochim. Biophys. Mol. Basis Dis.* **2019,** *1865*, 434-444.

(11) Kakinen, A.; Sun, Y.; Javed, I.; Faridi, A.; Pilkington, E. H.; Faridi, P.; Purcell, A. W.; Zhou, R.; Ding, F.; Lin, S.; Ke, P. C.; Davis, T. P., Physical and toxicological profiles of human IAPP amyloids and plaques, *Sci. Bull.* **2019,** *64,* 26-35.
(12) Ke, P. C.; Pilkington, E. H., Sun, Y., Javed, I.; Kakinen, A.; Peng, G.; Ding, F.; Davis, T. P., Mitigation of Amyloidosis with Nanomaterials, *Adv. Mater.* **2019,** 1901690.

Conference presentations

Pilkington, E. H.; Blin, T.; Käkinen, A.; Ding, F.; Ke, P. C.; Davis, T. P.; Nanotechnologies for IAPP Aggregation Inhibition and Anti-Protein Fouling, **Warwick Polymer Conference,** Coventry, UK, 2016.

Pilkington, E. H.; Gustafsson, O. J. R.; Ding, F.; Wilson, P.; Ke, P. C.; Davis, T. P.; Protein Corona, in a New Context of Amyloidogenesis, **International Conference on Nanoscience and Nanotechnology (ICONN),** Wollongong, Australia, 2018.

Pilkington, E. H.; Gustafsson, O. J. R.; Ding, F.; Wilson, P.; Ke, P. C.; Davis, T. P.; Protein Corona, in a New Context of Amyloidogenesis, **Macro Group UK Young Researcher's Meeting (YRM),** Dublin, Ireland, 2018.

Pilkington, E. H.; Gustafsson, O. J. R.; Ding, F.; Wilson, P.; Ke, P. C.; Davis, T. P.; Protein Corona, in a New Context of Amyloidogenesis, **EuCheMS,** Liverpool, UK, 2018.

Pilkington, E. H.; Gustafsson, O. J. R.; Ding, F.; Wilson, P.; Ke, P. C.; Davis, T. P.; Protein Corona, in a New Context of Amyloidogenesis, **PolymerVic,** Melbourne, Australia, 2018.

Thesis including published works declaration

I hereby declare that this thesis contains no material which has been accepted for the award of any other degree or diploma at any university or equivalent institution and that, to the best of my knowledge and belief, this thesis contains no material previously published or written by another person, except where due reference is made in the text of the thesis.

This thesis includes two original papers published in peer reviewed journals. The core theme of the thesis is amyloidosis. The ideas, development and writing up of all the papers in the thesis were the principal responsibility of myself, the student, working within the Monash Institute of Pharmaceutical Sciences (Monash University) and the Faculty of Chemistry (University of Warwick) under the supervision of Dr Pu Chun Ke, Dr Paul Wilson & Prof Tom Davis.

The inclusion of co-authors reflects the fact that the work came from active collaboration between researchers and acknowledges input into team-based research.

In the case of Chapters 3 and 4 my contribution to the work involved the following:

Thesis Chapter	**Publication Title**	**Status** *(published, in press, accepted or returned for revision, submitted)*	**Nature and % of student contribution**	**Co-author name(s) Nature and % of Co-author's contribution***	**Co-author(s), Monash student Y/N***
3	Profiling the Serum Protein Corona of Fibrillar Human Islet Amyloid Polypeptide	Published	50%. Concept and collecting data and analyses, writing first draft and additional editing	1. Ove J. R. Gustafsson: *data analysis, input into manuscript 19%* 2. Yanting Xing: *computational analysis, input into manuscript 1%* 3. Juan Hernandez-Fernaud: *LC-MS/MS, input into manuscript 1%* 4. Cleidi Zampronio: *LC-MS/MS, input into manuscript 1%* 5. Aleksandr Kakinen: *supplementary experiments, input into manuscript 1%* 6. Ava Faridi: *cell culture, input into manuscript 1%*	1. No 2. No 3. No 4. No 5. No 6. Yes 7. No 8. No 9. No 10. No

				7. Feng Ding: *computational analysis, input into manuscript 1%* 8. Paul Wilson: *supervision, input into manuscript 5%* 9. Pu Chun Ke: *concept, supervision, input into manuscript 15%* 10. Thomas P. Davis: *concept, supervision, input into manuscript 5%*	
4	Star Polymers Reduce Islet Amyloid Polypeptide Toxicity via Accelerated Amyloid Aggregation	Published	50%. Concept and collecting data and analyses, writing first draft and additional editing	1. May Lai: *polymer synthesis, input into manuscript 8%* 2. Xinwei Ge: *computational analysis, input into manuscript 2%* 3. William J. Stanley: *ex vivo experiments, input into manuscript 1%* 4. Bo Wang: *computational analysis, input into manuscript 1%* 5. Miaoyi Wang: *data analysis, input into manuscript 1%* 6. Aleksandr Kakinen: *data analysis, input into manuscript 1%* 7. Marc-Antoine Sani: *CD, input into manuscript 1%* 8. Michael R. Whittaker: *concept, input into manuscript 1%* 9. Esteban N. Gurzov: *ex vivo experiments, input into manuscript 1%* 10. Feng Ding: *computational*	1. Yes 2. No 3. No 4. No 5. No 6. No 7. No 8. No 9. No 10. No 11. No 12. No 13. No

				analysis, input into manuscript 1% 11. John F. Quinn: *concept, input into manuscript 2%* 12. Thomas P. Davis: *concept, supervision, input into manuscript 10%* 13. Pu Chun Ke: *concept, supervision, input into manuscript 20%*	

I have renumbered sections of submitted or published papers in order to generate a consistent presentation within the thesis.

Student signature: **Emily Pilkington** **Date: 26/11/2019**

The undersigned hereby certify that the above declaration correctly reflects the nature and extent of the student's and co-authors' contributions to this work. In instances where I am not the responsible author I have consulted with the responsible author to agree on the respective contributions of the authors.

Main Supervisor signature: **Pu Chun Ke** **Date: 26/11/2019**

Acknowledgements

This research was supported by an Australian Government Research Training Program (RTP) Scholarship, and additionally by the 2018 Vaughan Scholarship and an Australian Bicentennial Scholarship (2016). I am also thankful for a travel bursary from the Monash-Warwick Alliance.

First and foremost, to my brilliant supervisors – Dr Paul Wilson, Prof Tom Davis and especially to my primary supervisor, Dr Pu Chun Ke, who has worked with me tirelessly every step of the way. I am exceptionally fortunate to have had the guidance and wealth of experience each of you have brought behind me during the past four years. I am so grateful for the opportunities you have given me, from attending and presenting at international conferences to lab visits with collaborators, access to resources and facilities that developed my skills as an experimentalist, to workshops, seminars, and soft-skills training that enabled my growth as a well-rounded researcher. To be able to publish over twenty papers within these last few years is a privilege many candidates aren't afforded, and for all the hard work I put in, you were willing to work twice as hard to get me there. Through your efforts, I go forward knowing my future is bright, and I could not be more thankful.

Thank you to my panel, Prof Colin Pouton, Dr Esteban Gurzov and Dr Nghia Truong, for their guidance and insight throughout my candidature. I also could not have had the incredibly productive PhD that I had without fantastic collaborators: Dr Feng Ding and the Ding group at Clemson University, USA, provided computational simulations that have complemented and elevated so much of the experimental work I have been involved in thus far. To Dr Esteban Gurzov and his team at St Vincent Institute for excellent *ex vivo* mouse work. Dr Johan Gustafsson, who took 40 GB of proteomic data sent from England and turned it into gold down in sunny Adelaide, and to Drs John Quinn and Michael Whittaker, and May Lai at MIPS, all-stars of star polymer synthesis. It has been such a pleasure to know and work with all of you, and I hope we can continue to do so for years to come.

To members of the Ke group, past and present – Dr Aleksandr Kakinen, Dr Miaoyi Wang, Dr Ibrahim Javed, Ava Faridi, Aparna Nandakumar, Nikolaos Andrikopoulos, Kairi Koppel – thank you for all of your support in the lab, the office and beyond. I am honoured to have known each of you for the brilliant scientists you are, and your dedication and drive inspires me to be a better scientist myself. To the lovely lads in the Haddleton/Wilson groups at the University of Warwick for always being supportive and accommodating to the migratory researcher in their midst, and who, as I was the lone amyloid scientist, gave me the nickname 'Emyloid' – with a particular thank

you to Chris and Gavin, who helped me through a very difficult period. To the admin and staff at the CBNS/MIPS Nanomed, who have each been endlessly helpful and generous through the years. To great scientists and greater friends in the wider Nanomed group, past and present, for their advice and encouragement – in particular to Ayaat, Carlos, Cheng, James, Jo, John, Lars, May, and Song-and-Elly, who went from friends to marriage within my candidature (and I got to catch the bouquet!)

It's been a long journey to get here – and I'm not just referring to the 24 hour UK-Australia flights I've been taking twice a year! To my long-suffering friends outside of work, who I might actually now see more than once every few months, and particularly to Ronnie, who might actually now see me in our own apartment – you mean the world to me, thank you for sticking with me through it all. And, finally, to Mum, Dad, and Meg, my wonderful, generous family, who don't quite understand what I do (and to my sweet cat, who definitely doesn't), but support me unconditionally anyway. I love you dearly, and could not have done this without you.

Table of contents.

Chapter One: Introduction

1.1 Protein aggregation: an overview

1.1.1 Defining protein aggregation: species and mechanics

Protein aggregation can be defined as the interfacing of misfolded proteins to form micro- to macrostructures with either regular or amorphous morphology. Due to the large number of possible conformations a protein can take, the process of protein folding can be highly complex and heterogeneous, and reliant on weak, non-covalent interactions to correctly assume the native state.[1] Modulation of a native protein's net charge, for example, could destabilize electrostatic interactions and result in misfolding.[2] Overarchingly, however, intramolecular folding of protein and protein aggregation are both driven by hydrophobic interactions: for soluble protein, folding mechanisms ensure hydrophobic residues are buried in the protein interior, and are particularly prescient for proteins 100 amino acids or larger (comprising around ~90% of all cellular proteins), which have a propensity for rapid hydrophobic collapse to compact, globular morphology.[3] In aggregating species, these moieties – in the context of

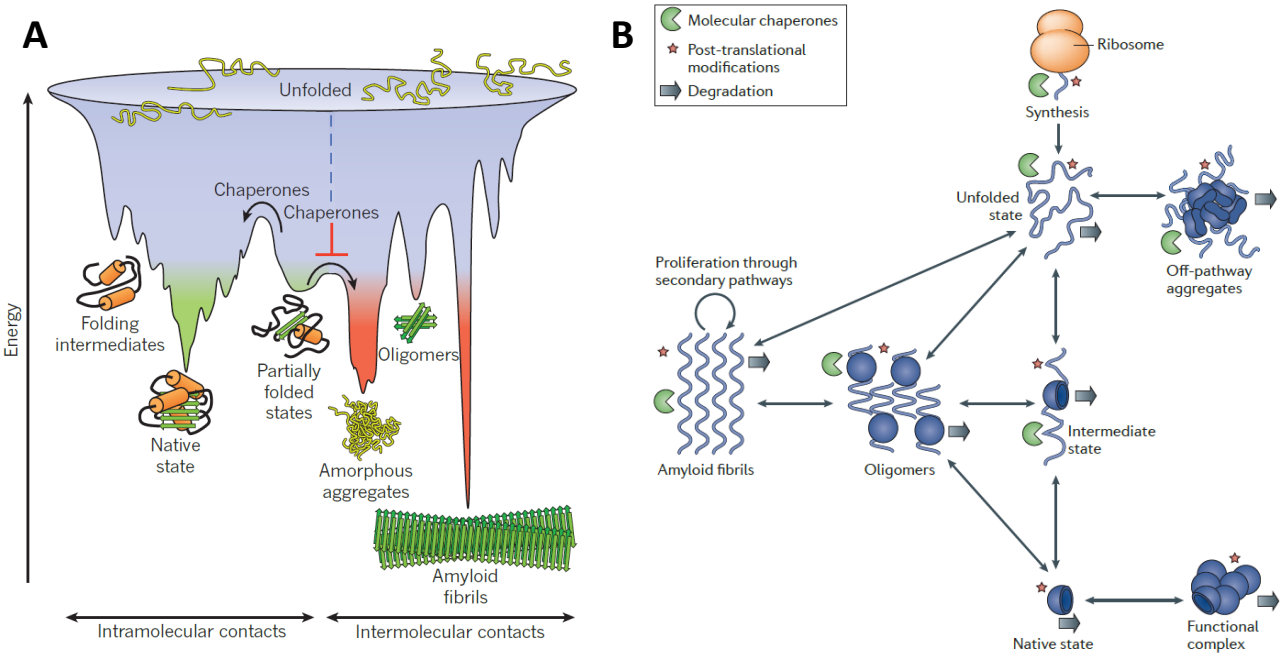

Figure 1: **Physical aspects of amyloid aggregation. A: Free energy landscape of protein aggregation,** visually demonstrating the energy requirements for the transition of a protein from its native state to different aggregation species, and how molecular chaperones attempt to return early aggregates to their native state while preventing further aggregation. Reproduced with permission from Hartl *et al.* 2011.[1] **B: Simplified scheme of amyloid aggregation pathway**, revealing the relationships between native states, intermediate and endpoint aggregates, in addition to which cellular mechanisms (molecular chaperones, post-translational modifications and degradation) can modify each pathway or off-pathway species. Reproduced with permission from Knowles *et al.* 2014.[4]

amyloid aggregation, referred to as 'amyloidogenic regions' – promoting intermolecular hydrophobic contacts in a concentration-dependent manner.[4-5] Accordingly, protein misfolding is surprisingly common – folding efficiency in secretory pathways frequently won't exceed 50%, and it has been estimated that up to 30% of all newly synthesized cellular proteins are defective ribosomal products, targeted for degradation shortly after synthesis.[6]

Figure 1A depicts the protein folding funnel model as a simplified representation of the free energy landscape of protein aggregation, with unfolded conformations populating the broad top of the funnel and the native protein structure situated at the narrow bottom.[1] Typically, aggregation occurs over several stages, each requiring a certain energy threshold to be met for the transition between different states to take place (**Fig. 1B**), with the process often conforming to sigmoidal kinetics (**Fig. 2**): these pertain to a lag phase, wherein negligible aggregate populations are present, to an exponential phase, where aggregation proceeds rapidly, and finally to the saturation phase, as populations of 'seeding' species required to propagate further aggregation are exhausted. Numerous intermediate species can be produced during aggregation, and can be generally classed as either low-order species (dimers, trimers, low molecular weight oligomers), or higher-order species, (high molecular weight oligomers and protofibrils), towards the formation of endpoint aggregates, typically either amorphous or amyloid structures. Rarely, crystalline conformations[7] (the absolute free-energy ground state with regards to protein conformation[8]) or superstructures such as protein particulates and spherulites[9] can be formed as endpoint species of protein aggregation under certain environmental conditions. However, amorphous aggregates, i.e. with no regular macroscopic structure, are the most common fate of aggregating protein. These aggregates are generally nontoxic, but result in loss-of-function of the protein.[10]

In contrast to amorphous aggregates, amyloid fibrils are highly ordered: constructed of typically two or more stacked protofilaments and defined by their cross-β structure, wherein β-sheets run perpendicular to the long fibril axis. Mesoscopically polymorphic, the morphology of fibrils can range from flat tapes to twisted or helical ribbons and nanotubes, dependent on fibrillization conditions.[8, 11] Nearly all proteins are capable of forming amorphous aggregates, yet only a fraction of human proteins – known as 'amyloidogenic' proteins and peptides – are capable of forming amyloid within a physiological environment,[10] though some metabolites can form 'amyloid-like' structures under certain conditions.[12] Though the amyloid state is defined by β-sheet-rich fibrils, amyloidogenic proteins and peptides can have a diversity of native structures – from the β-sheet sandwich structures of β2-microglobulin (β2m),

immunoglobulin light chain and transthyretin to the α+β structure of lysozyme and even α-rich, in the case of serum amyloid A.[13] Remarkably, it has been demonstrated that ultrashort peptides of two[14] to three[15] residues, down to single amino acids (i.e. phenylalanine)[16] are capable of amyloidosis. Furthermore, endpoint products of aggregation are not necessarily conserved for amyloidogenic species: for example, β2m forms either amyloid fibrils or amorphous aggregates at pH 2.5 depending on local NaCl concentration.[7]

Amyloidosis has been modelled as a process of secondary nucleation for most major amyloid species. In secondary nucleation, amyloid fibrils provide a scaffold for new amyloid nuclei or 'seeds' to assemble, subsequently continuing to grow and provide catalytic surfaces for more nuclei to form.[17] Under these parameters, the rate of amyloid fibrillization is highly dependent on concentration, and a large and varied population of intermediate aggregates[18-19] are generated during the exponential phase of aggregation. For major amyloid species such as amyloid-beta (Aβ) and alpha-synuclein (αSyn), complete amyloidosis under physiological conditions takes place over days *in vitro*,[20-21] allowing more granular explorations of fibrillization kinetics and the categorization of intermediates to be feasibly achieved. This has perpetuated the 'oligomer hypothesis', pertaining to the theory that oligomers and intermediate aggregate species are the arbiters of amyloid-associated cytotoxicity rather than mature fibrils.[19] However, for amyloidogenic species with rapid fibrillization kinetics, such as human islet amyloid polypeptide (IAPP), where amyloidosis can reach the saturation phase within minutes *in vitro* dependent on concentration,[22] the transition point from majority lower order to higher order aggregate populations cannot be easily delineated, and their elicited toxicity less clearly defined.[23]

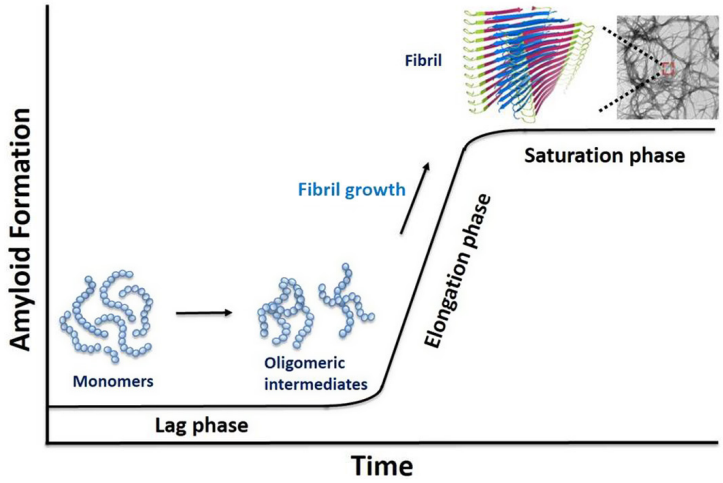

Figure 2: **Fibrillization kinetics of amyloidogenesis as they pertain to solution populations of amyloid pathway species.** Reproduced with permission from Raleigh *et al.* 2017.[117]

1.1.2 Pathological amyloid and dysfunctional aggregation

Aggregation can be a vital, functional process, with the generation of various protein aggregates along the pathway contributing to integral cellular and metabolic functions. It has been theorized that amyloidogenesis in humans could be an evolutionarily flawed attempt at an antimicrobial defense mechanism,[24-25] or that, in a primordial earth, amyloids could have even functioned as a primitive extracellular matrix.[26] These concepts can be reflected in the roles of functional amyloid in bacteria: both acting as antimicrobial agents against competing bacteria and utilized in biofilm formation, in addition to facilitating pathogen-host interactions and rendering 'stealth' status of the bacterium against host immune processes.[27-28] Indeed, proteinaceous oligomers form the blocks of key biological machinery, from bacterial membrane channels [29-30] to human vision,[31] and large, complex amyloid-like aggregate structures, including Balbiani bodies and nuclear amyloid bodies, have crucial roles in cellular health and maintenance.[32-33] Furthermore, the rapid amyloidogenesis of pmel17 (**Fig. 3**) within melanosomes to form nontoxic, functional fibrils is a key step in melanogenesis, i.e. pigmentation of the skin.[34]

Ultimately, however, the majority of amyloidogenic processes in humans are found to be pathological. There are 22 different amyloidogenic proteins and peptides in the human body, which are implicated in over 50 diseases,[5] with the misfolding that accompanies their pathologies generally correlating to a toxic 'gain of function' of the aggregating protein. A selection of amyloidogenic species in amyloid-associated disease are outlined in **Table 1**.

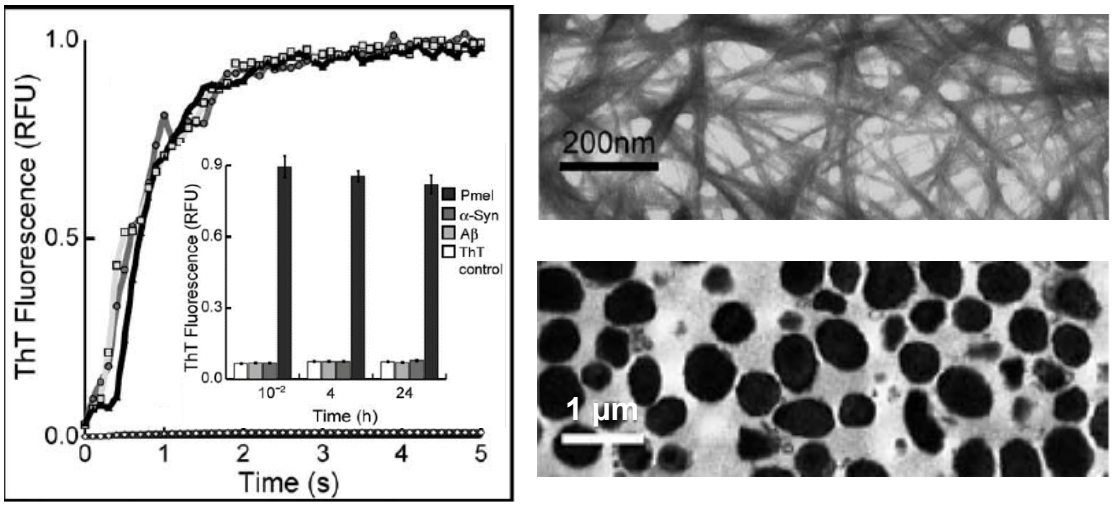

Figure 3: **Rapid pmel17 fibrillization during melanogenesis.** Left panel: ThT fluorescence of pmel17 fibrillization at pH 7.4 (black line), 6.0 (dark grey line) and 4.85 (light grey line). Inset: ThT fluorescence of pmel17 compared to major pathogenic amyloid species up to 24 h of fibrillization. Right panels: TEM imagery of pmel17 amyloid fibrils (top) and melanosomes with stored melanin. Adapted with permission from Fowler *et al.* 2005.[34]

Major amyloid-associated diseases include Alzheimer's disease (AD), type II diabetes mellitus (T2D), and Parkinson's disease (PD); these are associated, respectively, with the amyloidogenic peptides Aβ, IAPP, tau and the amyloidogenic protein αSyn.

Table 1: **Selected amyloidogenic species and associated diseases***

Disease	Aggregating species	Polypeptide length (number of residues)	Native structure
Neurodegenerative diseases			
Alzheimer's disease (AD)	Amyloid-beta (Aβ)	37-43	Intrinsically disordered
Frontotemporal dementia with Parkinsonism	Tau	352-441	Intrinsically disordered
Parkinson's disease (PD)	Alpha-synuclein (αSyn)	140	Intrinsically disordered
Frontotemporal dementia with Lewy bodies			
Spongiform encephalopathies	Prion protein and fragments	230	Intrinsically disordered and α-helical
Huntington's disease (HD)	Huntingtin fragments	Variable	Mostly intrinsically disordered
Amyotrophic lateral sclerosis	Superoxide dismutase 1	153	β-sheets, Ig-like
Non-neuropathic systemic amyloidosis			
Amyloid light chain (AL) amyloidosis	Immunoglobulin (Ig) light chains or fragments	90	β-sheets, Ig-like
Amyloid A (AA) amyloidosis	Serum amyloid A1 fragments	76-104	α-helical, unknown fold
Senile systemic amyloidosis	Transthyretin (TTR) Wild type	127	β-sheets
Familial amyloidotic polyneuropathy	Mutants		
Haemodialysis-related amyloidosis	β_2-microglobulin (β2m)	99	β-sheets, Ig-like
Lysozyme amyloidosis	Lysozyme mutants	130	α-helical and β-sheets
Non-neuropathic localized amyloidosis			
Type II diabetes mellitus (T2D)	Human islet amyloid polypeptide (IAPP; amylin)	37	Intrinsically disordered
Apolipoprotein A1 (ApoA1) amyloidosis	ApoA1 fragments	80-93	Intrinsically disordered
Injection-localized amyloidosis	Insulin	21 and 30	α-helical, insulin-like

**Adapted with permission from Knowles et al. 2014.[4] A comprehensive list of amyloid-associated diseases in humans can be found in Chiti & Dobson, 2006.[5]*

Dysfunctional aggregation can be triggered by various factors. In an *in silico* study of human sequence variations that may potentiate aggregation, mutations in human disease were found more likely to induce aggregation than non-disease associated mutations.[35] In the context of protein aggregation, the introduction of mutant sequences can result in either loss- or gain-of-function for the aggregating species. With 'loss-of-function' mutations, excessive aggregation of a key protein is nontoxic but its consequent deficiency is the major burden of disease, e.g. in cystic fibrosis and α1-antitrypsin deficiency.[1] In contrast, 'gain-of-function' mutations allow the aggregating species to elicit new biological effects unavailable to the wild-type monomer, often found to be highly deleterious. For example, non-amyloid aggregation of mutant p53 prevents apoptosis and allows cancerous cells to proliferate,[36-37] and aggregating mutant α-galactosidase acquires resistance to the chemical chaperone DGJ-1, limiting the treatment of familial Fabry disease.[38] In amyloid-associated disease, the acquired 'gain-of-function' is typically pathogenic: huntingtin is only capable of amyloidosis upon mutation to introduce a polyglutamine sequence near its N-terminus, thus conferring pathogenicity in HD.[39] Chiti *et al.* examined sixteen mutated forms of amyloidogenic species (Aβ, ApoA1, tau and the fibrinogen α-chain) and found that mutation induced a reduction in net charge of fourteen of these species, leading to enhanced aggregation and pathogenicity.[2] Indeed, in Aβ1-42, the Arctic mutation (E22G) induces enhanced amyloidogenesis of Aβ, with mutant aggregate species found highly resistant to intracellular degradation mechanisms *in vitro*[40] and additionally capable of enhancing the misfolding of Aβ1-40 through cross-amyloid seeding.[41] Mutation in amyloidogenesis may present as a double-edged sword: mutant amyloid species overarchingly display enhanced pathogenicity, but, in some cases, their specific recognition by monoclonal antibodies[42] or allele-selective compounds[43] could provide more direct avenues of treatment.

Faulty post-translational processing of polypeptides can also readily generate aggregating species. The hyperphosphorylation of tau, for example, is known to be a hallmark in its fibrillization and pathology.[44] Phosphorylation of Aβ at Ser8[45-46] or Ser26[47] or nitration at Tyr10[48] have each been demonstrated to promote amyloid aggregation while extending the lifetime of oligomeric intermediates, resulting in increased pathogenicity. Interestingly, phosphorylation of tau at Thr205 was shown to confer a protective role against Aβ cytotoxicity *in vivo*.[49] 'Unwanted' post-translational modifications, such as protein glycation, also contribute to protein misfolding. Glycated αSyn[50] and tau[51] form globule-like deposits, and the methylglyoxal-mediated glycation of Aβ enhanced its neurotoxicity *in vitro*.[52] Though the roles

of glycation and advanced glycation endproducts (AGEs) in aggregation are yet to be fully elucidated, AGE-associated aggregation has been implicated in the pathologies of neurodegenerative diseases and a number of cancers.[53]

Disruptions to the physiological environment can induce or promote protein aggregation, and can even induce amyloid formation without initial unfolding and destabilization of its native state.[54] Oxidative stress, and the generation of radical oxygen species (ROS), facilitate residue oxidation-induced aggregation of proteins such as γD-crystallin,[55] linked to cataract formation, and tryptophan hydroxylase 2 (TPH2),[56] associated with pathologies of PD, under physiological conditions. High temperature and low pH are required to induce protein misfolding towards amyloid aggregation in naturally non-amyloidogenic proteins, such as cow's milk-derived β-lactoglobulin (bLg).[57] Small changes in physiological temperature (which can range from 33.4 – 42°C under certain conditions, such as within tumors and neurological disease) can also accelerate aggregation of amyloidogenic species: the amyloidogenic region of Aβ monomers was shown to be increasingly exposed, i.e. allowing more amyloid contact, when increasing environmental temperature from 37 to 42 °C.[58] With regards to pH, human pmel17 fibrillates only under the mildly acidic conditions present within the melanosome, with the formed amyloid fibrils solubilizing at neutral pH.[59]

Lastly, the intracellular environment is densely crowded, with 30-40% of its volume taken up by biomolecules[60] – the roles of biomolecules, and proteins in particular, in amyloidosis is discussed in **Section 1.3.** In general, macromolecular crowding has been shown to accelerate the aggregation of αSyn[61-62] and apolipoprotein C-II.[63] The ionic strength of the milieu also contributes to amyloidogenesis, driving β2m aggregation from amorphous to toxic amyloidosis.[7] Furthermore, the coordination of metal ions such as Cu^{2+}, Zn^{2+} and Fe^{3+} with amyloidogenic species can trigger aggregation through destabilization of the native protein structure and/or facilitating intermolecular amyloid contact through cross-linking with the incorporated metal ion.[64] As would be expected, environmental stressors can intersect or even impede their respective promotional actions on aggregation. Interfacing amyloid species with redox-active ions, i.e. Cu^{2+} and Fe^{3+}, can facilitate ROS-induced aggregation – for example, Cu^{2+} drives the formation of dityrosine dimers of IAPP[65] and Aβ,[66] – but the phosphorylation of Aβ actually limits the action of Cu^{2+}.[67] Interestingly, the selection pressure induced by aggregate-causing environmental stressors can, in some cases, be advantageous: exposing *E. coli* to stressors (heat, oxidative stress and antibiotic treatment) that induced the formation of

intracellular protein aggregates could instill increased resistance in subsequent generations to these conditions comparative to aggregate-free bacteria.[68]

In the absence of a strong genetic link to their onset, some amyloid diseases – most prominently late-onset diseases such as AD, PD and HD – are ultimately considered diseases of ageing.[69] The triggers of protein misfolding listed above – mutation, post-translational processing, and environmental interactions – can be generated or their effects enhanced by the breakdown and dysfunction of biological machinery typical of ageing. In yeast, for instance, approximately 480 proteins have recently been identified as age-related aggregators.[70] Weids and colleagues screened proteins in *S. cerevisiae* triggered to aggregate by stressful conditions – oxidative stress, heavy metal exposure, and amino acid stressors – significantly overlapped with proteins known to aggregate due to ageing; and, additionally, that these stress-induced aggregators also aligned with ageing-induced aggregators in *C. elegans*.[71] There is some debate, however, as to whether protein aggregation is causative of ageing, or a consequence therein, and thus this relationship warrants further investigation.

Deleterious aggregation is further spurred by the failure of systems designed to correct protein misfolding, and remove harmful aggregation species from the circulation. Protein aggregation can be ostensibly 'kept in check' so long as it is controllable, reversible, and localized temporally and spatially – so that, ultimately, local protein concentrations are always kept below their critical aggregation-concentration threshold.[72] The conservation of this equilibrium is known as proteostasis – a complex collection of cellular mechanisms to employ the functional benefits of protein aggregation and limit associated pathologies (**Fig. 4**). Amyloid species can build up to overwhelm the cellular systems that maintain proteostasis, but can also actively interfere with certain components of these systems, further accelerating their cytotoxicity. A cell can attempt to quarantine toxic aggregates within intracellular compartments, such as inclusion bodies[6] and the Insoluble Protein Deposit (IPOD) in yeast[73] – ultimately, however, if all internal systems fail and the cell is unable to restore proteostasis, the cell can decide to self-terminate to minimize further damage mediated to the local environment by uncontrolled protein aggregation.[69]

Proteostasis can be essentially grouped into maintenance at two levels: the 'nucleic acid' level and the 'protein' level. At the regulatory level, it is estimated that over 75% of proteins contain hydrophobic regions that significantly promote aggregation nucleation[74] – consequently, amino acids can be encoded adjacent to these regions to counteract aggregation through charge

repulsion (arginine, lysine, aspartate, glutamate), the entropic penalty relating to aggregate formation (arginine and lysine) or inability to conform to β-sheet structure (proline).[75] Two or more of these so-called 'gatekeeping' residues have been predicted to flank up to 60% of aggregation-prone regions in a multiproteome study, with some guarded by up to six.[74] Gatekeeping residues have been identified in amyloid-forming bacterial proteins such as the *E. coli* curli protein CsgA[76] and microcin E492 in *Klebsiella pneumoniae*.[77] Interestingly, it has been shown that employing this tactic at the regulatory level can provide a 'barcode' to be read by protein-mediated quality control processes: namely, that chaperones can recognize a pattern of charged residues before a hydrophobic region, aiding in the efficacy of processing misfolded protein.[74] Similarly, the encoding of a KFERQ motif, known as a consensus sequence, directs chaperone-mediated autophagy (CMA) for amyloid precursor protein (APP),[78] αSyn[79] and huntingtin (associated with pathologies in HD),[80] among others. Tight control can also be elicited over the translation of αSyn and APP through an iron response element (IRE) in their respective 5'UTR.[81-83]

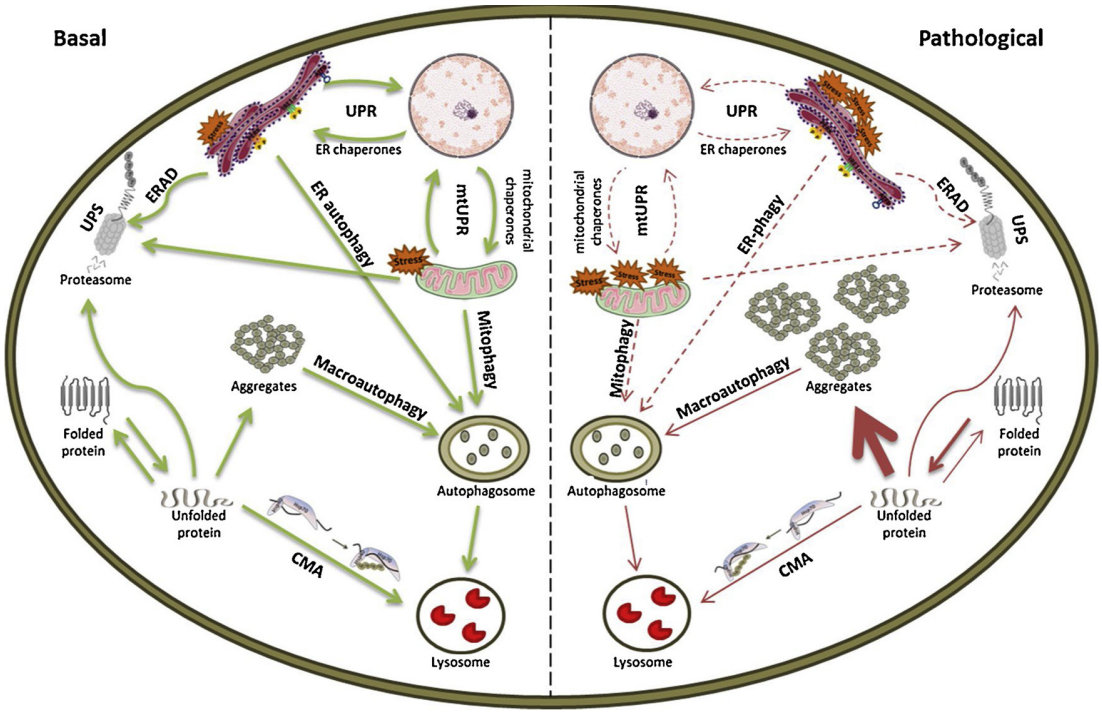

Figure 4: **Cellular mechanisms in which to maintain proteostasis, i.e. amelioration or elimination of misfolded protein, and how the failure of these systems can result in aggregation-based pathologies.** Basal state mechanisms associated with proteostasis are represented by green arrows, with red arrows representing the pathological state – dashed arrows are impaired processes, and bold arrows are increased protein aggregation. Hsp70, heat shock protein of 70 kDa; Ub, ubiquitin; CMA, chaperone-mediated autophagy; ERAD, endoplasmic reticulum-associated protein degradation; UPS, ubiquitin-proteasome system; UPR, unfolded protein response; mtUPR, mitochondrial unfolded protein response. Reproduced with permission from Trigo *et al.*, 2019.[69]

At the 'protein' level, defensive strategies to maintain proteostatic equilibrium fall into three main categories: disaggregation and refolding of misfolded protein by molecular chaperones,[1] and, if the chaperone system becomes overwhelmed, targeted destruction of protein aggregates by the ubiquitin-proteasome system (UPS)[84] or the autophagy-lysosome system (ALS).[85] Within the UPS – predominantly responsible for the removal of short-lived proteins (which, on average, have a high aggregation propensity[86]) and over 90% of oxidatively damaged protein within the cytosol – damaged and dysfunctional proteins are tagged for destruction with ubiquitin and subsequently recognized and degraded by the proteasome. Comparatively, the ALS, which disposes of longer-lived proteins and aggregates, involves the activation protein complexes encoded by autophagic genes (ATG) to form the autophagosome, which in turn leads to lysosomal degradation of dysfunctional protein cargo. In both normal and pathological proteostasis, combinations of these pathways are possible, such as in the case of CMA. The chaperone system majorly consists of heat shock proteins (Hsp) and small heat shock proteins (smHsps), delineated by their kilodalton molecular weight, i.e. Hsp70, Hsp90 and Hsp100,[87] and typically interact with longer-lived, low turnover proteins.[86] Hsp70, in particular, has a central role in protein folding and proteostasis control – its increased expression has been shown to ameliorate toxicity associated with the aggregation of αSyn in an *in vivo* PD model.[88] However, buildup of αSyn oligomers can conversely limit the chaperone action of Hsp70, rendering it unable to functionally fold other protein.[89] Hyperphosphorylated tau also facilitates the displacement of TDP-43 from cdc37, a co-chaperone of Hsp90, resulting in accumulation of TDP-43 fragments in the cytosol which subsequently form inclusions typically associated with the pathologies of amyotrophic lateral sclerosis and frontotemporal dementia.[90] Though tau aggregates can subsequently be cleared by the ALS,[91] the presence of autophagic vacuoles in dystrophic neurites of AD patient brains, a disease also subject to tauopathies, implicates that the process is overall malfunctional in the disease state.[92] Similarly, there is a tight relationship between Aβ and the UPS that contributes to the pathologies in AD, wherein the UPS readily degrades Aβ aggregates under endogenous conditions but Aβ species competitively inhibit proteasome activity under disease conditions.[93]

Individual organelles additionally have their own mechanisms in place to mitigate protein-misfolding under stress-response, such as the unfolded protein response (UPR) system within the endoplasmic reticulum (ER) and mitochondria (denoted as the mtUPR). The UPR follows the aforementioned dual strategies: corrective refolding of proteins mediated by chaperones, or their enforced degradation via the ER-associated protein degradation pathway (ERAD).

Concordantly, increased Aβ deposition in the brain of mouse models was correlated with the downregulation of membralin, a component of the ERAD system.[94] Sorrentino and colleagues demonstrated cross-species conservation, from *C. elegans* to human models, of mtUPR-mediated suppression of Aβ toxicity, and posit that strategies to enhance the mtUPR may rescue aggregation-based pathologies in amyloid diseases.[95]

1.2 Islet amyloid polypeptide: type II diabetes as an amyloid disease

1.2.1 Overview

T2D is a metabolic disease currently affecting approximately 5% of the global adult population,[96] with prevalence expected to double by 2035.[97] Though the major burden of the disease is largely preventable through healthy diet and exercise, T2D is predicted to become the seventh leading cause of death by 2030.[98] A key hallmark during the onset of T2D is dysfunction and death of pancreatic β-cells, located within the islets of Langerhans (**Fig. 5**).[99-101] Once β-cell mass decreases by 40-60%, development of T2D is irreversible.[99]

The 37-residue peptide IAPP, also known as amylin, is directly correlated with β-cell loss in T2D.[102-108] In its native state, IAPP is positively charged and hydrophobic, due to an amidated C-terminus and lack of acidic residues, and is 'intrinsically disordered' i.e. does not conform to a rigid, globular morphology. Endogenously, IAPP is co-secreted with insulin by pancreatic β-cells and has a number of both established and purported functions: centrally, in glycemic control and energy balance, though new evidence indicates there may be further roles for amylin in neurodegeneration and cognition.[109-110] However, it is highly amyloidogenic, and can aggregate in a concentration-dependent manner through intermolecular amyloid contact at its amyloidogenic region, known to be primarily at residues 20-29 (**Fig. 6**).[111] Rodent IAPP (rIAPP), which does not naturally fibrillate, differs in six amino acids in this region, with the most important substitutions considered the three proline residues at positions 25, 28 and 29 of rIAPP,[112] due to the capacity of proline to disrupt H-bonding and β-sheet formation.[75] Additionally, a His18 residue in IAPP that is replaced by Arg increases the positive charge of the sidechain in rIAPP under physiological conditions, likely further limiting aggregation.[113] Ultimately, the insoluble amyloid fibrils and plaques formed in IAPP amyloidogenesis, present in 90% of T2D patients, are implicated in the development, progression and burden of the disease.[114] A deviation in IAPP secretion within a single cell could be capable of initiating

amyloid fibrillation,[115] and recent evidence has also suggested that amyloidosis in monomeric IAPP can be triggered by existing amyloid species in a prion-like mechanism.[116]

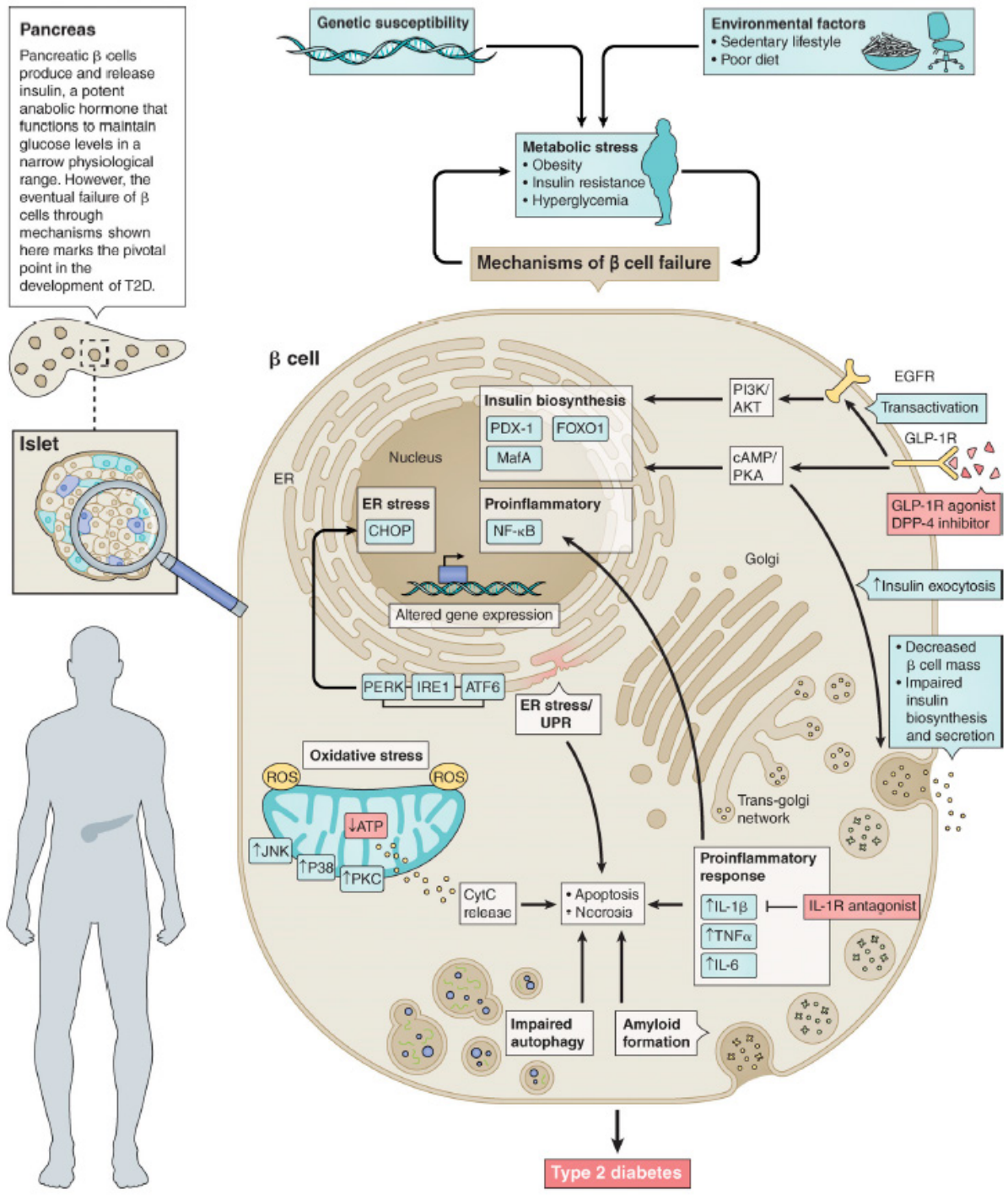

Figure 5: **Mechanisms of pancreatic β-cell dysfunction as the hallmark of T2D.** Reproduced with permission from Park & Woo, 2019.[101]

1.2.2 IAPP within pancreatic β-cells

IAPP is generated via the translational processing of proIAPP, a propeptide whose expression is regulated by the glucose-responsive IAPP gene promoter.[117] IAPP is capable of undergoing further 'unwanted' post-translational modifications, such as glycation, which may enhance its pathogenicity. For example, glycated IAPP has been shown to undergo more rapid fibrillization than IAPP lacking AGEs, and was further capable of expediting the fibrillization of non-glycated IAPP.[118] Gong *et al.* observed increased local plasma concentration of IAPP and amyloid deposition in the kidneys of T2D patients with diabetic nephropathy (DN), hypothesizing that IAPP could bind AGE receptors (RAGEs) and potentially trigger inflammatory signal transduction pathways, thus contributing to localized cell death.[119] Concordantly, in a study conducted by Abedini and colleagues, RAGEs were shown to be upregulated in response to a human IAPP challenge in the islets of transgenic, human IAPP-producing mouse models *ex vivo*. Interestingly, RAGEs demonstrated selective binding of IAPP intermediate species over fibrillar amyloid, with isolated extracellular ligand-binding domains of soluble RAGE (sRAGE) capable of inhibiting IAPP amyloid formation and associated cytotoxicity.[120]

ER stress has been shown to have a role in β-cell death and dysfunction in diabetes, and has been specifically linked to pathological IAPP fibrillization.[121-123] IAPP upregulation *in vitro* was associated with the inhibition of autophagy signaling and, in particular, mitophagy – resulting in accumulation of damaged mitochondria, ROS production, and rendering β-cells more prone to dysfunction and apoptosis induced by ER stress.[124] Concordantly, molecular

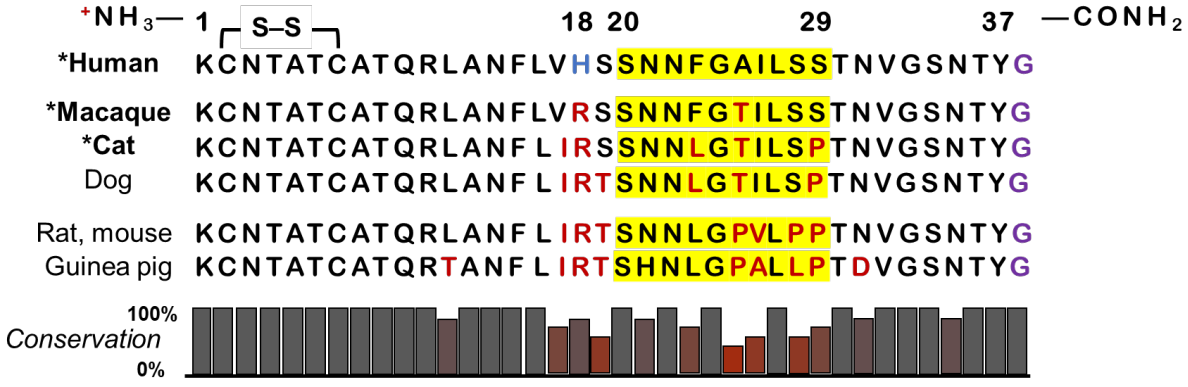

Figure 6: **Sequence of human IAPP compared to other mammals.** The amyloidogenic region of human IAPP (20-29) is highlighted, and residue substitutions across species (as compared to human IAPP) are in red. Bolded, starred species indicate IAPP can natively form amyloids. The disulfide bridge between C2 and C7 is indicated, with the amidated C-terminus denoted in purple and His18 in human IAPP labeled in blue. Relative overall sequence conservation across all species, including those omitted from this figure, is illustrated below. Adapted with permission from Raleigh *et al.* 2017.[117]

(GRP78, protein disulfide isomerase: PDI) and chemical (taurine-conjugated ursodeoxycholic acid, 4-phenylbutyrate) chaperones have been shown to mitigate IAPP-induced ER stress *in vitro*.[125-126] A proteomic study into the contents of the β-cell granules identified a number of molecular chaperones sequestered within, including Hsps 5, 70, 72 and 90, in addition to PDIs and GRP58.[127] In a follow-up study, Chien and co-workers demonstrated that Hsp70 and the co-chaperone Hsp40 inhibit IAPP fibrillization *in vitro;*[126] Hsp72 has additionally been shown capable of rescuing IAPP pathology *in vivo* in *C. elegans*.[128] Recently, in fact, a hybrid of Hsp70 grafted with IAPP demonstrated cytoprotective effects in pancreatic β-cells against IAPP-mediated toxicity *in vitro*.[129] Press and colleagues recently reviewed the current literature regarding the role of IAPP in proteostasis, specifically concerning the UPS and ALS.[130] There is little or conflicting evidence regarding the relationship between IAPP and the UPS, though there is some consensus that IAPP can act to impair it – more specifically, inhibiting proteasomal activity in addition to downregulating expression of Hsp90 and UCH-L1, a deubiquitination enzyme. Similarly, though the ALS plays a role in IAPP clearance, fundamental understanding of the impact IAPP in the disease state elicits on ALS is limited – though IAPP may interfere with autophagic pathways, the increase in dysfunctional autophagy with age may exacerbate IAPP-mediated toxicity. Furthermore, it is not currently known if IAPP-associated autophagosome accumulation is due to an increased response to IAPP challenge, or, as IAPP aggregates are resistant to proteolytic degradation,[131] due to IAPP burden impairing lysosomal degradation.

Upon completion of processing through the ER and Golgi, IAPP is natively stored at millimolar concentrations within the high pH environment of the β-cell granules, under conditions which favor the retention of monomeric IAPP over amyloidogenesis.[132] It has been previously thought that insulin, co-stored in β-cell granules at a 100:1 molar ratio to IAPP, is the major inhibitor of intracellular IAPP fibrillation.[133] Though insulin has been shown to be a potent IAPP aggregation inhibitor *in vitro,*[134] hyper-production or -secretion of IAPP is often not complemented by upregulation of insulin *in vivo*, and intercellular concentrations of IAPP have been shown to be comparatively heterogeneous.[115] Additionally, IAPP is localized nearly exclusively in the soluble halo fraction of β-cell granules, whereas insulin forms insoluble hexameric crystals within the core.[135] Consequently, it is more plausible to postulate that additional granule components, co-localized with IAPP, contribute to this crucial role within β-cells. Two such candidates include C-peptide, a part of the proinsulin sequence which precursors insulin synthesis, and zinc ions (Zn^{2+}).[136] Interestingly, Zn^{2+} concentration within

pancreatic β-cells represents one of the highest in the human body, and is maintained by a zinc transporter (ZnT8) specific to β-cells.[137] Zn^{2+} is known to form hexamers with insulin, and as such is important in effective insulin storage within the β-cell granules.[138] It has been recently demonstrated that C-peptide, Zn^{2+}, and IAPP form a stable, heteromolecular complex that is capable of preventing IAPP fibrillation *in vitro*, and thus potentially maintain the IAPP native state within β-cell granular storage.[139]

1.2.3 IAPP amyloidogenesis

The initiation of IAPP amyloid fibrillation remains a debate of 'chicken versus egg': whether intracellular amyloidogenesis triggers death of the β-cell and provides a 'seed' for larger plaque formation extracellularly,[115] or if IAPP fibrillation occurs post-secretion within the extracellular space, and subsequently leads to β-cell death.[104] Conclusive evidence to support either hypothesis remains forthcoming. In addition to the question of intracellular versus extracellular amyloidogenesis, there has been considerable debate in the literature as to the primary IAPP conformation that induces β-cell toxicity[23] – namely, monomeric IAPP, intermediate species or mature amyloids – and, additionally, the mechanisms thereof. Within an *in vitro* aqueous environment, IAPP fibrillates rapidly, and multiple forms can co-exist at any given stage until the amyloid saturation point has been long reached.[4] When compared to the well-characterized Aβ, which has a slower aggregation rate of days *in vitro*, isolation of different IAPP species to examine their cytotoxic effects has thus far been difficult to accomplish,[23] further contributing to ambiguity with regards to IAPP toxicity.

Mature IAPP amyloids have been historically favored as a causative agent of β-cell failure, with physical association between plaques and cells posited to result in membrane perturbation, production of ROS, and/or apoptosis.[22] A Japanese population who produced a mutated form of IAPP with an increased aggregation propensity showed that they subsequently developed T2D in clinical studies.[140-141] Lorenzo *et al.* identified amyloid-membrane contact triggering apoptosis as the primary mechanism of toxicity (**Fig. 7A**), proposing that β-cell viability is only reduced when IAPP concentration is high enough to mediate fibrillization.[104] Additionally, Schubert and colleagues screened a number of amyloid peptides in B12 cells for production of ROS with 2,7-dichlorofluorescin diacetate (DCFDA), and determined that IAPP was correlated with ROS production and subsequent loss of β-cell viability, while no such species were measured with the non-amyloidogenic rIAPP.[108] Furthermore, exposure of pancreatic β-cells

to sublethal levels of IAPP aggregates *in vitro* resulted in ROS-independent upregulation of antioxidant enzymes, indicating an in-built defensive mechanism to IAPP-mediated oxidative stress.[142] There is evidence that amphiphilic amyloid can mediate formation of ion channels or pores in the β-cell membrane through its high propensity for contacting and integrating phospholipids into growing fibrils, i.e. 'lipid stripping', leading to cell death by unregulated calcium ion influx or cytosol leakage (**Fig. 7B-C**).[143-147] IAPP fibrils can be phagocytosed *in vitro* but amyloid-associated factors may limit the capacity of macrophages to clear localized plaques *in vivo*, potentiating long-term perturbation of the tissues they are deposited within.[131]

In more recent years, however, the focus has shifted to the soluble oligomeric form of IAPP as the main toxic species, but considering similar mechanisms of toxicity as were postulated for IAPP amyloids. As such, many working paradigms concerning IAPP toxicity have been influenced by mechanistic studies of Aβ toxicity in AD – known to be mediated by Aβ oligomers[23] – in light of the biophysical and biochemical connections between IAPP and Aβ fibrillization. This approach remains to be validated, though evidence to suggest a toxic role for IAPP oligomers is abundant. Ritzel and coworkers observed that IAPP oligomers mediated a disruption in islet architecture *ex vivo*, impairing cell coupling and insulin secretion and inducing apoptosis.[107] Research from Kayed *et al.* and Meier *et al.* described cell membrane permeation induced by IAPP oligomers (**Fig. 7B-C**), while monomeric IAPP or amyloid fibrils showed no adverse effects,[105] and prevention of amyloid fibrillization did not mitigate toxicity.[106] Rifampicin was utilized in the latter study to inhibit the formation of amyloid plaques, demonstrating its anti-aggregation properties through Thioflavin-T (ThT) staining – an established method to detect amyloid protein. However, Meng and colleagues refuted this, revealing that rifampicin had no effect on IAPP fibrillization and demonstrating that the ligand could interfere with ThT fluorescence.[148] Furthermore, studies interrogating the toxicity of

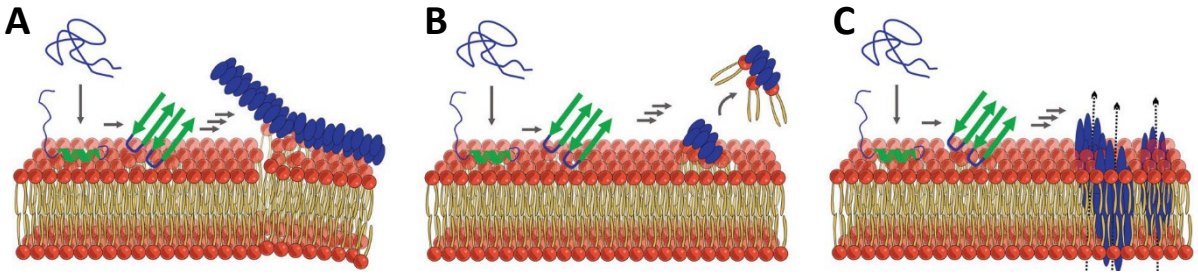

Figure 7: **Proposed mechanisms of lipid membrane damage elicited by amyloid pathway species such as IAPP.** A: Non-specific membrane disruption by fibril growth and physical perturbation. B: Detergent-like membrane disruption and 'lipid stripping' by oligomeric and fibrillating species. C: Pore formation by low-order intermediate species. Adapted with permission from Owen *et al.* 2019.[147]

different IAPP species *in vivo* are predominantly conducted with antibodies, e.g. anti-oligomer antibodies such as A11, which can be problematic when applied in a complex environment as these antibodies are not sequence-specific – rather, they recognize conformational shape.[149] Given the polymorphic nature of oligomers, and the wealth of biomolecules *in vivo* that share β-rich conformations, the reliability of antibodies to delineate IAPP aggregation species in the context of their associated pathogenicity is called into question.[23] Collectively, this illustrates the limitations of current methodology to characterize IAPP species, and warrants a more comprehensive approach towards establishing fundamental tenets of IAPP pathogenicity.

1.2.4 IAPP pathologies beyond the pancreas

Per its role in glycemic control, IAPP is capable of crossing the blood-brain barrier (BBB), and is ubiquitously present in the circulation. Lack of confinement to the pancreas becomes problematic in the context of T2D, as IAPP amyloid deposits have been reported in the kidneys,[119] heart,[150] and brain[151] of T2D patients, with associated tissue degradation and health complications observed in each case. Srodulski *et al.* proposed a mechanism for IAPP wherein oligomerized IAPP translocated from the pancreas to the brain, mediating damage to the BBB, which subsequently allowed diffusion of IAPP oligomers into the brain tissue.[151] Indeed, IAPP amyloid deposition has been reported in brain blood vessels and perivascular spaces of AD patients with or without T2D, causing extensive damage to the surrounding tissue.[152] Interestingly, unchanged or decreased blood plasma concentrations of IAPP have been reported in T2D patients, likely due to increasing amyloid accumulation in the pancreas inhibiting the translocation of monomeric IAPP.[153-154] The reason for this disparity, i.e. between IAPP plasma concentration and increased systematic amyloid deposition in T2D, has not been fully elucidated. Oskarsson and colleagues posit that IAPP could be expressed within the brain, which could contribute to the formation of local Aβ-IAPP co-amyloids.[155] Though there is some evidence that extra-pancreatic expression of IAPP occurs in several animal models,[156-157] there is no current evidence to suggest a similar mechanism in humans.[152]

Compared to other amyloid protein species, including Aβ and αSyn, IAPP is understudied, with fundamental knowledge of its endogenous and pathogenic behavior found lacking: further interrogation into IAPP at the biological interface should thus be pursued, particularly in light of the significant proportion of the global population that are affected by T2D.

1.3 Amyloid in the extracellular environment

1.3.1 Modulation of amyloidosis by extracellular biomolecules

Post-secretion, amyloid species are introduced to a complex extracellular milieu, with various circulating species likely to elicit significant effects on amyloid morphology and cytotoxicity. For instance, nucleic acids can mediate aggregation of αSyn, prion protein and Aβ, among others,[158] and lipids additionally impact amyloid aggregation of various species, from small peptides such as Aβ and IAPP to apolipoprotein B, one of the largest proteins present in nature.[159] How lipids, and more specifically, phospholipids, play a role in amyloidogenesis is of particular interest, given the deleterious seeding and conformational change of amyloid species on synthetic and endogenous phospholipid bilayers.[105, 144-145, 160] In the presence of unimolecular lysophosphatidylcholine (LPC), a product of lipid peroxidation and the most abundant single-tailed phospholipid in the blood,[161] fibrillization of Aβ1-40 was repressed – but, surprisingly, a promotional effect was observed on the aggregation of Aβ1-42,[162] further augmenting its cytotoxicity *in vitro*.[163] Contrastingly, IAPP fibrillization was inhibited in the presence of both unimolecular and micellar LPC, with micellar LPC driving IAPP to adopt a majority α-helical conformation, as has been reported in the presence of sodium dodecyl sulfate (SDS) micelles.[164] The stark contrast in the elicited effect of singular lipids and model biomembranes between different amyloid species highlights the necessity to examine amyloid interactions at the biological interface on a case-by-case basis, in order to fully reflect the complex endogenous environments they inhabit.

Concordantly, though thousands of proteins have been identified in the circulation,[165] few have been investigated as non-specific interactors or aggregation inhibitors of amyloid species. Human serum albumin (HSA), as the most abundant protein in blood plasma, has been reported to bind >90% of circulating Aβ and up to half of Aβ within the cerebrospinal fluid, and act to inhibit its fibrillization.[166] Recently, HSA also demonstrated the capacity to inhibit amyloid aggregation of IAPP and αSyn, in addition to mitigating amyloid-associated hemolysis *in vitro*.[167] Extracellular proteins α-casein, lysozyme (Lys), alpha-lactalbumin (aLac), bLg, albumin, pyruvate kinase and catalase have been shown to bind non-specifically to Aβ1-40 and inhibit its fibrillization *in vitro*.[168-170] Various amyloidogenic species, including Aβ1-40 and Aβ1-42 peptides, pulmonary lung surfactant protein C[171] and the ageing-associated arterial amyloid medin,[172] were inhibited through *in vitro* interactions with proteins with the BRICHOS domain (sequence alignments related to BRI proteins associated with British and Danish

dementia, in addition to chondromodulin and proSP-C) such as proSP-C,[173-174] Bri2,[174-175] and gastrokine 1.[176]

Non-chaperone specific interference of molecular chaperones with amyloidogenesis has also been described. α2-Macroglobulin (α2M) and haptoglobin (Hp), glycoproteins with the capacity to rescue proteins from stress-induced amorphous aggregation, demonstrated anti-amyloidosis properties through their association with Aβ1-42, in addition to various other aggregating proteins.[177] Concordantly, smHsps such as αB-crystallin and Hsp27 prevented amyloidogenesis and/or amyloid-associated toxicity through transient interactions with Aβ1-42,[178-179] Aβ1-40 in wild type and a mutant with higher pathogenicity,[179] in addition to αSyn.[180]

With regards to IAPP, interactions with intracellular components beyond the granular space have been reported,[181] but, surprisingly, little is known so far concerning the association of IAPP with extracellular proteins and their biological and pathological implications. Several co-factors, including serum amyloid P (SAP) component,[182] apolipoprotein E (ApoE)[183] and glycosaminoglycans (GAGs), in particular heparan sulfate proteoglycans,[184] have been shown to associate with IAPP amyloid deposits *in vivo*. GAGs are also known to enhance fibrillization of IAPP[185-186] and can promote aggregation of incompletely processed IAPP.[187] Secretory chaperones have additionally demonstrated some capacity to prevent IAPP fibrillation *in vitro.*[188] However, association with IAPP does not necessarily affect residual IAPP-mediated cytotoxicity – in the cases of ApoE and GAGs, only the latter is implicated in IAPP toxicity.[189-190] This paradigm was further highlighted via the exposure of fibrillating IAPP to aLac and Lys as two model protein interactors, with analogous molecular weight and morphology but opposing charges, to gauge how their presence impacted IAPP aggregation and associated cytotoxicity *in vitro*.[191] Net positively-charged Lys inhibited IAPP aggregation while net negatively charged aLac elicited a promotional effect, yet the application of neither protein was able to significantly mitigate the cytotoxicity of IAPP.

Lastly, amyloidogenic peptides have also been found to co-localize, with Aβ, tau and αSyn frequently reported to interact and generate enhanced pathologies within *in vivo* neurodegenerative disease models.[192-193] Accordingly, circulating IAPP species have been shown capable of forming co-amyloids with other extra-pancreatic amyloidogenic peptides. For example, residues within the amyloidogenic region of IAPP show a strong binding affinity for Aβ.[194] IAPP-Aβ cross-seeding and co-amyloid generation has been widely reported,[195-197] particularly in the context of T2D at the interface of neurological disorders and AD. How IAPP

contributes to the overall toxicity of these co-amyloids, however, remains unclear. IAPP-Aβ co-aggregates have been shown to contain properties intermediate to each respective amyloidogenic peptide; Seeliger *et al*. demonstrated that IAPP-Aβ permeabilized β-cell lipid membranes at a slower rate than IAPP alone, but more rapidly than Aβ species.[196] Clearance of toxic Aβ amyloids in the brain by circulating low order IAPP species has actually been proposed as a therapeutic effect of their association.[152, 197] However, though IAPP was found to co-localize with cerebral and vascular Aβ plaques, Aβ was not detected in IAPP plaques isolated from T2D patients.[155] Elucidating the interplay of IAPP with extracellular biomolecules, in addition to other amyloidogenic species, would shed further light on IAPP pathologies, towards developing targeted, effective treatment strategies against T2D.

1.3.2 Amyloid and the 'protein corona'

The 'protein corona' was first coined in 2007 by Dawson, Linse and colleagues to describe the fouling of synthetic nanomaterials when exposed to a biological environment, defined therein as "proteins compete for the nanoparticle 'surface,' leading to a protein 'corona' that largely defines the biological identity of the particle."[198] In this sense, the enrichment of nanomaterial surface-exposed proteins leads to an *in vivo* response which may not necessarily align with the applied nanomaterial's intended target. In the decade since, elucidating the protein corona of a given nanomaterial has become a key point of characterization in order to more accurately predict its *in vivo* behavior.[199] Recently, it has been proposed that so-called 'native' nanomaterials, i.e. biomolecular structures naturally present *in vivo*, likely form a protein corona in the complex extracellular environment, which may have additional implications on their biological fate. As of writing, protein corona formation has been reported on virions,[200] collagen matrices,[201] unfolded fibronectin,[202] protofibrils of a synthetic Aβ1-42 variant,[203] and, recently, per the author, mature IAPP amyloid fibrils (**Fig. 8**).[191, 204]

As an emerging field, the general literature on protein-amyloid species interactions do not ascribe a 'coronal' effect to protein interactors in the case that they have inhibitory action on amyloidosis but specific binding mechanics are not elucidated: rather, 'non-specific', 'transient' or 'unknown' protein-amyloid interactions are reported. Potential coronal interference in amyloidogenesis is exemplified in many studies pertaining to amyloid-molecular chaperone associations. Clusterin, known also as apolipoprotein J and found in all disease-associated extracellular amyloid deposits, was capable of inhibiting amyloidogenesis of multiple aggregating species *in vitro*, including Aβ1-42 and αSyn.[205] It has been posited that the interaction of clusterin with Aβ species enhances its amyloid-associated pathogenicity, as loss of clusterin directed amyloid deposition to the cerebrovasculature and relieved hemorrhage and inflammation in an AD mouse model *in vivo*.[206] Concordantly, clusterin associated with engineered Aβ1-42 protofibrils as a component of its protein corona,[203] potentiating clusterin as an alternative target for anti-amyloidosis treatment strategies. Aβ1-42 oligomers formed in the presence of the chaperone prefoldin (PFD) were shown to elicit approximately 30-40% less

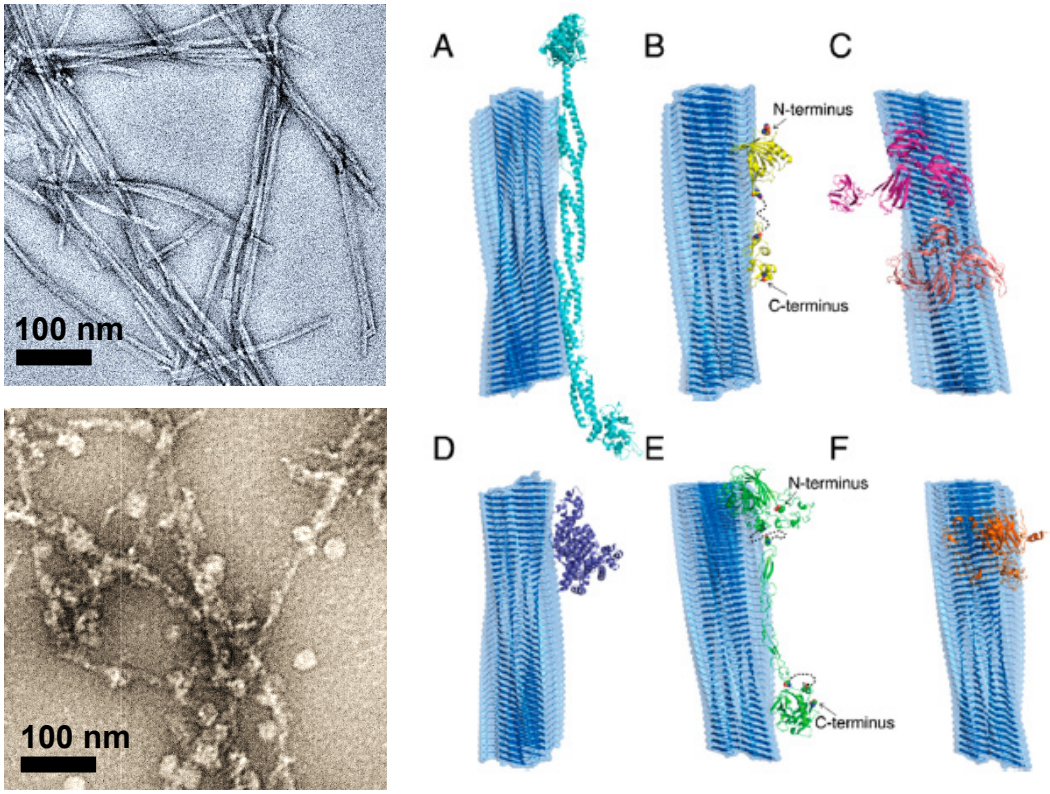

Figure 8: **Formation of the amyloid-protein corona within biological media.** Left panels: Transmission electron microscopy (TEM) images of IAPP amyloid in the absence (top) and presence (bottom) of complex biological media *in vitro*. Right panels: docking simulations of amyloid fibrils (dark blue) with identified coronal proteins of IAPP amyloids after exposure to fetal bovine serum *in vitro*. A: alpha-actinin-4; B: protein AMBP; C: neuropilin, in both 'open' and 'closed' conformations; D: serum albumin; E: thrombospondin-1; F: cartilage oligomeric matrix protein. Adapted with permission from Pilkington *et al.* 2018.[204]

cytotoxicity to PC12 cells and murine primary cortical neurons *in vitro* comparative to oligomers generated in its absence, suggesting the interfacing of PFD with Aβ1-42 aggregates to form a corona may prevent cytotoxic contact.[207] Lastly, DNAJB6, a member of the Hsp40 family, did not interact with unfolded Aβ1-42 monomers but was able to truncate the fibrillization of aggregated species;[208] similarly, Hsp104 was also capable of arresting Aβ1-42 aggregation at multiple stages, but unable to mediate disaggregation of formed aggregates.[209] In this context, the changed identity of the amyloid surface via corona formation presents two key paradigms: firstly, limiting amyloid fibrillization through obfuscation of nucleation sites, but, antithetically, rendering chaperones unable to interact and perform amyloid disaggregation. This underscores the need to interrogate the amyloid-protein corona within different environments, and how applied conditions may act to both help and hinder treatment strategies.

Towards a more comprehensive understanding of proteins enriched within the amyloid plaque microenvironment *in vivo*, Liao *et al.* isolated plaques from clinical patients with AD and described the co-localization of 488 proteins with senile plaques from postmortem brain tissues, with 26 found conserved between two patients.[210] Proteomic analysis characterized the plaques as majorly Aβ-based, with tau also identified as a co-amyloid. Non-amyloid proteins such as cystatin C, capable of binding soluble Aβ peptides,[211] and 14-3-3 proteins, which comprise of up to 1% of soluble protein within the brain,[212] were identified in the plaques, with the zeta isoform found to be the most enriched. As 14-3-3 ζ is known to bind and promote the phosphorylation of tau,[213] and, accordingly, has been found enriched in tau neurofibrillary tangles,[214] the presence of tau within these plaques may have influenced its localization, indicating that co-amyloids – and their relative makeup, with regards to ratios of different amyloid species – likely impact the diversity of enriched ligands. Furthermore, the increased localization of a number of lysosomal ATPases and cathepsin D to the AD plaques comparative to the surrounding tissue implicated the plaque interior as an area of high proteolytic activity. Overarchingly, the AD plaque-localized proteins Liao and colleagues identified pertained to a number of biological processes, including cell adhesion, inflammation, membrane trafficking and proteolysis, thus potentiating interference in these mechanisms elicited by these plaques through artificial enrichment of specific proteins within the local microenvironment.

The first *in vitro* characterization of amyloid-protein corona formation in biological media, wherein corona formation was tracked under different environmental conditions and coronal proteins identified through proteomic analysis, was performed on IAPP amyloid fibrils *in vitro*

by the author and colleagues,[204] as a follow-up study to an initial examination of protein corona formation of IAPP fibrils in the presence of single model protein interactors.[191] Singular protein interactors were able to induce fibril conformational change and mitigate low-level cytotoxicity elicited in primary cells *in vitro*;[191] accordingly, the amyloid-protein corona in complex media was found extensive and nonuniform, and further induced changes in morphology of cultured pancreatic β-cells.[204] Concordantly, proteins from the amyloid corona formed in complex media generally favored fibrillar conformations and structural plasticity (**Fig. 8**), and pertained to roles in a variety of biological processes, including focal adhesion, ECM-receptor interaction, the PI3K-Akt signaling pathway and metabolism. Remarkably, exposure of amyloids to the same biological media under different conditions, i.e. flow, generated divergent coronae, further illustrating how factors within the local microenvironment may influence plaque composition. Interestingly, the enrichment of APP was conserved under these parameters, a continued testament to the high propensity of amyloid-fated species to co-localize. Further examination of enriched proteins in plaques *in vivo* in tandem with the controlled interrogation of amyloid-corona formation conditions *in vitro* can build a fundamental understanding of how amyloid, as a scaffold for protein interactors, may elicit a biological impact beyond the scope of short-term cytocidal action, and further reveal as-yet undiscovered pathologies of amyloid-associated disease.

1.4 Anti-amyloidosis strategies: from nano to micro

1.4.1 Overview and models

Amyloid inhibition is essentially achieved through the introduction of exogenous ligands or chaperones to disrupt and/or outcompete the self-assembly of amyloid proteins from initiating nucleation, driving toxic intermediate species off-pathway or sequestering them for degradation, and, lastly, the disaggregation or remodeling of mature fibrils into nontoxic amorphous aggregates. In principle, this can be accomplished by introducing engineered nanoparticles (NPs) that mediate – in no particular order – hydrogen bonding (H-bonding), hydrophobic and electrostatic interactions, as well as π stacking, either individually or in combination with amyloid proteins. In practice, however, controlling such an array of interactions through nanomaterials design (for both the core and the surface) and synthesis remains a major challenge, further complicated by the necessity of installing the nanoparticles with good dispersity, biocompatibility and bioavailability *in vitro* and *in vivo*.

Over the last decade, there has been an active search for efficacious anti-amyloidosis agents. A myriad of nanomaterials and small molecules, from simple polyphenols to complex nanostructures with a range of different surface chemistries, have been screened *in vitro* for their capacity to mitigate amyloidosis, with the majority of anti-amyloidosis studies – from benchtop to clinic – focused on Aβ aggregation.[215] An overview of nanomaterials utilized to combat amyloid aggregation, in addition to prototypical experimental models to which they are applied, is shown in **Figure 9**. Recent efforts have not shown a trend towards a particular material – rather, multiple species are still being explored *in vitro* towards their application *in vivo*.

Assessing anti-amyloidosis candidates *in vitro* involves immortalized and primary cell lines from humans, mice, and sometimes bacteria, frequently undertaken in static, 2D conditions, but additionally can be performed under flow[216] and/or in a 3D microenvironment.[217-218] Cells can also be co-cultured to generate organoids, towards a more realistic biological environment – for example, mimicking pancreatic islet biology through the co-culture of α-cells, β-cells and epithelial cells in a specific ratio to investigate IAPP-elicited cytotoxicity and its amelioration by a given treatment strategy.[219]

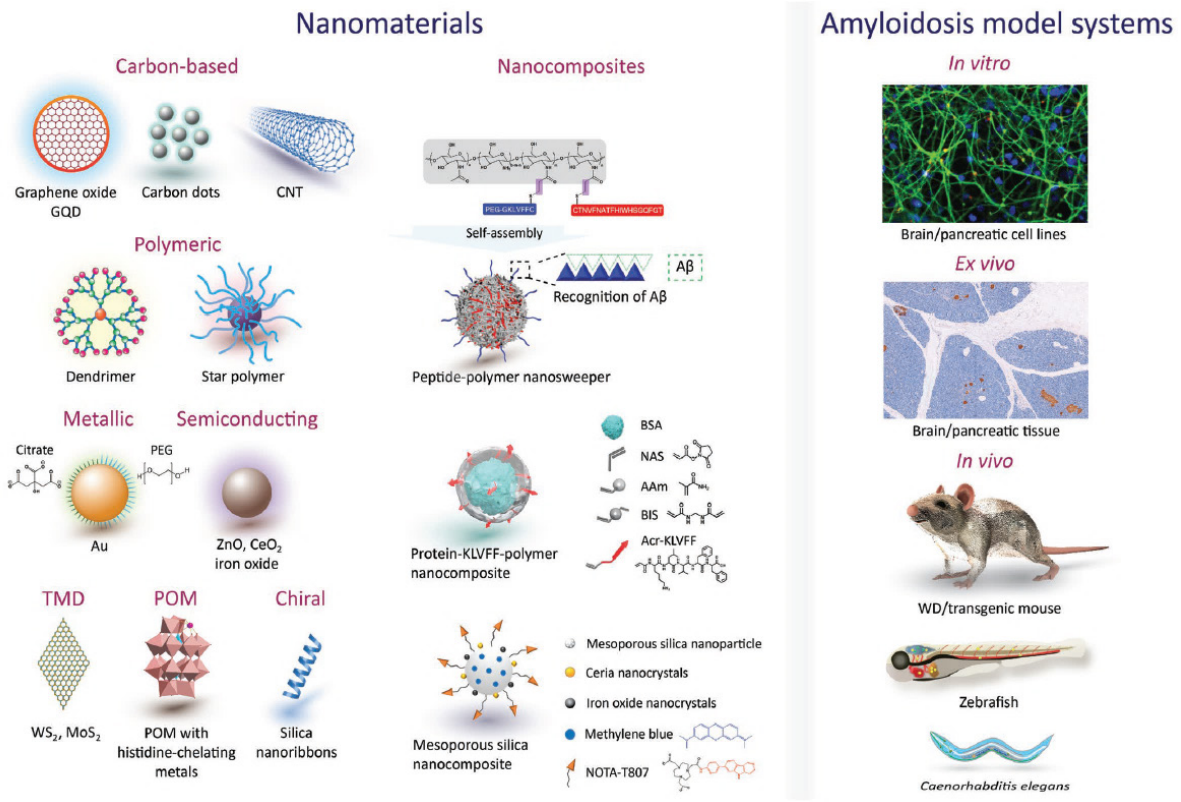

***Figure 9*: Selected anti-amyloidosis agents and model systems of amyloidosis.** Reproduced with permission from Ke *et al.* 2019.[215]

In vivo models exploited to investigate amyloidosis can range from the nematode *C. elegans* to recent studies utilizing zebrafish (*Danio rerio*),[215] and, more rarely, non-human primates.[220] Rodent models, primarily mice and occasionally rats, are the most frequently utilized *in vivo* platform for anti-amyloidosis research. However, these models can differ from human biology in key areas that are essential to mimic human disease – for instance, the non-amyloidogenic nature of rIAPP.[117] Consequently, to best approximate the conditions of human disease, two overarching strategies are utilized: firstly, generating transgenic (tg) mice to overexpress human amyloidogenic proteins or peptides, optionally excising affected organs and applying treatment strategies *ex vivo*; secondly, direct injection of human amyloid species into the circulation or specific tissues of wild-type (WT) animals to produce disease pathologies. To evaluate the burden of disease in these models, animal behavior is assessed in addition to tissue damage and amyloid deposition, and, specifically, the presence of neurotransmitters such as acetylcholine esterase, serum glutamate and GABA (γ-amino butyric acid) for AD, tyrosine hydroxylase for PD, and insulin levels for T2D can be monitored as indicators for each respective disease.[221-222]

1.4.2 Small molecules

Small molecules, both natural and synthetic, are capable of complexing with amyloid proteins or intercalating into the amyloidogenic regions of aggregating species, resulting in effective inhibition of amyloid aggregation.[11, 223] Plant-derived polyphenols, including resveratrol, curcumin and epigallocatechin gallate (EGCG), are additionally cytoprotective due to their antioxidant properties, capable of scavenging amyloid-associated ROS and thereby preventing lipid peroxidation of cell membranes.

Discrete molecular dynamics simulations indicate that resveratrol and curcumin are capable of forming IAPP-polyphenol nanoassemblies.[224] EGCG has been shown to intercalate between beta sheets of fibrillating IAPP via π-π stacking and hydrophobic interactions, and capable of driving amyloid aggregation off-pathway.[11] How their anti-aggregation properties correlate to mitigation of IAPP toxicity, however, can vary – resveratrol-stabilized IAPP oligomers were found toxic to β-cells *in vitro,*[225] whereas a reduction in cytotoxicity was reported for IAPP and other amyloidogenic peptides stabilized by the polyphenols 1,2,3,4,6-penta-O-galloyl-β-$_D$-glucose[226] and EGCG[227] respectively. Polyphenols have additionally been investigated for amyloid-remodelling properties: EGCG has been shown to cleave IAPP fibrils without

changing their morphology,[11] with remodelled species delegated off-pathway and so unable to refibrillate.[228] Bieschke *et al*. demonstrated that EGCG-mediated remodelling of Aβ and αSyn rendered them unable to reform fibrils, and conferred reduced cytotoxicity *in vitro.*[227]

The molecular promiscuity[229] and poor aqueous solubility of polyphenols, however, limit their direct application *in vivo* – consequently, polyphenolic compounds are frequently utilized as anti-amyloidosis agents in the context of a payload delivered by a carrier nanoparticle. For example, in an APPswe/PS1dE9 AD mouse model, EGCG loaded into polyethylene glycol (PEG)-functionalized poly(lactic-co-glycolic acid) (PLGA) NPs, ostensibly intended to target the brain, was able to cross the BBB when given orally to mice – but was additionally found present in every other organ. Furthermore, no specific pathway was shown to be employed by the EGCG-loaded NPs to cross the BBB. Regardless, treatment did result in significant amelioration of spatial learning and memory and other AD pathologies, including a notable rise in synapses and decreased neuroinflammation in addition to a reduced presence of Aβ(1-42) species and overall plaque load.[230] Synthesis of biocompatible, targeted nanostructures with analogous properties to small molecules, e.g. aromatic and tertiary hydroxyl groups, may present superior efficacy as anti-amyloidosis agents.

1.4.3 Metallic and semi-conducting nanomaterials

Metallic and semi-conducting NPs, including gold (AuNPs),[231] silver (AgNPs),[232] cadmium telluride (CdTe),[233] iron oxides (IONPs),[232] zinc oxides (ZnO NPs)[234] and ceria nanocrystals,[235] among others, have been widely applied in anti-amyloidosis treatment strategies. Gold nanoparticles (AuNPs), in particular, have been frequently exploited, given both their inert nature and their capacity to bind amyloid cysteines, potentiating their development as both inhibitors and indicators of amyloid aggregation.[231] For example, improved acquisition and retention of special learning and memory in addition to neural survival was observed in Aβ-treated mice after the application of citrate-coated AuNPs.[236] Zhang *et al.* examined the anti-amyloidosis capacity of AuNPs coated with a metal-phenolic network, comprising of tannic acid coordinated with various metal ions (Al^{3+}, Fe^{3+}, Co^{2+}, Ni^{2+}, Cu^{2+}, Zn^{2+}), and demonstrated that AuNPs coated with a cobalt-tannic acid network were most effective in inhibiting Aβ1-40 fibrillization *in vitro*, likely due to the specific geometry of the cobalt-tannic acid network favoring interactions with histidine and methionine residues in Aβ peptides.[237] Recently, AuNPs functionalized with sonicated β-sheet rich bLg amyloid acted as probes for fibrillating

IAPP, wherein dark-field microscopy visualized the T-cell mediated phagocytosis of AuNP-decorated fibrils through the intrinsic surface plasmon resonance (SPR) property of gold.[238] Similarly, quercetin-modified gold-palladium NPs promoted clearance of Aβ through inducing autophagy in SH-SY5Y cells.[239] Gladytz *et al.* have recently interfaced AuNPs with amyloid proteins, hypothesizing that the amyloid aggregation of IAPP and prion protein SUP35 hinged on a balance between peptide-nanoparticle and peptide-peptide interactions.[240] Specifically, anionic citrate-coated AuNPs intercalated with cationic IAPP through stronger Coulombic interactions, while PEG-coated AuNPs adsorbed onto IAPP fibrils via binding forces weaker than those involved in IAPP self-assembly.

Magnetic NPs (MNPs), such as superparamagnetic IONPs, NPs with a metallic core (i.e. nickel, zinc, cobalt) or magnetic doping agent (e.g. gadolinium; Gd), are effective T_2 contrast agents for magnetic resonance imaging (MRI).[241] The complexation of MNPs with a targeting motif can allow them to act as theranostics, for both the detection and mitigation of amyloidoses. Gd-based NPs grafted with the nanobody B10AP specifically targeted IAPP, Aβ and TTR amyloid deposits *ex vivo* in murine pancreas, brain and stomach tissue sections, respectively.[242] PEGylated superparamagnetic IONPs were conjugated with an oligomer-specific scFv antibody (W20) and, after intravenous injection into PD and HD mouse models, were demonstrated by MRI to be capable of targeting amyloid oligomers in the brain.[243] In separate studies, IONPs[222] and Gd-doped PLGA NPs with a curcumin cargo and cationic carrier peptide (K16ApoE)[244] were complexed with the plaque-binding antibody IgG4.1, and visualized through MRI to penetrate the BBB and localize to Aβ plaques in the murine cerebrovasculature. In the latter work, however, nonspecific immune reactions and meningoencephalitis were observed during human pre-clinical studies.[245] Bypassing extra-circulatory *in vivo* contact may present a more biocompatible route for anti-amyloidosis treatment: Kim and colleagues utilized an innovative 'magnetic dialysis' methodology to cleanse toxic Aβ species from the blood of 5XFAD mice.[246] Blood was first extracted from the femoral artery, and circulating Aβ species captured by magnetite/ceria NPs within in a closed system – subsequently, with the aid of a magnet and peristaltic pump, magnetite/ceria NPs with bound Aβ were sequestered, allowing 'cleansed' blood to return to the mouse via the jugular vein. Treated mice demonstrated decreased levels of circulating Aβ and additionally did not develop spatial working memory deficits.

Physiological metals are known to have key roles in both regular and dysfunctional cellular biology. Cysteines, for example, can complex with heavy metal ions – exploited in functional

amyloid-based biomaterials for wastewater purification and iron fortification[247-248] – and recent studies have demonstrated the potential for amyloids to act as pseudo-enzymes via the sequestration of metal ions,[249] potentially altering materials that interface with the amyloid surface. Polyoxometalates (POMs) have been demonstrated to effectively inhibit Aβ *in vitro*,[250-251] with POM-Dawson derivatives functionalized with histidine-chelating metals (Cu, Fe, Ni, Co, Mn) shown further capable of crossing the BBB in rodent models *in vivo*.[251] However, as metallic and metal oxide NPs have the capacity to release metal ions, several of which – notably, Fe^{3+}, Cu^{2+} and Zn^{2+} – are known to impact amyloidosis *in vivo*, further investigation is warranted to assess whether ion leakage may be exploited to combat amyloid-associated pathologies. A recent study demonstrated that, while IONPs stabilized by PEG and phosphorylcholine (PC) had little impact on IAPP fibrillization *in vitro*, Fe^{3+} ions strongly inhibited amyloid aggregation.[232] On the other hand, limiting ion release or leaching through particle surface coating can be beneficial: consider the case of zinc, where Zn^{2+} ions have been shown to promote formation of toxic oligomers during amyloidosis.[252] Utilizing hen's egg white lysozyme (HEWL) as the amyloid model, Ban & Paul demonstrated that ZnO NPs capped with starch induced less β-sheet formation and reduced amyloid-associated cytotoxicity *in vitro* comparative to bare NPs.[234] Consequently, amyloid aggregation inhibition achieved through concentration-dependent application of certain metallic or semi-conducting NPs may be induced through increased local ion concentration, rather than mediated by the surface properties of the particles themselves.

1.4.4 Carbon-based and inorganic nanomaterials

Carbon-based nanomaterials, comprised of infinitely repeating aromatic structures and including fullerenes,[253] graphene oxide (GO),[254-255] carbon nanotubes (CNTs)[256-257] and quantum dots (QDs),[258-259] have shown efficacy in sequestering amyloid species and reducing amyloid-associated cytotoxicity *in vitro*.[256] Surface functionalization of carbonaceous materials is generally required, however, to improve their biocompatibility and provide stable dispersion within the aqueous *in vivo* environment. Accordingly, aqueous solubility was conferred to fullerene derivatives via functionalization with phenylbutyric acid, aminocaproic acid and thiocarboxylic acid, with each construct demonstrating effective anti-amyloidosis properties and low acute toxicity in mouse models *in vivo*.[253] Concordantly, graphene or GO nanosheets can provide scaffolds for effective scavenging of toxic amyloid species[255] and/or surface functionalizations[260] to enhance anti-amyloidosis detection, targeting and delivery. For

example, He *et al.* interfaced fluorescently-tagged resveratrol with GO to create a FRET-based probe for effectively detecting Aβ amyloid species *in vitro,* towards a potential method to screen for AD.[260] Though not carbon-based, MoS_2 and WS_2 nanosheets are graphene-like in their physical structure, i.e. composed of vertically-stacked 2D layers: MoS_2 was able to modulate the aggregation of amyloidogenic Aβ33-42 and IAPP20-29 fragments,[261] while WS_2 scavenged Aβ1-40 monomers and permitted dissolution of bound aggregates upon near-infrared radiation.[262] The large size of these nanomaterials can, however, limit their practicality at the biological interface.

Recently, multi-walled CNTs functionalized with bLg amyloid fragments were able to form a bLg-IAPP double protein corona through H-bonding and hydrophobic interactions by sequestering toxic IAPP species pre-injected into zebrafish embryos, effectively neutralizing their pathogenicity.[257] Hybridization of carbon-based materials with amyloids even has applications outside the scope of nanomedicine and into biotechnology, e.g. for developing conductive nanowires[256] and the selective removal of fluoride from contaminated waterways.[263] CNTs require careful design and functionalization to be effective at the biological interface, however, given the capacity for longer, rigid structures (i.e. with a high aspect ratio) to induce 'frustrated phagocytosis' – thus pertaining to a long circulation lifetime – in addition to oxidative stress caused by the partitioning of CNTs through the lipid cell membrane.[264-265] Shorter, tangled CNTs may thus be more biocompatible, but, due to a smaller available surface area, likely pose less effective amyloid scavengers.

On the other hand, graphene QDs, due to their small size, good biocompatibility and intrinsic photoluminescent properties, provide promising candidates for the development of anti-amyloidosis biosensors. Huang and colleagues demonstrated that graphene QDs were able to track Aβ aggregation *in vitro*, providing an analogous kinetic profile to ThT for probing amyloid fibrillization.[266] Furthermore, nonfunctionalized graphene QDs were able to translocate across the BBB and induced the clearance of amyloid from αSyn-treated WT mice,[221] additionally mitigating IAPP-associated toxicity in zebrafish larvae *in vivo*.[259] However, given that the surface of carbon-based materials is highly fouling in lieu of stealth polymer functionalization,[256] consideration should be taken to protein corona formation when materials are introduced to the biological interface, and how it may impact their trafficking and behavior *in vivo*.

Given the left-handedness of most major amyloid species under physiological conditions,[267] chirality presents a novel mesoscopic target for anti-amyloidosis strategies. Direct chiral modulation of Aβ1-42 aggregation and associated *in vitro* cytotoxicity was demonstrated by enantiomeric carbon dots synthesized from L-lysine over those synthesized by D-lysine.[268] Accordingly, right-handed silica nanoribbons provided a nucleation site for IAPP, allowing fibrillization to occur perpendicularly to the ribbon axis, consequently rescuing zebrafish larvae from IAPP-associated toxicity.[269] In addition to nanoribbons, mesoporous silica NPs (MSNs) are well-established as vehicles for drug delivery in nanomedicine, and have recently been explored for their capacity to mitigate amyloidosis.[270] For example, defect-related luminescent MSNs, surface-modified by chitosan and conjugated to the small peptide NF(NMe)GA(N-Me)IL, inhibited IAPP fibrillization and associated generation of ROS, further demonstrating intervention of this nanocomposite stabilized the mitochondrial membrane potential in INS-1 cells *in vitro*.[271]

1.4.5 Biomimetic nanomaterials

The utilization of nanostructures either directly constructed of or synthetically mimicking native biomolecular components can ensure robust biocompatibility and low immunogenicity, thus allowing safe passage of so-called 'biomimetic' nanomaterials through complex biological milieu. Chitosan NPs, derived from the degradation of crustacean chitin shells, were conjugated with the peptide KLVFF via a PEG cross-linker, with a Beclin-1 protein also attached to induce autophagy.[272] KLVFF, a 'β-sheet breaker' derived from Aβ1-42, selectively targeted Aβ plaques in APPswe/PS1dE9 mice via H-bonding between NP-bound KVLFF and the twin sequence inherent in Aβ aggregates. The NP-amyloid complex was then effectively endocytosed and degraded through the ALS, resulting in the clearance of approximately 59% of insoluble and 32% of soluble Aβ *in vivo,* respectively, and restored memory deficits within the mice. Mirror image phage display identified two peptides, TGNYKALHPHNG (TGN) and QSHYRHISPAQV (QSH), predicted to target the BBB and Aβ fibrils. Conjugation of the peptides to PEGylated polylactic acid NPs resulted in concentration of the NPs at Aβ plaques in the hippocampus after intravenous injection into Aβ-treated nude adult mice.[273] Mitigation of AD-associated behavioral and memory deficits, however, was not assessed in this approach.

HSA nanoparticles were used to encapsulate and deliver the drug andrographolide, derived from the Asian medicinal plant *Andrographis paniculate,* across the BBB to target Aβ plaques

in the brain of TgCRND8 mice. Though this approach did not succeed in counteracting Aβ aggregation and toxicity, significantly reduced oxidative stress levels were reported in treated mice.[274] Ma and colleagues developed a xenograft mouse model of immunoglobulin light-chain amyloidosis (LC), and, selecting 306-O18B3 lipidoid nanoparticles as model candidates for anti-LC gene therapy, they demonstrated that NP-encapsulated siRNA targeting κ LC constant region-encoding mRNA was capable of reducing circulating LC in the mice after 8 days of daily injections.[275] Lastly, bridging the gap between lipid and protein, apolipoprotein E3 (ApoE3) and high-density lipoproteins (HDLs) were complexed to generate biomimetic 'nanodiscs'. These nanodiscs demonstrated stealth properties upon intravenous administration into Aβ-treated WT mice, avoiding the accumulation of a protein corona within the plasma and cerebrospinal fluid as they crossed the BBB via ApoE3 specific receptors, and specifically targeted low order Aβ species, subsequently promoting clearance of Aβ from astrocytes and microglial cells.[276]

1.4.6 Polymeric nanomaterials

Polymeric NPs have facilely tuneable structures, allowing the generation of NPs with a diverse range of properties. Given the propensity for cationic nanomaterials to undergo protein fouling and inflict membrane damage, anionic or neutrally charged polymeric materials may prove superior agents for combating amyloidosis. For example, Aso and colleagues functionalized poly(propylene imine) core dendrimers with a maltose-histidine shell, neutralizing the positive charge of the amino groups and subsequently demonstrating improved biocompatibility and BBB penetration in APP/PS1 mice, in addition to mediating neuroprotectivity against AD pathologies.[277] Tuning the hydrophobicity of polymeric NPs is also necessary to both (1) promote hydrophobic interactions of the NP with the amyloidogenic region of aggregating species while (2) allowing effective dispersion of the NPs in aqueous solution, as posited by Evgrafova and colleagues, who demonstrated that inhibition of Aβ1-40 was best achieved through balancing the hydrophobic and hydrophilic properties of polymeric anti-amyloidosis candidates.[278]

Though several types of polymeric NPs have been investigated as for the inhibition of amyloidogenic peptides,[277-282] a paucity of data exists for IAPP. Poly-ε-caprolactone NPs were designed with an IAPP cargo towards an *in vivo* system of controlled IAPP release, allowing the endogenous functions of IAPP to be performed while maintaining its localized concentration below the aggregation threshold, and were able to regulate glycemia in fasting mice over 36 h.[283] As IAPP aggregation-inhibition agents, hydrophobic, neutrally charged NiPAM:BAM co-polymers have shown some efficacy in inhibiting IAPP fibrillization,[284] and OH-terminated polyamidoamine (PAMAM-OH) dendrimers were recently shown to interact with IAPP within the amyloidogenic region, preventing IAPP fibrillization through amyloid contact and mitigating cytotoxicity *in vitro* and in mouse islets.[285] Interestingly, some neutral polymers have been shown to promote amyloid aggregation, particularly at higher concentrations, likely due to molecular crowding – recently, for example, PEG 12 polymer was shown to promote fibrillization of αSyn, increasing with increasing concentration of PEG in solution.[280] The promotion of amyloid aggregation, however, is not necessarily correlated with increased cytotoxicity – through reducing the lifetime of toxic oligomeric species via their

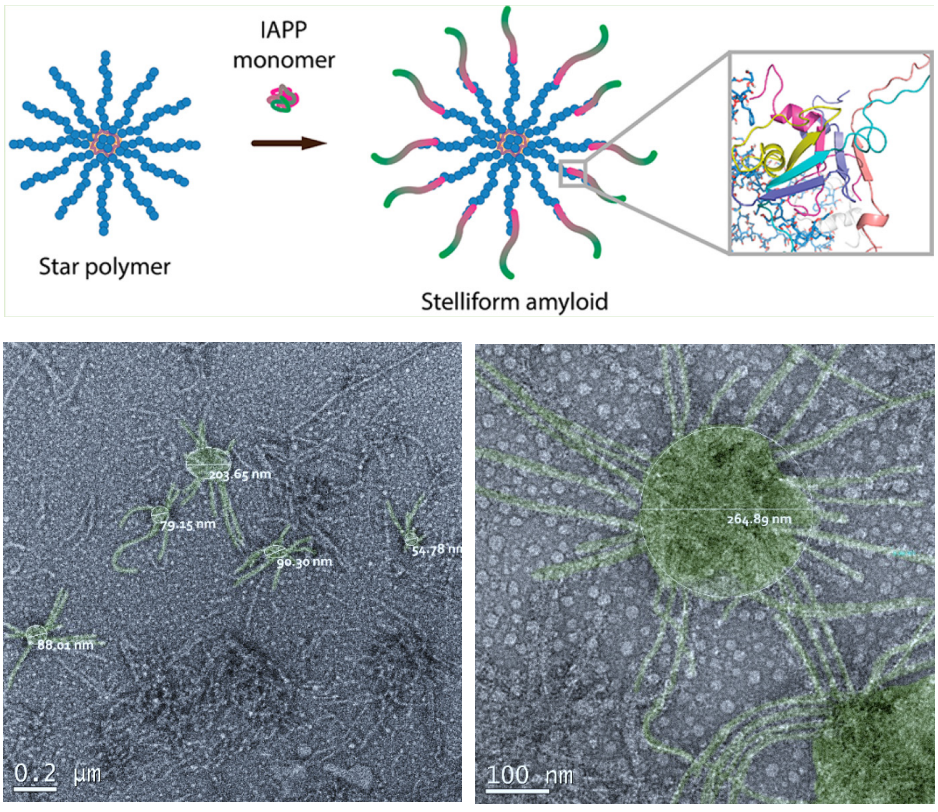

Figure 10: Star polymers sequester IAPP and provide a scaffold to promote fibrillization, generating 'stelliform' amyloids. Top panel: simplified cartoon scheme of poly (2-hydroxyl ethyl acrylate) stars interacting with IAPP monomers. Bottom panel: TEM imagery of stelliform amyloids, as nanostructures with compact cores and radiating fibrils, highlighted in green with the diameter of the core indicated. Upper panel reproduced with permission from Pilkington *et al.* 2017.[290]

conversion to fibrils, a net reduction in amyloid-associated toxicity may be observed, and could provide an alternative treatment strategy for amyloidosis. Accordingly, anionic sulfated dendrimers prevented IAPP-associated cytotoxicity in β-cells *in vitro*, with dendrimer-mediated modulation of the amyloid pathway dependent on dendrimer morphology: G0 dendrimers were shown to inhibit amyloidogenesis, whereas G1 dendrimers enhanced it, through providing a scaffold that promoted IAPP amyloid contact and aggregation.[286]

Despite the potential of dendrimers as effective anti-amyloidosis agents, their synthesis is expensive and labour intensive, limiting their practical application in IAPP research. Hyperbranched and star polymers, on the other hand, lack the cost and difficulty of synthesis of dendrimers and other polymeric species, yet are capable of analogous structural complexity, potentiating their development as treatment agents for amyloid-associated pathologies. For example, a hyperbranched PEG polymer containing a dopamine moiety was effective in inhibiting the fibrillization of αSyn *in vitro.*[280] Star polymers have historically been utilized for engineering and materials science applications, while their usage in a biological context is relatively new[287] – a frequent application within the scope of nanomedicine being the delivery of interference RNA for anti-cancer purposes[288] and for diabetic-related wound healing[289] *in vivo*. In pancreatic β-cells *in vitro*, and additionally *ex vivo* in mouse islets, poly (2-hydroxyl ethyl acrylate) star polymers were shown to accelerate IAPP fibrillization through formation of a polymer-IAPP 'stelliform amyloid' complex (**Fig. 10**), resulting in a significant reduction of IAPP-mediated cytotoxicity.[290] This reflects the aforementioned rapid fibrillization kinetics of pmel17 in melanogenesis, as an endogenous mechanism to reduce the lifetime of toxic intermediate species.[34] Thus, the development of hyperbranched and star polymers with aromatic or hydroxyl terminal moieties as novel anti-IAPP agents may provide an effective approach for mitigating the toxic effect of IAPP in T2D.

1.5 State-of-the-art and current paradigms in amyloid science

1.5.1 State-of-the-art in amyloid technologies and anti-amyloidosis strategy

Amyloid science represents a diverse field, and encapsulates not only the interrogation of amyloid pathologies, but additionally harnessing amyloids for use in engineering and nanotechnology beyond the scope of associated disease – namely, taking the pathological and rendering it functional. Reches & Gazit pioneered the use of modified amyloidogenic peptides as scaffolding for nanomaterial production, utilizing Aβ-diphenylalanine ultrashort peptides

assembled into nanotubes to internally cast silver nanowires, subsequently 'breaking' the cast via enzymatic digestion and revealing discrete nanowires with long persistence length.[14] Fifteen years later, Jain *et al.* fibrillized ultrashort dipeptides into an amyloid-like hydrogel which was utilized as a staging area for the synthesis of rectangular platonic gold nanoparticles, attaining size control through tuning pH.[291] *Bacillus subtilis* biofilms generated through tunable TasA amyloid fibrillization can be 3D printed into diverse shapes for a wide variety of applications in biomedicine;[292] similarly, fibrillization under certain conditions allows αSyn to form flat sheets that may have potential in biosensing.[293] Amyloid oligomers have even been exploited as NPs to target macrophages.[294] With regards to IAPP, a synthetic nanovaccine for Chikungunya fever was generated by merging the amyloidogenic region (20-29) of IAPP with an 18mer antigenic sequence from a glycoprotein exposed on the Chikungunya viral envelope. The fibrillization of the synthetic nanovaccine, facilitated by IAPP20-29, provided superior surface area for IgG response and macrophage uptake in immunized mice.[295] Increased manipulation of the intrinsic properties of amyloid species comes hand in hand with new insight into fundamental aspects of their fibrillogenesis and toxic states, towards understanding and combating amyloid pathologies.

Within the biomedical context of amyloid science, a theory recently gaining traction is that bacteria may contribute to the development and/or pathologies of a number of amyloid-associated diseases.[296] Of particular interest is how bacterial infection and the microbiota contribute to AD development,[297] but these could also have implications in T2D.[298-299] The capacity for bacterial toxins to interface with neurodegenerative disorder was recently illustrated through the delivery of superparamagnetic IONPs and thioflavin S – neither capable of crossing the BBB under normal circumstances – to Aβ plaques within the brain of mouse models, as facilitated by their complexation with the toxin lipopolysaccharide (LPS).[300] LPS was able to induce inflammation at the BBB of 5XFAD mice, consequently allowing uptake of the Aβ-targeting materials – however, this effect was only seen in ageing mice, not in young or wild-type mice, potentiating that the BBB in older models is more susceptible to leakiness upon inflammation. Accordingly, systemic inflammation induced by LPS also impacted the health of older models: highlighting both the risk of the approach and the implications of the role of bacteria in neurodegenerative disease. Anti-amyloidosis, on the other hand, may offer new solutions to multi-drug resistance (MDR), a paramount challenge for modern medicine due to the antibiotic-focused global pharmaceutical industry.

CRISPR-Cas9 presents a new frontier for a wide range of gene therapy applications, and has found recent application in the field of amyloid science. Sun *et al.* demonstrated that β-cleavage of APP to generate toxic Aβ species can be redirected to neuroprotective α-cleavage through the editing of APP at the extreme C-terminus, and that this methodology is well-tolerated in human iPSC-derived neuronal cells and *in vivo* within mouse models. CRISPR-Cas9 amphiphilic nanocomplexes were further utilized by Park and colleagues to target β-secretase 1 (*Bace1*), an enzyme required for the production of Aβ peptides through APP cleavage. This approach was able to rescue AD pathologies in two mouse models (5XFAD and *App* knock-in mice) of AD.[301] Harnessing nanotechnology to target the source of protein aggregation rather than the outcome could be highly effective in ameliorating the pathologies of amyloid diseases, particularly for mutation-induced amyloidoses.[43]

Overall, the development and application of novel and innovative anti-amyloidosis agents, from molecular tweezers[302] to plasmon-activated water,[303] generates a broad catalogue of treatment strategies to potentially bring to the market. Exploiting the propensity for amyloids to sequester other amyloid species and co-fibrillate presents such a venture: from prion-functionalized AuNPs[304] and Aβ1-40 tethered to MNPs[305] for Aβ-sensing, to protein-capped NPs against tau,[306] and recent work with inexpensive, biocompatible bLg amyloid fragments absorbed to NPs that, when administered to the circulation of zebrafish, crossed the BBB to sequester Aβ in the brain and mitigate its toxicity.[307] Further utilizing the promotion of amyloid protein fibrillization to combat its associated toxicity could provide a new treatment strategy for amyloid-associated pathologies, particularly for IAPP. Though the application of NPs to deliberately enhance amyloid aggregation in order to decrease toxic oligomer lifetime has been explored for Aβ,[223, 308-309] anti-amyloidosis candidate design has trended overarchingly towards inhibition strategies for IAPP. This strategy was applied successfully via the application of poly (2-hydroxyl ethyl acrylate) star polymers to promote IAPP fibrillization, wherein the formation of polymer-IAPP complexes mitigated IAPP-associated cytotoxicity in pancreatic β-cells and mouse islets.[290] Biocompatible polymeric nanostructures with facile synthesis therefore represent an understudied class of nanomaterials with potential development as effective agents against IAPP pathologies in T2D.

1.5.2 Prevailing issues and future directions in amyloid science

As of 2016, 51 FDA-approved medicinal NPs and 77 NP products were in clinical trials for a wide range of applications,[310] yet decades of research has produced only one candidate against amyloid disease to clear the clinic and seek FDA approval to enter the market.[311] Overarchingly, efforts to develop anti-amyloidosis technologies are likely stymied by two key issues: a lack of fundamental knowledge of how amyloid species and NPs interact with each other and the surrounding milieu at the biological interface, and, furthermore, a lack of appropriate models for the interrogation of these conditions at pre-clinical stages.

Firstly, in light of recent failures of antibody-based strategies to promote the clearance of amyloid species in clinical trials,[312] it was hypothesized that the amyloid surface may prove highly heterogeneous and thus difficult to specifically target due to obfuscation by circulating proteins. Indeed, the first investigations into the amyloid-protein corona[191, 204] revealed that amyloid species form a nonuniform, viscoelastic corona capable of remodeling mature fibrils, and that proteins absorbed to the amyloid surface have roles in a number of key metabolic and biological functions. These insights were supported by proteomic profiling of *in vivo* plaques,[210] and provide new implications for the endogenous state of mature amyloid fibrils and plaques within different areas of the body, in addition to how enriched proteins may influence the biological processes of the local environment. Consequently, further characterization of amyloid plaques in different microenvironments could provide novel targeting strategies for anti-amyloidosis treatment agents.

Autosomal dominant mutations in APP, PSEN1 or PSEN2 are causative of early onset familial AD (FAD), and represent < 1% of AD cases – yet these mutated forms of APP and PS1 are expressed in all major transgenic rodent models of AD.[220] Similarly, in rodent models transgenic for human IAPP, multiple copies of the transgene can be expressed – in one case, up to 74 copies were recorded[313] – with the IAPP gene promoter found 2-5× more responsive to glucose challenge than under endogenous conditions, causing artificial overexpression of IAPP.[314-315] 3D cultures, including spheroids and organoids, represent an alternative to the use of animal models. Recently, Choi and coworkers developed a human neural stem cell 3D model of FAD supported by a gel matrix, demonstrating that the bioengineered tissue deposited Aβ into the gel, with plaques forming after 5-6 weeks.[218] Remarkably, tau neurofibrillary tangles were also observed a week later, representative of clinical pathologies in human AD yet never replicated in animal models of the disease. Low volume microfluidic platforms further reduce

waste while providing a highly controlled platform to investigate the behavior of amyloid species and NPs under flow. For example, a dynamic flow sandwich immunoassay utilizing antibody-conjugated AuNPs to detect captured protein within multi-channel microfluidic chips allowed detection of Aβ and tau at femtomolar levels.[216]

Ultimately, in order to attain successful translation of anti-amyloidosis agents from *in vitro* to *in vivo*, fundamental aspects of the nature and behavior of amyloid in complex biological environments must be elucidated. Providing a complex microenvironment that more accurately approximates human biology, while benefiting from the tight control of an *in vitro* platform, endogenous amyloid and/or NP interactions can be more effectively addressed.

1.6 Context of thesis

In this introduction, it has been established that elucidating the mechanics of IAPP amyloid aggregation and associated pathologies in their native context has, for decades, been obfuscated by the complexity of the biological milieu to which they are introduced post-secretion from pancreatic β-cells – from the pancreatic extracellular space to the circulation, and beyond, to pathologies in tissues and organs throughout the body that contribute to the symptomatic burden of T2D. Though oligomers have been cited as the key mediators of amyloid-associated cytotoxicity for other amyloids, this paradigm is still contested for IAPP. Moreover, the rapid fibrillization of IAPP has presented a challenge for the characterization of intermediate species, with morphologies described in theory but not in practice. Given, further, that fibrillating and mature IAPP amyloid interface with a complex extracellular environment – consisting of numerous circulating proteins and lipids – its impact on the structure and biological behavior of IAPP species has been found lacking. For example, the 'protein corona' described for synthetic nanomaterials interfacing with a biological environment had yet to be demonstrated for an endogenously generated, proteinaceous nanomaterial such as amyloid.

As a result of knowledge gaps regarding IAPP at the biological interface, numerous studies utilizing a wide variety of nanomaterials towards mitigating IAPP pathologies have not, at the time of writing, succeeded in clinical translation. The majority of anti-amyloid research utilizes inhibition of fibrillization as a strategy, with a 'fibrillization promotion' approach far less frequently employed. Considering the effective application of this strategy in nature through nontoxic melanogenesis, an approach utilizing a biocompatible polymeric nanostructure, e.g. a star polymer, designed with aromatic and hydroxyl moieties to effectively sequester IAPP

species and, additionally, acting to promote IAPP fibrillization, could present a new agent and a new strategy to be employed towards mitigating IAPP-mediated toxicity in T2D.

Concordantly, this thesis aims to bridge the gap between fundamental knowledge and practical application in the context of IAPP aggregation and associated cytotoxicity, through gaining deeper understanding of an understudied amyloidogenic peptide towards strategies to mitigate its pathologies. Herein, fundamental mechanisms and biological interactions of IAPP amyloidosis and associated pathway species are established, and this knowledge utilized to advise the design and application of an anti-amyloidosis agent. These paradigms are explored over three experimental chapters, as outlined in two key aims:

1. **Establish fundamental paradigms of IAPP species at the biological interface**
    a. Characterize the morphology and associated cytotoxicity of IAPP species *in vitro*
    b. Examine the modulation of IAPP fibrillization and biological behavior by the extracellular environment utilizing model proteins, lipids and ultrasmall membranes *in vitro*
    c. Explore the formation of an 'amyloid-protein corona' within a model complex biological milieu *in vitro*
2. **Explore a new strategy and agent for mitigation of IAPP-mediated cytotoxicity**
    a. Design and assess the efficacy of a star polymer to inhibit IAPP-mediated toxicity *in vitro* and *ex vivo*

The experimental section of this thesis is thus structured as follows: first, the fibrillization pathway of IAPP is interrogated and intermediate species characterized (**Chapter Two,** *Aim 1A*). Second, IAPP amyloid pathway species are explored at the *in vitro* biological interface: with regards to their cytotoxic impact on primary cells and their interactions with model proteins, lipids and ultrasmall membranes (**Chapter Two,** *Aim 1B*). The formation of the 'amyloid-protein corona' in a complex *in vitro* environment (*Aim 1C*) is then explored in-depth, through a biophysical and proteomics-based study published in *ACS Nano* (**Chapter Three**). Lastly, the novel synthesis of a poly (2-hydroxyl ethyl acrylate) 'PHEA' star polymer and its capacity to mitigate IAPP-mediated cytotoxicity in pancreatic β-cells *in vitro*, in addition to mouse islets *ex vivo (Aim 2),* is described in **Chapter Four**, as published in *Biomacromolecules*. Conclusions and future directions are finally summarized in **Chapter Five**.

1.7 References

(1) Hartl, F. U.; Bracher, A.; Hayer-Hartl, M., Molecular chaperones in protein folding and proteostasis. *Nature* **2011,** *475*, 324-332.

(2) Chiti, F.; Calamai, M.; Taddei, N.; Stefani, M.; Ramponi, G.; Dobson, C. M., Studies of the aggregation of mutant proteins *in vitro* provide insights into the genetics of amyloid diseases. *Proc. Natl. Acad. Sci. U.S.A.* **2002,** *99*, 16419-16426.

(3) Bartlett, A. I.; Radford, S. E., An expanding arsenal of experimental methods yields an explosion of insights into protein folding mechanisms. *Nat. Struc. Mol. Biol.* **2009,** *16*, 582-588.

(4) Knowles, T. P. J.; Vendruscolo, M.; Dobson, C. M., The amyloid state and its association with protein misfolding diseases. *Nat. Rev. Mol. Cell Biol.* **2014,** *15*, 384-396.

(5) Chiti, F.; Dobson, C. M., Protein Misfolding, Functional Amyloid, and Human Disease. *Annu. Rev. Biochem.* **2006,** *75*, 333-366.

(6) Kopito, R. R., Aggresomes, inclusion bodies and protein aggregation. *Trends Cell Biol.* **2000,** *10*, 524-530.

(7) Yoshimura, Y.; Lin, Y.; Yagi, H.; Lee, Y.-H.; Kitayama, H.; Sakurai, K.; Masatomo, S.; Ogi, H.; Naiki, H.; Goto, Y., Distinguishing crystal-like amyloid fibrils and glass-like amorphous aggregates from their kinetics of formation. *Proc. Natl. Acad. Sci. U.S.A.* **2012,** *109*, 14446-14451.

(8) Adamcik, J.; Mezzenga, R., Amyloid Polymorphism in the Protein Folding and Aggregation Energy Landscape. *Angew. Chem., Int. Ed. Engl.* **2018,** *57*, 8370-8382.

(9) Vetri, V.; Foderà, V., The route to protein aggregate superstructures: Particulates and amyloid-like spherulites. *FEBS Lett.* **2015,** *589*, 2448-2463.

(10) Dobson, C. M., Principles of protein folding, misfolding and aggregation. *Semin. Cell Dev. Biol.* **2004,** *15*, 3-16.

(11) Käkinen, A.; Adamcik, J.; Wang, B.; Ge, X.; Mezzenga, R.; Davis, T. P.; Ding, F.; Ke, P. C., Nanoscale inhibition of polymorphic and ambidextrous IAPP amyloid aggregation with small molecules. *Nano Res.* **2017,** *11*, 3636-3647.

(12) Sade, D.; Shaham-Niv, S.; Arnon, Z. A.; Tavassoly, O.; Gazit, E., Seeding of proteins into amyloid structures by metabolite assemblies may clarify certain unexplained epidemiological associations. *Open Biol.* **2018,** *8*, 170229.

(13) Sipe, J. D.; Benson, M. D.; Buxbaum, J. N.; Ikeda, S.-I.; Merlini, G.; Saraiva, M. J. M.; Westermark, P., Nomenclature 2014: Amyloid fibril proteins and clinical classification of the amyloidosis. *Amyloid* **2014,** *21*, 221-224.

(14) Reches, M.; Gazit, E., Casting metal nanowires within discrete self-assembled peptide nanotubes. *Science* **2003,** *300*, 625-627.

(15) Tamamis, P.; Adler-Abramovich, L.; Reches, M.; Marshall, K.; Sikorski, P.; Serpell, L.; Gazit, E.; Archontis, G., Self-Assembly of Phenylalanine Oligopeptides: Insights from Experiments and Simulations. *Biophys. J.* **2009,** *96*, 5020-5029.

(16) Adler-Abramovich, L.; Vaks, L.; Carny, O.; Trudler, D.; Magno, A.; Caflisch, A.; Frenkel, D.; Gazit, E., Phenylalanine assembly into toxic fibrils suggests amyloid etiology in phenylketonuria. *Nat. Chem. Biol.* **2012,** *8*, 701-706.

(17) Törnquist, M.; Michaels, T. C. T.; Sanagavarapu, K.; Yang, X.; Meisl, G.; Cohen, S. I. A.; Knowles, T. P. J.; Linse, S., Secondary nucleation in amyloid formation. *Chem. Commun.* **2018,** *54*, 8667-8684.

(18) van Diggelen, F.; Tepper, A. W. J. W.; Apetri, M. M.; Otzen, D. E., α-Synuclein Oligomers: A Study in Diversity. *Isr. J. Chem.* **2016,** *57*, 699-723.

(19) Walsh, D. M.; Selkoe, D. J., Aβ Oligomers - a decade of discovery. *J. Neurochem.* **2007,** *101*, 1172-1184.

(20) Bellomo, G.; Bologna, S.; Gonnelli, L.; Ravera, E.; Fragai, M.; Lelli, M.; Luchinat, C., Aggregation kinetics of the Aβ1–40 peptide monitored by NMR. *Chem. Commun.* **2018,** *54*, 7601-7604.

(21) Wördehoff, M. M.; Bannach, O.; Shaykhalishahi, H.; Kulawik, A.; Schiefer, S.; Willbold, D.; Hoyer, W.; Birkmann, E., Single Fibril Growth Kinetics of α-Synuclein. *J. Mol. Biol.* **2015,** *427*, 1428-1435.

(22) Pillay, K.; Govender, P., Amylin Uncovered: A Review on the Polypeptide Responsible for Type II Diabetes. *Biomed Res. Int.* **2013,** *2013*, 826706.

(23) Zraika, S.; Hull, R. L.; Verchere, C. B.; Clark, A.; Potter, K. J.; Fraser, P. E.; Kahn, S. E., Toxic oligomers and islet beta cell death: guilty by association or convicted by circumstantial evidence? *Diabetologia* **2010,** *53*, 1046-1056.

(24) Kumar, D. K. V.; Choi, S. H.; Washicosky, K. J.; Eimer, W. A.; Tucker, S.; Ghofrani, J.; Lefkowitz, A.; McColl, G.; Goldstein, L. E.; Tanzi, R. E.; Moir, R. D., Amyloid-β peptide protects against microbial infection in mouse and worm models of Alzheimer's disease. *Sci. Transl. Med.* **2016,** *8*, 340ra72.

(25) Moir, R. D.; Lathe, R.; Tanzi, R. E., The antimicrobial protection hypothesis of Alzheimer's disease. *Alzheimers Dement.* **2018,** *14*, 1602-1614.

(26) Jacob, R. S.; Das, S.; Singh, N.; Patel, K.; Datta, D.; Sen, S.; Maji, S. K., Amyloids Are Novel Cell-Adhesive Matrices. In *Biochemical and Biophysical Roles of Cell Surface Molecules*, Chattopadhyay, K.; Basu, S., Eds. Springer: Singapore, 2018.

(27) Blanco, L. P.; Evans, M. L.; Smith, D. R.; Badtke, M. P.; Chapman, M. R., Diversity, biogenesis and function of microbial amyloids. *Trends Microbiol.* **2012,** *20*, 66-73.

(28) Romero, D.; Kolter, R., Functional amyloids in bacteria. *Int. Microbiol.* **2014,** *17*, 65-73.

(29) Nakae, T.; Ishii, J.; Tokunaga, M., Subunit Structure of Functional Porin Oligomers That Form Permeability Channels in the Outer Membrane of *Escherichia coli*. *J. Biol. Chem.* **1978,** *254*, 1457-1461.

(30) Pyle, E.; Kalli, A. C.; Amillis, S.; Hall, Z.; Lau, A. M.; Hanyaloglu, A. C.; Diallinas, G.; Byrne, B.; Politis, A., Structural Lipids Enable the Formation of Functional Oligomers of the Eukaryotic Purine Symporter UapA. *Cell Chem. Biol.* **2018,** *25*, 840-848.

(31) Filipek, S.; Krzysko, K. A.; Fotiadis, D.; Liang, Y.; Saperstein, D. A.; Engel, A.; Palczewski, K., A concept for G protein activation by G protein-coupled receptor dimers: the transducin/rhodopsin interface. *Photochem. Photobiol. Sci.* **2004,** *3*, 628-638.

(32) Woodruff, J. B.; Hyman, A. A.; Boke, E., Organization and Function of Non-dynamic Biomolecular Condensates. *Trends Biochem. Sci.* **2018,** *43*, 81-94.

(33) Audas, T. E.; Audas, D. E.; Jacob, M. D.; Ho, J. J. D.; Khacho, M.; Wang, M.; Perera, J. K.; Gardiner, C.; Bennett, C. A.; Head, T.; Kryvenko, O. N.; Jorda, M.; Daunert, S.; Malhotra, A.; Trinkle-Mulcahy, L.; Gonzalgo, M. L.; Lee, S., Adaptation to Stressors by Systemic Protein Amyloidogenesis. *Dev. Cell* **2016,** *39*, 155-168.

(34) Fowler, D. M.; Koulov, A. V.; Alory-Jost, C.; Marks, M. S.; Balch, W. E.; Kelly, J. W., Functional Amyloid Formation within Mammalian Tissue. *PLoS Biol.* **2006,** *4*, 0100-0107.

(35) De Baets, G.; Van Doorn, L.; Rousseau, F.; Shymkowitz, J., Increased Aggregation Is More Frequently Associated to Human Disease-Associated Mutations Than to Neutral Polymorphisms. *PLoS Comput. Biol.* **2015,** *11*, e1004374.

(36) Xu, J.; Reumers, J.; Couceiro, J. R.; De Smet, F.; Gallardo, R.; Rudyak, S.; Cornelis, A.; Rozenski, J.; Zwolinska, A.; Marine, J.-C.; Lambrechts, D.; Suh, Y.-A.; Rousseau, F.; Schymkowitz, J., Gain of function of mutant p53 by coaggregation with multiple tumor suppressors. *Nat. Chem. Biol.* **2011,** *7*, 285-295.

(37) Jang, H. H., Regulation of Protein Degradation by Proteasomes in Cancer. *J. Cancer Prev.* **2018,** *23*, 153-161.

(38) Siekierska, A.; De Baets, G.; Reumers, J.; Gallardo, R.; Rudyak, S.; Broersen, K.; Couceiro, J.; Van Durme, J.; Schymkowitz, J.; Rousseau, F., α-Galactosidase Aggregation Is a Determinant of Pharmacological Chaperone Efficacy on Fabry Disease Mutants. *J. Biol. Chem.* **2012,** *287*, 28386-28397.

(39) Huang, C. C.; Faber, P. W.; Persichetti, F.; Mittal, V.; Vonsattel, J.-P.; MacDonald, M. E.; Gusella, J. F., Amyloid Formation by Mutant Huntingtin: Threshold, Progressivity and Recruitment of Normal Polyglutamine Proteins. *Somatic Cell Mol. Genet.* **1998,** *24*, 217-233.

(40) Lu, M.; Williamson, N.; Mishra, A.; Michel, C. H.; Kaminski, C. F.; Tunnacliffe, A.; Schierle, G. S. K., Structural progression of amyloid-β Arctic mutant aggregation in cells revealed by multiparametric imaging. *J. Biol. Chem.* **2018,** *294*, 1478-1487.

(41) Yoo, B. K.; Xiao, Y.; McElheny, D.; Ishii, Y., E22G Pathogenic Mutation of *β*-Amyloid (A*β*) Enhances Misfolding of A*β*40 by Unexpected Prion-like Cross Talk between A*β*42 and A*β*40. *J. Am. Chem. Soc.* **2018,** *140*, 2781-2784.

(42) Hatami, A.; Monjazeb, S.; Milton, S.; Glabe, C. G., Familial Alzheimer's Disease Mutations within the Amyloid Precursor Protein Alter the Aggregation and Conformation of the Amyloid-β Peptide. *J. Biol. Chem.* **2017,** *292*, 3172-3185.

(43) Li, Z.; Wang, C.; Wang, Z.; Zhu, C.; Li, J.; Sha, T.; Ma, L.; Gao, C.; Yang, Y.; Sun, Y.; Wang, J.; Sun, X.; Lu, C.; Difiglia, D.; Mei, Y.; Ding, C.; Luo, S.; Dang, Y.; Ding, Y.; Fei, Y.; Lu, B., Allele-selective lowering of mutant HTT protein by HTT–LC3 linker compounds. *Nature* **2019,** *575*, 203-209.

(44) Noble, W.; Hanger, D. P.; Miller, C. C. J.; Lovestone, S., The Importance of Tau Phosphorylation for Neurodegenerative Diseases. *Front. Neurol.* **2013,** *4*, 83.

(45) Rezaei-Ghaleh, N.; Amininasab, M.; Kumar, S.; Walter, J.; Zweckstetter, M., Phosphorylation modifies the molecular stability of β-amyloid deposits. *Nat. Commun.* **2016,** *7*, 11359.

(46) Kumar, S.; Walter, J., Phosphorylation of amyloid beta (Aβ) peptides - a trigger for formation of toxic aggregates in Alzheimer's disease. *Aging* **2011,** *3*, 803-812.

(47) Kumar, S.; Wirths, O.; Stüber, K.; Wunderlich, P.; Koch, P.; Theil, S.; Rezaei-Ghaleh, N.; Zweckstetter, M.; Bayer, T. A.; Brüstle, O.; Thal, D. R.; Walter, J., Phosphorylation of the amyloid β-peptide at Ser26 stabilizes oligomeric assembly and increases neurotoxicity. *Acta Neuropathol.* **2016,** *131*, 525-537.

(48) Guivernau, B.; Bonet, J.; Valls-Comamala, V.; Bosch-Morató, M.; Godoy, J. A.; Inestrosa, N. C.; Perálvarez-Martin, A.; Fernández-Busquets, X.; Andreu, D.; Oliva, B.; Muñoz, F. J., Amyloid-β Peptide Nitrotyrosination Stabilizes Oligomers and Enhances NMDAR-Mediated Toxicity. *J. Neurosci.* **2016,** *36*, 11693-11703.

(49) Ittner, A.; Chua, S. W.; Bertz, J.; Volkerling, A.; van der Hoven, J.; Gladbach, A.; Przybyla, M.; Bi, M.; van Hummel, A.; Stevens, C. H.; Ippati, S.; Suh, L. S.; Macmillan, A.; Sutherland, G.; Kril, J. J.; Silva, A. P. G.; Mackay, J. P.; Poljak, A.; Delerue, F.; Ke, Y. D.; Ittner, L. M., Site-specific phosphorylation of tau inhibits amyloid-β toxicity in Alzheimer's mice. *Science* **2016,** *354*, 904-908.

(50) Chen, L.; Wei, Y.; Wang, X.; He, R., Ribosylation Rapidly Induces α-Synuclein to Form Highly Cytotoxic Molten Globules of Advanced Glycation End Products. *PLoS ONE* **2010,** *5*, e9052.

(51) Chen, L.; Wei, Y.; Wang, X.; He, R., d-Ribosylated Tau forms globular aggregates with high cytotoxicity. *Cell. Mol. Life Sci.* **2009,** *66*, 2559-2571.

(52) Li, X.-H.; Du, L.-L.; Cheng, X.-S.; Jiang, X.; Zhang, Y.; Lv, B.-L.; Liu, R.; Wang, J.-Z.; Zhou, X.-W., Glycation exacerbates the neuronal toxicity of β-amyloid. *Cell Death Dis.* **2013,** *4*, e673.

(53) Haque, E.; Kamil, M.; Hasan, A.; Irfan, S.; Sheikh, S.; Khatoon, A.; Nazir, A.; Mir, S. S., Advanced Glycation End Products (AGEs), Protein Aggregation and their Crosstalk: New Insight in Tumorigenesis. *Glycobiology* **2019**, cwz073.

(54) Soldi, G.; Bemporad, F.; Torrassa, S.; Relini, A.; Ramazzotti, M.; Taddei, N.; Chiti, F., Amyloid Formation of a Protein in the Absence of Initial Unfolding and Destabilization of the Native State. *Biophys. J.* **2005,** *89*, 4234-4244.

(55) Serebryany, E.; Woodard, J. C.; Adkar, B. V.; Shabab, M.; King, J. A.; Shakhnovich, E. I., An Internal Disulfide Locks a Misfolded Aggregation-prone Intermediate in Cataract-linked Mutants of Human γD-Crystallin. *J. Biol. Chem.* **2016,** *291*, 19172-19183.

(56) Kuhn, D. M.; Sykes, C. E.; Geddes, T. J.; Jaunarajs, K. L. E.; Bishop, C., Tryptophan hydroxylase 2 aggregates through disulfide cross-linking upon oxidation: possible link to serotonin deficits and non-motor symptoms in Parkinson's disease. *J. Neurochem.* **2011,** *116*, 426-437.

(57) Bolisetty, S.; Harnau, L.; Jung, J.; Mezzenga, R., Gelation, Phase Behavior, and Dynamics of *β*-Lactoglobulin Amyloid Fibrils at Varying Concentrations and Ionic Strengths. *Biomacromolecules* **2012,** *13*, 3241-3252.

(58) Ghavami, M.; Rezaei, M.; Ejtehadi, R.; Lofti, M.; Shokrgozar, M. A.; Emamy, B. A.; Raush, J.; Mahmoudi, M., Physiological Temperature Has a Crucial Role in Amyloid Beta in the Absence and Presence of Hydrophobic and Hydrophilic Nanoparticles. *ACS Chem. Neurosci.* **2013,** *4*, 375-378.

(59) McGlinchey, R. P.; Shewmaker, F.; McPhie, P.; Monterroso, B.; Thurber, K.; Wickner, R. B., The repeat domain of the melanosome fibril protein Pmel17 forms the amyloid core promoting melanin synthesis. *Proc. Natl. Acad. Sci. U.S.A.* **2009,** *106*, 13731-13736.

(60) Zimmerman, S. B.; Trach, S. O., Estimation of macromolecule concentrations and excluded volume effects for the cytoplasm of *Escherichia coli*. *J. Mol. Biol.* **1991,** *222*, 599-620.

(61) Uversky, V. N.; Cooper, M. E.; Bower, K. S.; Li, J.; Fink, A. L., Accelerated α-synuclein fibrillation in crowded milieu. *FEBS Lett.* **2002,** *515*, 99-103.

(62) Shtilerman, M. D.; Ding, T. D.; Lansbury, P. T., Molecular Crowding Accelerates Fibrillization of α-Synuclein: Could an Increase in the Cytoplasmic Protein Concentration Induce Parkinson's Disease? *Biochemistry* **2002,** *41*, 3855-3860.

(63) Hatters, D. M.; Minton, A. P.; Howlett, G. J., Macromolecular Crowding Accelerates Amyloid Formation by Human Apolipoprotein C-II. *J. Biol. Chem.* **2002,** *277*, 7824-7830.

(64) Viles, J. H., Metal ions and amyloid fiber formation in neurodegenerative diseases. Copper, zinc and iron in Alzheimer's, Parkinson's and prion diseases. *Coord. Chem. Rev.* **2012,** *256*, 2271-2284.

(65) Dong, X.; Svantesson, T.; Sholts, S. B.; Wallin, C.; Jarvet, J.; Gräslund, A.; Wärmländer, S. K. T. S., Copper ions induce dityrosine-linked dimers in human but not in murine islet amyloid polypeptide (IAPP/amylin). *Biochem. Biophys. Res. Communs.* **2019,** *510*, 520-524.

(66) Smith, D. P.; Ciccotosto, G. D.; Tew, D. J.; Fodero-Tavoletti, M. T.; Johanssen, T.; Masters, C. L.; Barnham, K. J.; Cappai, R., Concentration Dependent Cu^{2+} Induced Aggregation and Dityrosine Formation of the Alzheimer's Disease Amyloid-β Peptide. *Biochemistry* **2007,** *46*, 2881-2891.

(67) Zhao, J.; Gao, W.; Yang, Z.; Li, H.; Gao, Z., Nitration of amyloid-β peptide (1–42) as a protective mechanism for the amyloid-β peptide (1–42) against copper ion toxicity. *J. Inorg. Biochem.* **2019,** *190*, 15-23.

(68) Govers, S. K.; Mortier, J.; Adam, A.; Aertsen, A., Protein aggregates encode epigenetic memory of stressful encounters in individual *Escherichia coli* cells. *PLoS Biol.* **2018,** *16*, e2003853.

(69) Trigo, D.; Nadais, A.; da Cruz e Silva, O. A. B., Unravelling protein aggregation as an ageing related process or a neuropathological response. *Ageing Res. Rev.* **2019,** *51*, 67-77.

(70) Peters, T. W.; Rardin, M. J.; Czerwieniec, G.; Evani, U. S.; Reis-Rodrigues, P.; Lithgow, G. J.; Mooney, S. D.; Gibson, B. W.; Hughes, R. E., Tor1 regulates protein solubility in *Saccharomyces cerevisiae*. *Mol. Biol. Cell* **2012,** *23*, 4679-4688.

(71) Weids, A. J.; Ibstedt, S.; Tamás, M. J.; Grant, C. M., Distinct stress conditions result in aggregation of proteins with similar properties. *Sci. Rep.* **2016,** *6*, 24554.

(72) Gsponer, J.; Babu, M. M., Cellular Strategies for Regulating Functional and Nonfunctional Protein Aggregation. *Cell Reports* **2012,** *2*, 1425-1437.

(73) Rothe, S.; Prakash, A.; Tyedmers, J., The Insoluble Protein Deposit (IPOD) in Yeast. *Front. Mol. Neurosci.* **2018,** *11*, 237.

(74) Reumers, J.; Maurer-Stroh, S.; Schymkowitz, J.; Rousseau, F., Protein sequences encode safeguards against aggregation. *Hum. Mutat.* **2009,** *30*, 431-437.

(75) Rousseau, F.; Schymkowitz, J.; Serrano, L., Protein aggregation and amyloidosis: confusion of the kinds? *Curr. Opin. Struct. Biol.* **2006,** *16*, 118-126.

(76) Wang, X.; Zhou, Y.; Ren, J.-J.; Hammer, N. D.; Chapman, M. R., Gatekeeper residues in the major curlin subunit modulate bacterial amyloid fiber biogenesis. *Proc. Natl. Acad. Sci. U.S.A.* **2010,** *107*, 163-168.

(77) Aguilera, P.; Marcoleta, A.; Lobos-Ruiz, P.; Arranz, R.; Valpuesta, J. M.; Monasterio, O.; Lagos, R., Identification of Key Amino Acid Residues Modulating Intracellular and *In vitro* Microcin E492 Amyloid Formation. *Front. Microbiol.* **2016,** *7*, 35.

(78) Park, J.-S.; Kim, D.-H.; Yoon, S.-Y., Regulation of amyloid precursor protein processing by its KFERQ motif. *BMB Rep.* **2016,** *49*, 337-342.

(79) Vogiatzi, T.; Xilouri, M.; Vekrellis, K.; Stefanis, L., Wild Type α-Synuclein Is Degraded by Chaperone-mediated Autophagy and Macroautophagy in Neuronal Cells. *J. Biol. Chem.* **2008,** *283*, 23542-23556.

(80) Bauer, P. O.; Goswami, A.; Wong, H. K.; Kurosawa, M.; Yamada, M.; Miyazaki, H.; Matsumoto, G.; Kino, Y.; Nagai, Y.; Nukina, N., Harnessing chaperone-mediated autophagy for the selective degradation of mutant huntingtin protein. *Nat. Biotechnol.* **2010,** *28*, 256-263.

(81) Friedlich, A. L.; Tanzi, R. E.; Rogers, J. T., The 5'-untranslated region of Parkinson's disease α-synuclein messengerRNA contains a predicted iron responsive element. *Mol. Psychiatry* **2007,** *12*, 222-223.

(82) Rogers, J. T.; Randall, J. D.; Cahill, C. M.; Eder, P. S.; Huang, X.; Gunshin, H.; Leiter, L.; McPhee, J.; Sarang, S. S.; Utsuki, T.; Greig, N. H.; Lahiri, D. K.; Tanzi, R. E.; Bush, A. I.; Giordani, T.; Gullans, S. R., An iron-responsive element type II in the 5'-untranslated region of the Alzheimer's amyloid precursor protein transcript. *J. Biol. Chem.* **2002,** *277*, 45518-45528.

(83) Avramovich-Tirosh, Y.; Amit, T.; Bar-Am, O.; Weinreb, O.; Youdim, M. B. H., Physiological and pathological aspects of Abeta in iron homeostasis via 5'UTR in the APP mRNA and the therapeutic use of iron-chelators. *BMC Neurosci.* **2008,** *9 (Suppl 2)*, S2.

(84) Glickman, M. H.; Ciechanover, A., The Ubiquitin-Proteasome Proteolytic Pathway: Destruction for the Sake of Construction. *Physiol. Rev.* **2001,** *82*, 373-428.

(85) Dikic, I.; Elazar, Z., Mechanism and medical implications of mammalian autophagy. *Nat. Rev. Mol. Cell Biol.* **2018,** *19*, 349-364.

(86) De Baets, G.; Reumers, J.; Blanco, J. D.; Dopazo, J.; Schymkowitz, J.; Rousseau, F., An Evolutionary Trade-Off between Protein Turnover Rate and Protein Aggregation Favors a Higher Aggregation Propensity in Fast Degrading Proteins. *PLoS Comput. Biol.* **2011,** *7*, e1002090.

(87) Liberek, K.; Lewandowska, A.; Zietkiewicz, S., Chaperones in control of protein disaggregation. *EMBO J.* **2008,** *27*, 328-335.

(88) Auluck, P. K.; Chan, H. Y. E.; Trojanowski, J. Q.; Lee, V. M. Y.; Bonini, N. M., Chaperone Suppression of α-Synuclein Toxicity in a Drosophila Model for Parkinson's Disease. *Science* **2002,** *295*, 865-868.

(89) Hinault, M.-P.; Cuendet, A. F. H.; Mattoo, R. U. H.; Mensi, M.; Dietler, G.; Lashuel, H. A.; Goloubinoff, P., Stable α-Synuclein Oligomers Strongly Inhibit Chaperone Activity of the Hsp70 System by Weak Interactions with J-domain Co-chaperones. *J. Biol. Chem.* **2010,** *285*.

(90) Zhang, Y.-J.; Gendron, T. F.; Xu, Y.-F.; Ko, L.-W.; Yen, S.-H.; Petrucelli, L., Phosphorylation regulates proteasomal-mediated degradation and solubility of TAR DNA binding protein-43 C-terminal fragments. *Mol. Neurodegener.* **2010,** *5*, 33.

(91) Wang, Y.; Mandelkow, E., Degradation of tau protein by autophagy and proteasomal pathways. *Biochem. Soc. Trans.* **2012,** *40*, 644-652.

(92) Liu, J.; Li, L., Targeting Autophagy for the Treatment of Alzheimer's Disease: Challenges and Opportunities. *Front. Mol. Neurosci.* **2019,** *12*, 203.

(93) Hong, L.; Huang, H.-C.; Jiang, Z.-F., Relationship between amyloid-beta and the ubiquitin–proteasome system in Alzheimer's disease. *Neurol. Res.* **2014,** *36*, 276-282.

(94) Zhu, B.; Jiang, L.; Huang, T.; Zhao, Y.; Liu, T.; Li, X.; Campos, A.; Pomeroy, K.; Masliah, E.; Zhang, D.; Xu, H., ER-associated degradation regulates Alzheimer's amyloid pathology and memory function by modulating γ-secretase activity. *Nat. Commun.* **2017,** *8*, 1472.

(95) Sorrentino, V.; Romani, M.; Mouchiroud, L.; Beck, J. S.; Zhang, H.; D'Amico, D.; Moullan, N.; Potenza, F.; Schmid, A. W.; Rietsch, S.; Counts, S. E.; Auwerx, J., Enhancing mitochondrial proteostasis reduces amyloid-β proteotoxicity. *Nature* **2017,** *552*, 187-193.

(96) Mendis, S. *Global status report on noncommunicable diseases 2014*; World Health Organisation: Geneva, 2014.

(97) Guariguata, L.; Whiting, D. R.; Hambleton, I.; Beagley, J.; Linnenkamp, U.; Shaw, J. E., Global estimates of diabetes prevalence for 2013 and projections for 2035. *Diabetes Res. Clin. Pract.* **2014,** *103*, 137-149.

(98) Mathers, C. D.; Loncar, D., Projections of Global Mortality and Burden of Disease from 2002 to 2030. *PLoS Med.* **2006,** *3*, 2011-2030.

(99) Leahy, J. L., Pathogenesis of Type 2 Diabetes Mellitus. *Arch. Med. Res.* **2005,** *36*, 197-209.

(100) Kahn, S. E.; Zraika, S.; Utzschneider, K. M.; Hull, R. L., The beta cell lesion in type 2 diabetes: there has to be a primary functional abnormality. *Diabetologia* **2009,** *52*, 1003-1012.

(101) Park, Y. J.; Woo, M., Pancreatic β cells: Gatekeepers of type 2 diabetes. *J. Cell Biol.* **2019,** *218,* 1094.

(102) Kamata, K.; Mizukami, H.; Inaba, W.; Tsuboi, K.; Tateishi, Y.; Yoshida, T.; Yagihashi, S., Islet amyloid with macrophage migration correlates with augmented β-cell deficits in type 2 diabetic patients. *Amyloid* **2014,** *21*, 191-201.

(103) Jurgens, C. A.; Toukatly, M. N.; Fligner, C. L.; Udayasankar, J.; Subramanian, S. L.; Zraika, S.; Aston-Mourney, K.; Carr, D. B.; Westermark, P.; Westermark, G. T., β-Cell Loss and β-Cell Apoptosis in Human Type 2 Diabetes Are Related to Islet Amyloid Deposition. *Am. J. Pathol.* **2011,** *178*, 2632-2640.

(104) Lorenzo, A.; Razzaboni, B.; Weir, G. C.; Yankner, B. A., Pancreatic islet cell toxicity of amylin associated with type-2 diabetes mellitus. *Nature* **1994,** *368*, 756-760.

(105) Kayed, R.; Sokolov, Y.; Edmonds, B.; McIntire, T. M.; Milton, S. C.; Hall, J. E.; Glabe, C. G., Permeabilization of Lipid Bilayers Is a Common Conformation-dependent Activity of Soluble Amyloid Oligomers in Protein Misfolding Diseases. *J. Biol. Chem.* **2004,** *279*, 46363-46366.

(106) Meier, J. J.; Kayed, R.; Lin, C.-Y.; Gurlo, T.; Haataja, L.; Jajasinghe, S.; Langen, R.; Glabe, C. G.; Butler, P. C., Inhibition of human IAPP fibril formation does not prevent β-cell death: evidence for distinct actions of oligomers and fibrils of human IAPP. *Am. J. Physiol. Endocrinol. Metab.* **2006,** *291*, E1317-E1324.

(107) Ritzel, R. A.; Meier, J. J.; Lin, C.-Y.; Veldhuis, J. D.; Butler, P. C., Human Islet Amyloid Polypeptide Oligomers Disrupt Cell Coupling, Induce Apoptosis, and Impair Insulin Secretion in Isolated Human Islets. *Diabetes* **2007,** *56*, 65-71.

(108) Schubert, D.; Behl, C.; Lesley, R.; Brack, A.; Dargusch, R.; Sagara, Y.; Kimura, H., Amyloid peptides are toxic via a common oxidative mechanism. *Proc. Natl. Acad. Sci. U.S.A.* **1995,** *92*, 1989-1993.

(109) Scherbaum, W. A., The role of amylin in the physiology of glycemic control. *Exp. Clin. Endocrinol. Diabetes* **1998,** *106*, 97-102.

(110) Mietlick-Baase, E. G., Amylin-mediated control of glycemia, energy balance, and cognition. *Physiol. Behav.* **2016,** *162*, 130-140.

(111) Zhang, S.; Andreasen, M.; Nielson, J. T.; Liu, L.; Nielson, E. H.; Song, J.; Ji, G.; Sun, F.; Skrydstrup, T.; Besenbacher, F.; Nielson, N. C.; Otzen, D. E.; Dong, M., Coexistence of ribbon and helical fibrils originating from $hIAPP_{20-29}$ revealed by quantitative nanomechanical atomic force microscopy. *Proc. Natl. Acad. Sci. U.S.A.* **2013,** *110*, 2798-2803.

(112) Betsholtz, C.; Christmansson, L.; Engström, U.; Rorsman, F.; Svensson, V.; Johnson, K. H.; Westermark, P., Sequence divergence in a specific region of islet amyloid polypeptide (IAPP) explains differences in islet amyloid formation between species. *FEBS Lett.* **1989,** *251*, 261-264.

(113) Abedini, A.; Raleigh, D. P., The Role of His-18 in Amyloid Formation by Human Islet Amyloid Polypeptide. *Biochemistry* **2005,** *44*, 16284-16291.

(114) Kahn, S. E., The Importance of the β-Cell in the Pathogenesis of Type 2 Diabetes Mellitus. *Am. J. Med.* **2000,** *108*, 2S-8S.

(115) Westermark, P.; Andersson, A.; Westermark, G. T., Islet Amyloid Polypeptide, Islet Amyloid, and Diabetes Mellitus. *Physiol. Rev.* **2011,** *91*, 795-826.

(116) Moreno-Gonzalez, I.; Soto, C., Misfolded Protein Aggregates: Mechanisms, Structures and Potential for Disease Transmission. *Semin. Cell Dev. Biol.* **2011,** *22*, 482-487.

(117) Raleigh, D.; Zhang, X.; Hastoy, B.; Clark, A., The β-cell assassin: IAPP cytotoxicity. *J. Mol. Endocrinol.* **2017,** *59*, R121-R140.

(118) Hsu, Y.-H.; Chen, Y.-W.; Wu, M.-H.; Tu, L.-H., Protein Glycation by Glyoxal Promotes Amyloid Formation by Islet Amyloid Polypeptide. *Biophys. J.* **2019,** *116*, 2304-2313.

(119) Gong, W.; Liu, Z. H.; Zeng, C. H.; Peng, A.; Chen, H. P.; Zhou, H.; Li, L. S., Amylin deposition in the kidney of patients with diabetic nephropathy. *Kidney Int.* **2007,** *72*, 213-218.

(120) Abedini, A.; Cao, P.; Plesner, A.; He, M.; Derk, J.; Patil, S. A.; Rosario, R.; Lonier, J.; Song, F.; Koh, H.; Li, H.; Raleigh, D. P.; Schmidt, A. M., RAGE binds preamyloid IAPP intermediates and mediates pancreatic β cell proteotoxicity. *J. Clin. Invest.* **2018,** *128*, 682-698.

(121) Huang, C. J.; Haataja, L.; Gurlo, T.; Butler, A. E.; Wu, X.; Soeller, W. C.; Butler, P. C., Induction of endoplasmic reticulum stress-induced beta-cell apoptosis and accumulation of polyubiquitinated proteins by human islet amyloid polypeptide. *Am. J. Physiol. Endocrinol. Metab.* **2007,** *293*, E1656-E1662.

(122) Huang, C.-J.; Lin, C.-Y.; Haataja, L.; Gurlo, T.; Butler, A. E.; Rizza, R. A.; Butler, P. C., High Expression Rates of Human Islet Amyloid Polypeptide Induce Endoplasmic Reticulum Stress–Mediated β-Cell Apoptosis, a Characteristic of Humans With Type 2 but Not Type 1 Diabetes. *Diabetes* **2007,** *56*, 2016-2027.

(123) Casas, S.; Gomis, R.; Gribble, F. M.; Altirriba, J.; Knuutila, S.; Novials, A., Impairment of the Ubiquitin-Proteasome Pathway is a Downstream Endoplasmic Reticulum Stress Response Induced by

Extracellular Human Islet Amyloid Polypeptide and Contributes to Pancreatic β-cell Apoptosis. *Diabetes* **2007,** *56*, 2284-2294.

(124) Hernández, M. G.; Aguilar, A. G.; Burillo, J.; Oca, R. G.; Manca, A. M.; Novials, A.; Alcarraz-Vizan, G.; Guillén, C.; Benito, M., Pancreatic β cells overexpressing hIAPP impaired mitophagy and unbalanced mitochondrial dynamics. *Cell Death Dis.* **2018,** *9*, 481.

(125) Cadavez, L.; Montane, J.; Alzarraz-Vizán, G.; Visa, M.; Vidal-Fàbrega, L.; Servitja, M.; Novials, A., Chaperones Ameliorate Beta Cell Dysfunction Associated with Human Islet Amyloid Polypeptide Overexpression. *PLoS ONE* **2014,** *9*, e101797.

(126) Chien, V.; Aitken, J. F.; Zhang, S.; Buchanan, C. E.; Hickey, A.; Brittain, T.; Cooper, G. J.; Loomes, K. M., The chaperone proteins HSP70, HSP40/DnaJ and GRP78/BiP suppress misfolding and formation of β-sheet-containing aggregates by human amylin: a potential role for defective chaperone biology in Type 2 diabetes. *Biochem. J.* **2010,** *432*, 113-121.

(127) Hickey, A. J. R.; Bradley, J. W. I.; Skea, G. L.; Middleditch, M. J.; Buchanan, C. M.; Phillips, A. R. J.; Cooper, G. J. S., Proteins Associated with Immunopurified Granules from a Model Pancreatic Islet β-Cell System: Proteomic Snapshot of an Endocrine Secretory Granule. *J. Proteome Res.* **2009,** *8*, 178-186.

(128) Rosas, P. C.; Nagaraja, G. M.; Kaur, P.; Panossia, A.; Wickman, G.; Garcia, L. R.; Al-Khamis, F. A.; Asea, A. A. A., Hsp72 (HSPA1A) Prevents Human Islet Amyloid Polypeptide Aggregation and Toxicity: A New Approach for Type 2 Diabetes Treatment. *PLoS ONE* **2016,** *11*, e0149409.

(129) Bongiovanni, M. N.; Aprile, F. A.; Sormanni, P.; Vendruscolo, M., A Rationally Designed Hsp70 Variant Rescues the Aggregation-Associated Toxicity of Human IAPP in Cultured Pancreatic Islet β-Cells. *Int. J. Mol. Sci.* **2018,** *19*, 1443.

(130) Press, M.; Jung, T.; König, J.; Grune, T.; Höne, A., Protein aggregates and proteostasis in aging: Amylin and β-cell function. *Mech. Ageing Dev.* **2019,** *177*, 46-54.

(131) Badman, M. K.; Pryce, R. A.; Chargé, S. B. P.; Morris, J. F.; Clark, A., Fibrillar islet amyloid polypeptide (amylin) is internalised by macrophages but resists proteolytic degradation. *Cell Tissue Res.* **1998,** *291*, 285-294.

(132) Khemtémourian, L.; Doménech, E.; Doux, J. P. F.; Koorengevel, M. C.; Killian, J. A., Low pH Acts as Inhibitor of Membrane Damage Induced by Human Islet Amyloid Polypeptide. *J. Am. Chem. Soc.* **2011,** *133*, 15598-15604.

(133) Jaikaran, E. T. A. S.; Nilsson, M. R.; Clark, A., Pancreatic *β*-cell granule peptides form heteromolecular complexes which inhibit islet amyloid polypeptide fibril formation. *Biochem. J.* **2004,** *377*, 709-716.

(134) Larson, J. L.; Miranker, A. D., The Mechanism of Insulin Action on Islet Amyloid Polypeptide Fiber Formation. *J. Mol. Biol.* **2004,** *335*, 221-231.

(135) Westermark, P.; Li, Z.-C.; Westermark, G. T.; Leckström, A.; Steiner, D. F., Effects of beta cell granule components on human islet amyloid polypeptide fibril formation. *FEBS Lett.* **1996,** *379*, 203-206.

(136) DeToma, A. S.; Salamekh, S.; Ramamoorthy, A.; Lim, M. H., Misfolded Proteins in Alzheimer's Disease and Type II Diabetes. *Chem. Soc. Rev.* **2012,** *41*, 608-621.

(137) Chimienti, F.; Favier, A.; Seve, M., ZnT-8, a pancreatic beta-cell-specific zinc transporter. *BioMetals* **2005,** *18*, 313-317.

(138) Lemaire, K.; Ravier, M. A.; Schraenen, A.; Creemers, J. W. M.; Van de Plas, R.; Granvik, M.; Van Lommel, L.; Waelkens, E.; Chimienti, F.; Rutter, G. A.; in't Veld, P. A.; Schuit, F. C., Insulin crystallization depends on zinc transporter ZnT8 expression, but is not required for normal glucose homeostasis in mice. *Proc. Natl. Acad. Sci. U.S.A.* **2009,** *106*, 14872-14877.

(139) Ge, X.; Kakinen, A.; Gurzov, E. N.; Pang, L.; Pilkington, E. H.; Separovic, F.; Davis, T. P.; Ke, P. C.; Ding, F., Zinc-coordination and C-peptide complexation: a potential mechanism for the endogenous inhibition of IAPP aggregation. *Chem. Commun.* **2017,** *53*, 9394-9397.

(140) Sakagashira, S.; Hiddinga, H. J.; Tateishi, K.; Sanke, T.; Hanabusa, T.; Nanjo, K.; Eberhardt, N. L., S20G Mutant Amylin Exhibits Increased *in Vitro* Amyloidogenicity and Increased Intracellular Cytotoxicity Compared to Wild-Type Amylin. *Am. J. Pathol.* **2000,** *157*, 2101-2109.

(141) Seino, S.; Study Group of Comprehensive Analysis of Genetic Factors in Diabetes Mellitus, T., S20G mutation of the amylin gene is associated with Type II diabetes in Japanese. *Diabetologia* **2001,** *44*, 906-909.

(142) Borchi, E.; Bargelli, V.; Guidotti, V.; Berti, A.; Stefani, M.; Nediani, C.; Rigacci, S., Mild exposure of RIN-5F β-cells to human islet amyloid polypeptide aggregates upregulates antioxidant enzymes via NADPH oxidase-RAGE: An hormetic stimulus. *Redox Biol.* **2014,** *2*, 114-122.

(143) Kawahara, M.; Kuroda, Y.; Arispe, N.; Rojas, E., Alzheimer's β-Amyloid, Human Islet Amylin, and Prion Protein Fragment Evoke Intracellular Free Calcium Elevations by a Common Mechanism in a Hypothalamic GnRH Neuronal Cell Line. *J. Biol. Chem.* **2000,** *275*, 14077-14083.

(144) Mirzabekov, T. A.; Lin, M.-C.; Kagan, B. L., Pore Formation by the Cytotoxic Islet Amyloid Peptide Amylin. *J. Biol. Chem.* **1996,** *271*, 1988-1992.

(145) Sparr, E.; Engel, M. F. M.; Sakharov, D. V.; Sprong, M.; Jacobs, J.; de Kruijff, B.; Höppener, J. W. M.; Killian, J. A., Islet amyloid polypeptide-induced membrane leakage involves uptake of lipids by forming amyloid fibres. *FEBS Lett.* **2004,** *577*, 117-120.

(146) Engel, M. F. M.; Khemtémourian, L.; Kleijer, C. C.; Meeldijk, H. J. D.; Jacobs, J.; Verkleij, A. J.; de Kruijff, B.; Killian, J. A.; Höppener, J. W. M., Membrane damage by human islet amyloid polypeptide through fibril growth at the membrane. *Proc. Natl. Acad. Sci. U.S.A.* **2008,** *105*, 6033-6038.

(147) Owen, M. C.; Gnutt, D.; Gao, M.; Wärmländer, S. K. T. S.; Jarvet, J.; Gräslund, A.; Winter, R.; Ebbinghaus, S.; Strodel, B., Effects of *in vivo* conditions on amyloid aggregation. *Chem. Soc. Rev.* **2019,** *48,* 3946-3996.

(148) Meng, F.; Marek, P.; Potter, K. J.; Verchere, C. B.; Raleigh, D. P., Rifampicin Does Not Prevent Amyloid Fibril Formation by Human Islet Amyloid Polypeptide but Does Inhibit Thioflavin-T Interactions: Implications for Mechanistic Studies of *β*-cell Death. *Biochemistry* **2008,** *47*, 6016-6024.

(149) Glabe, C. G., Structural Classification of Toxic Amyloid Oligomers. *J. Biol. Chem.* **2008,** *283*, 29639-29643.

(150) Despa, S.; Margulies, K. B.; Chen, L.; Knowlton, A. A.; Havel, P. J.; Taegtmeyer, H.; Bers, D. M.; Despa, F., Hyperamylinemia Contributes to Cardiac Dysfunction in Obesity and Diabetes: A Study in Humans and Rats. *Circ. Res.* **2012,** *110*, 598-608.

(151) Srodulski, S.; Sharma, S.; Bachstetter, A. B.; Brelsford, J. M.; Pascual, C.; Xie, X. S.; Saatman, K. E.; Van Eldik, L. J.; Despa, F., Neuroinflammation and neurologic deficits in diabetes linked to brain accumulation of amylin. *Mol. Neurodegener.* **2014,** *9*.

(152) Jackson, K.; Barisone, G. A.; Diaz, E.; Jin, L.-W.; DeCarli, C.; Despa, F., Amylin Deposition in the Brain: A Second Amyloid in Alzheimer Disease? *Ann. Neurol.* **2013,** *74*, 517-526.

(153) Mäkimattila, S.; Fineman, M. S.; Yki-Järvinen, H., Deficiency of Total and Nonglycosylated Amylin in Plasma Characterizes Subjects with Impaired Glucose Tolerance and Type 2 Diabetes. *J. Clin. Endocrinol. Metab.* **2000,** *85*, 2822-2827.

(154) Sanke, T.; Hanabusa, T.; Nakano, Y.; Oki, C.; Okai, K.; Nishimura, S.; Kondo, M.; Nanjo, K., Plasma islet amyloid polypeptide (Amylin) levels and their responses to oral glucose in Type 2 (non-insulin-dependent) diabetic patients. *Diabetologia* **1991,** *34*, 129-132.

(155) Oskarsson, M. E.; Paulsson, J. F.; Schultz, S. W.; Ingelsson, M.; Westermark, P.; Westermark, G. T., *In Vivo* Seeding and Cross-Seeding of Localized Amyloidosis. *Am. J. Pathol.* **2015,** *185*, 834-846.

(156) Ferrier, G. J. M.; Pierson, A. M.; Bloom, S. R.; Girgis, S. I.; Legon, S., Expression of the rat amylin (IAPP/DAP) gene. *J. Mol. Endocrinol.* **1989,** *3*, R1-4.

(157) D'Este, L.; Wimalawansa, S. J.; Renda, T. G., Distribution of Amylin-Immunoreactive Neurons in the Monkey Hypothalamus and their Relationships with the Histaminergic System. *Arch. Histol. Cytol.* **2001,** *64*, 295-303.

(158) Liu, C.; Zhang, Y., Nucleic acid-mediated protein aggregation and assembly. *Adv. Protein Chem. Struct. Biol.* **2011,** *84*, 1-40.

(159) Gursky, O., *Lipids in Protein Misfolding*. Springer: Cham, Switzerland, 2015; Vol. 855.

(160) Grey, M.; Linse, S.; Nilsson, H.; Brundin, P.; Sparr, E., Membrane Interaction of α-Synuclein in Different Aggregation States. *J. Parkinsons Dis.* **2011,** *1*, 359-371.

(161) Kishimoto, T.; Soda, Y.; Matsuyama, Y.; Mizuno, K., An enzymatic assay for lysophosphatidylcholine concentration in human serum and plasma. *Clin. Biochemistry* **2002,** *35*, 411-416.

(162) Sheikh, A. M.; Nagai, A., Lysophosphatidylcholine modulates fibril formation of amyloid beta peptide. *FEBS J.* **2011,** *278*, 634-642.

(163) Sheikh, A. M.; Michikawa, M.; Kim, S. U.; Nagai, A., Lysophosphatidylcholine increases the neurotoxicity of Alzheimer's amyloid β1-42 peptide: Role of oligomer formation. *Neuroscience* **2015,** *292*, 159-169.

(164) Xing, Y.; Pilkington, E. H.; Wang, M.; Nowell, C. J.; Käkinen, A.; Sun, Y.; Wang, B.; Davis, T. P.; Ding, F.; Ke, P. C., Lysophosphatidylcholine modulates the aggregation of human islet amyloid polypeptide. *Phys. Chem. Chem. Phys.* **2017,** *19*, 30627-30635.

(165) Ponomarenko, E. A.; Poverennaya, E. V.; Ilgisonis, E. V.; Pyatnitskiy, M. A.; Kopylov, A. T.; Zgoda, V. G.; Lisitsa, A. V.; Archakov, A. I., The Size of the Human Proteome: The Width and Depth. *Int. J. Anal. Chem.* **2016,** *2016*, 7436849.

(166) Stanyon, H. F.; Viles, J. H., Human Serum Albumin Can Regulate Amyloid-β Peptide Fiber Growth in the Brain Interstitium. *J. Biol. Chem.* **2012,** *2012*, 28163-28168.

(167) Käkinen, A.; Javed, I.; Faridi, A.; Davis, T. P.; Ke, P. C., Serum albumin impedes the amyloid aggregation and hemolysis of human islet amyloid polypeptide and alpha synuclein. *Biochim. Biophys. Acta, Biomembranes* **2018,** *1860*, 1803-1809.

(168) Luo, J.; Wärmländer, S. K. T. S.; Gräslund, A.; Abrahams, J. P., Human lysozyme inhibits the *in vitro* aggregation of Aβ peptides, which *in vivo* are associated with Alzheimer's disease. *Chem. Commun.* **2013,** *49*, 6507-6509.

(169) Luo, J.; Wärmländer, S. K. T. S.; Gräslund, A.; Abrahams, J. P., Non-chaperone Proteins Can Inhibit Aggregation and Cytotoxicity of Alzheimer Amyloid *β* Peptide. *J. Biol. Chem.* **2014,** *289*, 27766-27775.

(170) Carrotta, R.; Canale, C.; Diaspro, A.; Trapani, A.; Biagio, P. L. S.; Bulone, D., Inhibiting effect of α(s1)-casein on Aβ(1-40) fibrillogenesis. *Biochim. Biophys. Acta* **2012,** *1820*, 124-132.

(171) Gustafsson, M.; Thyberg, J.; Näslund, J.; Eliasson, E.; Johansson, J., Amyloid fibril formation by pulmonary surfactant protein C. *FEBS Lett.* **1999,** *464*, 138-142.

(172) Peng, S.; Glennert, J.; Westermark, P., Medin-amyloid: A recently characterized age-associated arterial amyloid form affects mainly arteries in the upper part of the body. *Amyloid* **2005,** *12*, 96-102.

(173) Nerelius, C.; Gustafsson, M.; Nordling, K.; Larsson, A.; Johansson, J., Anti-Amyloid Activity of the C-Terminal Domain of proSP-C against Amyloid β-Peptide and Medin. *Biochemistry* **2009,** *48*, 3778-3786.

(174) Willander, H.; Presto, J.; Askarieh, G.; Biverstal, H.; Frohm, B.; Knight, S. D.; Johansson, J.; Linse, S., BRICHOS domains efficiently delay fibrillation of amyloid β-peptide. *J. Biol. Chem.* **2012,** *287*, 31608-31617.

(175) Peng, S.; Fitzen, M.; Jörnvall, H.; Johansson, J., The extracellular domain of Bri2 (ITM2B) binds the ABri peptide (1–23) and amyloid β-peptide (Aβ1–40): Implications for Bri2 effects on processing of amyloid precursor protein and Aβ aggregation. *Biochem. Biophys. Res. Commun.* **2010,** *393*, 356-361.

(176) Altieri, F.; Di Stadio, C. S.; Severino, V.; Sandomenico, A.; Minopoli, G.; Miselli, G.; Di Maro, A.; Ruvo, M.; Chambery, A.; Quagliariello, V.; Masullo, M.; Rippa, E.; Arcari, P., Anti-amyloidogenic property of human gastrokine 1. *Biochimie* **2014,** *106*, 91-100.

(177) Yerbury, J. J.; Kumita, J. R.; Meehan, S.; Dobson, C. M.; Wilson, M. R., α2-Macroglobulin and Haptoglobin Suppress Amyloid Formation by Interacting with Prefibrillar Protein Species. *J. Biol. Chem.* **2009,** *284*, 4246-4254.

(178) Raman, B.; Ban, T.; Sakai, M.; Pasta, S. Y.; Ramakrishna, T.; Naiki, H.; Goto, Y.; Rao, C. M., αB-crystallin, a small heat-shock protein, prevents the amyloid fibril growth of an amyloid β-peptide and β2-microglobulin. *Biochem. J.* **2005,** *392*, 573-581.

(179) Wilhelmus, M. M. M.; Boelens, W. C.; Otte-Höller, I.; Kamps, B.; de Waal, R. M. W.; Verbeek, M. M., Small heat shock proteins inhibit amyloid-β protein aggregation and cerebrovascular amyloid-β protein toxicity. *Brain Res.* **2006,** *1089*, 67-78.

(180) Cox, D.; Selig, E.; Griffin, M. D. W.; Carver, J. A.; Ecroyd, H., Small Heat-shock Proteins Prevent α-Synuclein Aggregation via Transient Interactions and Their Efficacy Is Affected by the Rate of Aggregation. *J. Biol. Chem.* **2016,** *291*, 22618-22629.

(181) Gao, M.; Estel, K.; Seeliger, J.; Friedrich, R. P.; Dogan, S.; Wanker, E. E.; Winter, R.; Ebbinghaus, S., Modulation of human IAPP fibrillation: cosolutes, crowders and chaperones. *Phys. Chem. Chem. Phys.* **2015,** *17*, 8338-8348.

(182) Westermark, P.; Skinner, M.; Cohen, A. S., The P-Component of Amyloid of Human Islets of Langerhans. *Scand. J. Immunol.* **1975,** *4*, 95-97.

(183) Chargé, S. B. P.; Esiri, M. M.; Bethune, C. A.; Hansen, B. C.; Clark, A., Apolipoprotein E is Associated With Islet Amyloid and Other Amyloidoses: Implications for Alzheimer's Disease. *J. Pathol.* **1996,** *179*, 443-447.

(184) Young, I. D.; Ailles, L.; Narindrasorasak, S.; Tan, R.; Kisilevsky, R., Localization of the basement membrane heparan sulfate proteoglycan in islet amyloid deposits in type II diabetes mellitus. *Arch. Pathol. Lab. Med.* **1992,** *116*, 951-954.

(185) Jha, S.; Patil, S. M.; Gibson, J.; Nelson, C. E.; Alder, N. N.; Alexandrescu, A. T., Mechanism of Amylin Fibrillization Enhancement by Heparin. *J. Biol. Chem.* **2011,** *286*, 22894-22904.

(186) Li, Y.; Wang, L.; Lu, T.; Wei, Y.; Li, F., The effects of chondroitin sulfate and serum albumin on the fibrillation of human islet amyloid polypeptide at the phospholipid membranes. *Phys. Chem. Chem. Phys.* **2016,** *18*, 12000-12008.

(187) Meng, F.; Abedini, A.; Song, B.; Raleigh, D. P., Amyloid Formation by Pro-Islet Amyloid Polypeptide Processing Intermediates: Examination of the Role of Protein Heparan Sulfate Interactions and Implications for Islet Amyloid Formation in Type 2 Diabetes. *Biochemistry* **2007,** *46*, 12091-12099.

(188) Peinado, J. R.; Sami, F.; Rajpurohit, N.; Lindberg, I., Blockade of islet amyloid polypeptide fibrillation and cytotoxicity by the secretory chaperones 7B2 and proSAAS. *FEBS Lett.* **2013,** *587*, 3406-3411.

(189) Oskarsson, M. E.; Singh, K.; Wang, J.; Vlodavsky, I.; Li, J.-P.; Westermark, G. T., Heparan Sulfate Proteoglycans are important for Islet Amyloid Formation and Islet Amyloid Polypeptide-Induced Apoptosis. *J. Biol. Chem.* **2015,** *290*, 15121-15132.

(190) Vidal, J.; Verchere, C. B.; Andrikopoulos, S.; Wang, F.; Hull, R. L.; Cnop, M.; Olin, K. L.; LeBoeuf, R. C.; O'Brien, K. D.; Chait, A.; Kahn, S. E., The effect of apolipoprotein E deficiency on islet amyloid deposition in human islet amyloid polypeptide transgenic mice. *Diabetologia* **2003,** *46*, 71-79.

(191) Pilkington, E. H.; Xing, Y.; Wang, B.; Käkinen, A.; Wang, M.; Davis, T. P.; Ding, F.; Ke, P. C., Effects of Protein Corona on IAPP Amyloid Aggregation, Fibril Remodelling, and Cytotoxicity. *Sci. Rep.* **2017,** *7*, 2455.

(192) Masliah, E.; Rockenstein, E.; Veinbergs, I.; Sagara, Y.; Mallory, M.; Hashimoto, M.; Mucke, L., β-Amyloid peptides enhance α-synuclein accumulation and neuronal deficits in a transgenic mouse model linking Alzheimer's disease and Parkinson's disease. *Proc. Natl. Acad. Sci. U.S.A.* **2001,** *98*, 12245-12250.

(193) Clinton, L. K.; Blurton-Jones, M.; Myczek, K.; Trojanowski, J. Q.; LaFerla, F. M., Synergistic Interactions between Aβ, Tau, and α-Synuclein: Acceleration of Neuropathology and Cognitive Decline. *J. Neurosci.* **2010,** *30*, 7281-7289.

(194) Andreetto, E.; Yan, L.-M.; Tatarek-Nossol, M.; Velkova, A.; Frank, R.; Kapurniotu, A., Identification of Hot Regions of the Aβ–IAPP Interaction Interface as High-Affinity Binding Sites in both Cross- and Self-Association. *Angew. Chem. Int. Ed., Engl.* **2010,** *49*, 3081-3085.

(195) O'Nuallain, B.; Williams, A. D.; Westermark, P.; Wetzel, R., Seeding Specificity in Amyloid Growth Induced by Heterologous Fibrils. *J. Biol. Chem.* **2004,** *279*, 17490-17499.

(196) Seeliger, J.; Weise, K.; Opitz, N.; Winter, R., The effect of Aβ on IAPP aggregation in the presence of an isolated β-cell membrane. *J. Mol. Biol.* **2012,** *421*, 348-363.

(197) Qiu, W. Q.; Wallack, M.; Dean, M.; Liebson, E.; Mwamburi, M.; Zhu, H., Association between Amylin and Amyloid-β Peptides in Plasma in the Context of Apolipoprotein E4 Allele. *PLoS ONE* **2014,** *9*, e88063.

(198) Cedervall, T.; Lynch, I.; Lindman, S.; Berggård, T.; Thulin, E.; Nilsson, H.; Dawson, K. A.; Linse, S., Understanding the nanoparticle-protein corona using methods to quantify exchange rates and affinities of proteins for nanoparticles. *Proc. Natl. Acad. Sci. U.S.A.* **2007,** *104*, 2050-2055.

(199) Ke, P. C.; Lin, S.; Parak, W. J.; Davis, T. P.; Caruso, F., A Decade of the Protein Corona. *ACS Nano* **2017,** *11*, 11773-11776.

(200) Ezzat, K.; Pernemalm, M.; Palsson, S.; Roberts, T. C.; Jarver, P.; Dondalska, A.; Bestas, B.; Sobkowiak, M. J.; Levanen, B.; Skold, M.; Thompson, E. A.; Saher, O.; Kari, O. K.; Lajunen, T.; Ekström, E. S.; Nilsson, C.; Ischenko, Y.; Malm, T.; Wood, M. J. A.; Power, U. F.; Masich, S.; Linden, A.; Sandberg, J. K.; Lehtio, J.; Spetz, A.-L.; Andaloussi, S. E. L., The viral protein corona directs viral pathogenesis and amyloid aggregation. *Nat. Commun.* **2018,** *10*, 2331.

(201) Serpooshan, V.; Mahmoudi, M.; Zhao, M.; Wei, K.; Sivanesan, S.; Motamedchaboki, K.; Malkovskiy, A. V.; Goldstone, A. B.; Cohen, J. E.; Yang, P. C.; Rajadas, J.; Bernstein, D.; Woo, Y. J.; Ruiz-Lozano, P., Protein Corona Influences Cell–Biomaterial Interactions in Nanostructured Tissue Engineering Scaffolds. *Adv. Funct. Mater.* **2015,** *25*, 4379-4389.

(202) Little, W. C.; Schwartlander, R.; Smith, M. L.; Gourdon, D.; Vogel, V., Stretched Extracellular Matrix Proteins Turn Fouling and Are Functionally Rescued by the Chaperones Albumin and Casein. *Nano Lett.* **2009,** *9*, 4158-4167.

(203) Rahman, M.; Zetterberg, H.; Lendel, C.; Härd, T., Binding of Human Proteins to Amyloid-β Protofibrils. *ACS Chem. Biol.* **2015,** *10*, 766-774.

(204) Pilkington, E. H.; Gustafsson, O. J. R.; Xing, Y.; Hernandez-Fernaud, J.; Zampronio, C.; Käkinen, A.; Faridi, A.; Ding, F.; Wilson, P.; Ke, P. C.; Davis, T. P., Profiling the Serum Protein Corona of Fibrillar Human Islet Amyloid Polypeptide. *ACS Nano* **2018,** *12*, 6066-6078.

(205) Yerbury, J. J.; Poon, S.; Meehan, S.; Thompson, B.; Kumita, J. R.; Dobson, C. M.; Wilson, M. R., The extracellular chaperone clusterin influences amyloid formation and toxicity by interacting with prefibrillar structures. *FASEB J.* **2007,** *21*, 2312-2322.

(206) Wojtas, A. M.; Kang, S. S.; Olley, B. M.; Gatherer, M.; Shinohara, M.; Loranzo, P. A.; Liu, C. C.; Kurti, A.; Baker, K. E.; Dickson, D. W.; Yue, M.; Petrucelli, L.; Bu, G.; Carare, R. O.; Fryer, J. D., Loss of clusterin shifts amyloid deposition to the cerebrovasculature via disruption of perivascular drainage pathways. *Proc. Natl. Acad. Sci. U.S.A.* **2017,** *114*, E6962-E6971.

(207) Sörgjerd, K. M.; Zako, T.; Sakono, M.; Stirling, P. C.; Leroux, M. R.; Saito, T.; Nilsson, P.; Sekimoto, M.; Saido, T. C.; Maeda, M., Human Prefoldin Inhibits Amyloid-β (Aβ) Fibrillation and Contributes to Formation of Nontoxic Aβ Aggregates. *Biochemistry* **2013,** *52*, 3532-3542.

(208) Mansson, C.; Arosio, P.; Hussein, R.; Kampinga, H. H.; Hashem, R. M.; Boelens, W. C.; Dobson, C. M.; Knowles, T. P. J.; Linse, S.; Emanuelsson, C., Interaction of the molecular chaperone DNAJB6 with growing amyloid-beta 42 (Aβ42) aggregates leads to sub-stoichiometric inhibition of amyloid formation. *J. Biol. Chem.* **2014,** *289*, 31066-31076.

(209) Arimon, M.; Grimminger, V.; Sanz, F.; Lashuel, H. A., Hsp104 Targets Multiple Intermediates on the Amyloid Pathway and Suppresses the Seeding Capacity of Aβ Fibrils and Protofibrils. *J. Mol. Biol.* **2008,** *384*, 1157-1173.

(210) Liao, L.; Cheng, D.; Wang, J.; Duong, D. M.; Losik, T. G.; Gearing, M.; Rees, H. D.; Lah, J. J.; Levey, A. I.; Peng, J., Proteomic Characterization of Postmortem Amyloid Plaques Isolated by Laser Capture Microdissection. *J. Biol. Chem.* **2004,** *279*, 37061-37068.

(211) Mi, W.; Pawlik, M.; Sastre, M.; Jung, S. S.; Radvinsky, D. S.; Klein, A. M.; Sommer, J.; Schmidt, S. D.; Nixon, R. A.; Mathews, P. M.; Levy, E., Cystatin C inhibits amyloid-β deposition in Alzheimer's disease mouse models. *Nat. Genet.* **2007,** *39*, 1440-1442.

(212) Foote, M.; Zhou, Y., 14-3-3 proteins in neurological disorders. *Int. J. Biochem. Mol. Biol.* **2012,** *3*, 152-164.

(213) Sadik, G.; Tanaka, T.; Kato, K.; Yamamori, H.; Nessa, B. N.; Morihara, T.; Takeda, M., Phosphorylation of tau at Ser214 mediates its interaction with 14-3-3 protein: implications for the mechanism of tau aggregation. *J. Neurochem.* **2009,** *108*, 33-43.

(214) Umahara, T.; Uchihara, T.; Tsuchiya, K.; Nakamura, A.; Iwamoto, T.; Ikeda, K.; Takasaki, M., 14-3-3 proteins and zeta isoform containing neurofibrillary tangles in patients with Alzheimer's disease. *Acta Neuropathol.* **2004,** *108*, 279-286.

(215) Ke, P. C.; Pilkington, E. H.; Sun, Y.; Javed, I.; Käkinen, A.; Peng, G.; Ding, F.; Davis, T. P., Mitigation of Amyloidosis with Nanomaterials. *Adv. Mater.* **2019**, 1901690.

(216) Kim, H. S.; Lee, S. H.; Choi, I., On-chip plasmonic immunoassay based on targeted assembly of gold nanoplasmonic particles. *Analyst* **2019,** *144*, 2820-2826.

(217) Choi, S. H.; Kim, Y. H.; Quinti, L.; Tanzi, R. E.; Kim, D. Y., 3D culture models of Alzheimer's disease: a road map to a "cure-in-a-dish". *Mol. Neurodegener.* **2016,** *11*, 75.

(218) Choi, S. H.; Kim, Y. H.; Hebisch, M.; Sliwinski, C.; Lee, S.; D'Avanzo, C.; Chen, H.; Hooli, B.; Asselin, C.; Muffat, J.; Klee, J. B.; Zhang, C.; Wainger, B. J.; Peitz, M.; Kovacs, D. M.; Woolf, C. J.; Wagner, S. L.; Tanzi, R. E.; Kim, D. Y., A three-dimensional human neural cell culture model of Alzheimer's disease. *Nature* **2014,** *515*, 274-278.

(219) Jo, Y. H.; Jang, I. J.; Nemeno, J. G.; Lee, S.; Kim, B. Y.; Nam, B. M.; Yang, W.; Lee, K. M. K., H.; Takebe, T.; Kim, Y. S.; Lee, J. I., Artificial Islets From Hybrid Spheroids of Three Pancreatic Cell Lines. *Transplant. Proc.* **2014,** *46*, 1156-1160.

(220) Drummond, E.; Wisniewski, T., Alzheimer's disease: experimental models and reality. *Acta Neuropathol.* **2017,** *133*, 155-175.

(221) Kim, H. Y.; Kim, H. V.; Jo, S.; Lee, J.; Choi, S. Y.; Kim, D. J.; Kim, Y., EPPS rescues hippocampus-dependent cognitive deficits in APP/PS1 mice by disaggregation of amyloid-β oligomers and plaques. *Nat. Commun.* **2015,** *6*, 8997.

(222) Poduslo, J. F.; Hultman, K. L.; Curran, G. L.; Preboske, G. M.; Chamberlain, R.; Marjanska, M.; Garwood, M.; Jack Jr., C. R.; Wengenack, T. M., Targeting vascular amyloid in arterioles of Alzheimer disease transgenic mice with amyloid β protein antibody-coated nanoparticles. *J. Neuropathol. Exp. Neurol.* **2011,** *70*, 653-661.

(223) Bieschke, J.; Herbst, M.; Wiglenda, M.; Friedrich, R. P.; Boeddrich, A.; Schiele, F.; Kleckers, D.; del Amo, J. M. L.; Grüning, B. A.; Wang, Q.; Schmidt, M. R.; Lurz, R.; Anwyl, R.; Schnoegl, S.; Fändrich, M.; Frank, R. F.; Reif, B.; Günther, S.; Walsh, D. M.; Wanker, E. E., Small-molecule conversion of toxic oligomers to nontoxic β-sheet–rich amyloid fibrils. *Nat. Chem. Biol.* **2011,** *8*, 93-101.

(224) Govindan, P. N.; Käkinen, A.; Pilkington, E. H.; Davis, T. P.; Ke, P. C.; Ding, F., Stabilizing Off-pathway Oligomers by Polyphenol Nanoassemblies for IAPP Aggregation Inhibition. *Sci. Rep.* **2016,** *6*, 19463.

(225) Pilkington, E. H.; Gurzov, E. N.; Käkinen, A.; Litwak, S. A.; Stanley, W. J.; Davis, T. P.; Ke, P. C., Pancreatic β-Cell Membrane Fluidity and Toxicity Induced by Human Islet Amyloid Polypeptide Species. *Sci. Rep.* **2016,** *6*, 21274.

(226) Bruno, E.; Pereira, C.; Roman, K. P.; Takiguchi, M.; Kao, P.-Y.; Nogaj, L. A.; Moffet, D. A., IAPP aggregation and cellular toxicity are inhibited by 1,2,3,4,6-penta-O-galloyl-β-$_D$-glucose. *Amyloid* **2013,** *20*, 34-38.

(227) Bieschke, J.; Russ, J.; Friedrich, R. P.; Ehrnhoefer, D. E.; Wobst, H.; Neugebauer, K.; Wanker, E. E., EGCG remodels mature α-synuclein and amyloid-β fibrils and reduces cellular toxicity. *Proc. Natl. Acad. Sci. U.S.A.* **2010,** *107*, 7710-7715.

(228) Cao, P.; Raleigh, D. P., Analysis of the Inhibition and Remodeling of Islet Amyloid Polypeptide Amyloid Fibers by Flavanols. *Biochemistry* **2012,** *51*, 2670-2683.

(229) Barrajón-Catalán, E.; Herranz-López, M.; Joven, J.; Segura-Carretero, A.; Alonso-Villaverde, C.; Menéndez, J. A.; Micol, V., Molecular Promiscuity of Plant Polyphenols in the Management of Age-Related Diseases: Far Beyond Their Antioxidant Properties. *Adv. Exp. Med. Biol.* **2014,** *824*, 141-159.

(230) Cano, A.; Ettcheto, M.; Chang, J.-H.; Barroso, E.; Espina, M.; Kühne, B. A.; Barenys, M.; Auladell, C.; Folch, J.; Souto, E. B.; Camins, A.; Turowski, P.; García, M. L., Dual-drug loaded nanoparticles of Epigallocatechin-3-gallate (EGCG)/Ascorbic acid enhance therapeutic efficacy of EGCG in a APPswe/PS1dE9 Alzheimer's disease mice model. *J. Control. Release* **2019,** *301*, 62-75.

(231) John, T.; Gladytz, A.; Kubeil, C.; Martin, L. L.; Risselada, H. J.; Abel, B., Impact of nanoparticles on amyloid peptide and protein aggregation: a review with a focus on gold nanoparticles. *Nanoscale* **2018,** *10*, 20894-20913.

(232) Wang, M.; Käkinen, A.; Pilkington, E. H.; Davis, T. P.; Ke, P. C., Differential Effects of Silver and Iron Oxide Nanoparticles on IAPP Aggregation and Toxicity. *Biomater. Sci.* **2017,** *5*, 485-493.

(233) Yoo, S. I.; Yang, M.; Brender, J. R.; Subramanian, V.; Sun, K.; Joo, N. E.; Jeong, S.-H.; Ramamoorthy, A.; Kotov, N. A., Inhibition of Amyloid Peptide Fibrillation by Inorganic Nanoparticles: Functional Similarities with Protein. *Angew. Chem. Int. Ed. Engl.* **2011,** *50*, 5110-5115.

(234) Ban, D. K.; Paul, S., Nano Zinc Oxide Inhibits Fibrillar Growth and Suppresses Cellular Toxicity of Lysozyme Amyloid. *ACS Appl. Mater. Interfaces* **2016,** *8*, 31587-31601.

(235) Dowding, J. M.; Song, W.; Bossy, K.; Karakoti, A.; Kumar, A.; Kim, A.; Bossy, B.; Seal, S.; Ellisman, M. H.; Perkins, G.; Self, W. T.; Bossy-Wetzel, E., Cerium oxide nanoparticles protect against Aβ-induced mitochondrial fragmentation and neuronal cell death. *Cell Death Differ.* **2014,** *21*, 1622-1632.

(236) Sanati, M.; Khodagholi, F.; Ghasemi, F.; Gholami, M.; Kebriaeezadeh, A.; Sabzevari, O.; Hajipour, M. J.; Imani, M.; Mahmoudi, M.; Sharifzadeh, M., Impact of Gold Nanoparticles on Amyloid β-Induced Alzheimer's Disease in a Rat Animal Model: Involvement of STIM Proteins. *ACS Chem. Neurosci.* **2019,** *10*, 2299-2309.

(237) Zhang, W.; Christofferson, A. J.; Besford, Q. A.; Richardson, J. J.; Guo, J.; Ju, Y.; Kempe, K.; Yarovsky, I.; Caruso, F., Metal-dependent inhibition of amyloid fibril formation: synergistic effects of cobalt–tannic acid networks. *Nanoscale* **2019,** *11*, 1921-1928.

(238) Javed, I.; Sun, Y.; Adamcik, J.; Wang, B.; Käkinen, A.; Pilkington, E. H.; Ding, F.; Mezzenga, R.; Davis, T. P.; Ke, P. C., Cofibrillization of Pathogenic and Functional Amyloid Proteins with Gold Nanoparticles against Amyloidogenesis. *Biomacromolecules* **2017,** *18*, 4316-4322.

(239) Liu, Y.; Zhou, H.; Yin, T.; Gong, Y.; Yang, G.; Chen, L.; Liu, J., Quercetin-modified gold-palladium nanoparticles as a potential autophagy inducer for the treatment of Alzheimer's disease. *J. Colloid Interface Sci.* **2019,** *552*, 388-400.

(240) Gladytz, A.; Abel, B.; Risselada, H. J., Gold-Induced Fibril Growth: The Mechanism of Surface-Facilitated Amyloid Aggregation. *Angew. Chem. Int. Ed., Engl.* **2016,** *55*, 11242-11246.

(241) Pansierei, J.; Gerstenmayer, M.; Lux, F.; Mériaux, S.; Tillement, O.; Forge, V.; Larrat, B.; Marquette, C., Magnetic Nanoparticles Applications for Amyloidosis Study and Detection: A Review. *Nanomaterials* **2018,** *8*, 740.

(242) Pansierei, J.; Plissonneau, M.; Stransky-Heilkron, N.; Dumoulin, M.; Heinrich-Balard, L.; Rivory, P.; Morfin, J.-F.; Toth, E.; Saraiva, M. J.; Allémann, E.; Tillement, O.; Forge, V.; Lux, F.; Marquette, C., Multimodal imaging Gd-nanoparticles functionalized with Pittsburgh compound B or a nanobody for amyloid plaques targeting. *Nanomedicine* **2017,** *12*, 1675-1687.

(243) Liu, X. G.; Lu, S.; Liu, D. Q.; Zhang, L.; Zhang, L. X.; Yu, X. L.; Liu, R. T., ScFv-conjugated superparamagnetic iron oxide nanoparticles for MRI-based diagnosis in transgenic mouse models of Parkinson's and Huntington's diseases. *Brain Res.* **2019,** *1707*, 141-153.

(244) Ahlschwede, K. M.; Curran, G. L.; Rosenberg, J. T.; Grant, S. C.; Sarkar, G.; Jenkins, R. B.; Ramakrishnan, S.; Poduslo, J. F.; Kandimalla, K. K., Cationic carrier peptide enhances cerebrovascular targeting of nanoparticles in Alzheimer's disease brain. *Nanomedicine* **2019,** *16*, 258-266.

(245) Dodart, J.-C.; Bales, K. R.; Paul, S. M., Immunotherapy for Alzheimer's disease: will vaccination work? *Trends Mol. Med.* **2003,** *9*, 85-87.

(246) Kim, D.; Kwon, H. J.; Hyeon, T., Magnetite/Ceria Nanoparticle Assemblies for Extracorporeal Cleansing of Amyloid-β in Alzheimer's Disease. *Adv. Mater.* **2019,** *31*, e1807965.

(247) Bolisetty, S.; Mezzenga, R., Amyloid-carbon hybrid membranes for universal water purification. *Nat. Nanotechnol.* **2016,** *11*, 365-372.

(248) Shen, Y.; Posavec, L.; Bolisetty, S.; Hilty, F. M.; Nyström, G.; Kohlbrecher, J.; Hilbe, M.; Rossi, A.; Baumgartner, J.; Zimmermann, M. B.; Mezzenga, R., Amyloid fibril systems reduce, stabilize and deliver bioavailable nanosized iron. *Nat. Nanotechnol.* **2017,** *12*, 642-647.

(249) Al-Garawi, Z. S.; McIntosh, B. A.; Neill-Hall, D.; Hatimy, A. A.; Sweet, S. M.; Bagley, M. C.; Serpell, L. C., The amyloid architecture provides a scaffold for enzyme-like catalysts. *Nanoscale* **2017,** *9*, 10773-10783.

(250) Geng, J.; Li, M.; Ren, J.; Wang, E.; Qu, X., Polyoxometalates as Inhibitors of the Aggregation of Amyloid β Peptides Associated with Alzheimer's Disease. *Angew. Chem. Int Ed., Engl.* **2011,** *50*, 4184-4188.

(251) Gao, N.; Sun, H.; Dong, K.; Ren, J.; Duan, T.; Xu, C.; Qu, X., Transition-metal-substituted polyoxometalate derivatives as functional anti-amyloid agents for Alzheimer's disease. *Nat. Commun.* **2014,** *5*, 3422.

(252) Lee, M.-C.; Yu, W.-C.; Shih, Y.-H.; Chen, C.-Y.; Guo, Z.-H.; Huang, S.-J.; Chan, J. C. C.; Chen, Y.-R., Zinc ion rapidly induces toxic, off-pathway amyloid-β oligomers distinct from amyloid-β derived diffusible ligands in Alzheimer's disease. *Sci. Rep.* **2018,** *8*, 4772.

(253) Bobylev, A. G.; Kraevaya, O. A.; Bobyleva, L. G.; Khakina, E. A.; Fadeev, R. S.; Zhilenkov, A. V.; Mishchenko, D. V.; Penkov, N. V.; Teplov, I. Y.; Yakupova, E. I.; Vikhlyantsev, I. M.; Troshin, P. A., Anti-amyloid activities of three different types of water-soluble fullerene derivatives. *Colloids Surf. B Biointerfaces* **2019,** *183*, 110426.

(254) Mahmoudi, M.; Akhavan, O.; Ghavami, M.; Rezaee, F.; Ghiasi, S. M. A., Graphene oxide strongly inhibits amyloid beta fibrillation. *Nanoscale* **2012,** *4*, 7322-7325.

(255) Govindan, P. N.; Gurzov, E. N.; Chen, P.; Pilkington, E. H.; Stanley, W. J.; Litwak, S. A.; Davis, T. P.; Ke, P. C.; Ding, F., Graphene Oxide Inhibits hIAPP Amyloid Fibrillation and Toxicity in Insulin-Producing NIT-1 Cells. *Phys. Chem. Chem. Phys.* **2015,** *18*, 94-100.

(256) Li, C.; Mezzenga, R., The interplay between carbon nanomaterials and amyloid fibrils in bio-nanotechnology. *Nanoscale* **2013,** *5*, 6207-6218.

(257) Javed, I.; Yu, T.; Peng, G.; Sánchez-Ferrer, A.; Faridi, A.; Käkinen, A.; Zhao, M.; Mezzenga, R.; Davis, T. P.; Lin, S.; Ke, P. C., In Vivo Mitigation of Amyloidogenesis through Functional−Pathogenic Double-Protein Coronae. *Nano Lett.* **2018,** *18*, 5797-5804.

(258) Liu, Y.; Xu, L.-P.; Dai, W.; Dong, H.; Wen, Y.; Zhang, X., Graphene quantum dots for the inhibition of β amyloid aggregation. *Nanoscale* **2015,** *7*, 19060-19065.

(259) Wang, M.; Sun, Y.; Cao, X.; Peng, G.; Javed, I.; Käkinen, A.; Davis, T. P.; Lin, S.; Liu, J.; Ding, F.; Ke, P. C., Graphene quantum dots against human IAPP aggregation and toxicity *in vivo*. *Nanoscale* **2018,** *10*, 19995-20006.

(260) He, X.-P.; Deng, Q.; Cai, L.; Wang, C.-Z.; Zang, Y.; Li, J.; Chen, G.-R.; Tian, H., Fluorogenic Resveratrol-Confined Graphene Oxide For Economic and Rapid Detection Of Alzheimer's Disease. *ACS Appl. Mater. Interfaces* **2014,** *6*, 5379-5382.

(261) Wang, J.; Liu, L.; Ge, D.; Zhang, H.; Feng, Y.; Zhang, Y.; Chen, M.; Dong, M., Differential Modulating Effect of MoS_2 on Amyloid Peptide Assemblies. *Chem. Eur. J.* **2018,** *24*, 3397-3402.

(262) Li, M.; Zhao, A.; Dong, K.; Li, W.; Ren, J.; Qu, X., Chemically exfoliated WS_2 nanosheets efficiently inhibit amyloid β-peptide aggregation and can be used for photothermal treatment of Alzheimer's disease. *Nano Res.* **2015,** *8*, 3216-3227.

(263) Zhang, Q.; Bolisetty, S.; Cao, Y.; Handschin, S.; Adamcik, J.; Peng, Q.; Mezzenga, R., Selective and Efficient Removal of Fluoride from Water: In Situ Engineered Amyloid Fibril/ZrO2 Hybrid Membranes. *Angew. Chem. Int. Ed., Engl.* **2019,** *58*, 6012-6016.

(264) Kostarelos, K., The long and short of carbon nanotube toxicity. *Nat. Biotechnol.* **2008,** *26*, 774-776.

(265) Ke, P. C.; Qiao, R., Carbon nanomaterials in biological systems. *J. Phys. Condens. Matter* **2007,** *19*, 373101.

(266) Huang, H.; Li, P.; Zhang, M.; Yu, Y.; Huang, Y.; Gu, H.; Wang, C.; Yang, Y., Graphene quantum dots for detecting monomeric amyloid peptides. *Nanoscale* **2017,** *9*, 5044-5048.

(267) Dzwolak, W., Chirality and Chiroptical Properties of Amyloid Fibrils. *Chirality* **2014,** *26*, 580-587.

(268) Malishev, R.; Arad, E.; Bhunia, S. K.; Shaham-Niv, S.; Kolusheva, S.; Gazit, E.; Jelinek, R., Chiral modulation of amyloid beta fibrillation and cytotoxicity by enantiomeric carbon dots. *Chem. Commun.* **2018,** *54*, 7762-7765.

(269) Faridi, A.; Sun, Y.; Okazaki, Y.; Peng, G.; Gao, J.; Käkinen, A.; Faridi, P.; Zhao, M.; Javed, I.; Purcell, A. W.; Davis, T. P.; Lin, S.; Oda, R.; Ding, F.; Ke, P. C., Mitigating Human IAPP Amyloidogenesis In Vivo with Chiral Silica Nanoribbons. *Small* **2018,** *14*, 1802825.

(270) Tang, F.; Li, L.; Chen, D., Mesoporous Silica Nanoparticles: Synthesis, Biocompatibility and Drug Delivery. *Adv. Mater.* **2012,** *24*, 1504-1534.

(271) Zhu, X.; Wen, Y.; Zhao, Y.; Liu, Y.; Sun, J.; Liu, J.; Chen, L., Functionalized chitosan-modified defect-related luminescent mesoporous silica nanoparticles as new inhibitors for hIAPP aggregation. *Nanotechnology* **2019,** *30*, 315705.

(272) Luo, Q.; Lin, Y.-X.; Yang, P.-P.; Wang, Y.; Qi, G.-B.; Qiao, Z.-Y.; Li, B.-N.; Zhang, K.; Zhang, J.-P.; Wang, L.; Wang, H., A self-destructive nanosweeper that captures and clears amyloid β-peptides. *Nat. Commun.* **2018,** *9*, 1802.

(273) Zhang, C.; Wan, X.; Zheng, X.; Shao, X.; Liu, Q.; Zhang, Q.; Qian, Y., Dual-functional nanoparticles targeting amyloid plaques in the brains of Alzheimer's disease mice. *Biomaterials* **2014,** *35*, 456-465.

(274) Bilia, A. R.; Nardiello, P.; Piazzini, V.; Leri, M.; Bergonzi, M. C.; Bucciantini, M.; Casamenti, F., Successful Brain Delivery of Andrographolide Loaded in Human Albumin Nanoparticles to TgCRND8 Mice, an Alzheimer's Disease Mouse Model. *Front. Pharmacol.* **2019,** *10*, 910.

(275) Ma, X.; Zhou, P.; Kugelmass, A.; Toskic, D.; Warner, M.; Lee, L.; Fogaren, T.; Godara, A.; Wang, M.; Li, Y.; Yang, L.; Xu, Q.; Comenzo, R. L., A novel xenograft mouse model for testing approaches targeting human kappa light-chain diseases. *Gene Ther.* **2019,** *26*, 187-197.

(276) Song, Q.; Huang, M.; Yao, L.; Wang, X.; Gu, X.; Chen, J.; Chen, J.; Huang, J.; Hu, Q.; Kang, T.; Rong, Z.; Qi, H.; Zheng, G.; Chen, H.; Gao, X., Lipoprotein-Based Nanoparticles Rescue the

Memory Loss of Mice with Alzheimer's Disease by Accelerating the Clearance of Amyloid-Beta. *ACS Nano* **2014,** *8*, 2345-2359.

(277) Aso, E.; Martinsson, I.; Appelhans, D.; Effenberg, C.; Benseny-Cases, N.; Cladera, J. C.; Gouras, G.; Ferrer, I.; Klementieva, O., Poly(propylene imine) dendrimers with histidine-maltose shell as novel type of nanoparticles for synapse and memory protection. *Nanomedicine* **2019,** *17*, 198-209.

(278) Evgrafova, Z.; Voigt, B.; Roos, A. H.; Hause, G.; Hinderberger, D.; Balbach, J.; Binder, W. H., Modulation of amyloid β peptide aggregation by hydrophilic polymers. *Phys. Chem. Chem. Phys.* **2019,** *21*, 20999-21006.

(279) Cabaleiro-Lago, C.; Quinlan-Pluck, F.; Lynch, I.; Lindman, S.; Minogue, A. M.; Thulin, E.; Walsh, D. M.; Dawson, K. A.; Linse, S., Inhibition of Amyloid β Protein Fibrillation by Polymeric Nanoparticles. *J. Am. Chem. Soc.* **2008,** *130*, 15437-15443.

(280) Breydo, L.; Newland, B.; Zhang, H.; Rosser, A.; Werner, C.; Uversky, V. N.; Wang, W., A hyperbranched dopamine-containing PEG-based polymer for the inhibition of α-synuclein fibrillation. *Biochem. Biophys. Res. Commun.* **2016,** *469*, 830-835.

(281) Chowdhury, S. R.; Agarwal, M.; Meher, N.; Muthuraj, B.; Iyer, P. K., Modulation of Amyloid Aggregates into Nontoxic Coaggregates by Hydroxyquinoline Appended Polyfluorene. *ACS Appl. Mater. Interfaces* **2016,** *8*, 13309-13319.

(282) Debnath, K.; Shekhar, S.; Kumar, V.; Jana, N. R.; Jana, N. R., Efficient Inhibition of Protein Aggregation, Disintegration of Aggregates, and Lowering of Cytotoxicity by Green Tea Polyphenol-Based Self-Assembled Polymer Nanoparticles. *ACS Appl. Mater. Interfaces* **2016,** *8*, 20309-20318.

(283) Guerreiro, L. H.; Da Silva, D.; Ricci-Junior, E.; Girard-Dias, W.; Mascarenhas, C. M.; Sola-Penna, M.; Miranda, K.; Lima, L. M. T. R., Polymeric particles for the controlled release of human amylin. *Colloids Surf. B Biointerfaces* **2012,** *94*, 101-106.

(284) Cabaleiro-Lago, C.; Lynch, I.; Dawson, K. A.; Linse, S., Inhibition of IAPP and $IAPP_{(20-29)}$ Fibrillation by Polymeric Nanoparticles. *Langmuir* **2009,** *26*, 3453-3461.

(285) Gurzov, E. N.; Wang, B.; Pilkington, E. H.; Chen, P.; Käkinen, A.; Stanley, W. J.; Litwak, S. A.; Hanssen, E. G.; Davis, T. P.; Ding, F.; Ke, P. C., Inhibition of hIAPP Amyloid Aggregation and Pancreatic β-Cell Toxicity by OH-Terminated PAMAM Dendrimer. *Small* **2016,** *12*, 1615-1626.

(286) Nguyen, P. T.; Sharma, R.; Rej, R.; De Carufel, C. A.; Roy, R.; Bourgault, S., Low generation anionic dendrimers modulate islet amyloid polypeptide self-assembly and inhibit pancreatic β-cell toxicity. *RSC Adv.* **2016,** *6*, 76360-76369.

(287) Ren, J. M.; McKenzie, T. G.; Fu, Q.; Wong, E. H. H.; Xu, J.; An, Z.; Shanmugam, S.; Davis, T. P.; Boyer, C.; Qiao, G. C., Star Polymers. *Chem. Rev.* **2016,** *116*, 6743-6836.

(288) Teo, J.; McCarroll, J. A.; Boyer, C.; Youkhana, J.; Sagnella, S. M.; Duong, H. T. T.; Liu, J.; Sharbeen, G.; Goldstein, D.; Davis, T. P.; Kavallaris, M.; Phillips, A. P., A Rationally Optimized Nanoparticle System for the Delivery of RNA Interference Therapeutics into Pancreatic Tumors in Vivo. *Biomacromolecules* **2016,** *17*, 2337-2351.

(289) Li, N.; Luo, H.-C.; Yang, C.; Deng, J.-J.; Ren, M.; Xie, X.-Y.; Lin, D.-Z.; Yan, L.; Zhang, L.-M., Cationic star-shaped polymer as an siRNA carrier for reducing MMP-9 expression in skin fibroblast cells and promoting wound healing in diabetic rats. *Int. J. Nanomedicine* **2014,** *9*, 3377-3387.

(290) Pilkington, E. H.; Lai, M.; Ge, X.; Stanley, W. J.; Wang, B.; Wang, M.; Käkinen, A.; Sani, M.-A.; Whittaker, M. R.; Gurzov, E. N.; Ding, F.; Quinn, J. F.; Davis, T. P.; Ke, P. C., Star Polymers Reduce Islet Amyloid Polypeptide Toxicity via Accelerated Amyloid Aggregation. *Biomacromolecules* **2017,** *18*, 4249-4260.

(291) Jain, R.; Khandelwal, G.; Roy, S., Unraveling the Design Rules in Ultrashort Amyloid-Based Peptide Assemblies toward Shape-Controlled Synthesis of Gold Nanoparticles. *Langmuir* **2019,** *35*, 5878-5889.

(292) Huang, J.; Liu, S.; Zhang, C.; Wang, X.; Pu, J.; Ba, F.; Xue, S.; Ye, H.; Zhao, T.; Li, K.; Wang, Y.; Zhang, J.; Wang, L.; Fan, C.; Lu, T. K.; Zhong, C., Programmable and printable *Bacillus subtilis* biofilms as engineered living materials. *Nat. Chem. Biol.* **2019,** *15*, 34-41.

(293) Lee, S.; Lee, D.; Hong, C.-S.; Yang, J. E.; Kang, J. S.; Sung, Y.-E.; Paik, S. R., Alternative Assembly of α-Synuclein Leading to Protein Film Formation and Its Application for Developing Polydiacetylene-Based Sensing Materials. *Langmuir* **2019,** *35*, 11923-11931.

(294) Kumar, S. T.; Meinhardt, J.; Fuchs, A.-K.; Aumüller, T.; Leppert, J.; Büchele, B.; Knüpfer, U.; Ramachandran, R.; Yadav, J. K.; Prell, E.; Morgado, I.; Ohlenschläger, O.; Horn, U.; Simmet, T.; Görlach, M.; Fändrich, M., Structure and Biomedical Applications of Amyloid Oligomer Nanoparticles. *ACS Nano* **2014,** *8*, 11042-11052.

(295) Babych, M.; Bertheau-Mailhot, G.; Zottig, X.; Dion, J.; Gauthier, L.; Archambault, D.; Bourgault, S., Engineering and evaluation of amyloid assemblies as a nanovaccine against the Chikungunya virus. *Nanoscale* **2018,** *10*, 19547-19556.

(296) Mayer, E. A.; Knight, R.; K., M. S.; Cryan, J. F.; Tillisch, K., Gut Microbes and the Brain: Paradigm Shift in Neuroscience. *J. Neurosci.* **2014,** *34*, 15490-15496.

(297) Dominy, S. S.; Lynch, C.; Ermini, F.; Benedyk, M.; Marczyk, A.; Konradi, A.; Nguyen, M.; Haditsch, U.; Raha, D.; Griffin, C.; Holsinger, L. J.; Arastu-Kapur, S.; Kaba, S.; Lee, A.; Ryder, M. I.; Potempa, B.; Mydel, P.; Hellvard, A.; Adamowicz, K.; Hasturk, H.; Walker, G. D.; Reynolds, E. C.; Faull, R. L. M.; Curtis, M. A.; Dragunow, M.; Potempa, J., *Porphyromonas gingivalis* in Alzheimer's disease brains: Evidence for disease causation and treatment with small-molecule inhibitors. *Sci. Adv.* **2019,** *5*, eaau3333.

(298) Koh, A.; Molinaro, A.; Ståhlman, M.; Khan, M. T.; Schmidt, C.; Mannerås-Holm, L.; Wu, H.; Carreras, A.; Jeong, H.; Olofsson, L. E.; Bergh, P.-O.; Gerdes, V.; Hartstra, A.; de Brauw, M.; Perkins, R.; Nieuwdorp, M.; Bergström, G.; Bäckhed, F., Microbially Produced Imidazole Propionate Impairs Insulin Signaling through mTORC1. *Cell* **2018,** *175*, 947-961.

(299) Meijnikman, A. S.; Gerdes, V. E.; Nieuwdorp, M.; Herrema, H., Evaluating Causality of Gut Microbiota in Obesity and Diabetes in Humans. *Endocr. Rev.* **2018,** *39*, 133-153.

(300) Barton, S. M.; Janve, V. A.; McClure, R.; Anderson, A.; Matsubara, J. A.; Gore, J. C.; Pham, W., Lipopolysaccharide Induced Opening of the Blood Brain Barrier on Aging 5XFAD Mouse Model. *J. Alzheimers Dis.* **2019,** *67*, 503-513.

(301) Park, H.; Oh, J.; Shim, G.; Cho, B.; Chang, Y.; Kim, S.; Baek, S.; Kim, H. S.; Shin, J.; Choi, H.; Yoo, J.; Kim, J.; Jun, W.; Lee, M.; Lengner, C.; Oh, Y.-K.; Kim, J., In vivo neuronal gene editing via CRISPR-Cas9 amphiphilic nanocomplexes alleviates deficits in mouse models of Alzheimer's disease. *Nat. Neurosci.* **2019,** *22*, 524-528.

(302) Lopes, D. H. J.; Attar, A.; Nair, G.; Hayden, E. Y.; Du, Z.; McDaniel, K.; Dutt, S.; Bandmann, H.; Bravo-Rodriguez, K.; Mittal, S.; Klärner, F.-G.; Wang, C.; Sanchez-Garcia, E.; Schrader, T.; Bitan, G., Molecular Tweezers Inhibit Islet Amyloid Polypeptide Assembly and Toxicity by a New Mechanism. *ACS Chem. Biol.* **2015,** *10*, 1555-1569.

(303) Cheng, C.-H.; Lin, K.-J.; Hong, C.-T.; Wu, D.; Chang, H.-M.; Liu, C.-H.; Hsiao, I.-T.; Yang, C.-P.; Liu, Y.-C.; Hu, C.-J., Plasmon-Activated Water Reduces Amyloid Burden and Improves Memory in Animals with Alzheimer's Disease. *Sci. Rep.* **2019,** *9*, 13252.

(304) Qin, J.; Cho, M.; Lee, Y., Ultrasensitive Detection of Amyloid-β Using Cellular Prion Protein on the Highly Conductive Au Nanoparticles–Poly(3,4-ethylene dioxythiophene)–Poly(thiophene-3-acetic acid) Composite Electrode. *Anal. Chem.* **2019,** *91*, 11259-11265.

(305) Wadghiri, Y. Z.; Sigurdsson, E. M.; Sadowski, M.; Elliott, J. I.; Li, Y.; Scholtzova, H.; Tang, C. Y.; Aguinaldo, G.; Pappolla, M.; Duff, K.; Wisniewski, T.; Turnbull, D. H., Detection of Alzheimer's amyloid in transgenic mice using magnetic resonance microimaging. *Magn. Res. Med.* **2003,** *50*, 293-302.

(306) Sonawane, S. K.; Ahmad, A.; Chinnathambi, S., Protein-Capped Metal Nanoparticles Inhibit Tau Aggregation in Alzheimer's Disease. *ACS Omega* **2019,** *4*, 12833-12840.

(307) Javed, I.; Peng, G.; Xing, Y.; Yu, T.; Zhao, M.; Käkinen, A.; Faridi, A.; Parish, C. L.; Ding, F.; Davis, T. P.; Ke, P. C.; Lin, S., Inhibition of amyloid beta toxicity in zebrafish with a chaperone-gold nanoparticle dual strategy. *Nat. Commun.* **2019,** *10*, 3780.

(308) Chen, J.; Armstrong, A. H.; Koehler, A. N.; Hecht, M. H., Small Molecule Microarrays Enable the Discovery of Compounds that Bind the Alzheimer's Aβ Peptide and Reduce its Cytotoxicity. *J. Am. Chem. Soc.* **2010,** *132*, 17015-17022.

(309) Limbocker, R.; Chia, S.; Ruggeri, F. S.; Perni, M.; Cascella, R.; Heller, G. T.; Meisl, G.; Mannini, B.; Habchi, J.; Michaels, T. C. T.; Challa, P. K.; Ahn, M.; Casford, S. T.; Fernando, N.; Xu, C. K.; Kloss, N. D.; Cohen, S. I. A.; Kumita, J. R.; Cecchi, F.; Zasloff, M.; Linse, S.; Knowles, T. P. J.; Chiti, F.; Vendruscolo, M.; Dobson, C. M., Trodusquemine enhances Aβ42 aggregation but suppresses its toxicity by displacing oligomers from cell membranes. *Nat. Commun.* **2019,** *10*, 225.

(310) Van der Munnik, N. P.; Moss, M. A.; Uline, M. J., Obstacles to translating the promise of nanoparticles into viable amyloid disease therapeutics. *Phys. Biol.* **2019,** *16*, 021002.

(311) Wadman, M.; Servick, K., Alzheimer's drug resurrected, as company claims clinical benefits. *Science* **2019**.

(312) Abbott, A.; Dolgin, E., Leading Alzheimer's theory survives drug failure. *Nature* **2016,** *540*, 15-16.

(313) Zhang, S.; Liu, H.; Chuang, C. L.; Li, X.; Au, M.; Zhang, L.; Phillips, A. R. J.; Scott, D. W.; Cooper, G. J. S., The pathogenic mechanism of diabetes varies with the degree of overexpression and oligomerization of human amylin in the pancreatic islet β cells. *FASEB J.* **2014,** *28*, 5083-5096.

(314) Fox, N.; Schrementi, J.; Nishi, M.; Ohagi, S.; Chan, S. J.; Heisserman, J. A.; Westermark, G. T.; Leckström, A.; Westermark, P.; Steiner, D. F., Human islet amyloid polypeptide transgenic mice as a model of non-insulin-dependent diabetes mellitus (NIDDM). *FEBS Lett.* **1993,** *323*, 40-44.

(315) Matveyenko, A. V.; Butler, P. C., Islet Amyloid Polypeptide (IAPP) Transgenic Rodents as Models for Type 2 Diabetes. *ILAR J.* **2006,** *47*, 225-233.

Chapter Two: Model Interactions of Amyloid Protein Species

Preamble: Fundamental insight into IAPP amyloid aggregation in model environments *in vitro* (*Aims 1A & 1B*) was first sought to provide context for further studies of amyloid behavior within complex environments (**Chapter Three**) and how nanomaterials might be designed to mimic endogenous mechanisms of IAPP amyloidosis inhibition (**Chapter Four**). Selected data in this chapter has been published as Xing, Y.; Pilkington, E. H. *et al. Phys. Chem. Chem. Phys*. **2017,** *19,* 30627 (**Fig. 4**), reproduced by permission of the PCCP Owner Societies; and Pilkington, E. H. *et al. Sci. Rep.* **2017,** *7,* 2455 (**Figs. 5 & 6**), as indicated in respective figure captions. All experiments and analyses presented herein were undertaken by the candidate, excepting FibreApp fibril persistence length analysis in **Figure 5E**, which was performed by Dr. Aleksandr Kakinen.

2.1. Chapter abstract

The amyloid aggregation of islet amyloid polypeptide (IAPP) is associated with dysfunction and death of pancreatic β-cells, a hallmark of type 2 diabetes (T2D), but is capable of further damage to extra-pancreatic tissues due to the propensity of circulating IAPP species to translocate throughout the body. Though studies have been conducted with Alzheimer's-associated amyloid-beta (Aβ) and Parkinson's-associated alpha-synuclein (αSyn), the rapid amyloidosis of IAPP has previously limited characterization of amyloid pathway species, with respect to their morphology and associated cytotoxicity. Through timepoint-based high resolution transmission electron microscopy (TEM), a diverse profile of IAPP intermediate species was generated, including a biannular oligomer morphology that has not been previously reported. A cytotoxicity assay, utilizing primary human umbilical vein endothelial cells (HUVECs) to provide a more accurate approximation of vascular tissue encountered by circulating IAPP *in vivo*, demonstrated differential cytotoxic effects of thioflavin T (ThT)-probed IAPP species, with early and intermediate IAPP species proving highly deleterious in both 'fresh' and preincubated states regardless of different fibrillization kinetics, and mature amyloid plaques eliciting low-level cytotoxicity.

A number of biophysical studies have highlighted membranes, both biological and synthetic, as eliciting a promotional effect on Aβ, αSyn and IAPP, through electrostatic and hydrophobic

interactions between amyloidogenic species and the lipid membranes. Utilizing a ThT kinetic assay, TEM and circular dichroism (CD) spectroscopy, micellar lysophosphatidylcholine (LPC), the most abundant lysophospholipid in the blood, is shown to inhibit IAPP amyloid aggregation through nonspecific interactions while elevating α-helical peptide secondary structure. This surprising finding suggests a native protective mechanism against IAPP aggregation *in vivo*.

The ubiquity of extracellular proteins in both the pancreatic islets of Langerhans and the vascular circulation belies an impact on fibrillating and amyloid IAPP, though the effects of protein association with IAPP species are largely unknown. Two homologous proteins, cationic lysozyme (Lys) and anionic alpha-lactalbumin (aLac), both of which can be found in the circulation, were examined for their capacity to modulate IAPP behavior in a controlled *in vitro* environment. Biophysical characterizations and a cell viability assay revealed distinct effects of Lys and aLac on IAPP amyloid aggregation, fibril remodeling and associated cytotoxicity, pointing to the role of a protein 'corona' in conferring the biological impact of amyloidogenic peptides. Collectively, this chapter provides fundamental characterizations and interactions of IAPP aggregation species individually and with model proteins, lipids, and ultrasmall membranes within a controlled *in vitro* environment, towards understanding endogenous behaviors of IAPP and its associated pathologies *in vivo*.

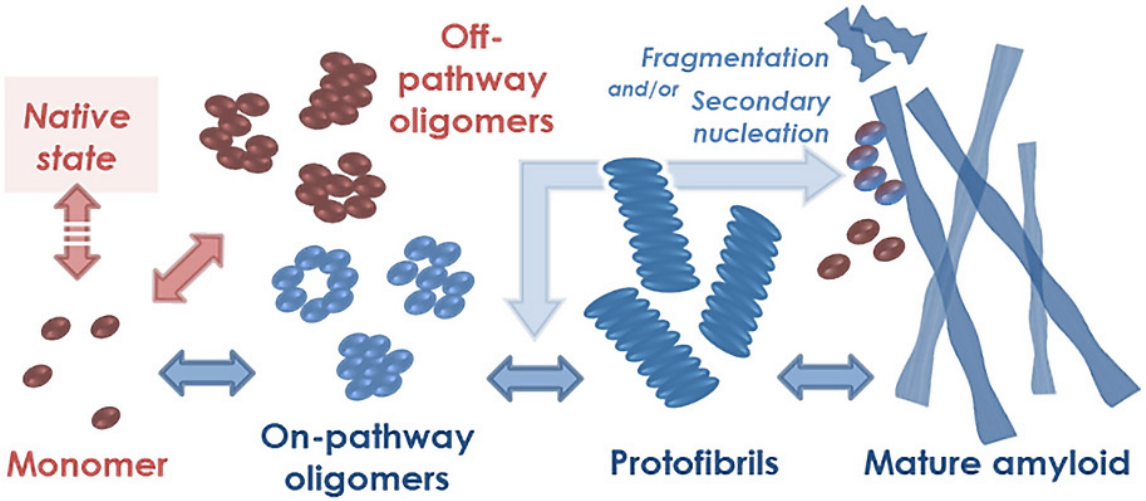

Figure 1. Simplified scheme of the amyloid fibrillization pathway (blue), in addition to off-pathway or native/unfolded species (red).

2.2. Introduction

IAPP is a 37-residue peptide hormone that, along with insulin, plays an essential role in glycemic control.[1] The soluble, monomeric peptide is stored at millimolar concentrations in the islets of Langerhans before being released to the bloodstream. However, IAPP is aggregation prone sans the stabilization of insulin, physiological metal ions, low pH,[2-7] or their complexation with zinc and C-peptide[8] per endogenous inhibitory measures employed by pancreatic β-cells.[9] Lacking a stabilizing microenvironment, *in vitro* studies have revealed that, at micromolar concentrations, IAPP can readily fibrillate into amyloids within hours – accumulating evidence has implicated IAPP amyloid aggregation as a key causative agent of pancreatic β-cell death and, subsequently, the development of T2D, a debilitating disease impairing 368 million people worldwide.[10]

Earlier studies ascribed IAPP amyloids as the toxic species,[11-12] while more recent studies pointed to IAPP oligomers as the causative toxic agent for β-cell loss.[13] The ambiguities surrounding IAPP toxicity largely stem from the difficulty in isolating IAPP monomers from oligomers, protofibrils and amyloids due to the rapid fibrillization kinetics of the peptide, as well as the complex intra- and extra-cellular environments of the IAPP species where peptides, proteins, lipids and fatty acids occur in abundance.[13] Intermediate species, spanning the breadth of the amyloid fibrillization pathway from monomer to fibril (**Fig. 1**), further complicate IAPP-induced pathogenicity. The structural diversity in IAPP oligomeric species,[14] wherein < 10% are predicted to have the β-rich secondary structure associated with eliciting cytotoxicity,[15] in addition to the rapid rate in which they progress from low order structures into higher order fibrils and protofibrils, dynamically changing conformation[16-17] and facilitating the nucleation of other fibrillating species,[9, 18] all present particular challenges for their characterization. The presence of IAPP fibrils and plaques in the extracellular space of the islets of Langerhans further suggests a role of cell membranes in inducing aberrant IAPP aggregation. Cell membranes as well as lipid vesicles have generally been shown to promote IAPP aggregation,[19-30] as also observed for Aβ and αSyn in neurodegenerative disorders.[31-32] Conversely, IAPP disrupts membrane integrity through lipid extraction or pore formation.[24, 26, 30-31] On the molecular level, the binding between IAPP and a lipid interface is initiated by the N-terminus of the peptide, through electrostatic interaction with the anionic lipids and facilitated by hydrophobic interaction engaging the lipid bilayer and the amphiphilic peptide oligomers, protofibrils and fibrils.[16-17, 19-23, 25]

In consideration of the changing conformation and hydrophobicity of IAPP during its fibrillization process, it is reasonable to postulate that the molecular ligands encountered by IAPP from cradle to grave may exert effects on the physical and biological identities of the IAPP species. Surprisingly, little is known concerning IAPP-protein interactions and their biological and pathological implications. IAPP amyloid deposition *in vivo* has been associated with various co-factors, including apolipoprotein E (ApoE),[33] serum amyloid P (SAP) component,[34] and glycosaminoglycans (GAGs), in particular heparan sulfate proteoglycans.[35] The fibrillization of IAPP has been shown to be enhanced by GAGs,[36-37] which can further augment aggregation of incompletely processed IAPP.[38] IAPP fibrillization *in vitro* has also been inhibited, to varying extents, by secretory chaperones and serum albumins.[37, 39-40] Protein-IAPP association is not necessarily correlated with mitigation of IAPP-mediated cytotoxicity, as is evidenced with ApoE and GAGs, wherein only the latter is implicated in IAPP toxicity.[41-42]

In this chapter, fundamental questions into the native state and behaviors of IAPP amyloid species are explored, utilizing controlled *in vitro* environments as a platform for elucidating endogenous processes in complex *in vivo* milieu. Firstly, a structure-based analysis of intermediate fibrillar species generated during a 24-hour period in aqueous solution was undertaken using TEM. Four distinct morphologies were identified – spherical, annular, biannular and complex aggregates – and additionally profiled by diametric size. Furthermore, by lowering the reaction temperature, the progression of intermediates to a predominantly fibrillar state was delayed, allowing for selection of reaction conditions that favor predominantly oligomeric species (e.g., 4 h at 4 ^{o}C) for use in comparative studies. Concordantly, an *in vitro* toxicity study was performed on three IAPP populations: monomeric IAPP, oligomeric/fibrillating IAPP, and mature IAPP amyloid. Utilizing HUVECs, a primary endothelial cell line corresponding to cells present in the vasculature that may interface with circulating IAPP, fibrillization and associated cytotoxicity of each IAPP species was compared. Under the applied conditions, monomeric and fibrillating IAPP species had near-identical toxicity profiles, demonstrating sigmoidal kinetics and an endpoint toxicity value of ~60%, despite notable differentiation in their fibrillization behavior. IAPP amyloid elicited around ~20% cytotoxicity, giving precedence to early and intermediate species of IAPP as causative of the majority of cell damage and death within an initial period of exposure.

In order to assess the impact of circulating proteins and lipids on IAPP behavior, model proteins and lipids were introduced to early ('fibrillating' or 'fresh') IAPP and mature amyloid IAPP, and their impact on IAPP fibrillization, morphology and associated cytotoxicity were explored for the first time.[43-44] In the first study, the effects of zwitterionic LPC on IAPP aggregation at both below and above its critical micelle concentration (CMC, 40-50 μM)[45] were examined. LPC, a product of lipid peroxidation, is the most abundant single-tailed phospholipid in the blood (234 μM)[46] as well as a signaling molecule in the cell membrane. At concentrations above the CMC, such as in the blood, LPC molecules render ultra-small micelles (~4 nm in diameter)[47-48] in size similar to that of sodium dodecyl sulfate (SDS). From the perspective of a model membrane the zwitterionic LPC micelles mimic the largely neutral pancreatic β-cell membranes (97.5% neutral, plus 2.5% anionic lipids)[49] more closely than the anionic SDS that has been used as a model system for examining protein-membrane interactions. The fibrillization of IAPP in the presence of linear and micellar LPC was quantified by a ThT kinetic assay and high-resolution TEM, with the changing secondary structure of IAPP in the presence of linear and micellar forms of the lipid probed with CD spectroscopy. A surprising inhibition effect of LPC micelles on IAPP amyloid aggregation was revealed, characterized by a prolonged lag time, a reduction in the β-sheet content at saturation in favor of majority α-helical conformations, and sparse formation of soft, braided IAPP fibrils.

Lastly, the interactions of the two IAPP populations with two model proteins, Lys and aLac, was examined, in order to determine how the binding of amyloid species with model circulatory proteins affects their biological fate. Lys and aLac are homologous proteins with similar tertiary structures (14 kDa, 41% helical and 9% β-sheets) while carrying opposite net charges. Lys is an enzyme commonly found in saliva and tears responsible for hydrolyzing peptidoglycans in bacterial cell wall, while aLac from mammal milk regulates lactose biosynthesis. Both Lys[50] and aLac[51] can also be found in circulation. ThT assay and high-resolution TEM were used to assess IAPP aggregation and fibril remodeling, and a viability assay with HUVECs was performed to evaluate the toxicities of fresh IAPP and IAPP amyloids in the presence of the model proteins. Specifically, co-incubated with IAPP peptides at a 1:1 molar ratio, Lys inhibited IAPP aggregation with no visible fibril formation while aLac induced amorphous aggregation containing significant β-sheet content. TEM imaging revealed that both aLac and Lys bound mature fibrils and binding of aLac led to fibril softening. Surprisingly, the cell viability study indicated that Lys enhanced but aLac reduced the cytotoxicity of IAPP

peptides, whereas binding of either Lys or aLac with mature IAPP fibrils mitigated the fibril toxicity.

This controlled *in vitro* study has revealed the polymorphic nature of intermediate IAPP aggregation species in addition to the contrasting effects of proteins and lipids on IAPP amyloidogenesis, fibril remodeling and cytotoxicity, depending on the physicochemical properties as well as the relative concentrations between the proteins and IAPP peptides – pointing to a natural defense mechanism of biological systems in mitigating the toxicities elicited by amyloidogenic species.

2.3. Results and discussion

2.3.1. Profiling IAPP fibrillization species and their associated toxicity in vitro

2.3.1.1. Characterization of IAPP intermediate species

Kinetic fluorescence-based studies of IAPP aggregation can indicate increasing β-sheet content over time but do not provide information about aggregate species morphology, particularly which populations are dominant at a given point in time. This study utilized TEM to characterize the formation of nonfibrillar IAPP aggregates, with regards to their size and morphology, during amyloidosis in a controlled environment. When monomeric IAPP was applied to aqueous solution at room temperature, nonfibrillar, globular aggregates were initially generated (**Fig. 2A**; 30 min) but a transition to fibrillar species was observed after 2 h of incubation, concordant with ThT assays of IAPP fibrillization kinetics (**Figs. 4A & 5A**). Non-fibrillar aggregates were gated into four categories based on their morphology: spherical, annular, biannular and complex aggregates (**Fig. 2B**). Spherical aggregates averaged around 22 nm in diameter, with annular and biannular species doubling in size to 44 nm and 48 nm respectively. Complex aggregates exhibited the broadest range of species, averaging a diameter of 63 nm, though the diametric variation of spherical species represented the largest proportional standard deviation (± 10 nm). Interestingly, some larger (100-400 nm) species with complex surface structure were observed across multiple timepoints at both 4 ºC and RT, potentially corresponding to off-pathway amyloid 'particulates'[52] (**Fig. S1A**). Given the extensive and heterogeneous population of oligomers predicated by secondary nucleation in

amyloidosis,[18] reports of oligomer formation *in vitro* with regards to size have varied – one review defines oligomers as smaller than 50 nm, generally consisting of under 50 misfolded monomer units.[52] Sedimentation velocity experiments have previously failed to detect IAPP oligomeric species under 100 units associating with mature fibrils, positing that IAPP intermediates form larger structures than those observed for Aβ1-42.[53] Indeed, the observation of aggregates > 50 nm here supports this hypothesis, and further investigation *in vivo* will determine if endogenous IAPP aggregates pertain to an analogous profile.

Annular oligomers, pertaining to 'doughnut' or 'cylinder-like' morphologies, have been previously reported for IAPP in addition to a number of amyloidogenic[54-55] and artificially

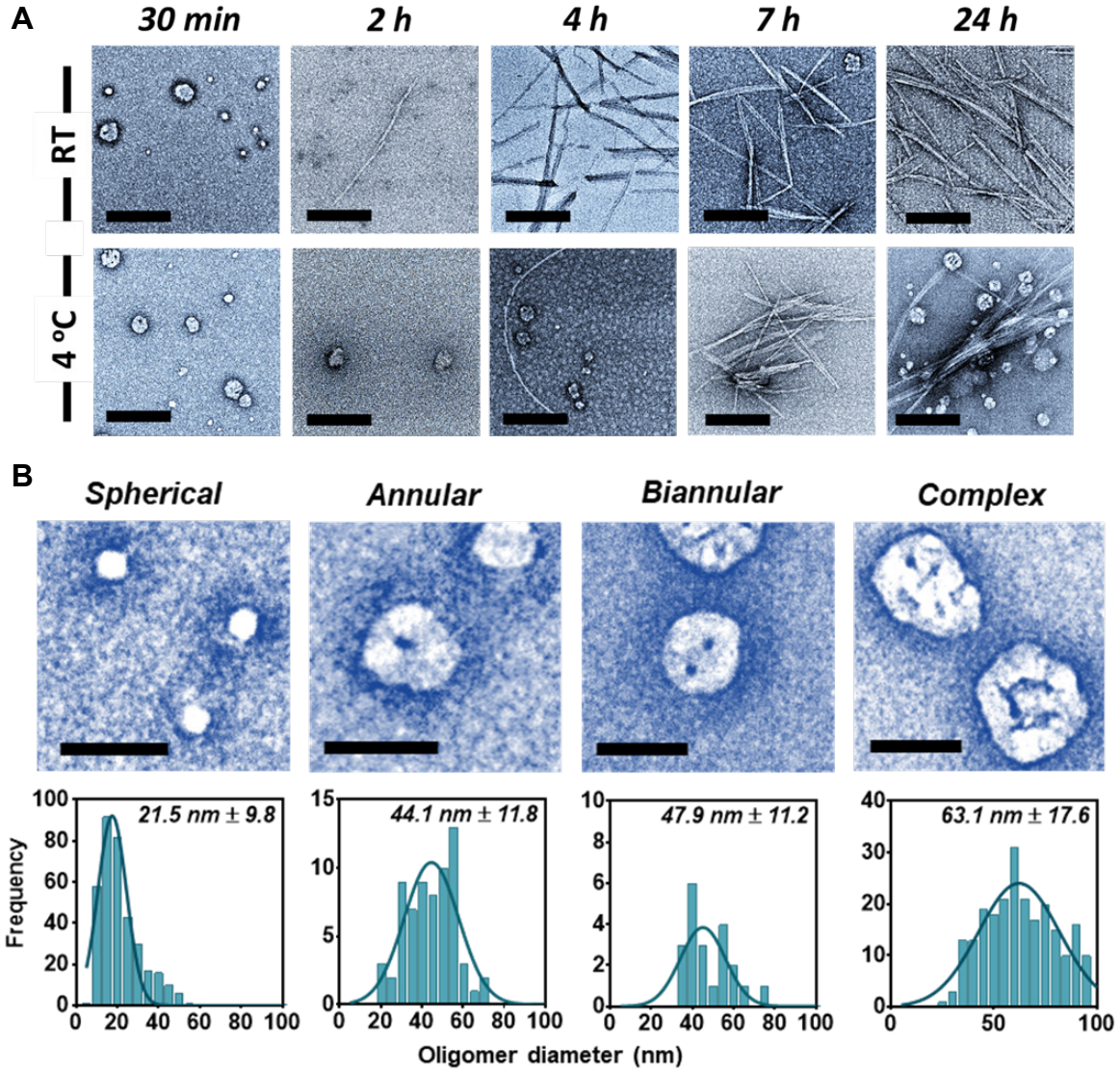

Figure 2. Characterization of IAPP intermediate aggregates by TEM. A: Fibrillization of IAPP (25 μM) in aqueous solution over time at either RT or 4 °C. Scale = 200 nm. B: Identification of different aggregate morphologies and corresponding diametric analysis. Scale = 50 nm.

fibrillated[56] species under various conditions. Previous *in vitro* studies of annular IAPP oligomer formation have either been investigated in a surface-mediated context, i.e. at a lipid membrane interface,[55] or omitted their morphological characterization.[57] Herein annular oligomeric IAPP is characterized *in vitro* in the absence of lipid membrane catalyzation. The presence of annular structures is in line with the observance of so-called 'β-barrel' oligomers,[15] which are purported to instigate pore formation when interfaced at the cell membrane and thus contribute to amyloid-associated pathologies. The low sample size of these morphologies in the population, comparative to spherical and complex aggregates (see section 2.5.3.1, Materials and Methods) correlates with the low abundance of β-barrel species within an aggregate population predicted by computational studies, estimated to comprise less than 10% of aggregates.[15] Biannular oligomers, to the candidate's knowledge, have not been previously reported elsewhere. Oligomerizing Aβ1-42 generated a few biannular oligomers by 24-28 hours (**Fig. S1B**), implicating these structures are not unique to IAPP.

Ultimately, the lack of nonfibrillar aggregate populations by 24 h at room temperature (**Fig. 2A**; RT), where fibrillar species overwhelmingly dominate, likely indicates that the observed aggregate morphologies are on-pathway species, given the saturation point of IAPP fibrillization is reached within several hours in aqueous solution at room temperature.[58] The wealth of diversity of IAPP intermediate species revealed in this study potentiates that a thorough, fine-grained approach to their characterization in further studies could provide further insight into computational and theoretically predicted amyloid aggregation mechanics.

Finally, reducing the environmental temperature to 4 ºC favored the production of lower-order aggregate species (**Fig. 2A;** 4 ºC), extending the observable 'lag' period of amyloidosis up to 7 h before fibrillar aggregates were observed as the majority population. These observations are concordant with the energy landscape for amyloidosis: specifically, that a reduction in temperature and thus a reduction in the kinetic energy facilitating intermolecular interactions between lower-order oligomeric species limits their further transition into mature fibrils. Though detailed methodologies for the preparation of different pathway species of Aβ have been published,[59-60] efforts to generate discrete populations of IAPP aggregates have often relied on the introduction of a foreign stabilizing agent.[61] Pre-incubating IAPP at a low temperature thus presents a facile, practical approach for curating intermediate populations.

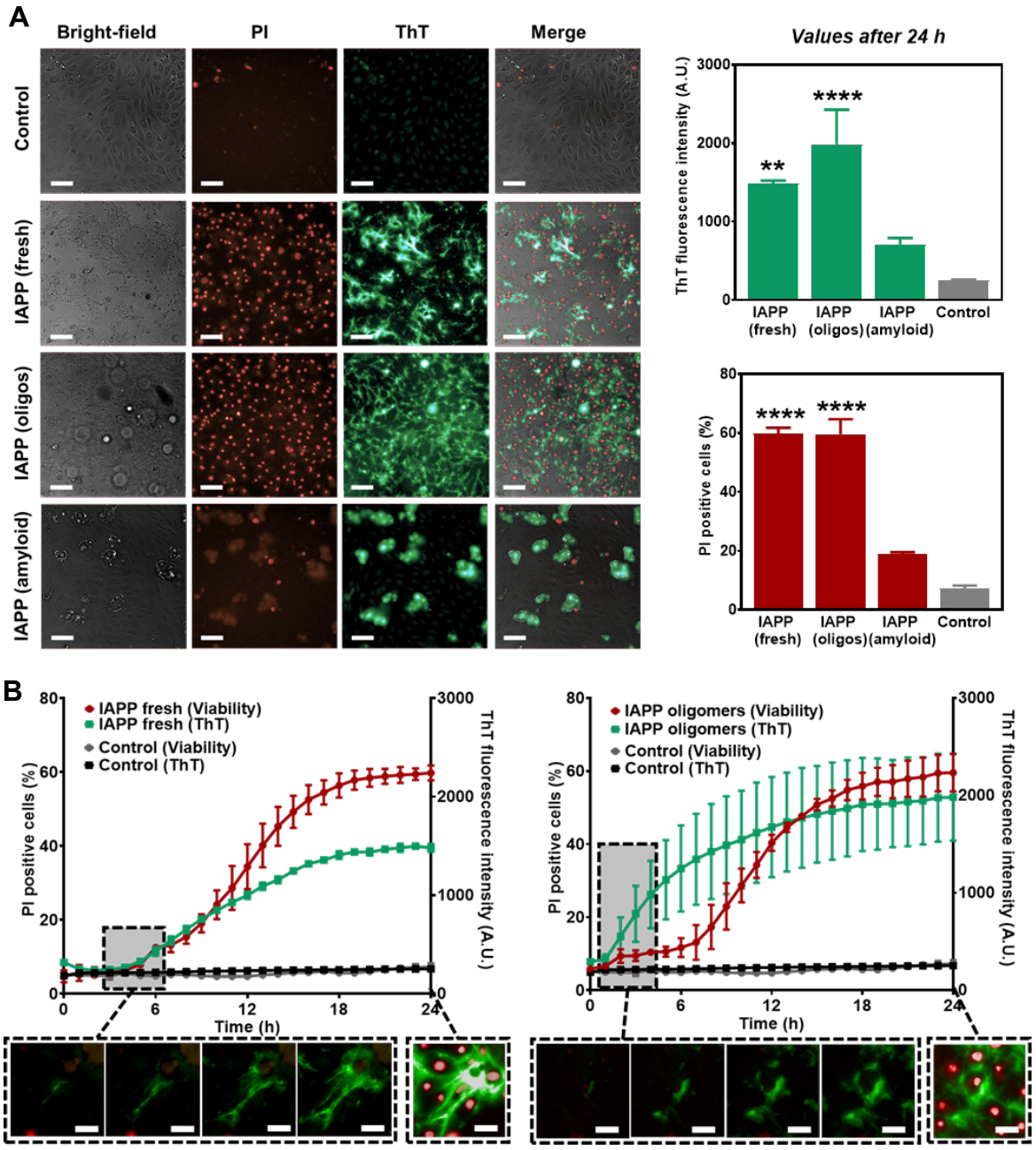

Figure 3. Visualizing and quantifying *in vitro* fibrillization and cytotoxicity of IAPP species. A: Fluorescence microscopy of IAPP species (25 μM), either fresh (lyophilized monomers), oligos (low order aggregates, pre-incubated for 4 h in aqueous at 4 °C) and amyloid (mature fibrils, pre-incubated for ~2 weeks in aqueous at room temperature) incubated with HUVECs after 24 h. Propidium iodide (PI) indicates dead cell nuclei, and the formation of β-rich amyloid is probed by thioflavin T (ThT), as then quantified in the right-hand panels. Scale = 100 μm. Statistical significance, as calculated by a 2-way ANOVA with Tukey's correction, is comparative to control: ** $p < 0.01$, **** $p < 0.0001$. Error bars represent standard error of mean (SEM), n = 3. B: Fibrillization of fresh and oligomeric IAPP over 24 h demonstrating the kinetic profile of endpoint data seen in A, i.e. β-rich amyloid formation (ThT fluorescence intensity) juxtaposed against cell death (PI positive cells) over time. Scale = 25 μm.

2.3.1.2. Cytotoxicity and fibrillization kinetics of IAPP species in primary endothelial cells

Given the diversity of IAPP pathway species able to be generated, the impact of different populations on *in vitro* primary cell viability and how it correlates with IAPP fibrillization over time was assessed. Fibrillating IAPP species were delineated as 'fresh' IAPP, i.e. lyophilized, monomeric IAPP directly dissolved into solution, and 'oligomeric' IAPP, i.e. majority-intermediate populations generated through the pre-incubation of IAPP in aqueous solution for 4 h at 4 ^{o}C, in addition to non-fibrillating, mature IAPP amyloids (at least one week old to eliminate oligomers and protofibrils). ThT was utilized as a probe for the generation of β-sheet rich aggregates, indicative of amyloid fibrillization (**Fig. 3**, in green). Both fibrillating IAPP populations demonstrated a significantly increased ThT fluorescence by 24 h comparative to the control (**Fig. 3A**), each displaying a prototypical sigmoidal increase in fluorescence over time (**Fig. 3B**). Though endpoint ThT fluorescence was conserved across the populations, notable differentiation was observed in their kinetic profiles. 'Fresh' IAPP underwent a lag phase of 5 h before progressing to exponential aggregation, and finally achieving saturation at ~18 h; contrastingly, oligomeric IAPP had a lag time of only 1 h, reaching saturation by approximately 16 h. As IAPP intermediate populations pertain to amyloid 'seeds' that can be utilized to propagate fibril growth and initiate the nucleation of further seed aggregates (**Fig. 1**), the unfavorable energetics of the lag phase were more readily overcome, allowing the IAPP oligomer samples to proceed more rapidly into the saturation phase compared to IAPP monomers. As expected, mature IAPP amyloid, in the absence of nucleating 'seeds', did not undergo further fibrillization, and maintained a steady fluorescence value of ~600 AU over 24 h (**Fig. S2A**). Though multiple ThT-labeled plaques are clearly visible in solution (**Figs. S3 & 3A**), statistical analysis did not deem the overall fluorescence significantly differentiated from background levels, potentially due to some free-floating aggregates not interfacing with cells at the analysis focal plane.

Membrane-impermeable propidium iodide (PI) traffics to the nucleus upon disruption of the cell membrane and complexes with fragmented DNA as an indicator of cell apoptosis (**Fig. 3**, in red). Overall, fibrillating species, i.e. fresh and intermediate populations, elicited the most toxic effect *in vitro*. IAPP amyloid did not display evolving cytocidal action on HUVECs over 24 h, maintaining a consistent value of PI-positive cells at 15-20% of the population (**Fig. S2**), found significantly differentiated to the untreated cells in the ThT- control group (**Fig. S2A;** $p < 0.05$ by two-way ANOVA). Fibrillating IAPP species, on the other hand, were highly

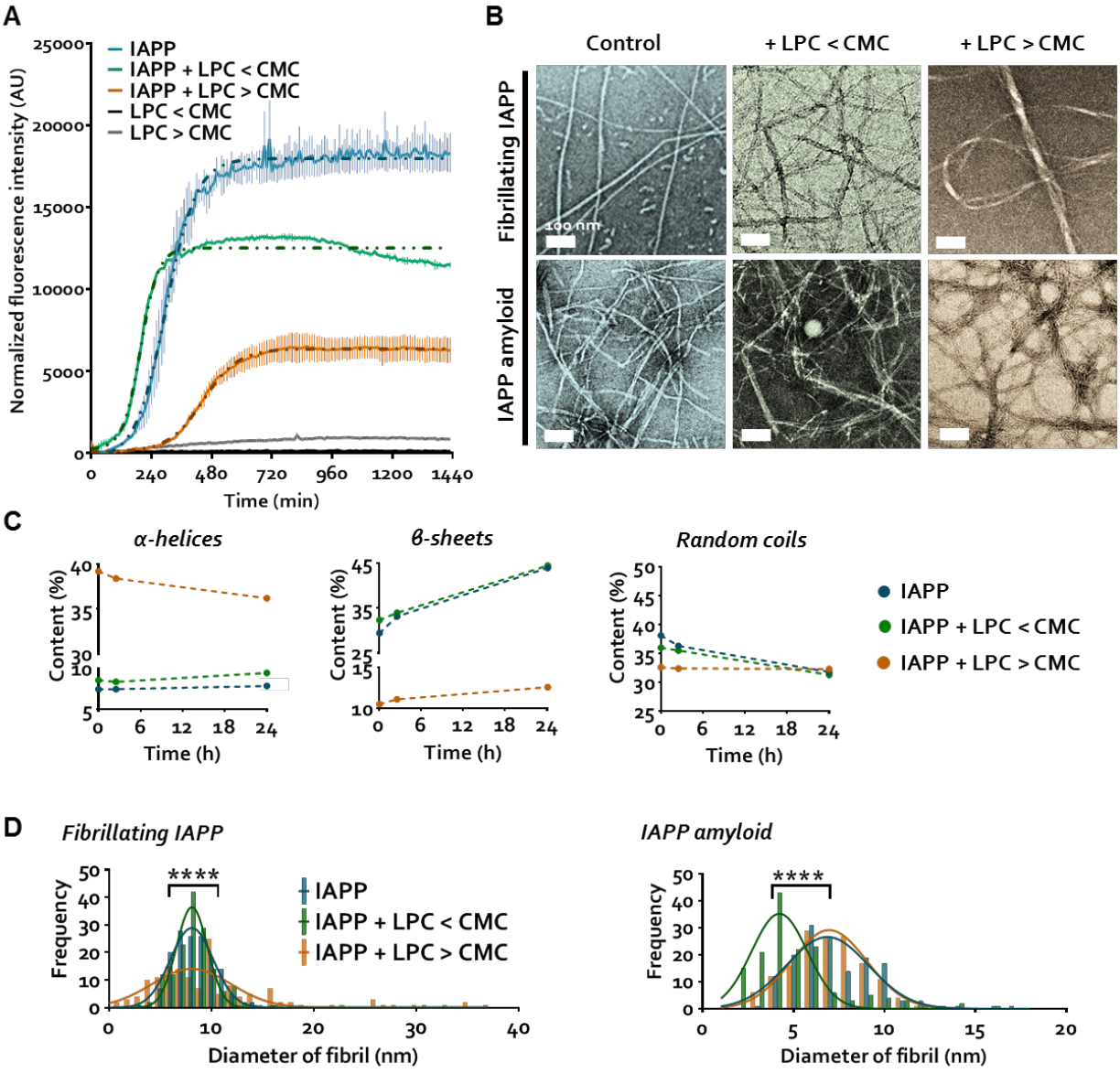

Figure 4. Effects of micellar (> CMC) and non-micellar (< CMC) LPC on IAPP fibrillization and amyloid remodeling. Concentrations of IAPP (25 μM), LPC < CMC (25 μM) and > CMC (2 mM) were fixed in all experiments. (A) ThT fluorescence assay of IAPP and LPC alone (both above and below the CMC) or as mixed samples, with sigmoidal least-squares fit (dotted lines); error = SEM. (B) TEM imaging of IAPP and IAPP amyloids after 24 h incubation with or without LPC, scale = 100 nm. (C) IAPP secondary structures in the presence and absence of LPC as determined through circular dichroism spectroscopy. Lines are intended to guide the eye. (D) Diameter frequencies of IAPP amyloid fibrils with Gaussian least-squares fit, ****$p < 0.0001$ (*one-way ANOVA, n = 100*). Reproduced with permission from Xing, Pilkington *et al.* 2017.[44]

deleterious, and appeared to seed and propagate along the cell membranes, accumulating for several hours prior to the death of the associated cells (**Fig. 3B**, images). Interestingly, monomeric IAPP appeared to form more concentrated deposits comparative to a more even distribution of the IAPP intermediate population across sampled areas (**Fig. 3A**, images), highlighting the role of cell membranes in accelerating amyloid fibrillization of localized aggregating species. Given that preformed seeds may not necessarily permeabilize the cell membrane,[57] the fibrillization of IAPP intermediate populations herein potentially represents a balance between surface-assisted nucleation at the interface of the intermediate species themselves (i.e., secondary nucleation) in addition to at the lipid cell membrane.

Assessing cell death over time rather than taking an endpoint value allowed the kinetics of IAPP-associated cytotoxicity to be visualized and compared between species. Accordingly, though fibrillization progressed more rapidly for the preincubated oligomeric IAPP, cell death kinetics were conserved between fresh IAPP and IAPP oligomers (**Fig. 3B**), with exponential death rates reached ~ 6 h post IAPP-exposure and both stabilizing at around 60% by ~ 18 h. The good correlation between IAPP fibrillization and cell death, particularly with regards to 'fresh' IAPP, leads further credence to membrane disruption as a major mechanism of IAPP-induced cytotoxicity – indeed, previous studies have demonstrated that monomeric IAPP elicited the largest shift in membrane fluidity in pancreatic β-cells *in vitro* comparative to oligomeric and mature amyloid IAPP.[62] Conversely, for oligomeric IAPP, as a mixed population of complex intermediate species (**Fig. 2**), the mechanisms of its elicited cytotoxicity at the cell membrane may be similarly diverse. Pore formation, 'lipid stripping' and physical perturbation have all been proposed as mechanisms of amyloid-associated cytotoxicity at the interface of lipid membranes,[24, 26, 30-31] as facilitated by different aggregate species:[63] accordingly, intermediate population demographics[15] likely determine which mechanism predominates. For example, preformed annular oligomers of αSyn and Aβ elicited less membrane permeabilization than spherical aggregates, though the effect of IAPP annular species was not reported.[57] Consequently, the generation of intermediate species under different conditions may have different roles in IAPP-associated pathologies, in particular given the propensity for extra-pancreatic translocation of toxic IAPP species, and merits further investigation *in vivo*.

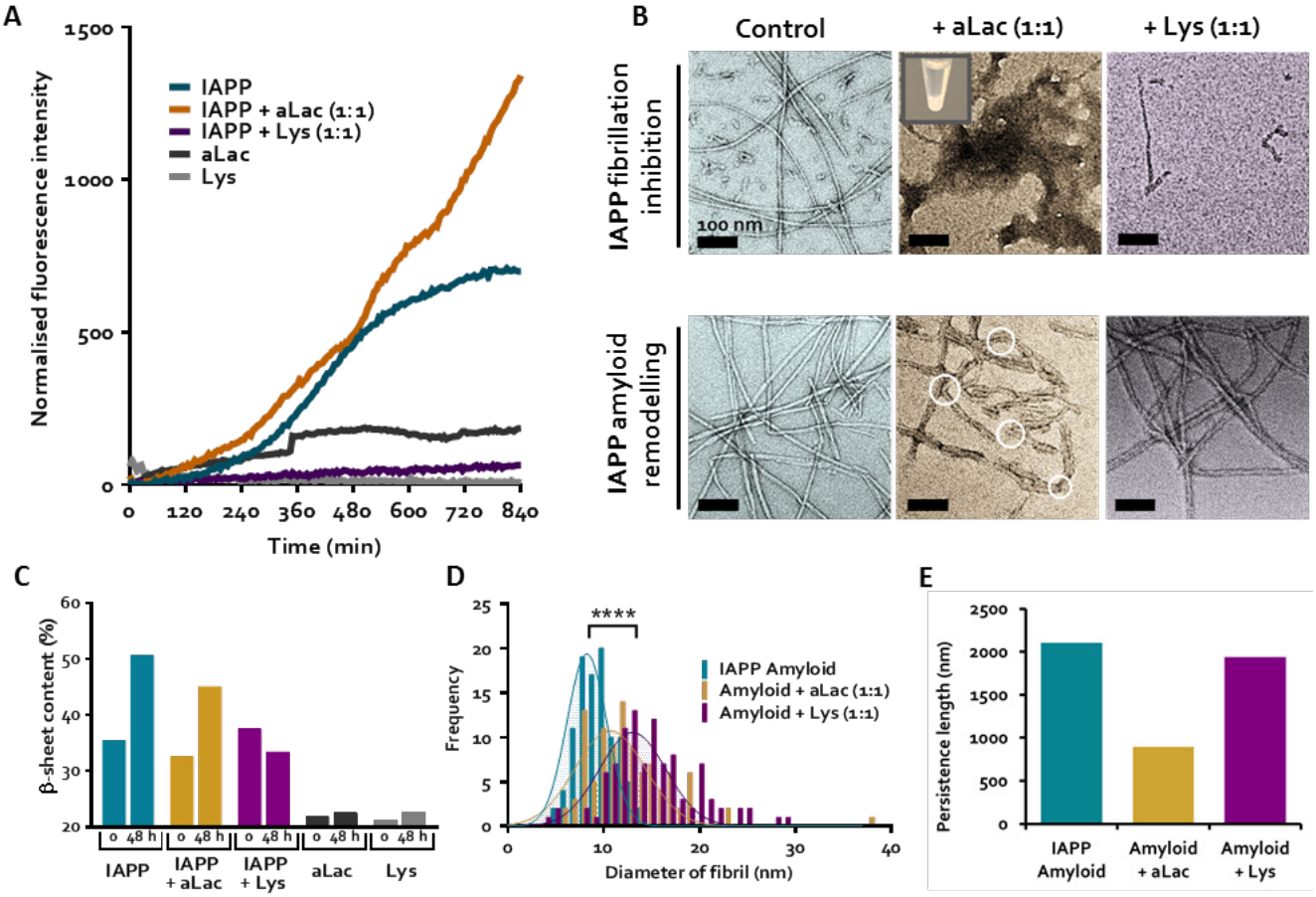

Figure 5. IAPP fibrillization inhibition and amyloid remodeling by lysozyme (Lys) and α-lactalbumin (aLac). (A) Thioflavin T (ThT) fluorescence assay shows IAPP fibrillization in the presence of Lys and aLac over 14 h. (B) TEM images of IAPP fibrillization inhibition (upper panel) and IAPP amyloid remodeling (lower panel) mediated by Lys and aLac at a 1:1 molar ratio after incubation in Milli-Q water for 24 h at 25 °C. Formation of a visible IAPP-aLac precipitate (upper middle panel, inset) and soft aLac-amyloids (lower middle panel, white circles) are shown. Scale = 200 nm. (C) Circular dichroism (CD) shows β-sheet content of IAPP in the presence of aLac and Lys, in addition to aLac and Lys controls, over 48 h. (D, E) Analysis of IAPP amyloid fibril diameter (D) and persistence length (E) in the presence or absence of Lys and aLac. IAPP concentration = 25 μM for all experiments. **** $p < 0.0001$ *(unpaired t-test, n = 100).* Reproduced with permission from Pilkington *et al.* 2017.[43]

2.3.2. Biophysical characterizations of protein and lipid binding on IAPP aggregation and fibril remodeling

2.3.2.1. Effects of LPC binding on IAPP fibrillization and remodeling

Biophysical characterizations revealed the differential effects of micellar and non-micellar LPC on IAPP fibrillization, and additionally, their capacities in remodeling of mature IAPP amyloids (**Fig. 4**). Native fibrillization of IAPP, which formed semi-flexible amyloid fibrils in aqueous solution over 24 h, was notably inhibited by micellar LPC (**Fig. 4B**). ThT fluorescence indicated a reduction in the β-sheet content formed by IAPP in the presence of micellar LPC by 24 h, compared to the IAPP control (**Fig. 4A**). Non-micellar LPC induced a lag time of only ~10 min and the saturation point was reached ~2 h before the IAPP control. This effect has also been observed with Aβ, where LPC below the CMC was capable of reducing the fibril lag and elongation times of Aβ1-42, yet showed no notable increase in fibrillization after saturation was reached in each case.[64] Anionic non-micellar lipids, including SDS[65] and lysophosphatidic acid (LPA),[66] have demonstrated the capacity to promote fibrillization and fibril elongation of β_2-microglobulin (β2M) at a neutral pH, though zwitterionic LPC did not mediate any significant effect.

The interaction of micellar LPC with IAPP, in contrast, greatly reduced IAPP fibrillization, both in terms of fibrillization kinetics and overall amyloid formation by 24 h. CD spectroscopy revealed the transition of peptide secondary structure from random coils to β-sheets over 24 h (**Fig. 4C**). In the presence of non-micellar LPC, an increase in β-sheet content of ~15% was observed for IAPP by 24 h, while the α-helical content (< 10%) showed negligible variations over the experimental period. In contrast, interactions of IAPP with LPC micelles induced an immediate transition from β-sheets to α-helices (39.2%). Within the IAPP-LPC micelle complex, IAPP random coils remained stable over 24 h (~ 33%). In contrast, Patil *et al.* observed that upon complexation with SDS micelles, IAPP residues 5-28 were present in the α-helical conformation, with residues 5-19 embedded in the hydrophobic core, and the known amyloidogenic region (residues 20-29) positioned on the surface of the micelle at the lipid-solvent interface.[25]

Given the limited capacity for inter-peptide interactions between micelle-bound IAPP, disruption of IAPP fibrillization is expected. Indeed, visualization of IAPP amyloid fibrils after 24 h in aqueous solution demonstrated significant structural polymorphism of IAPP fibrils in

the presence of micellar LPC by TEM imaging (**Fig. 4B**) and subsequent analysis of fibril diameter (**Fig. 4D**). Large, braided amyloid fibrils larger than 30 nm in diameter were observed (**Fig. 4B**), displaying a significantly broadened distribution compared with the IAPP control or IAPP treated with non-micellar LPC (Fig. 4D), though fewer fibrils were seen. The fibrils appeared softer, with a persistence length of 458 ± 13 nm based on FiberApp statistical

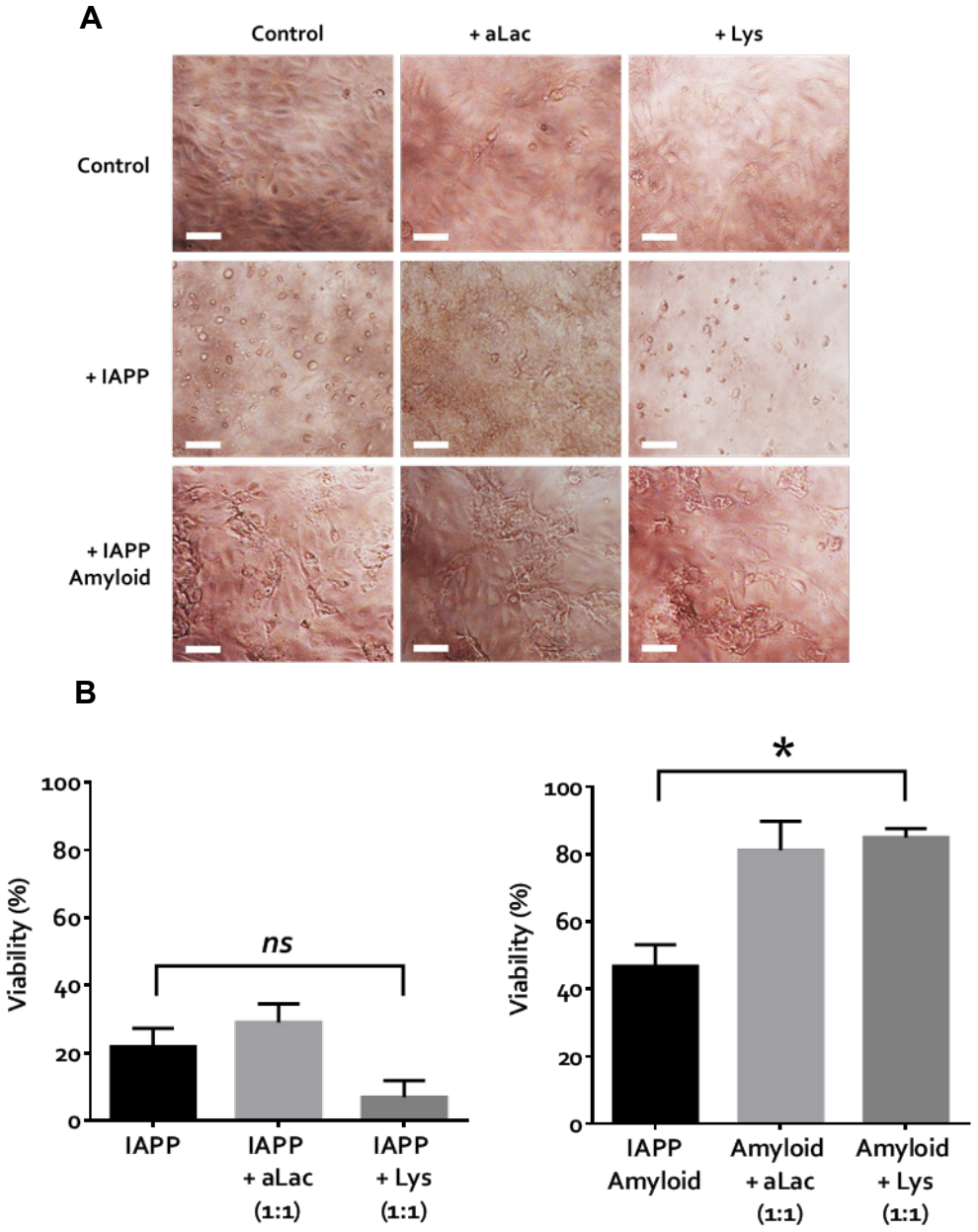

Figure 6. Viability of HUVECs exposed to 25 µM IAPP and amyloids in the presence of α-lactalbumin (aLac) and lysozyme (Lys) after 24 h. (A) Bright-field images reveal extensive cell death in the presence of fibrillating IAPP, and some loss of cells with IAPP amyloids. (B) The calcein-AM viability assay demonstrates high toxicity of IAPP (left) and, to a lesser extent, IAPP amyloids (right). Significant mitigation of toxicity in amyloids was observed when pre-treated with aLac and Lys. *Scale* = 25 µm*; * $p < 0.05$ (one-way ANOVA, $n = 3$)*. Reproduced with permission from Pilkington *et al.* 2017.[43]

analysis,[67] compared with that of 2,885 ± 60 nm for the IAPP control.[68] Below the CMC, LPC remodeled amyloid fibrils into filaments of thinner width (**Fig. 4D**). Micellar LPC (**Fig. S4**, 4-5 nm in size) did not remodel pre-formed fibrils, but similarly to their effect on fibrillating IAPP, individual fibrils were observed to closely associate, belying the 'glue-like' effect of LPC micelles on mature amyloids. The strong LPC-fibril binding suggests that LPC could coat the fibril and bundle multiple fibrils into a braided structure as observed in TEM (**Fig. 4B**). This can also explain the slightly reduced ThT intensity but increased β-sheet content observed for IAPP fibrillization in the presence and absence of LPC < CMC (**Fig. 4A** vs. **4C**, middle panel), as the strong binding of LPC monomers onto IAPP fibrils and protofibrils would sterically hinder ThT dye from binding thereby reducing its fluorescence. Concordantly, the combined ThT, CD and TEM results suggest that unimolecular LPC accelerated IAPP binding.

2.3.2.2. ThT and CD assay quantifications of IAPP fibrillization inhibition by proteins

IAPP, aLac and Lys were incubated with the amyloid-sensitive ThT dye to quantify the rate and kinetics of IAPP fibrillization over 14 h (**Fig. 5A**), in addition to visualizing change in protein secondary structure up to 48 h through CD spectroscopy (**Fig. 5C**). It was demonstrated that IAPP alone remained in the energetically unfavorable nucleation, or lag, phase up to 5 h, before entering the elongation phase, and by 14 h was within the saturation phase (**Fig. 5A**). This is in turn was complemented by an increase of IAPP β-sheet content from 35.4% at 0 h to 50.7% after 48 h (**Fig. 5C**), indicative of increasing prevalence of β-sheet rich amyloid species.

The secondary structure of IAPP mixed with aLac showed analogous increase in β-sheets to the IAPP control after 48 h (**Fig. 5C**), which was not complemented in aLac in the absence of IAPP. Comparative to IAPP alone, however, IAPP-aLac did not show evidence of sigmoidal fibrillization, and the increase in ThT fluorescence followed a more linear trend (**Fig. 5A**). IAPP-aLac also attained the largest increase in ThT fluorescence overall, indicating a promotional effect of aLac on IAPP aggregation. The non-sigmoidal fibrillization trend, however, was consistent in all experiments, with the combined intensity and kinetics observations therefore suggesting formation of unstructured, amorphous IAPP aggregates in the presence of aLac. In contrast, complete inhibition of IAPP was observed in the presence of Lys over the 14 h sampling period for ThT (**Fig. 5A**); concordantly, no increase in percentage of IAPP β-sheet structure in IAPP:Lys was seen after 48 h (**Fig. 5C**). Each protein consequently mediated opposing effects on IAPP fibrillization, both in terms of β-sheet content and kinetic behavior.

2.3.2.3. High-resolution TEM imaging of IAPP fibrillization inhibition and remodeling by proteins

TEM imaging was performed to complement ThT analysis through visualization of the aggregation products (**Fig. 5B**, upper panel), and also to examine IAPP amyloid remodeling mediated by aLac or Lys (**Fig. 5B**, lower panel). The TEM images were further analyzed with statistical software to determine the morphological and mesoscopic changes of mature IAPP amyloid fibrils incubated with aLac or Lys, including fibril diameter (**Fig. 5D**) and persistence length (fibril stiffness) (**Fig. 5E**).

By 24 h incubation of IAPP alone, both long fibrils and smaller protofibrillar aggregates appeared (**Fig. 5B**, upper panel). Neither of these structures were observed in the presence of aLac or Lys, however. Specifically, IAPP fibrillization was completely inhibited by Lys, with only a few small, worm-like structures present after 24 h. Electrostatic repulsion between the positively charged IAPP and Lys likely compromised IAPP-IAPP interactions. In comparison, the IAPP-aLac mixture was mainly present as large amorphous aggregates after 24 h, which were also observed as off-white precipitates in solution (**Fig. 5B** upper panel, inset). Based on the ThT assay (**Fig. 5A**), the amorphous aggregates were significantly β-sheet rich. Considering the opposing charges of IAPP and aLac, it is likely that electrostatic attraction with aLac strongly perturbed IAPP self-assembly into fibrils, while favored formation of amorphous structures. Alternatively, formation of non-fibrillar species has been observed in both IAPP and Aβ amyloidogenesis when monomers interact with hydrophobic surfaces.[69-70] This suggests that IAPP-aLac could act as a seed, promoting contact between monomeric or low-order oligomeric IAPP species, yet directing aggregation off-pathway.

Mature IAPP amyloids formed by IAPP alone after 30-60 days of incubation were long and semi-flexible (**Fig. 5B**, lower panel). The presence of some shorter species is attributed to the cross-linking and subsequent gelation of mature IAPP amyloids,[71] which can result in some fibril breakage during pipetting from the stock. Statistical analysis of these fibrils revealed an average diameter of ~ 8.9 nm (**Fig. 5D**) and an average persistence length of ~2,100 nm (**Fig. 5E**). When incubated with aLac and Lys, IAPP amyloids underwent remodeling, as indicated by changes in fibril diameter and morphology compared to IAPP amyloids alone (**Fig. 5B**, lower panels). Both aLac and Lys interacted with the fibrils, mediating a significant shift in average fibril diameter (**Fig. 5D**) from approximately 9 nm (IAPP amyloid control) to 12 nm (aLac) and 15 nm (Lys), correspondingly. Interestingly, interaction with aLac halved the

persistence length of amyloid fibrils (**Fig. 5E**) indicating significant fibril softening, while no difference was seen in IAPP stiffness with Lys binding.

The endogenous inhibition of Aβ1-40 fibrillization mediated by several non-chaperone proteins, including aLac and Lys, has been previously reported.[72] It was shown that fibrillization of the negatively charged Aβ was inhibited by aLac and Lys at a ~ 1:1 molar ratio, yet both proteins were unable to promote disaggregation of pre-formed Aβ fibrils. In the case of IAPP, although both aLac and Lys inhibited the fibrillization, aLac promoted the formation of large amorphous aggregates with significant β-sheet content while Lys prevented any formation of aggregates that could be detected by either ThT and TEM imaging. The differential impact on IAPP amyloid aggregation and remodeling of IAPP amyloids by aLac and Lys suggests that both electrostatic and hydrophobic interactions between proteins and IAPP can alter the intrinsic properties of IAPP amyloids. As such, it is likely that IAPP amyloids can facilitate interactions with a multitude of components in the environmental milieu. Formation of a 'protein corona'[73-74] on IAPP amyloids *in vivo* is likely to have a significant effect on IAPP amyloid toxicity, and merits further investigation.

2.3.3. Effects of protein binding on the viabilities of fresh IAPP and IAPP amyloids

Bright-field imaging (**Fig. 6A**) showed healthy control HUVECs as highly confluent and endothelial-like in morphology. Microscopic examination was additionally complemented by the calcein-AM assay (**Fig. 6B**) for quantitative measurement of cell viability against an untreated control. Large-scale cell damage and death was observed with IAPP, regardless of the presence or absence of aLac or Lys (**Fig. 6A**, middle row). Viability data (**Fig. 6B**, left panel) for IAPP (22% viability), IAPP-aLac (29%) and IAPP-Lys (7%) further demonstrated that aLac and Lys, though capable of inhibiting IAPP fibrillization, had no mitigating effect on the peptide toxicity. In fact, the IAPP-Lys mixture showed notably higher toxicity in HUVECs compared to IAPP alone, suggesting that Lys binding might increase the half-life of toxic low-order IAPP species towards eliciting further damage to exposed cells (**Fig. 5**). The reduced toxicity of IAPP-aLac mixture was likely due to the fact that the formed amorphous aggregates were very large and precipitated (**Fig. 6B**, IAPP-aLac inset), reducing their exposure and subsequent toxic effects to cells.

Interestingly, different phenomena were observed when aLac and Lys were incubated with IAPP amyloids. Large deposits of mature amyloid aggregates were seen with each condition (**Fig. 6A**, lower row); however, extensive cell destruction, as visualized with IAPP, was not present. In amyloid-aLac and amyloid-Lys, healthy cells were observed. This effect is corroborated by the viability data (**Fig. 6B**, right panel); the relatively lower level of toxicity mediated by IAPP amyloids (47% viability) was significantly reduced in the presence of both aLac (81% viability) and Lys (85% viability). Therefore, these results suggest that the formation of aLac or Lys 'corona' on the amyloid fibril surface likely screened the amyloid-cell interactions and thus reduced the low levels of amyloid fibril-induced cytotoxicity.

2.4. Conclusions

It is often said that one is a product of their environment. Collectively, these studies aimed to elucidate the behavior of IAPP fibrillization species within a model environment, and how representative lipids and proteins therein can impact the structure, morphology and induced cytotoxicity of these aggregation products, towards a more complete understanding of IAPP at the biological interface.

Amyloidosis, as a complex process with a variety of intermediate species produced in the exponential phase of fibrillization before fibrillar species dominate the saturation phase, is further complicated in the case of IAPP – given its rapid fibrillization in aqueous media, characterization of intermediate aggregates is challenging. A high-resolution electron microscopy-focused study into IAPP fibrillization within a controlled environment revealed a wide variety of intermediate aggregates, including spherical and annular morphologies prototypical of amyloidosis in various species,[54-56] but additionally biannular aggregates, revealing a new conformational morphology to be explored. Furthermore, monomeric and oligomeric IAPP demonstrated near-identical cytotoxicity profiles in primary endothelial cells *in vitro* regardless of the more rapid fibrillization kinetics of the intermediate population: potentiating that the known capacity of IAPP to mediate cytotoxic cell membrane disruption at the lipid interface is likely facilitated by diverse mechanisms, directed by proportions of different intermediate conformations adopted by IAPP in a given population. In a previous study, the candidate and co-workers explored the complex nature of IAPP fibrillization species and their associated toxicities.[62] It was demonstrated that fibrillating, stabilized oligomeric and

mature amyloid IAPP species played different roles in eliciting toxicity to pancreatic β-cells *in vitro*. This study supports this narrative with a different cell line and hence a different *in vitro* IAPP environment, and additionally provides new insight.

The uncovered phenomenon of IAPP aggregation inhibition by micellar LPC offers a new mechanism to the existing models of IAPP intracellular stabilization by insulin, low pH, metal ions,[2] or by zinc-C-peptide-IAPP complexation.[8] Unlike cell membranes and SDS micelles, which are net negatively charged, zwitterionic LPCs readily disperse in water as ultrasmall micelles which are then shown to interface with IAPP, subsequently inhibiting its aggregation. Some LPC species have been demonstrated to be five times more concentrated within β-cell secretory granules comparative to other cellular compartments – these are then downregulated 40-60% after glucose stimulation,[75] potentiating a connection between LPC abundance and IAPP activity. Consequently, these unique physicochemical characteristics exhibited by LPC may be crucial to IAPP stabilization *in vivo,* and could further advise the design and development of small molecules and nanoparticles against amyloidosis.

The binding of cationic IAPP to both cationic Lys and anionic aLac further illustrates the capacity for extracellular, circulating protein to differentially impact amyloid pathologies. Thousands of circulating proteins have been identified *in vivo*;[76] consequently, given the intrinsically disordered nature and high conformational flexibility of IAPP peptides, IAPP likely has the capacity to interface with numerous plasma proteins through electrostatic and hydrophobic interactions. Furthermore, depending on their physicochemical properties, proteins binding to IAPP may have drastically different effects on IAPP amyloidosis. For example, aLac and IAPP co-aggregated forming a large IAPP-aLac molecular complex driven by strong binding affinity and opposite charges. The large aggregates formed by IAPP and aLac mixture elicited low toxicity to HUVECs – Lys, on the other hand, could bind and stabilize IAPP intermediate species, where increased electrostatic repulsion prevented further aggregation of these clusters.[43] Stabilization of low molecular weight oligomers of IAPP by their associations with Lys resulted in increased toxicity of IAPP as toxic oligomers were transiently formed. Interestingly, protein binding of IAPP fibrils – i.e. formation of amyloid coronae – always reduced the relatively low toxicity of the fibril, suggesting a new mechanism for mitigating IAPP toxicity *in vivo*.

Despite the general binding of IAPP with globular proteins and the potential of proteins in promoting toxic IAPP species at comparable protein/IAPP concentrations, a crowded

environment with abundant globular proteins may inhibit the formation of IAPP oligomers. Interestingly, although not directly related to this study, it has been shown in the literature that whey protein α or β caseins, usually present in the form of micelles through mutual hydrophobic and electrostatic interactions, show a chaperone-like activity in inhibiting Aβ and insulin from aggregation through mechanisms not yet understood.[77-79] Conversely, however, IAPP has recently been shown to form toxic oligomers in plasma through interactions with glucose and low-density lipoproteins.[80] Further exploration is necessary to fully elucidate environmental proteins that may contribute to IAPP toxicity both in the pancreas and in circulation. Together, this new protein corona paradigm facilitates our understanding of the fate and transformation of IAPP *in vivo*, which may have consequential bearings on IAPP glycemic control and T2D pathology.

2.5. Materials and Methods

2.5.1 Materials

Human islet amyloid polypeptide (IAPP) (disulfide bridge: 2-7; MW: 3,906; 37-residue: KCNTATCATQRLANFLVHSSNNFGAILSSTNVGSNTY; > 95% pure by HPLC) was obtained as lyophilized powder from AnaSpec. Lysozyme (Lys) (from chicken egg white; MW: 14,300), α-lactalbumin (aLac) (calcium depleted, from bovine milk; MW: 14,178), and L-α-Lysophosphatidylcholine (LPC; from *Glycine max,* >99% pure by TLC) were purchased from Sigma-Aldrich. LPC derived from soybean is primarily composed of unsaturated C-18 fatty acids; typically, 40-60% linoleic, 25-30% palmitic, 10-12% oleic, 7-10% stearic and 4-6% linolenic acid. IAPP, aLac and Lys were weighed on a Cubis MSE balance (Sartorius, 0.01 mg resolution), dissolved in Milli-Q water (pH 6.5) to a concentration of 200 μM and used immediately for zeta potential, ThT, TEM and viability assay sample preparations. Pre-formed IAPP amyloids (30-60 days old in Milli-Q water, room temperature) were kept at a stock concentration of 200 μM. The stock solution of LPC was 16 mM in Milli-Q water. Thioflavin T (ThT) dye (Sigma) was dissolved in Milli-Q water to form a 250 μM stock solution immediately prior to use in ThT sample preparations unless otherwise specified. Calcein-AM (Sigma) and propidium iodide (PI) dyes (Thermo Fisher) were kept in a 1 mM stock solution in DMSO and 1.5 mM stock in water, respectively, and stored at -20 ºC.

2.5.2. Thioflavin T (ThT) assays

IAPP alone (25 μM) or in the presence of micellar (25 μM) and non-micellar (2 mM) LPC, aLac (25 μM) or Lys (25 μM), was mixed with 25 μM ThT dye in a black/clear bottom 96-well plate (Costar), with the remaining volume made up to 100 μL with Milli-Q water where necessary. ThT fluorescence (excitation: 440 nm/emission: 485 nm) was then read every 10 min for 24 h (144 time points) on an EnVision plate reader (Perkin Elmer) for IAPP-LPC studies, a Flexstation 3 plate reader (Molecular Devices) every 5 min for a total of 14 h (169 time points) for IAPP-protein studies (both at 25 ºC), and hourly on an Operetta High-Content Imaging System (Perkin Elmer) for 24 h (24 time points) at 37 ºC for IAPP characterization studies, as paired with an *in vitro* viability assay (see *Propidium iodide live-dead assay*, section 2.5.5.2). Error represents the standard error of mean of two (IAPP-LPC, IAPP-proteins) or three independent (IAPP characterization studies) experiments. Data was fit to a sigmoidal curve (least squares) using Prism (GraphPad) where required.

2.5.3. Transmission electron microscopy (TEM) and analysis

Carbon-coated formvar copper grids (400 mesh, ProSciTech) were glow discharged to promote hydrophilicity. A 10 μL aliquot of the sample to be imaged was placed on the grid and allowed to adsorb for 60 s. The remaining solution was then drawn off and the grid washed twice in 10 μL of Milli-Q water. The grid was then touched to 5 μL 1% uranyl acetate (in Milli-Q water), the solution immediately drawn off, and the grid then placed onto a 5 μL droplet of 1% uranyl acetate to stain for 15 s. Any remaining liquid was then drawn off and the sample allowed to dry. Grids were imaged using Tecnai TF20 (FEI), Talos L120C (FEI) and JEOL 2000FX transmission electron microscopes.

For IAPP characterization experiments, lyophilized monomeric IAPP (25 μM) was incubated in aqueous solution (PBS, pH 7) at either 4 ºC or room temperature for 24 h, with samples taken for imaging at 0 min (data not shown), 30 min, 2 h, 4 h, 7 h, and 24 h. Grids were not glow-discharged for these studies. For the experiments concerning IAPP and model interactors, IAPP, IAPP amyloids, aLac, Lys, monomeric LPC (25 μM; all materials 1:1 by mass) and micellar LPC (2 mM; IAPP:LPC = 1:40 by mass) were incubated in Milli-Q water at 25 ºC for 24 h prior to imaging.

2.5.3.1. Morphological and statistical analysis of IAPP species imaged using TEM

The size distribution profiles of IAPP aggregate species were generated using Digital Micrograph software (GMS3, Gatan), and Gaussian modelling of size distributions was applied in Prism (GraphPad, v. 7.01). For IAPP characterization experiments, lower order aggregates were gated into four distinct categories based on their morphologies – spherical (sphere shaped, no 'pores' or irregular structures), annular (pertaining to a singular pore), biannular (pertaining to two distinct pores), and complex (multipore, and/or demonstrating irregular globular structure). Size analysis was performed for each group, with sampling capped at 200 individual aggregates (spherical); for less common species, the sample pool was 126 (complex) 60 (annular) and 19 (biannular), respectively.

The distributions of fibril diameters for IAPP amyloids, IAPP-aLac, IAPP-Lys and IAPP-LPC were determined through randomly sampling > 100 points on the amyloid fibrils. Statistical significance was calculated via unpaired t-tests, utilizing the Holm-Sidak method for multiple comparisons, for protein binding experiments, and a one-way ANOVA with Tukey's correction was utilized for IAPP-LPC. Values wherein $p < 0.05$ were considered to be statistically significant.

The mesoscopic parameters of fibril persistence length (λ) and contour length (l) in the presence and absence of the proteins were analyzed with software FiberApp[67] by Dr. Aleksandr Kakinen. The FiberApp open-source code was developed from statistical polymer physics for the structural analysis of filamentous and macromolecular objects. The persistence length λ reflects the rigidity of a polymer and is mathematically defined via the bond correlation function (BCF) in 3D or 2D as the length over which angular correlations in the tangential direction decrease by a factor of e. Here the λ values of IAPP fibrils were estimated from the average values determined by the BCF, mean-squared end-to-end distance (MSED) and mean-squared midpoint displacement (MSMD) methods. The contour length corresponds to the end-to-end length of a polymer along its contour. The values of persistence length and contour length were obtained based on statistical analysis of 290 fibrils.

2.5.4. Circular dichroism (CD) spectroscopy

Experiments were performed on a Chirascan CD spectrometer (Applied Photophysics), with spectra read from 190-260 nm. Prior to sample loading, a baseline with no cuvette was run. 300 µL of 25 µM IAPP in Milli-Q water, alone or in the presence of LPC above (2 mM) and below (25 µM) the CMC, aLac (25 µM) or Lys (25 µM) was placed in a cuvette with a 0.1 cm pathlength and CD analysis was run at 0 h, 2.5 h and 24 h (LPC) or 0 and 48 h (aLac, Lys) time points after incubation at room temperature. Between samples, cuvettes were washed more than 5× with distilled water. Final spectra were an average of three reads, which were then normalized against background signal and, for IAPP:protein or IAPP:LPC samples, against individual protein/LPC controls at each respective timepoint. Data were then de-convoluted with CDNN software to give a final relative percentage content of secondary structure.

2.5.5. In vitro biological assays

2.5.5.1. Cell culture

Primary human umbilical vein endothelial cells (HUVECs), sourced from pooled donors and available commercially through Lonza, were seeded into a black/clear bottom 96 well plate (Corning) at a density of 1.0 x 10^5 cells/well in 200 µL EGM (Lonza) and incubated overnight (37 ºC, 95% humidity, 5% CO_2) or until 70-80% confluency was reached. Media was refreshed every 24-48 h during cell growth, with old media then removed before experimentation.

2.5.5.2. Propidium iodide live-dead assay

For IAPP characterization studies, 150 µL of media containing 1 µM propidium iodide (PI; Thermo Fisher) was added to wells and allowed to equilibrate with cells in the dark at 37 ºC, 5% CO_2, 95% humidity for ~ 30 min. IAPP stock solutions (200 µM) were mixed 1:1 with ThT (200 µM) and allowed to equilibrate before 50 µL of each sample was then added to each well to make a final volume of 200 µL (final concentration IAPP and ThT = 25 µM). 'Fresh' IAPP was lyophilized monomers dissolved directly into solution; IAPP 'oligos' was lyophilized monomers pre-incubated at 4 ºC for 4 h with gentle shaking; IAPP amyloid was lyophilized monomers pre-incubated for > 1 week at room temperature. The plate was then imaged on an Operetta High-Content Imaging System (PerkinElmer) at 37 ºC, 5% CO_2, 95% humidity for

24 h, with 5 readings at regions of interest in each well taken with a 20× lens every hour. PI was read at 535 nm excitation/617 nm emission, and 430 nm excitation/460-480 emission was utilized for ThT (refer to *Thioflavin T (ThT) assays,* section 2.5.2).

2.5.5.3. Calcein-AM viability assay

The calcein-AM live cell assay was used to provide quantitative data on cell viability. Calcein-AM is a colorless dye in aqueous solution, but fluoresces brightly in the green spectrum when cellular esterases cleave off the AM group. IAPP, IAPP amyloids, aLac and Lys (100 μM) were incubated in Milli-Q water for 24 h at 25 ºC prior to addition to cells. Media was refreshed and pre-incubated IAPP, IAPP amyloids, aLac and Lys were added to final concentrations of 25 μM. For control cells, an equal volume of Milli-Q water was added to each well. Samples were added to wells in triplicate and incubated for 24 h (37 ºC, 95% humidity, 5% CO_2). Bright-field images were taken prior to calcein-AM viability testing with a Nikon TS100 bright-field microscope, equipped with a DS-Fi1 CCD camera (Nikon) and Digital Sight software (Nikon). Media was then aspirated from wells, cells were gently washed 3× in warm HBSS (Gibco), and 100 μL aliquots of 2 μM calcein-AM dye in HBSS were added to each well. The dye was incubated with cells for 30 min at 37 ºC before endpoint fluorescence was read (excitation: 485 nm/emission: 538 nm) on a Flexstation 3 plate reader (Molecular Devices). Though lysozyme is capable of non-specific esterase activity,[81] a separate control confirmed the fluorescence of calcein-AM was not affected.

2.5.5.4. Statistical analysis

All data were analyzed using Prism (GraphPad, v. 7.01), with values considered statistically significant if $p < 0.05$.

For the PI live-dead assay, PI positive cells were calculated within sampling areas as an estimate of total well counts from total cell count vs PI-positive nuclei, utilizing digital phase contrast mapping to define nuclear and cell boundaries. A two-way ANOVA was performed utilizing Tukey's correction for multiple comparisons to compare cytotoxicity elicited by IAPP species at 24 h, and unpaired t-tests were performed (24 h timepoint) using the Holm-Sidak method for multiple comparisons to confirm the presence of ThT did not impact overall viability of control and IAPP-treated cells (refer to **Fig S2**).

For the calcein-AM viability assay, percentage viability of cells was calculated through direct comparison of calcein-AM fluorescence intensity with control cells (100% viable) after correcting for background fluorescence. Error bars represent the standard error of mean. A one-way ANOVA utilizing Tukey's multiple comparisons test was performed to test for statistical significance.

2.6. References

(1) Schmitz, O.; Brock, B.; Rungby, J., Amylin Agonists: A Novel Approach in the Treatment of Diabetes. *Diabetes* **2004,** *53*, S233-S238.

(2) Haataja, L.; Gurlo, T.; Huang, C. J.; Butler, P. C., Islet Amyloid in Type 2 Diabetes, and the Toxic Oligomer Hypothesis. *Endocrine Rev.* **2008,** *29*, 303-316.

(3) Ke, P. C.; Sani, M.-A.; Ding, F.; Käkinen, A.; Javed, I.; Separovic, F.; Davis, T. P.; Mezzenga, R., Implications of peptide assemblies in amyloid diseases. *Chem. Soc. Rev.* **2017,** *46*, 6492-6531.

(4) Brender, J. R.; Hartman, K.; Nanga, R. P. R.; Popovych, N.; de la Salud Bea, R.; Vivekanandan, S.; Marsh, E. N. G.; Ramamoorthy, A., Role of Zinc in Human Islet Amyloid Polypeptide Aggregation. *J. Am. Chem. Soc.* **2010,** *132*, 8973-8983.

(5) Nanga, R. P. R.; Brender, J. R.; Vivekanandan, S.; Ramamoorthy, A., Structure and membrane orientation of IAPP in its natively amidated form at physiological pH in a membrane environment. *Biochim. Biophys. Acta* **2011,** *2011*, 2337-2342.

(6) Larson, J. L.; Miranker, A. D., The Mechanism of Insulin Action on Islet Amyloid Polypeptide Fiber Formation. *J. Mol. Biol.* **2004,** *335*, 221-231.

(7) Sciacca, M. F. M.; Milardi, D.; Messina, G. M. L.; Marletta, G.; Brender, J. R.; Ramamoorthy, A.; La Rosa, C., Cations as Switches of Amyloid-Mediated Membrane Disruption Mechanisms: Calcium and IAPP. *Biophys. J.* **2013,** *104*, 173-184.

(8) Ge, X.; Kakinen, A.; Gurzov, E. N.; Pang, L.; Pilkington, E. H.; Separovic, F.; Davis, T. P.; Ke, P. C.; Ding, F., Zinc-coordination and C-peptide complexation: a potential mechanism for the endogenous inhibition of IAPP aggregation. *Chem. Commun.* **2017,** *53*, 9394-9397.

(9) Padrick, S. B.; Miranker, A. D., Islet amyloid: phase partitioning and secondary nucleation are central to the mechanism of fibrillogenesis. *Biochemistry* **2002,** *41*, 4694-4703.

(10) Kahn, S. E.; Andrikopoulos, S.; Verchere, C. B., Islet amyloid: a long-recognized but underappreciated pathological feature of type 2 diabetes. *Diabetes* **1999,** *48*, 241-253.

(11) Knowles, T. P. J.; Vendruscolo, M.; Dobson, C. M., The amyloid state and its association with protein misfolding diseases. *Nat. Rev. Mol. Cell Biol.* **2014,** *15*, 384-396.

(12) Eisenberg, D.; Jucker, M., The amyloid state of proteins in human diseases. *Cell* **2012,** *148*, 1188-1203.

(13) Zraika, S.; Hull, R. L.; Verchere, C. B.; Clark, A.; Potter, K. J.; Fraser, P. E.; Kahn, S. E., Toxic oligomers and islet beta cell death: guilty by association or convicted by circumstantial evidence? *Diabetologia* **2010,** *53*, 1046-1056.

(14) Young, L. M.; Cao, P.; Raleigh, D. P.; Ashcroft, A. E.; Radford, S. E., Ion Mobility Spectrometry-Mass Spectrometry Defines the Oligomeric Intermediates in Amylin Amyloid Formation and the Mode of Action of Inhibitors. *J. Am. Chem. Soc.* **2014,** *136*, 660-670.

(15) Sun, Y.; Käkinen, A.; Xing, Y.; Pilkington, E. H.; Davis, T. P.; Ke, P. C.; Ding, F., Nucleation of β-rich oligomers and β-barrels in the early aggregation of human islet amyloid polypeptide. *Biochim. Biophys. Mol. Basis Dis.* **2019,** *1865*, 434-444.

(16) Birol, M.; Kumar, S.; Rhoades, E.; Miranker, A. D., Conformational switching within dynamic oligomers underpins toxic gain-of-function by diabetes-associated amyloid. *Nat. Commun.* **2018,** *9*, 1312.

(17) Rawat, A.; Maity, B. K.; Chandra, B.; Maiti, S., Aggregation-induced conformation changes dictate islet amyloid polypeptide (IAPP) membrane affinity. *Biochim. Biophys. Acta* **2018,** *1860*, 1734-1740.

(18) Törnquist, M.; Michaels, T. C. T.; Sanagavarapu, K.; Yang, X.; Meisl, G.; Cohen, S. I. A.; Knowles, T. P. J.; Linse, S., Secondary nucleation in amyloid formation. *Chem. Commun.* **2018,** *54*, 8667-8684.

(19) Cao, P.; Abedini, A.; Wang, H.; Tu, L.-T.; Zhang, X.; Schmidt, A. M.; Raleigh, D. P., Islet amyloid polypeptide toxicity and membrane interactions. *Proc. Natl. Acad. Sci. USA* **2013,** *110*, 19279-19284.

(20) Duan, M.; Fan, J.; Huo, S., Conformations of islet amyloid polypeptide monomers in a membrane environment: implications for fibril formation. *PLoS ONE* **2012,** *7*, e47150.

(21) Guo, C.; Côté, S.; Mousseau, N.; Wei, G., Distinct Helix Propensities and Membrane Interactions of Human and Rat IAPP1–19 Monomers in Anionic Lipid Bilayers. *J. Phys. Chem. B* **2015,** *119*, 3366-3376.

(22) Porat, Y.; Kolusheva, S.; Jelinek, R.; Gazit, E., The Human Islet Amyloid Polypeptide Forms Transient Membrane-Active Prefibrillar Assemblies. *Biochemistry* **2003,** *42*, 10971-10977.

(23) Lopes, D. H. J.; Meister, A.; Gohlke, A.; Hauser, A.; Blume, A.; Winter, R., Mechanism of Islet Amyloid Polypeptide Fibrillation at Lipid Interfaces Studied by Infrared Reflection Absorption Spectroscopy. *Biophys. J.* **2007,** *93*, 3132-3141.

(24) Ritzel, R. A.; Meier, J. J.; Lin, C.-Y.; Veldhuis, J. D.; Butler, P. C., Human Islet Amyloid Polypeptide Oligomers Disrupt Cell Coupling, Induce Apoptosis, and Impair Insulin Secretion in Isolated Human Islets. *Diabetes* **2007,** *56*, 65-71.

(25) Patil, S. M.; Xu, S.; Sheftic, S. R.; Alexandrescu, A. T., Dynamic α-Helix Structure of Micelle-bound Human Amylin. *J. Biol. Chem.* **2009,** *284*, 11982-11991.

(26) Sparr, E.; Engel, M. F. M.; Sakharov, D. V.; Sprong, M.; Jacobs, J.; de Kruijff, B.; Höppener, J. W. M.; Killian, J. A., Islet amyloid polypeptide-induced membrane leakage involves uptake of lipids by forming amyloid fibres. *FEBS Lett.* **2004,** *577*, 117-120.

(27) Gao, M.; Winter, R., The Effects of Lipid Membranes, Crowding and Osmolytes on the Aggregation, and Fibrillation Propensity of Human IAPP. *J. Diabetes Res.* **2015,** *2015*, 849017.

(28) Sasahara, K.; Morigaki, K.; Shinya, K., Amyloid aggregation and deposition of human islet amyloid polypeptide at membrane interfaces. *FEBS J.* **2014,** *281*, 2597-2612.

(29) Hirakura, Y.; Yiu, W. W.; Yamamoto, A.; Kagan, B. L., Amyloid peptide channels: blockade by zinc and inhibition by Congo red (amyloid channel block). *Amyloid* **2000,** *7*, 194-199.

(30) Bag, N.; Ali, A.; Chauhan, V. S.; Wohland, T.; Mishra, A., Membrane destabilisation by monomeric hIAPP observed by imaging fluorescence correlation spectroscopy. *Chem. Commun.* **2013,** *49*, 9155-9157.

(31) Kayed, R.; Sokolov, Y.; Edmonds, B.; McIntire, T. M.; Milton, S. C.; Hall, J. E.; Glabe, C. G., Permeabilization of Lipid Bilayers Is a Common Conformation-dependent Activity of Soluble Amyloid Oligomers in Protein Misfolding Diseases. *J. Biol. Chem.* **2004,** *279*, 46363-46366.

(32) Galvagnion, C.; Buell, A. K.; Meisl, G.; Michaels, T. C. T.; Vendruscolo, M.; Knowles, T. P. J.; Dobson, C. M., Lipid vesicles trigger α-synuclein aggregation by stimulating primary nucleation. *Nat. Chem. Biol.* **2015,** *11*, 229-234.

(33) Chargé, S. B. P.; Esiri, M. M.; Bethune, C. A.; Hansen, B. C.; Clark, A., Apolipoprotein E is Associated With Islet Amyloid and Other Amyloidoses: Implications for Alzheimer's Disease. *J. Pathol.* **1996,** *179*, 443-447.

(34) Westermark, P.; Skinner, M.; Cohen, A. S., The P-Component of Amyloid of Human Islets of Langerhans. *Scand. J. Immunol.* **1975,** *4*, 95-97.

(35) Young, I. D.; Ailles, L.; Narindrasorasak, S.; Tan, R.; Kisilevsky, R., Localization of the basement membrane heparan sulfate proteoglycan in islet amyloid deposits in type II diabetes mellitus. *Arch. Pathol. Lab. Med.* **1992,** *116*, 951-954.

(36) Jha, S.; Patil, S. M.; Gibson, J.; Nelson, C. E.; Alder, N. N.; Alexandrescu, A. T., Mechanism of Amylin Fibrillization Enhancement by Heparin. *J. Biol. Chem.* **2011,** *286*, 22894-22904.

(37) Li, Y.; Wang, L.; Lu, T.; Wei, Y.; Li, F., The effects of chondroitin sulfate and serum albumin on the fibrillation of human islet amyloid polypeptide at the phospholipid membranes. *Phys. Chem. Chem. Phys.* **2016,** *18*, 12000-12008.

(38) Meng, F.; Abedini, A.; Song, B.; Raleigh, D. P., Amyloid Formation by Pro-Islet Amyloid Polypeptide Processing Intermediates: Examination of the Role of Protein Heparan Sulfate Interactions and Implications for Islet Amyloid Formation in Type 2 Diabetes. *Biochemistry* **2007,** *46*, 12091-12099.

(39) Peinado, J. R.; Sami, F.; Rajpurohit, N.; Lindberg, I., Blockade of islet amyloid polypeptide fibrillation and cytotoxicity by the secretory chaperones 7B2 and proSAAS. *FEBS Lett.* **2013,** *587*, 3406-3411.

(40) Käkinen, A.; Javed, I.; Faridi, A.; Davis, T. P.; Ke, P. C., Serum albumin impedes the amyloid aggregation and hemolysis of human islet amyloid polypeptide and alpha synuclein. *Biochim. Biophys. Acta Biomembranes* **2018,** *1860*, 1803-1809.

(41) Oskarsson, M. E.; Singh, K.; Wang, J.; Vlodavsky, I.; Li, J.-P.; Westermark, G. T., Heparan Sulfate Proteoglycans are important for Islet Amyloid Formation and Islet Amyloid Polypeptide-Induced Apoptosis. *J. Biol. Chem.* **2015,** *290*, 15121-15132.

(42) Vidal, J.; Verchere, C. B.; Andrikopoulos, S.; Wang, F.; Hull, R. L.; Cnop, M.; Olin, K. L.; LeBoeuf, R. C.; O'Brien, K. D.; Chait, A.; Kahn, S. E., The effect of apolipoprotein E deficiency on islet amyloid deposition in human islet amyloid polypeptide transgenic mice. *Diabetologia* **2003,** *46*, 71-79.

(43) Pilkington, E. H.; Xing, Y.; Wang, B.; Käkinen, A.; Wang, M.; Davis, T. P.; Ding, F.; Ke, P. C., Effects of Protein Corona on IAPP Amyloid Aggregation, Fibril Remodelling, and Cytotoxicity. *Sci. Rep.* **2017,** *7*, 2455.

(44) Xing, Y.; Pilkington, E. H.; Wang, M.; Nowell, C. J.; Käkinen, A.; Sun, Y.; Wang, B.; Davis, T. P.; Ding, F.; Ke, P. C., Lysophosphatidylcholine modulates the aggregation of human islet amyloid polypeptide. *Phys. Chem. Chem. Phys.* **2017,** *19*, 30627-30635.

(45) Bergmann, S. R.; Ferguson, T. B.; Sobel, B. E., Effects of amphiphiles on erythrocytes, coronary arteries, and perfused hearts. *Am. J. Physiol.* **1981,** *240*, H229-H237.

(46) Kishimoto, T.; Soda, Y.; Matsuyama, Y.; Mizuno, K., An enzymatic assay for lysophosphatidylcholine concentration in human serum and plasma. *Clin. Biochem.* **2002,** *35*, 411-416.

(47) Wu, Y.; Hudson, J. S.; Lu, Q.; Moore, J. M.; Mount, A. S.; Rao, A. M.; Alexov, E.; Ke, P. C., Coating Single-Walled Carbon Nanotubes with Phospholipids. *J. Phys. Chem. B* **2006,** *110*, 2475-2478.

(48) Qiao, R.; Ke, P. C., Lipid-Carbon Nanotube Self-Assembly in Aqueous Solution. *J. Am. Chem. Soc.* **2006,** *128*, 13656-13657.

(49) Seeliger, J.; Weise, K.; Opitz, N.; Winter, R., The effect of Aβ on IAPP aggregation in the presence of an isolated β-cell membrane. *J. Mol. Biol.* **2012,** *421*, 348-363.

(50) Flanagan, P.; Lionetti, F., Lysozyme Distribution in Blood. *Blood* **1955,** *10*, 497-501.

(51) Kleinberg, D. L., Human α-Lactalbumin: Measurement in Serum and in Breast Cancer Organ Cultures by Radioimmunoassay. *Science* **1975,** *190*, 276-278.

(52) Vetri, V.; Foderà, V., The route to protein aggregate superstructures: Particulates and amyloid-like spherulites. *FEBS Lett.* **2015,** *589*, 2448-2463.

(53) Vaiana, S. M.; Ghirlando, R.; Yau, W.-M.; Eaton, W. A.; Hofrichter, J., Sedimentation Studies on Human Amylin Fail to Detect Low-Molecular-Weight Oligomers. *Biophys. J.* **2008,** *94*, L45-L47.

(54) Chen, S. W.; Drakulic, S.; Deas, E.; Ouberai, M.; Aprile, F. A.; Arranz, R.; Ness, S.; Roodveldt, C.; Guilliams, T.; De-Genst, E. J.; Klenerman, D.; Wood, N. W.; Knowles, T. P. J.; Alfonso, C.; Ricas, G.; Abramov, A. Y.; Valpuesta, J. M.; Dobson, C. M.; Cremades, N., Structural characterization of toxic oligomers that are kinetically trapped during α-synuclein fibril formation. *Proc. Natl. Acad. Sci. U.S.A.* **2015,** *112*, E1194-E2003.

(55) Quist, A.; Doudevski, I.; Lin, H.; Azimova, R.; Ng, D.; Frangione, B.; Kagan, B.; Ghiso, J.; Lal, R., Amyloid ion channels: A common structural link for protein-misfolding disease. *Proc. Natl. Acad. Sci. U.S.A.* **2005,** *102*, 10427-10432.

(56) Arya, S.; Kumari, A.; Dalal, V.; Bhattacharya, M.; Mukhopadhyay, S., Appearance of annular ring-like intermediates during amyloid fibril formation from human serum albumin. *Phys. Chem. Chem. Phys.* **2015,** *17*, 22862-22871.

(57) Kayed, R.; Pensalfini, A.; Margol, L.; Sokolov, Y.; Sarsoza, F.; Head, E.; Hall, J.; Glabe, C., Annular Protofibrils Are a Structurally and Functionally Distinct Type of Amyloid Oligomer. *J. Biol. Chem.* **2009,** *284*, 4230-4237.

(58) Pillay, K.; Govender, P., Amylin Uncovered: A Review on the Polypeptide Responsible for Type II Diabetes. *Biomed Res. Int.* **2013,** *2013*, 826706.

(59) Stine, W. B.; Dahlgren, K. N.; Krafft, G. A.; LaDu, M. J., *In Vitro* Characterization of Conditions for Amyloid-β Peptide Oligomerization and Fibrillogenesis. *J. Biol. Chem.* **2003,** *278*, 11612-11622.

(60) Stine, W. B.; Jungbauer, L.; Yu, C.; LaDu, M. J., Preparing Synthetic Aβ in Different Aggregation States. *Methods Mol. Biol.* **2011,** *670*, 13-32.

(61) Govindan, P. N.; Käkinen, A.; Pilkington, E. H.; Davis, T. P.; Ke, P. C.; Ding, F., Stabilizing Off-pathway Oligomers by Polyphenol Nanoassemblies for IAPP Aggregation Inhibition. *Sci. Rep.* **2016,** *6*, 19463.

(62) Pilkington, E. H.; Gurzov, E. N.; Käkinen, A.; Litwak, S. A.; Stanley, W. J.; Davis, T. P.; Ke, P. C., Pancreatic β-Cell Membrane Fluidity and Toxicity Induced by Human Islet Amyloid Polypeptide Species. *Sci. Rep.* **2016,** *6*, 21274.

(63) Owen, M. C.; Gnutt, D.; Gao, M.; Wärmländer, S. K. T. S.; Jarvet, J.; Gräslund, A.; Winter, R.; Ebbinghaus, S.; Strodel, B., Effects of *in vivo* conditions on amyloid aggregation. *Chem. Soc. Rev.* **2019,** *48*, 3946-3996.

(64) Sheikh, A. M.; Nagai, A., Lysophosphatidylcholine modulates fibril formation of amyloid beta peptide. *FEBS J.* **2011,** *278*, 634-642.

(65) Yamamoto, S.; Hasegawa, K.; Yamaguchi, I.; Tsutsumi, S.; Kardos, J.; Goto, Y.; Gejyo, F.; Naiki, H., Low Concentrations of Sodium Dodecyl Sulfate Induce the Extension of β2-Microglobulin-Related Amyloid Fibrils at a Neutral pH. *Biochemistry* **2004,** *43*, 11075-11082.

(66) Ookoshi, T.; Hasegawa, K.; Ohhashi, Y.; Kimura, H.; Takahashi, N.; Yoshida, H.; Miyazaki, R.; Goto, Y.; Naiki, H., Lysophospholipids induce the nucleation and extension of beta2-microglobulin-related amyloid fibrils at a neutral pH. *Nephrol. Dial. Transplant.* **2008,** *23*, 3247-3255.

(67) Usov, I.; Mezzenga, R., FiberApp: An Open-Source Software for Tracking and Analyzing Polymers, Filaments, Biomacromolecules and Fibrous Objects. *Macromolecules* **2015,** *48*, 1269-1280.

(68) Wang, M.; Käkinen, A.; Pilkington, E. H.; Davis, T. P.; Ke, P. C., Differential Effects of Silver and Iron Oxide Nanoparticles on IAPP Aggregation and Toxicity. *Biomater. Sci.* **2017,** *5*, 485-493.

(69) Keller, A.; Fritzsche, M.; Yu, Y.-P.; Liu, Q.; Li, Y.-M.; Dong, M.; Besenbacher, F., Influence of Hydrophobicity on the Surface-Catalyzed Assembly of the Islet Amyloid Polypeptide. *ACS Nano* **2011,** *5*, 2770-2778.

(70) Moores, B.; Drolle, E.; Attwood, S. J.; Simons, J.; Leonenko, Z., Effect of Surfaces on Amyloid Fibril Formation. *PLoS ONE* **2011,** *6*, e25954.

(71) Jean, L.; Lee, C. F.; Hodder, P.; Hawkins, N.; Vaux, D. J., Dynamics of the formation of a hydrogel by a pathogenic amyloid peptide: islet amyloid polypeptide. *Sci. Rep.* **2016,** *6*, 32124.

(72) Luo, J.; Wärmländer, S. K. T. S.; Gräslund, A.; Abrahams, J. P., Non-chaperone Proteins Can Inhibit Aggregation and Cytotoxicity of Alzheimer Amyloid *β* Peptide. *J. Biol. Chem.* **2014,** *289*, 27766-27775.

(73) Cedervall, T.; Lynch, I.; Lindman, S.; Berggård, T.; Thulin, E.; Nilsson, H.; Dawson, K. A.; Linse, S., Understanding the nanoparticle-protein corona using methods to quantify exchange rates and affinities of proteins for nanoparticles. *Proc. Natl. Acad. Sci. U.S.A.* **2007,** *104*, 2050-2055.

(74) Ding, F.; Radic, S.; Chen, R.; Chen, P.; Geitner, N. K.; Brown, J. M.; Ke, P. C., Direct observation of a single nanoparticle-ubiquitin corona formation. *Nanoscale* **2013,** *5*, 9162-9169.

(75) MacDonald, M. J.; Ade, L.; Ntambi, J. M.; Ansari, I.-U. H.; Stoker, S. W., Characterization of Phospholipids in Insulin Secretory Granules and Mitochondria in Pancreatic Beta Cells and Their Changes with Glucose Stimulation. *J. Biol. Chem.* **2015,** *290*, 11075-11092.

(76) Ponomarenko, E. A.; Poverennaya, E. V.; Ilgisonis, E. V.; Pyatnitskiy, M. A.; Kopylov, A. T.; Zgoda, V. G.; Lisitsa, A. V.; Archakov, A. I., The Size of the Human Proteome: The Width and Depth. *Int. J. Anal. Chem.* **2016,** *2016*, 7436849.

(77) Carrotta, R.; Canale, C.; Diaspro, A.; Trapani, A.; Biagio, P. L. S.; Bulone, D., Inhibiting effect of α(s1)-casein on Aβ(1-40) fibrillogenesis. *Biochim. Biophys. Acta* **2012,** *1820*, 124-132.

(78) Librizzi, F.; Carrotta, R.; Spigolon, D.; Bulone, D.; Biagio, P. L. S., α-Casein Inhibits Insulin Amyloid Formation by Preventing the Onset of Secondary Nucleation Processes. *J. Phys. Chem. Lett.* **2014,** *5*, 3043-3048.

(79) Javed, I.; Peng, G.; Xing, Y.; Yu, T.; Zhao, M.; Käkinen, A.; Faridi, A.; Parish, C. L.; Ding, F.; Davis, T. P.; Ke, P. C.; Lin, S., Inhibition of amyloid beta toxicity in zebrafish with a chaperone-gold nanoparticle dual strategy. *Nat. Commun.* **2019,** *10*, 3780.

(80) Camargo, D. C. R.; Garg, D.; Buday, K.; Franko, A.; Camargo, A. R.; Schmidt, F.; Cox, S. J.; Suladze, S.; Haslbeck, M.; Mideksa, Y. G.; Gemmecker, G.; Aichler, M.; Mettenleiter, G.; Schulz, M.; Walch, A. K.; de Angelis, M. H.; Feige, M. J.; Sierra, C. A.; Conrad, M.; Tripsianes, K.; Ramamoorthy, A.; Reif, B., hIAPP forms toxic oligomers in plasma. *Chem. Commun.* **2018,** *54*, 5426-5429.

(81) Jollès, J.; Jollès, P., Lysozymes' esterase activity. *FEBS Lett.* **1983,** *162*, 120-121.

Chapter Three: Profiling the Serum Protein Corona of Fibrillar Human Islet Amyloid Polypeptide

This chapter pertains to a published work, reprinted with permission from Pilkington, E. H.; Gustafsson, O. J. R.; Xing, Y.; Hernandez-Fernaud, J.; Zampronio, C.; Käkinen, A.; Faridi, A.; Ding, F.; Wilson, P.; Ke, P. C.; Davis, T. P., Profiling the Serum Protein Corona of Fibrillar Human Islet Amyloid Polypeptide. *ACS Nano* **2018,** *12,* 6066-6078. Copyright 2018 American Chemical Society.

https://doi.org/10.1021/acsnano.8b02346

Preamble: In **Chapter Two**, it was demonstrated that IAPP aggregation species interact with model proteins, lipids and lipid micelles *in vitro*, and the capacity of these biomolecules to impact intrinsic physicochemical properties and biological behaviors of these species was established. In particular, proteins and lipids exerted conformational remodeling and reduced associated cytotoxicity upon binding to mature amyloid fibrils, resulting in the first report of the 'amyloid-protein corona'. In this chapter, these initial findings are further expanded through the interrogation of the amyloid-protein corona *in vitro* in complex biological media *(Aim 1C)*, as fibrils and plaques would be natively exposed to within the extracellular milieu *in vivo*.

ACS NANO

JUNE 2018 VOLUME 12 NUMBER 6

pubs.acs.org/acsnano

Defining nanoscience and nanotechnology

Profiling human islet amyloid polypeptide fibrils

Laser writing nanophotonic structures on contact lenses

Natural resources in Korea's demilitarized zone

ACS NANO
Cite This: ACS Nano 2018, 12, 6066−6078
www.acsnano.org

ARTICLE

Profiling the Serum Protein Corona of Fibrillar Human Islet Amyloid Polypeptide

Emily H. Pilkington,[†,‡] Ove J. R. Gustafsson,[§] Yanting Xing,[∥] Juan Hernandez-Fernaud,[⊥] Cleidi Zampronio,[⊥] Aleksandr Kakinen,[†] Ava Faridi,[†] Feng Ding,[∥] Paul Wilson,[†,‡] Pu Chun Ke,*[,†] and Thomas P. Davis*[,†,‡]

[†]ARC Centre of Excellence in Convergent Bio-Nano Science and Technology, Monash Institute of Pharmaceutical Sciences, 381 Royal Parade, Parkville, VIC 3052, Australia

[‡]Department of Chemistry, University of Warwick, Library Road, CV4 4AL Coventry, United Kingdom

[§]ARC Centre of Excellence in Convergent Bio-Nano Science and Technology, Future Industries Institute, University of South Australia, University Boulevard, Mawson Lakes, SA 5095, Australia

[∥]Department of Physics and Astronomy, Clemson University, Clemson, South Carolina 29634, United States

[⊥]Warwick Proteomics Research Technology Platform, School of Life Sciences, University of Warwick, Gibbet Hill Road, CV4 7AL Coventry, United Kingdom

Supporting Information

ABSTRACT: **Amyloids may be regarded as native nanomaterials that form in the presence of complex protein mixtures. By drawing an analogy with the physicochemical properties of nanoparticles in biological fluids, we hypothesized that amyloids should form a protein corona *in vivo* that would imbue the underlying amyloid with a modified biological identity. To explore this hypothesis, we characterized the protein corona of human islet amyloid polypeptide (IAPP) fibrils in fetal bovine serum using two complementary methodologies developed herein: quartz crystal microbalance and "centrifugal capture", coupled with nanoliquid chromatography tandem mass spectroscopy. Clear evidence for a significant protein corona was obtained. No trends were identified for amyloid corona proteins based on their physicochemical properties, whereas strong binding with IAPP fibrils occurred for linear proteins or multidomain proteins with structural plasticity. Proteomic analysis identified amyloid-enriched proteins that are known to play significant roles in mediating cellular machinery and processing, potentially leading to pathological outcomes and therapeutic targets.**

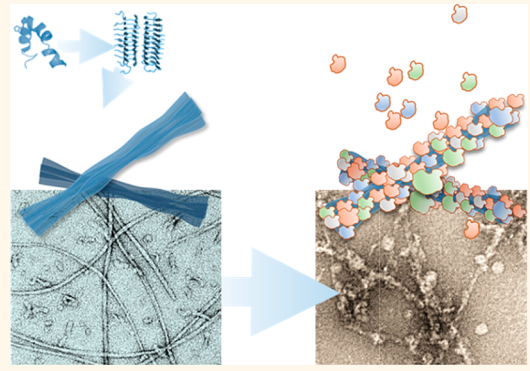

KEYWORDS: *amyloid, protein corona, liquid chromatography, mass spectrometry, amyloidogenesis*

[redacted]

[redacted]

Received: March 28, 2018
Accepted: May 10, 2018
Published: May 10, 2018

ACS Publications © 2018 American Chemical Society

DOI: 10.1021/acsnano.8b02346
ACS Nano 2018, 12, 6066−6078

Downloaded via UNIV OF WARWICK on June 27, 2018 at 10:28:14 (UTC).
See https://pubs.acs.org/sharingguidelines for options on how to legitimately share published articles.

Chapter Four: Star Polymers Reduce Islet Amyloid Polypeptide Toxicity via Accelerated Amyloid Aggregation

This chapter pertains to a published work, reprinted with permission from Pilkington, E. H.; Lai, M.; Ge, X.; Stanley, W. J.; Wang, B.; Wang, M.; Käkinen, A.; Sani, M.-A.; Whittaker, M. R.; Gurzov, E. N.; Ding, F.; Quinn, J. F.; Davis, T. P.; Ke, P. C., Star Polymers Reduce Islet Amyloid Polypeptide Toxicity via Accelerated Amyloid Aggregation. *Biomacromolecules* **2017,** *18,* 4249-4260. Copyright 2017 American Chemical Society.

https://doi.org/10.1021/acs.biomac.7b01301

Preamble: In **Chapters Two** and **Three**, fundamental understanding of IAPP species at the biological interface was achieved through characterizing the aggregation pathway and exploring the interactions of pathway species with natively circulating biomolecules in both model and complex environments. Drawing specifically on knowledge gained in **Chapter Two**, wherein fibrillating IAPP species demonstrated significantly higher cytotoxicity *in vitro* cytotoxicity in primary human endothelial cells comparative to mature IAPP amyloid (*Aim 1A*), with the charge of model interactors providing no significant differentiation to the toxic effect of oligomeric IAPP (*Aim 1B)*, **Chapter Four** highlights the application of 'fibrillization promotion' as an effective strategy for mitigating IAPP-associated cytotoxicity. Herein, the design and synthesis of a polymer-based anti-amyloidosis agent – poly (2-hydroxyl ethyl acrylate) 'PHEA' stars – is described *(Aim 2)*, comprised of aromatic moieties and terminal hydroxyls towards the sequestration of fibrillating IAPP, and carrying a neutral charge to enhance its biocompatibility. The cytoprotective capabilities of the PHEA stars against IAPP *in vitro* and *ex vivo* are demonstrated, through sequestering toxic intermediate IAPP species and enhancing their fibrillization towards noncytotoxic mature IAPP amyloid – presenting a new agent and new strategy towards mitigating IAPP pathologies in T2D.

Biomacromolecules
DECEMBER 2017 VOLUME 18, NUMBER 12 pubs.acs.org/Biomac

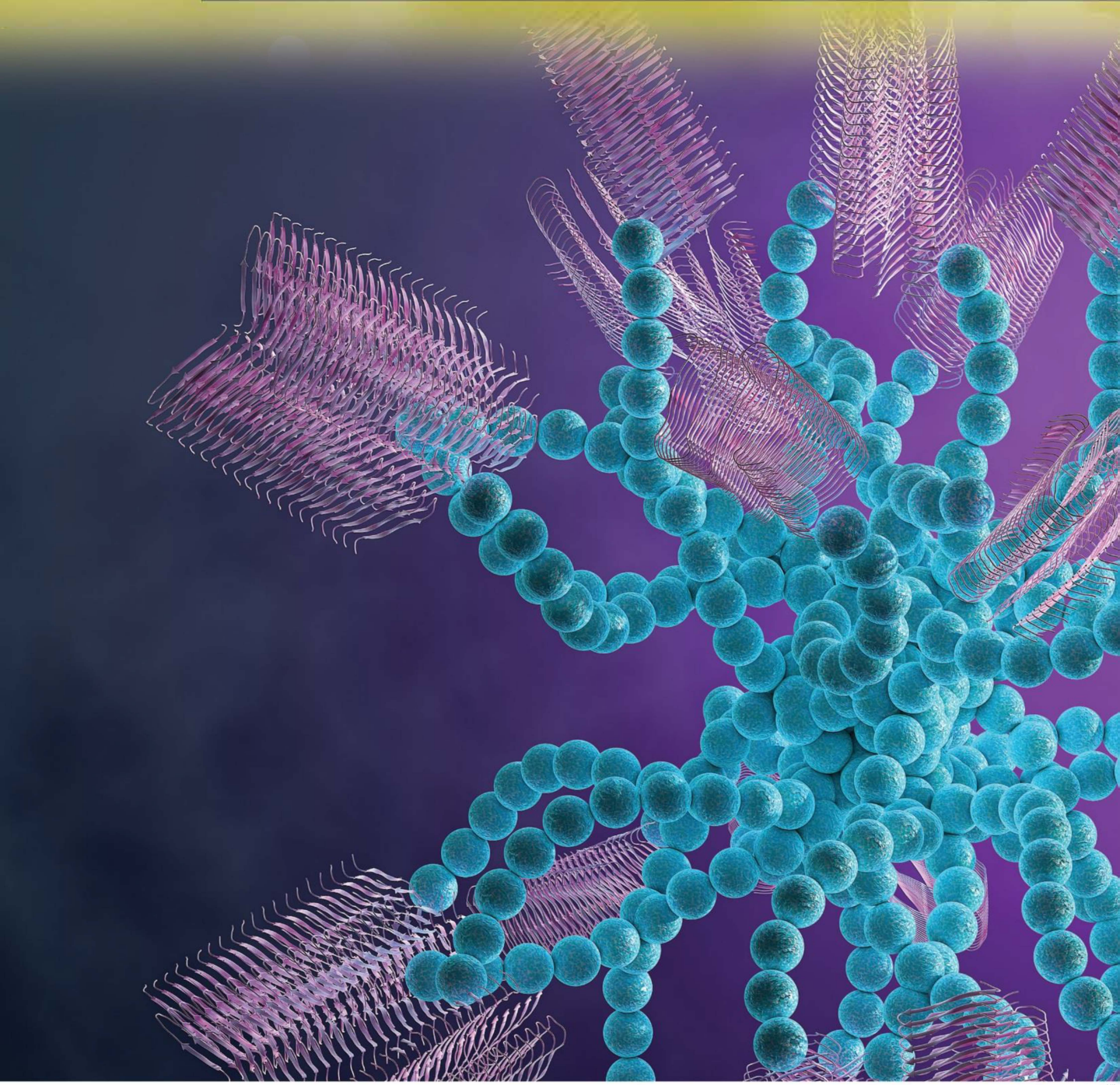

ACS Publications
Most Trusted. Most Cited. Most Read.
www.acs.org

This is an open access article published under an ACS AuthorChoice License, which permits copying and redistribution of the article or any adaptations for non-commercial purposes.

Article

pubs.acs.org/Biomac

Star Polymers Reduce Islet Amyloid Polypeptide Toxicity via Accelerated Amyloid Aggregation

Emily H. Pilkington,[†] May Lai,[†] Xinwei Ge,[‡] William J. Stanley,[¶,§] Bo Wang,[‡] Miaoyi Wang,[†] Aleksandr Kakinen,[†] Marc-Antonie Sani,[#] Michael R. Whittaker,[†] Esteban N. Gurzov,[¶,§] Feng Ding,[‡] John F. Quinn,*[,†] Thomas P. Davis,*[,†,∥] and Pu Chun Ke*[,†]

[†]ARC Centre of Excellence in Convergent Bio-Nano Science and Technology, Monash Institute of Pharmaceutical Sciences, Monash University, 381 Royal Parade, Parkville, Victoria 3052, Australia

[‡]Department of Physics and Astronomy, Clemson University, Clemson, South Carolina 29634, United States

[¶]St Vincent's Institute of Medical Research, 9 Princes Street, Fitzroy, Victoria 3065, Australia

[§]Department of Medicine, St. Vincent's Hospital, The University of Melbourne, Melbourne, Australia

[#]School of Chemistry, Bio21 Institute, The University of Melbourne, 30 Flemington Rd, Parkville, Victoria 3010, Australia

[∥]Department of Chemistry, University of Warwick, Gibbet Hill, Coventry CV4 7AL, United Kingdom

Supporting Information

ABSTRACT: Protein aggregation into amyloid fibrils is a ubiquitous phenomenon across the spectrum of neurodegenerative disorders and type 2 diabetes. A common strategy against amyloidogenesis is to minimize the populations of toxic oligomers and protofibrils by inhibiting protein aggregation with small molecules or nanoparticles. However, melanin synthesis in nature is realized by accelerated protein fibrillation to circumvent accumulation of toxic intermediates. Accordingly, we designed and demonstrated the use of star-shaped poly(2-hydroxyethyl acrylate) (PHEA) nanostructures for promoting aggregation while ameliorating the toxicity of human islet amyloid polypeptide (IAPP), the peptide involved in glycemic control and the pathology of type 2 diabetes. The binding of PHEA elevated the β-sheet content in IAPP aggregates while rendering a new morphology of "stelliform" amyloids originating from the polymers. Atomistic molecular dynamics simulations revealed that the PHEA arms served as rodlike scaffolds for IAPP binding and subsequently accelerated IAPP aggregation by increased local peptide concentration. The tertiary structure of the star nanoparticles was found to be essential for driving the specific interactions required to impel the accelerated IAPP aggregation. This study sheds new light on the structure−toxicity relationship of IAPP and points to the potential of exploiting star polymers as a new class of therapeutic agents against amyloidogenesis.

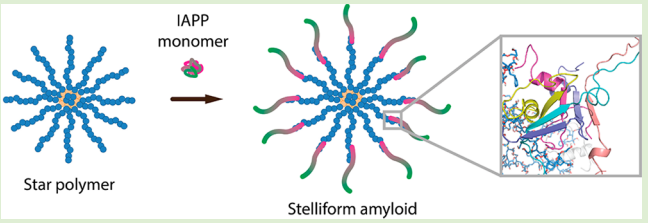

INTRODUCTION

Type 2 diabetes mellitus (T2D) is a metabolic disease affecting 5% of the global population.[1] Extensive research indicates that a major factor in the development and pathogenesis of T2D is dysfunction of human islet amyloid polypeptide (IAPP), a 37-residue peptide cosecreted with insulin from pancreatic β-cells, which undergoes fibrillization to form amyloid plaques found in 90% of T2D patients.[2,3] The toxic IAPP aggregation products are also capable of eliciting systemic damage in T2D patients with evidence of cardiac dysfunction and neurological deficits mediated by IAPP deposition increasing the burden of disease.[4,5] Concordantly, there is a crucial need for the development of treatment agents that are capable of mitigating IAPP-associated toxicity in vivo to reduce the morbidity of T2D and prevent its development in prediabetics.

Aggregation inhibition with the use of small molecules as well as metal, carbon, and polymeric nanoparticles (NPs)[6−9] has been a major strategy against amyloid-mediated toxicity. Polymeric NPs, specifically, have been explored as protein aggregation inhibitors utilizing their tunable hydrophobicity as well as their capacity for initiating H-bonding.[10−13] For example, antiprion activity has been demonstrated by phosphorus dendrimers, maltose-based glycodendrimers (mPPI), poly(propyleneimine) PPI, and poly(ethylenimine) hyperbranched polymers.[12−20] Of the myriad forms of polymeric NPs, hyperbranched polymers and dendrimers have demonstrated strong efficacies as antiamyloid agents,[11,12,15,21−26] though anti-IAPP applications have only been explored recently. PPI glycodendrimers and lysine dendrimers have been investigated as anti-Aβ aggregation agents,[22,23] and hyperbranched PEG-based polymers with a dopamine moiety were found to be capable of inhibiting α-

Received: September 8, 2017
Revised: October 13, 2017
Published: October 16, 2017

ACS Publications © 2017 American Chemical Society

DOI: 10.1021/acs.biomac.7b01301
Biomacromolecules 2017, 18, 4249−4260

synuclein (αS) aggregation.[11] Anionic low-generation dendrimers have been shown to modulate IAPP fibrillization and associated toxicity,[24] and inhibition of IAPP fibrillization and toxicity in vitro and ex vivo has recently been demonstrated by our team with OH-terminated polyamidoamine dendrimers (PAMAM-OH).[26]

Curiously, the amyloidogenesis of melanocyte protein Pmel17 in the human system is entirely nonpathogenic.[27] The rapid fibrillization of Pmel17, which transitions from monomeric form to mature amyloid fibrils within 3 s, is a cytoprotective mechanism, namely, through reducing the half-life of toxic intermediate products (i.e., oligomers and protofibrils) to favor the formation of nontoxic, mature amyloid fibrils. Indeed, this effect has been shown to extend to pathogenic amyloids; mice overexpressing the Alzheimer's-related amyloidogenic peptide amyloid-β (Aβ) with the "Artic" mutation, correlated with the acceleration of Aβ fibrillization, demonstrated higher plaque loading with lower or negligible impact on behavioral function comparable to mice expressing wild-type Aβ.[28] The concept of fibrillization promotion, rather than inhibition, thus provides a biomimetic and perhaps counterintuitive strategy in the mitigation of amyloid cytotoxicity.

Amyloid aggregation promotion as a strategy for mitigating cytotoxicity has thus far only been reported for a selected few small molecules.[29,30] Specifically, high-throughput screening identified aromatic small molecules capable of promoting Aβ fibrillization to provide a cytoprotective effect, including the orcein-related molecule O4[30] and the compound 2002-H20.[29] Small molecules, however, are imperfectly suited as antiamyloid agents when utilized without modifications to confer targeting specificity, as they frequently display molecular promiscuity.[31]

In this study, we synthesized and demonstrated the use of poly(2-hydroxyethyl acrylate) (PHEA) star polymers[32] as an anti-IAPP agent capable of cytoprotective rescue of pancreatic β-cells through the promotion of amyloid aggregation. PHEA stars were synthesized using a reversible addition-fragmentation chain-transfer (RAFT) polymerization methodology and were designed to mimic the chemistry of small molecule aggregation promoters through the incorporation of hydroxyls and aromatic rings via the RAFT end-groups.[33,34] The PHEA stars were weakly negatively charged, each possessing a hydrodynamic size of ~12 nm and containing on average 12 arms. Through biophysical characterizations, we demonstrated a significant, positive correlation between amyloid aggregation promotion induced by PHEA stars and reduction in IAPP-mediated cytotoxicity both in vitro and ex vivo and additionally identified a new amyloid morphology, named "stelliform amyloids", formed by coaggregation of IAPP and PHEA stars at a molar ratio of 5:1. Atomistic discrete molecular dynamics (DMD)[35] simulations revealed that the PHEA stars possessed rigid arms different from the porous and micellar PAMAM dendrimers. The rodlike arms served as linear scaffolds for IAPP binding and further accelerated the nucleation of β-sheet aggregates by increased local peptide concentration. Each arm of the PHEA stars could nucleate the fibrillization of IAPP resulting in the stelliform amyloid morphology. This study opens the door to the design and application of a new class of agents against amyloid diseases.

EXPERIMENTAL METHODS

Materials. 2-Hydroxyethyl acrylate (HEA) was purchased from Sigma-Aldrich and deinhibited by passing through a column of basic alumina. *S,S′*-Dibenzyl trithiocarbonate (DBTC), *N,N′*-methylenebis-(acrylamide) (X) was purchased from Sigma-Aldrich. Azobis-(isobutyronitrile) (AIBN) was purified by recrystallization from methanol before use. Dimethyl sulfoxide (DMSO) was purchased from Merck Millipore and used as received. Human islet amyloid polypeptide monomers (IAPP; disulfide bridge: 2−7; MW: 3,906; 37 residue: KCNTATCATQRLANFLVHSSNNFGAILSSTNVGSNTY; >95% pure by HPLC) were obtained in lyophilized powder form from AnaSpec and were made up to a 200 μM stock immediately prior to an experiment or allowed to fibrillate at 25 °C for >5 days to produce mature IAPP amyloids. All materials were weighed out on a Cubis MSE balance (Sartorius, 0.01 mg resolution) and made up fresh in Milli-Q water prior to experiments unless otherwise specified. Thioflavin T (ThT) dye (Sigma-Aldrich) was prepared fresh for each experiment at a 250 μM stock solution. Propidium iodide (PI) dye stock solution (1 mg/mL in water) was stored at −20 °C.

RAFT Synthesis of Poly(2-hydroxyl ethyl acrylate) Stars. *Synthesis of Poly(2-hydroxyl ethyl acrylate) (p(HEA)) Homopolymer.* Three homopolymers of PHEA were prepared by RAFT polymerization with molecular weights of 4,000, 8,000, and 16 000 g/mol.

The synthesis of PHEA 1 (M_n = 4000 g/mol) was carried out using the following stoichiometry: [DBTC]:[HEA]:[AIBN] = 1:38:0.1. In brief, 2-hydroxyethyl acrylate (4.00 g, 0.034 mol), DBTC RAFT agent (0.27 g, 9.12×10^{-4} mol), AIBN (15.4×10^{-3} g, 9.38×10^{-5} mol), and DMSO (26 mL) were placed into a 50 mL round-bottom flask equipped with a magnetic stirrer bar and capped with a rubber septum. The reaction mixture was deoxygenated for 1 h at 0 °C with nitrogen gas. The sealed deoxygenated reaction vessel was placed in a preheated oil bath at 70 °C, and the polymerization was carried for 4 h with stirring. Polymerization was stopped by placing the vessel in ice to cool. The product was analyzed by ^{1}H NMR and GPC. The monomer conversion was determined to be approximately 88% by NMR, thus resulting in a M_w of 4141 g/mol. By integrating the peaks associated with the benzyl group (7.1−7.4 ppm) and the hydroxyl group in the PHEA repeat unit (δ = 4.8 ppm), the $M_{n(NMR)}$ is found to be 4374 g/mol. Per arm, there are 32 units of the PHEA monomer because the homopolymer constitutes 64 units. The molecular number and polydispersity index were determined by GPC to be 8,276 M_n and 1.30, respectively.

A similar procedure was employed for the synthesis of PHEA 2 (M_n = 8000 g/mol) using the following stoichiometry: [DBTC]:[HEA]:[AIBN] = 1:75:0.1. In brief, 2-hydroxyethyl acrylate (4.00 g, 0.034 mol), DBTC RAFT agent (0.13 g, 4.58×10^{-4} mol), AIBN (7.2×10^{-3} g, 4.38×10^{-5} mol), and DMSO (26 mL) were placed into a 50 mL round-bottom flask equipped with a magnetic stirrer bar and capped with a rubber septum. The reaction mixture was deoxygenated for 1 h at 0 °C with nitrogen gas. The sealed deoxygenated reaction vessel was placed in a preheated oil bath at 70 °C, and the polymerization was carried for 4 h with stirring. Polymerization was stopped by placing the vessel in ice to cool. The product was analyzed by ^{1}H NMR and GPC. The monomer conversion was determined to be approximately 85% by NMR, thus resulting in an $M_{n(th)}$ of 7716 g/mol. By integrating the peaks associated with the benzyl group (7.1−7.4 ppm) and the hydroxyl group in the PHEA repeat unit (δ = 4.8 ppm), the $M_{n(NMR)}$ is found to be 7729 g/mol. Per arm, there are 32 units of the PHEA monomer; therefore, the homopolymer constitutes 64 units. The molecular number and polydispersity index were determined by GPC to be 14,688 M_n and 1.24, respectively.

The synthesis of PHEA 3 (M_n = 16,000 g/mol) was achieved in a similar method as above using the following stoichiometry: [DBTC]:[HEA]:[AIBN] = 1:144:0.1. In brief, 2-hydroxyethyl acrylate (4.91 g, 0.042 mol), DBTC RAFT agent (0.085 g, 2.93×10^{-4} mol), AIBN (5×10^{-3} g, 3.04×10^{-5} mol), and DMSO (32 mL) were placed into a 50 mL round-bottom flask equipped with a magnetic stirrer bar and capped with a rubber septum. The reaction mixture was deoxygenated for 1 h at 0 °C with nitrogen gas. The sealed deoxygenated reaction vessel was placed in a preheated oil bath at 70 °C and the polymerization was carried for 6 h with stirring. Polymerization was terminated by placing the vessel in ice to cool. The product was

DOI: 10.1021/acs.biomac.7b01301
Biomacromolecules 2017, 18, 4249−4260

analyzed by ^{1}H NMR and GPC. The monomer conversion was determined to be approximately 91% by NMR, thus resulting in an M_w of 15,553 g/mol. By integrating the peaks associated with the benzyl group (7.1−7.4 ppm) and the hydroxyl group in the PHEA repeat unit (δ = 4.8 ppm), the $M_{n(NMR)}$ is found to be 15,961 g/mol. The molecular number and polydispersity index were determined by GPC to be 26,676 M_n and 1.24, respectively.

Synthesis of PHEA Star. A typical PHEA star synthesis is carried out as follows. The synthesis of PHEA star was conducted using the following stoichiometry: [PHEA 2]:[HEA]:[AIBN]:[XL] = 1:12:0.4:18. In brief, a 1.86 mL aliquot (250 mg equivalent) of the solution above, AIBN (1.60 mg, 9.76 × 10^{-3} mol), methylene bis(acrylamide) (77.09 mg, 0.5 mol), and 930 μL of DMSO were added into a glass vial equipped with a magnetic stirrer bar and capped with a rubber septum. The reaction mixture was deoxygenated for 30 min at 0 °C with nitrogen gas. The sealed deoxygenated reaction vessel was placed in a preheated oil bath at 70 °C, and the polymerization was carried for 24 h with stirring. Polymerization was terminated by placing the vessel in ice to cool.

Purification was conducted by dialysis against water with a MWCO of 14 kDa for 2 days and then lyophilization. The product was analyzed by GPC, and its molecular number and polydispersity index were determined to be 85,500 M_n and 2.18, respectively. With the given M_n values from GPC, the star was calculated to have 12 arms. In theory, the molecular weight of the star is 47,295 g/mol.

Analysis Methods. *^{1}H Nuclear Magnetic Resonance Spectroscopy.* ^{1}H NMR spectra were recorded at 400 MHz on a Bruker UltraShield 400 MHz spectrometer running Bruker Topspin, version 1.3. Spectra were recorded in DMSO-d_6.

Gel Permeation Chromatography (GPC). GPC was performed using a Shimadzu modular system comprised of a SIL-20AD automatic injector, a RID-10A differential refractive-index detector, and a 50 × 7.8 mm guard column followed by three KF-805L columns (300 × 8 mm, bead size: 10 μm, pore size maximum: 5000 Å). *N,N′*-Dimethylacetamide (DMAc, HPLC grade, 0.03% w/v LiBr) at 50 °C was used for the analysis with a flow rate of 1 mL min^{-1}. Samples were filtered through 0.45 μm PTFE filters before injection. The GPC calibration was performed with narrow-polydispersity polystyrene standards ranging from 500 to 2 × 10^6 g mol^{-1}.

Dynamic Light Scattering (DLS). DLS was carried out on a Malvern Zetasizer Nano ZS Series running DTS software (laser, 4 mW, λ = 633; angle 173°). The polydispersity index (PDI) used to describe the average diameters and size distribution of prepared stars was determined via a cumulants analysis of the measured intensity autocorrelation function using the DTS software. Samples were filtered using 0.45 μm PTFE syringe filter to remove contaminants/dust prior to the measurement.

Fourier Transform Infrared Spectroscopy-Attenuated Total Reflectance (FTIR-ATR). ATR-FTIR measurements were performed using a Shimadzu IRTracer 100 Fourier transform infrared spectrometer with a GladiATR 10 single reflection ATR accessory. Spectra were obtained in the midinfrared region of 4000−600 cm^{-1} at a resolution of 8 cm^{-1} (512 scans) and analyzed using LabSolution IR software.

Thioflavin T Assay. Aliquots of IAPP (final concentration of 25 μM), ThT dye (25 μM), and PHEA polymers (5, 1, or 0.2 μM) were added directly to wells of a black/clear bottom 96-well plate (Costar) and mixed thoroughly. The final well volume of 100 μL was made up using Milli-Q water where necessary. The plate was run on a Flexstation 3 plate reader (Molecular Devices) with samples excited at 440 nm and the emission read at 485 nm every 5 min for a total of 14 h (169 readings).

Circular Dichroism (CD) Spectroscopy. Experiments were performed on a Chirascan CD spectrometer (Applied Photophysics) with spectra read from 190 to 260 nm. Prior to sample loading, a baseline with no cuvette was run. Then, 300 μL of 25 μM IAPP in Milli-Q water alone or in the presence of PHEA (5 μM), was placed in a cuvette with a 0.1 cm path length, and CD analysis was run at 0, 2.5, and 24 h time points. Between samples, cuvettes were washed more than 5× with distilled water. Reads are an average of 3 repeats. Raw data were offset to zero and normalized against the spectra of Milli-Q water for IAPP spectra and against PHEA alone for IAPP-PHEA mixed samples. Data were then deconvoluted with CDNN software to give a final relative percentage content of secondary structure.

Transmission Electron Microscopy. Samples were placed in Eppendorf tubes at a final IAPP concentration of 25 μM and incubated for 24 h at 25 °C. An aliquot (10 μL) was placed on 400 mesh carbon-coated Formvar copper grids (ProSciTech) that were glow-discharged to promote hydrophilicity. Samples were adsorbed onto the grid for 60 s, then drawn off using filter paper. Grids were washed twice with 10 μL of Milli-Q water. Five microliters of 1% uranyl acetate (in water) was then utilized to twice-stain grids by touching one droplet and immediately drawing the stain off, and then placing the grid atop the second droplet to stain for 15 s. TEM images were obtained on a Tecnai TF20 transmission electron microscope (FEI) with an UltraScan 1000 (2k × 2k) CCD camera (Gatan).

Determination of Fibril Morphology. Fibril tracking and analysis were performed with software FiberApp[36] to determine the morphology and mesoscopic parameters of persistence length (λ) and contour length (l) of IAPP fibrils. FiberApp was developed from statistical physics and enables structural analysis of tubular and macromolecular objects. The persistence length λ reflects the stiffness of a polymer and is mathematically defined via the bond correlation function (BCF) in 3D or 2D as the length over which angular correlations in the tangential direction decrease by a factor of e.[37] Here, the λ values of IAPP fibrils were estimated using the BCF, mean-squared end-to-end distance (MSED), and mean-squared midpoint displacement (MSMD) methods and presented as averaged values determined by the three methods. The contour length corresponds to the end-to-end length of a polymer along its physical contour. The values of persistence length and contour length were obtained based on statistical analysis of 1,243 fibrils.

Cell Culture and Viability. Insulin-producing βTC6 cells (ATCC) were cultured in complete DMEM (ATCC; 15% FBS). For viability assays, a 96-well plate (Corning) was coated with 70 μL of 70 μg/mL poly-D-lysine for >10 min; then, the wells were washed 3× in 100 μL of HBSS. Cells were seeded at a density of ∼50,000 cells per well in 200 μL of complete media and incubated at 37 °C in 5% CO_2 for 3 days. Fresh IAPP or mature IAPP amyloids (200 μM stock) were preincubated together with PHEA polymers (40, 8, and 3.2 μM stocks) at a 1:1 v/v ratio for 24 h at room temperature. Prior to cell treatment, the media was aspirated, and the wells were washed 1× in 100 μL of HBSS. One micromolar propidium iodide (PI; AnaSpec) dye solution was made up in complete media containing 1% penicillin/streptomycin, and 150 μL aliquots were added to each of the wells. The cells were returned to the incubator for 30 min to equilibrate with the dye solution. Each sample treatment was then added to the wells in triplicate, in addition to an IAPP control made up fresh immediately prior to adding to the wells (final well volume: 200 μL; final IAPP concentration: 25 μM). The cells were imaged on an Operetta High-Content Imaging System (PerkinElmer) utilizing standardized excitation/emission settings for PI with images of five areas within a single well taken every hour for 24 h. Total cell counts per well were estimated using phase-contrast mapping within sampling areas. Cell death over time was expressed as %PI positive cells within the total cell count.

Ex Vivo Viability. C57BL/6 male mice (age 10−14-week-old) were maintained at St. Vincent's Institute animal care facility on a 12 h light-dark cycle in a temperature-controlled room and obtained food and water ad libitum. Uniformly sized mouse islets from C57BL/6 mice were handpicked into 1 cm Petri dishes containing 1 mL of 25 μM hIAPP, 5 μM PHEA, or a combination of both and cultured for 48 h. At the end of the culture period, islets were dispersed with trypsin and resuspended in 250 μL of hypotonic buffer containing 50 μg/mL of propidium iodide, which stained nuclear DNA. The cells were analyzed by fluorescence-activated cell sorter (FACS), and cell death was identified by their subdiploid DNA content as previously described.[38] The study was conducted at St Vincent's Institute (Melbourne, Australia) following the guidelines of the Institutional Animal Ethics Committee.

DOI: 10.1021/acs.biomac.7b01301
Biomacromolecules 2017, 18, 4249−4260

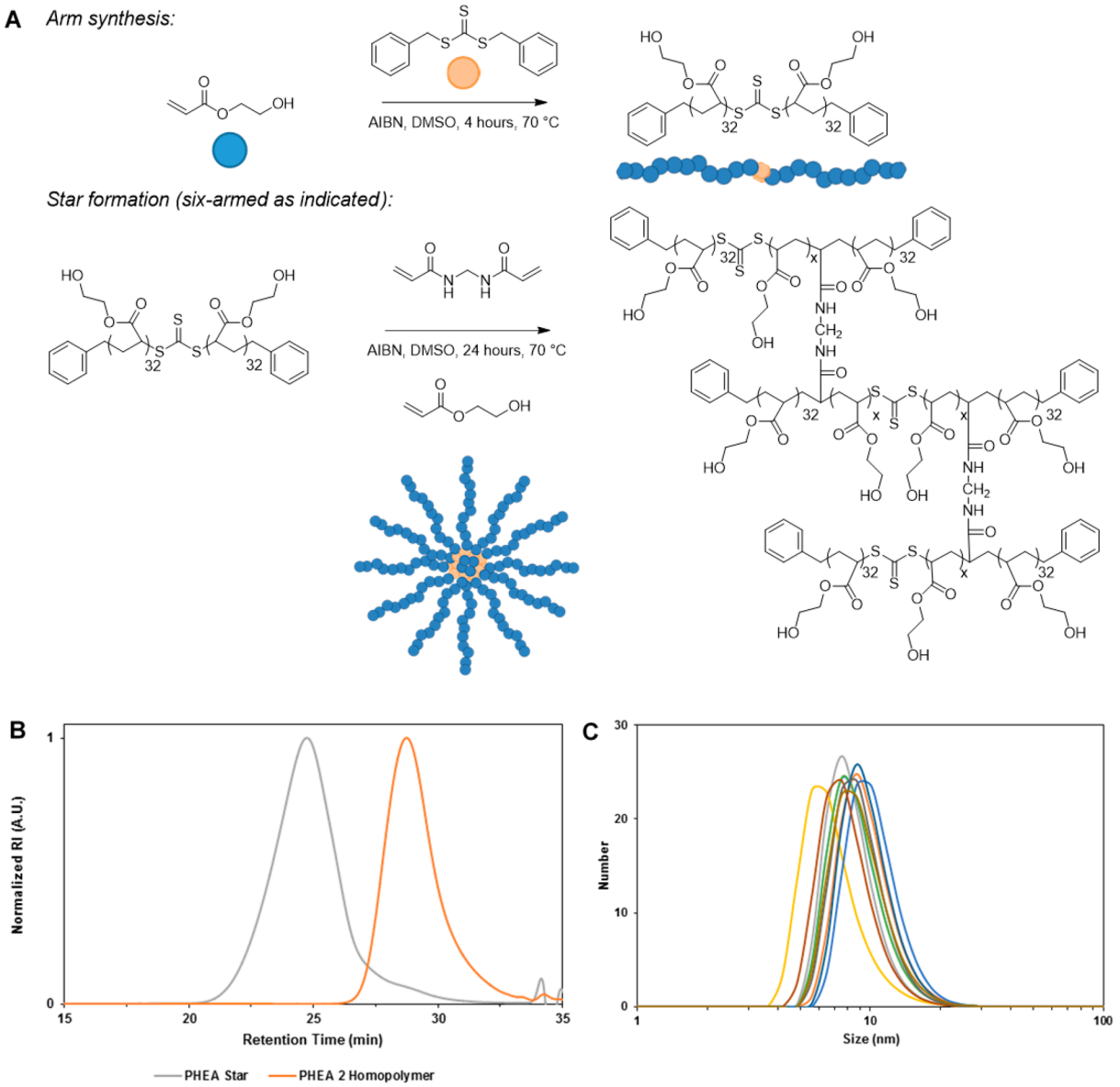

Figure 1. Synthesis and preliminary characterization of PHEA stars via RAFT polymerization. (A) Synthesis of PHEA stars using a symmetrical RAFT agent. (B) Gel permeation chromatograms for the PHEA arm (orange) and star (gray). (C) Size distribution by number from dynamic light scattering for PHEA stars.

Statistics. Where applicable, data were analyzed using a one-way ANOVA with Tukey's correction with $p < 0.05$ considered statistically significant.

DMD Simulations and Simulation Setup. DMD is a special form of molecular dynamics, where discrete step functions instead of continuous functions are used to mimic the constraints. The united-atom representation with all polar hydrogen and heavy atoms was used to model IAPPs and PHEA polymers. An adapted Medusa force field[35] with an implicit solvent model was used to describe the nonbonded interatomic interactions, including van der Waals, solvation, hydrogen bonding, and electrostatic terms. The Debye–Hückel approximation with a Debye length of ~10 Å was applied to capture the screened electrostatic interactions. Anderson's thermostat was used to maintain temperature, which was fixed at 300 K in all simulations. The DMD program is freely available to academic users at the Molecules in Action Web site (http://moleculesinaction.com), and all simulation parameters can be obtained upon request. Given the stochastic nature in the dynamics of a multimolecular system and the nucleation-dependent aggregation kinetics, we performed multiple independent long simulations with different starting configurations (e.g., randomized velocities, intermolecular distances and orientations) to ensure sufficient sampling and avoid potential bias associated with initial configurations. Thermodynamic and kinetic prosperities were then obtained by analyzing all the independent runs for each molecular system.

All the PHEA model structures were constructed with the Avogadro[39] molecular builder software and energy minimized with the MMFF94s force field.[40] MedusaScore,[41] an extension of the Medusa force field,[42] was adapted to model the polymers in addition to IAPP. The MedusaScore was parametrized on a large set of ligands and was transferrable to different molecular systems. The predictive power of MedusaScore has been validated in various benchmark studies, including recent community structure–activity resource (CSAR) blind ligand–receptor docking prediction exercises.[43,44]

For each 2-arm PHEA (Figure S3A), we performed 20 independent simulations at 300 K with different starting configurations. Each independent simulation lasted 300 ns, and thus, an accumulative 6 μs simulation was obtained for the polymer model. We used the last half of all simulations and computed the radius of gyration (R_g) values of the modeled polymers. For the 8-arm PHEA (Figure S3C), 20

DOI: 10.1021/acs.biomac.7b01301
Biomacromolecules 2017, 18, 4249–4260

independent simulations were performed at 300 K with different starting configurations, each of which lasted 200 ns.

The IAPP (PDB ID: 2L86) structure was obtained from PDB. Counterions Cl^{1-} were introduced to achieve a neutral charge condition if necessary. For systems containing six IAPPs (with and without a 6-arm PHEA as shown in Figure S3B), the peptide concentration was maintained by fixing the dimension of the simulation box as 120 Å, and periodic boundary conditions were applied. For each of the multimolecular systems, 20 independent simulations starting with different intermolecular distances and orientations were performed at 300 K, and each run lasted 100 ns.

Secondary structure analyses were performed using the dictionary secondary structure of protein (DSSP) method. For each snapshot structure, the secondary structure, such as helix, sheet, coil, and turn, for each residue was obtained. An empirical sigmoidal function

$$y = (I_{max} - I_{min})/(1 + \exp(-k(t - t_0))) + I_{min} \quad (1)$$

was adopted to fit the kinetics of the total number of residues in the β-sheet conformation, where fitting parameters A, B, t_0, and k corresponded to the max and min values of aggregation, the midpoint time of aggregation, and the elongation rate, respectively. The lag time was determined as

$$t_{lag} = t_0 - 2/k$$

In the potential of mean force (PMF) calculation, normalized sigmoidal function, $Q_{fibrillization} = 1/(1+ \exp(-k(t - t_0)))$, was used to quantify the extent of fibrillization for each independent simulation. For a given snapshot, the distribution of IAPP oligomers was analyzed, where any two peptides interconnected by at least one intermolecular heavy atom contact (the cutoff of 0.55 nm) was defined to belong to an oligomer. The size of an oligomer, $n_{oligomer}$, was defined by the number of IAPP peptides forming the aggregate. The two-dimensional PMF (or effective free energy) was computed according to

$$PMF = -K_B T \ln P(n_{oligomer}, Q_{fibrillization}) \quad (2)$$

where K_B is the Boltzmann constant, T corresponds to the simulation temperature 300 K, and $P(n_{oligomer}, Q_{fibrillization})$ is the probability of finding a peptide in an oligomer with the size of $n_{oligomer}$ and the extent of fibrillization $Q_{fibrillization}$ at the time.

RESULTS AND DISCUSSION

Synthesis and Characterization of PHEA Stars. PHEA stars were synthesized with constitutive elements similar to those observed in small molecule aggregation promoters. Specifically, the stars were designed to incorporate aromatic rings (on the distal end of the star arms) and pendant hydroxyls on the side chains of the arms. To actualize these design criteria, we chose *S,S′*-dibenzyltrithiocarbonate (DBTC) as the RAFT agent and employed in the polymerization of 2-hydroxethyl acrylate (Figure 1A). The polymerization was carried out in DMSO at 70 °C using AIBN as the radical initiator. To provide a suitable array of arm molecular weights for the subsequent star formation, we first synthesized three PHEA homopolymers with varying degrees of polymerization to approximately 80−90% conversion. The M_n of the homopolymers was determined via ^{1}H NMR analysis by comparing integrals for the peaks at δ = 7.1−7.4 ppm (corresponding to the benzyl leaving group of the RAFT agent, i.e., the polymer end group) with the integral for the peak corresponding to the hydroxyl group in the PHEA repeat unit (δ = 4.8 ppm). These results agreed well with the theoretical molecular weights determined from the ratio of the monomer to RAFT agent (see Table S1). GPC analysis of the various PHEA homopolymers revealed unimodal peaks with an acceptable dispersity of 1.2−1.3, although of course the M_n values from GPC differed considerably from those determined above due to calibration of the GPC against polystyrene standards.

The solutions of arm polymers (including unreacted HEA) were then used to form the PHEA stars by adding methylene(bis(acrylamide)) at various molar ratios and a further aliquot of AIBN and then heating at 70 °C for 24 h. Samples were taken periodically during the reaction with a further aliquot of AIBN injected after 12 h. A library of different core-cross-linked stars were formed with the results tabulated in Table S2. It is worth noting that the symmetrical nature of the RAFT agent used (DBTC) gave rise to arm polymer in which the thiocarbonylthio moiety was in the middle of the polymer chain. As such, subsequent introduction of the difunctional monomer (to facilitate formation of the cross-linked core) occurred in the middle of the arm polymer. The consequence of this architecture is that the final stars had an arm molecular weight that was half the value of the starting "arm" material. To our knowledge, this is the first time that this approach (i.e., the use of a symmetrical RAFT agent such as DBTC) has been employed in the preparation of star polymers. The resulting star polymers were analyzed by gel permeation chromatography to identify the best conditions for star formation. For all systems, there was a shift in the GPC trace for the PHEA homopolymer to shorter retention times, reflecting successful chain extension, with this shift typically most pronounced for higher ratios of cross-linker to polymer (Figure 1B; for [P]:[M]:[X] = 1:12:16 and $M_{n(GPC)}^{arm}$ = 14,500 g mol^{-1}). Estimation of approximate arm number could be made by dividing the $M_{n(GPC)}$ for the star by 1/2 $M_{n(GPC)}$ for the arm. The factor of 1/2 is introduced into this equation because of the symmetry of the chain transfer agent, as noted above. For each series, higher ratios of cross-linker led to higher arm numbers. It should be noted, however, that these values are only indicative of the true arm number due to the potential underestimation of molecular weight when applying GPC to hyperbranched materials. Moreover, the indicative nature of this approach is clearly evident in that the arm number should only ever be even given the symmetrical nature of the RAFT agent. Importantly, the use of DBTC as a RAFT agent for the HEA polymerization and the subsequent formation of star from DBTC-derived PHEA led to somewhat broader molecular weight distributions than have been achieved using other star polymer systems.[33] Although there is evidence in the literature that varying the solvent for star formation can improve arm incorporation and minimize polydispersity,[33] the scope for optimization of the current system was limited by the intransigent solubility of the stars in most solvents: we observed that the resulting materials were soluble only in DMSO or water. Even then, some difficulty was encountered when attempting to redisperse the star in these solvents after lyophilization. We attribute this effect to hydrogen bonding between the arms and as such allowed a minimum of 72 h for the polymer to equilibrate after redispersing in water.

From the GPC data, the star with the clearest shift to higher molecular weight accompanied by maintenance of a relatively unimodal molecular weight distribution was observed for the system where $M_{n(GPC)}^{arm}$ = 14,500 g mol^{-1} and [P]:[M]:[X] = 1:12:16. Analysis of this material by dynamic light scattering (Figure 1C) indicated a number-average hydrodynamic radius of approximately 9.8 nm for the stars when dispersed in water, which is consistent with other water-soluble star polymers synthesized via RAFT polymerization. Spectroscopic evaluation of these same PHEA stars was also conducted with the recorded ^{1}H NMR spectrum confirming that the desired

DOI: 10.1021/acs.biomac.7b01301
Biomacromolecules 2017, 18, 4249−4260

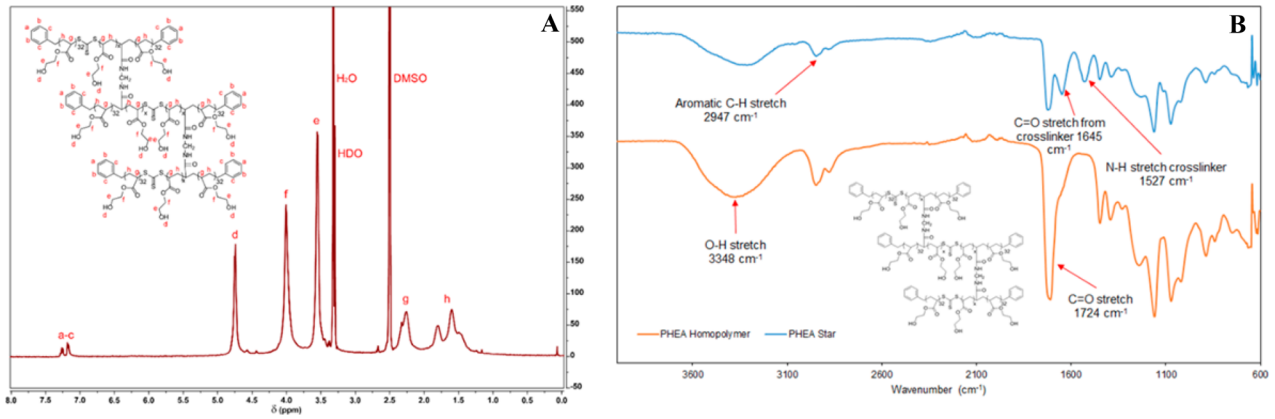

Figure 2. (A) ^{1}H NMR spectrum of purified PHEA stars recorded in DMSO-d_6 (400 MHz). The phenyl end-groups are evident at δ = 7.2−7.3 ppm. (B) FTIR-ATR spectra for the PHEA arm (orange) and star (blue).

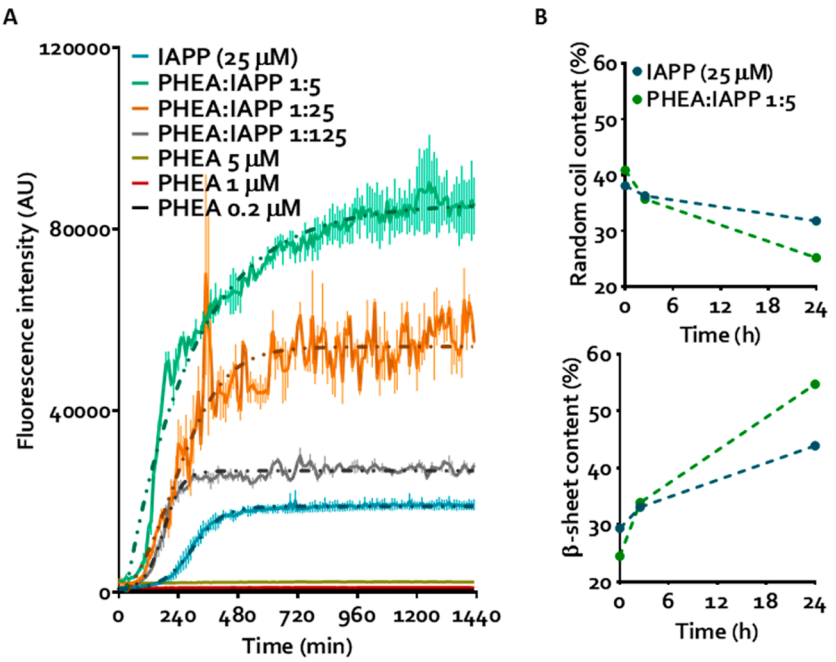

Figure 3. (A) ThT fluorescence of IAPP in the presence of PHEA stars over 24 h. Dotted lines represent sigmoidal curve fitting (least-squares fit); error is SEM (n = 2). (B) Secondary structure transitions in IAPP mapped by circular dichroism at 0, 2.5, and 24 h time points. Lines are intended to guide the eye. The concentration of IAPP in all experiments is 25 μM.

aromatic and hydroxyl moieties were present in the final polymer structure (Figure 2A). FTIR analysis before and after star formation provided further evidence of the high proportion of OH groups in the star in addition to demonstrating the presence of the methylene(bis(acrylamide)) linking groups in the star core (Figure 2B). Specifically, the emergence of peaks associated with amide C═O stretch (1,645 cm^{-1}) and amide N−H stretch (1,547 cm^{-1}) provide clear evidence that the amide cross-linking groups were successfully incorporated into the star structure.

Modulation of IAPP Fibrillization by PHEA Polymers. The thioflavin T (ThT) assay utilizes the amyloidophilic ThT dye to provide a measurement of both the extent and kinetics of amyloid fibrillization over time. The control IAPP was shown to fibrillate with a nucleation period of ∼2 h followed by an exponential period of ∼12 h before reaching saturation at 14 h (Figure 3A). Incubation of PHEA with IAPP at molar concentrations of 1:5 and 1:25 had a promotional effect on IAPP fibrillization both for the star NPs and their constituent subunits, referred to as "arms" (Figure S1), with the largest increase in ThT fluorescence observed at 1:5. Following the trend of increasing fibrillization with increasing concentration of PHEA, the energetically unfavorable nucleation period was also shown to significantly decrease with increasing concentration of PHEA, falling from ∼3.5 h in the IAPP control to less than 30 min with the highest concentration of PHEA. The reduction in IAPP lag time was also demonstrated through circular dichroism (CD) spectroscopy, wherein the presence of PHEA to IAPP at the 1:5 ratio notably promoted the amyloidogenic conversion of random coil content to β-sheets (Figures 3B and Figure S3). Over 2.5 h, β-sheet conversion in IAPP:PHEA 1:5 (25−34%) was 2.3× more rapid than that of IAPP alone (29−33%), and concordantly, IAPP contained 25% higher β-sheet content at 24 h in the presence of PHEA (55%) compared to that of IAPP alone (44%). This shift in prototypical IAPP aggregation kinetics, in addition to the

DOI: 10.1021/acs.biomac.7b01301
Biomacromolecules 2017, 18, 4249−4260

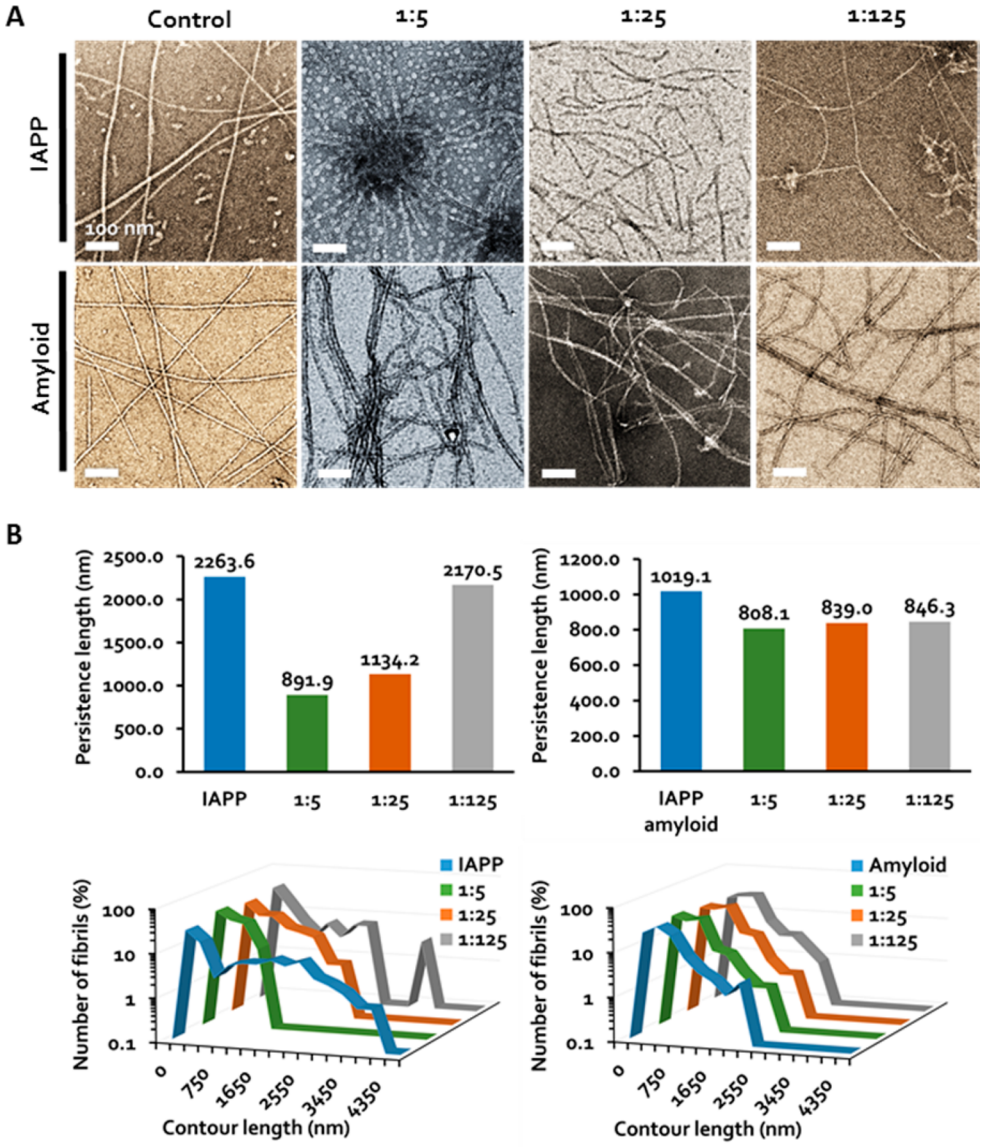

Figure 4. (A) TEM imaging of fibrillating IAPP (IAPP) and mature IAPP amyloids (Amyloid) in the presence and absence of PHEA stars after 24 h incubation. Stelliform amyloids are seen at PHEA:IAPP 1:5. Scale = 100 nm. (B) Structural analysis of amyloid fibrils visualized in (A). IAPP concentration in all experiments is 25 μM.

promotion of fibrillization overall, presents a case for rapid local sequestration of IAPP seeds by PHEA, whereas a lower PHEA concentration ratio would isolate aggregation "hotspots" and thus limit fibril elongation but promote coaggregation and thus enhance fibrillization at higher PHEA concentrations.

Stelliform Amyloid Formation and Amyloid Remodeling by PHEA. Transmission electron microscopy (TEM) imaging complemented ThT and CD analyses for fibrillating IAPP, allowing further analysis of persistence and contour length of amyloid fibrils generated after 24 h in aqueous solution in the presence and absence of PHEA. After 24 h, IAPP amyloidogenesis reached the saturation phase, and long, semiflexible fibrils can be observed by TEM with some shorter species still present (Figure 4A). Once fibril elongation and 3D cross-linking occurred at >5 days of amyloidogenesis, amyloids formed in-solution hydrogels, and generally, shorter species were absent.[45] "Stelliform amyloids" were observed when PHEA was incubated with IAPP at a 1:5 molar ratio (Figure 4A). These amyloids were characterized by a central nucleation "core", ranging from smaller clusters of 50−150 nm to micrometers in diameter. Fibrils of low persistence (average of 891.9 nm compared with that of 2,885 ± 60 nm for the IAPP control[6,7]) and contour length (<1,350 nm) were additionally observed radiating out from the core, forming the full stelliform structure of ∼0.5 μm in diameter for smaller cores and micrometers in diameter for larger cores with some macroscopic aggregates visible in solution (Figure 4A).

With lower concentrations of PHEA, the fibrillization products generally trended toward matching the structural morphology of IAPP alone (Figure 4B). IAPP amyloid fibrils with significantly reduced contour lengths were produced with increasing PHEA concentration, indicating polyphenol-like stabilization of growing fibrils through H-bonding; hydrophobic and $\pi-\pi$ interactions by PHEA[46] may have terminated fibril elongation, resulting in a fibril population with predominantly low contour lengths. As fibril elongation is mediated by amyloid seeds, the extensive exponential periods observed in the ThT assay (Figure 3A) could be indicative of the PHEA-IAPP

DOI: 10.1021/acs.biomac.7b01301
Biomacromolecules 2017, 18, 4249−4260

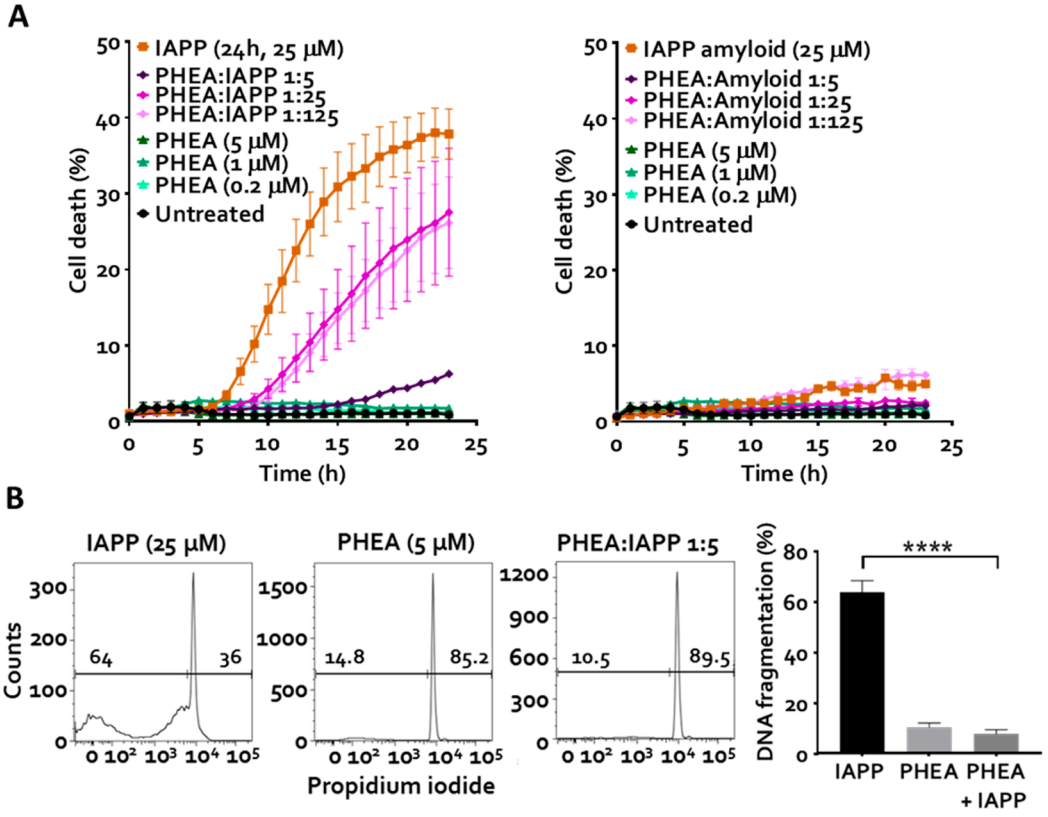

Figure 5. Protective effect of PHEA stars against IAPP-mediated cytotoxicity in pancreatic beta cells and islets. (A) In vitro cytotoxicity of fibrillating IAPP and mature IAPP amyloids in the presence and absence of PHEA in βTC6 cells over 24 h. Error = SEM (n = 3). (B) Ex vivo cytotoxicity of fibrillating IAPP and IAPP:PHEA at a 1:5 molar ratio in mouse islets after 48 h incubation. Flow cytometry data is representative of n = 5 experiments summarized in the graph. Error = SEM. ****p < 0.0001, one-way ANOVA with Tukey's correction.

complex rapidly sequestering amyloid seeds to render large populations of shorter fibrils, thus depleting the available seeding population to perform elongation. Interestingly, however, the shift in fibril persistence length induced by stars versus arms varied greatly; stars induced softer fibrils, whereas those generated in the presence of arms were notably stiffer. The capacity of PHEA to remodel IAPP amyloids was also assessed after coincubation for 24 h and demonstrated a similar trend. Amyloids were reduced in persistence length upon exposure to PHEA stars with the most notable effect seen as soft, limp fibrils "bundling" at PHEA:IAPP 1:5. Conversely, negligible amyloid remodeling was observed in the presence of PHEA arms. These observations could be attributed to the differences in morphology and surface physicochemical properties of the stars and arms.

Stelliform IAPP Amyloids Are Cytoprotective in Vitro and ex Vivo. IAPP-mediated cytotoxicity was assessed in an insulin-producing pancreatic β-cell line over a 24 h period (Figure 5A) and ex vivo in mouse islets after 48 h (Figure 5B). PHEA stars were completely biocompatible at all concentrations tested. In vitro, IAPP alone typically began to induce cytotoxicity at ~6 h post-treatment with cell death progressing exponentially up until the 20−24 h mark to an end point toxicity value of 38%. When incubated with IAPP at 1:25 and 1:125 ratios, PHEA stars delayed the progression of IAPP toxicity by ~2 h and reduced IAPP-mediated toxicity overall compared to that of the IAPP control. However, with PHEA stars:IAPP 1:5, cells were 94% viable after 24 h, and low levels of cytotoxicity were only observed more than 15 h post incubation. Per their aromatic structures,[31] PHEA arms successfully mitigated IAPP cytotoxicity at all concentrations tested (Figure S2). The cytoprotective capacity of PHEA stars at a 1:5 ratio to IAPP was also seen ex vivo, where mouse islets treated with IAPP in the presence of the highest concentration of PHEA stars (~8% relative cell death) demonstrated a significant reduction in toxicity compared to that of IAPP alone (64%) after 48 h treatment.

The near-complete mitigation in IAPP-mediated toxicity observed both in vitro and ex vivo when IAPP was incubated with PHEA stars correlated with stelliform amyloid formation at the PHEA:IAPP ratio of 1:5, as observed in Figure 4A. Likely the key to the cytoprotective nature of stelliform amyloids lies first in their mechanism of formation and additionally in terms of the structure itself. First, oligomeric and low-order protofibrillar species formed as intermediates during IAPP amyloidogenesis are widely considered responsible for the majority of IAPP-mediated cytotoxicity[3] with far less toxicity attributed to amyloid fibrils.[28] Seeding of IAPP oligomers to the plasma membrane of pancreatic β-cells resulted in destabilization of the lipid membrane[47] and cell death through "lipid stripping".[48] Concordantly, rapid sequestering of toxic low-order IAPP species through the formation of stelliform amyloids mediated by PHEA stars would reduce the local population of toxic species around the cell membrane.

Lastly, it has also been purported that the cytotoxicity of amyloid fibrils is mediated through partitioning of the hydrophobic, stiff fibrils into the cell membrane, leading to disruption of the membrane and production of radical oxygen species.[47,49,50] The structure of stelliform amyloids, with a compact core and vastly reduced persistence and contour

DOI: 10.1021/acs.biomac.7b01301
Biomacromolecules 2017, 18, 4249−4260

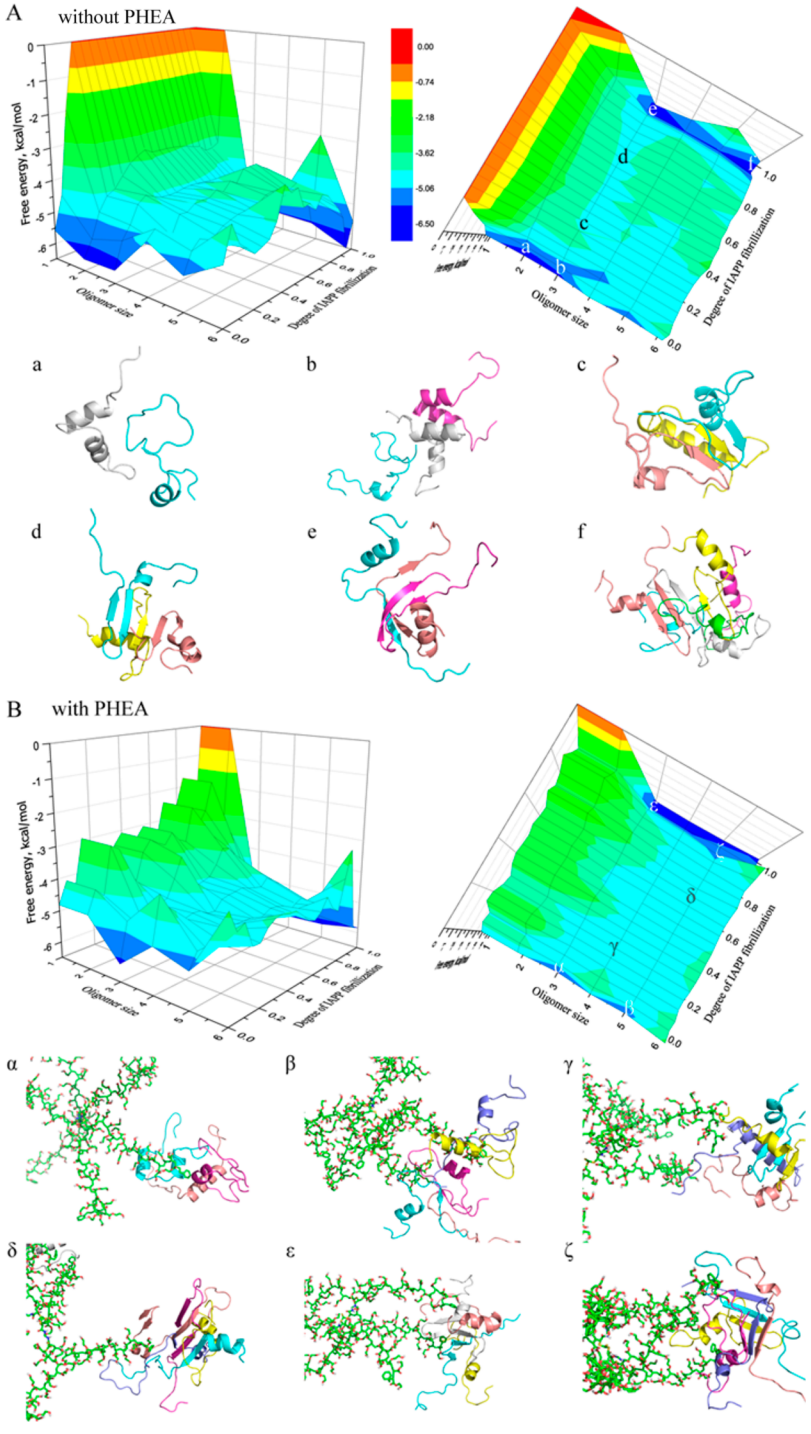

Figure 6. Aggregation free energy landscapes of IAPP without (A) and with (B) PHEA. Three-dimensional potentials of mean force (PMFs) with respect to IAPP oligomer size and degree of fibrillization were used to derive the free energy landscapes in front and top views. Snapshot structures with IAPP in cartoon and PHEA polymers in stick are shown to illustrate the basins and saddles of the energy landscapes.

lengths of radiating fibrils, would be unable to effectively partition into the lipid bilayer[51] and would also readily form a protein corona[52,53] within the extracellular milieu through electrostatic and hydrophobic interactions, further limiting any amyloid contact with cellular membranes. Importantly, we observed complete protection from IAPP-induced cell death in primary mouse islets treated with PHEA stars at a 1:5 molar ratio.

In Silico Study of the PHEA Polymers and Their Effects on IAPP Aggregation. To complement the experimental findings, we examined the structural properties of model PHEA polymers by all-atom DMD simulations[35] (see Experimental Methods, ESI). We first studied 2-arm PHEA polymers (Figure S4A) with different degrees of polymerization (DP) and computed their corresponding radius of gyration (R_g) values (Figure S4D). The data revealed an approximately linear dependence of R_g on DP (up to ~40, Figure S4D), suggesting that the PHEA stars were rather rigid. The autocorrelation analysis of the polymer dynamics in simulations resulted in an estimated Kuhn length of ~36 repeats (Figure

DOI: 10.1021/acs.biomac.7b01301
Biomacromolecules 2017, 18, 4249−4260

S4E), which confirmed the rigidity of the PHEA stars. To evaluate the structure and dynamics of PHEA stars, we studied an 8-arm PHEA model with molecular compositions resembling the experimental data (Figure S4C) in all-atom DMD simulations. A rapid equilibration in terms of R_g and ellipticity was observed (Figure S4F). The average R_g of the 8-arm polymer was ∼4.5 nm, consistent with the experimentally measured hydrodynamic radii (Figure 1C). The high ellipticity value (close to 1) suggests that the 8-arm PHEA adopted a nonspherical conformation as illustrated by a typical snapshot 3D structure (e.g., the inset of Figure S4F). Because of the high rigidity, the interactions between different arms were found minimal beyond the covalent cross-links. Therefore, the all-atom DMD simulations revealed a different morphology of the PHEA stars from that of PAMAM dendrimers, which feature a micellar structure with a porous interior for encapsulating small molecules[54] and IAPP peptides.[26]

To provide molecular insight into IAPP-PHEA binding and its effect on IAPP self-association, we performed DMD simulations on two sets of molecular systems with one containing six IAPP peptides along with a 6-arm PHEA polymer (Figure S4B) and another of six peptides alone as the control (see Experimental Methods in the ESI). We first monitored the size of the largest IAPP aggregates as a function of the simulation time and noted that the presence of PHEA indeed accelerated the self-association clusters in silico (Figure S5A). On the basis of the last 25 ns of the simulations where the largest IAPP aggregates were formed, the binding probability of each IAPP residue with PHEA indicated that both polar and nonpolar residues of IAPP could bind PHEA, though hydrophobic and aromatic residues showed a slightly higher binding propensity (Figure S5B). As a result, the generally nonspecific attraction between IAPP and PHEA led to the accumulation of peptides on PHEA arms, and the increased local peptide concentration accelerated the aggregation of IAPP consistently with a previous coarse-grained computational study.[55] We also examined the secondary structure of IAPPs and their binding with PHEA along the simulation trajectories (e.g., one of the independent simulations shown in Figure S6), where a general trend of correlation between IAPP-PHEA binding and β-sheet formation in IAPP aggregates was evident. Comparison-average secondary structure contents of the last 25 ns between simulations with and without PHEA (Figure S5C and D) suggest that the PHEA binding did not significantly affect the structures of the aggregates other than accelerated IAPP self-association (Figure S4A).

Next, the kinetics of β-sheet formation were analyzed for simulations of IAPPs with and without PHEA. The total number of IAPP residues in the β-sheet conformation followed sigmoidal-like kinetics (i.e., a lag phase followed by rapid growth/elongation and saturation as in Figure S7A) resembling experimentally observed aggregation kinetics. As expected for a nucleation-dependent process, each of the independent simulations rendered different lag times and elongation rates (see the fitting analysis in the Experimental Methods). The presence of PHEA significantly reduced the aggregation lag times (Figure S7B) and broadened the distribution of the elongation rates (Figure S7C), further suggesting that PHEA binding accelerated the nucleation of β-sheet aggregates and induced heterogeneity in β-sheet elongation, respectively. Additionally, the potential of mean force (PMF; i.e., the effective aggregate free energy landscape in Figure 6) was computed with respect to the size of IAPP oligomers, $n_{oligomer}$, and the degree of IAPP fibrillization, $Q_{fibrillization}$ (for details, see Experimental Methods in the ESI). Two major basins, one corresponding to IAPP monomers and oligomers with little β-sheets (e.g., highlighted as *a*,*b* in Figure 6A and α,β in Figure 6B) and the other denoting IAPP aggregates with high amounts of β-sheets (e.g., *e*,*f* in Figure 6A and ε,ζ in Figure 6B), could be observed in both IAPP aggregation free energy landscapes with and without PHEA stars. The saddles connecting the two basins corresponded to the aggregation pathways and intermediates (e.g., *c*,*d* in Figure 6A and γ,δ in Figure 6B). The presence of the PHEA star rendered the non-β-sheet basin shallower and the saddle broader (i.e., more pathways/routes toward final β-rich aggregates in Figure 6B), which accounted for the reduced aggregation lag times (Figure S7B) and heterogeneity in β-sheet elongation rates (Figure S7C).

CONCLUSIONS

Inspired by the mechanism of Pmel17 amyloidogenesis, we have developed and established that a polymeric star nanoparticle, PHEA, is capable of mitigating IAPP-mediated toxicity both in vitro and ex vivo through PHEA-mediated promotion of IAPP aggregation and formation of a unique "stelliform amyloid" morphology. Unlike the porous PAMAM-OH dendrimers, which inhibited both IAPP aggregation and toxicity through peptide sequestration,[26] the possession of high rigidity, long arm length, and rich aromatic moieties of PHEA stars facilitated rapid deposition and fibrillization of IAPP monomers into amyloid fibrils. Subsequently, this amyloid structure elicited significantly reduced toxicity in a pancreatic β-cell line and in mouse islets when compared to the long, semiflexible fibrils typically formed by IAPP. In light of the observation that both PHEA arms and stars elevated IAPP aggregation while mitigating IAPP toxicity, whereas dendrimers and hyperbranched polymers have been predominantly shown in the literature to inhibit amyloid protein aggregation,[11−18,21−26] it is plausible to attribute the observed phenomenon chiefly to the structure and physicochemical properties of the PHEA. Nonetheless, the shape/morphology of the PHEA stars was likely a contributing factor in the IAPP-PHEA interaction, as reflected by the difference in IAPP fibril stiffness associated with PHEA stars versus arms. Shortening of the oligomer lifetime through amyloid aggregation promotion represents a potential strategy to be explored within the larger context of amyloid research,[56] although implementation of such a strategy in vivo remains a challenge given the stochastic nature of secondary nucleation of amyloid proteins. This study has shed new light on the IAPP structure−toxicity relationship and presents an alternative blueprint for the design of polymeric nanomedicines against amyloidogenesis.

ASSOCIATED CONTENT

Supporting Information

The Supporting Information is available free of charge on the ACS Publications website at DOI: 10.1021/acs.biomac.7b01301.

Details of star polymer characterization, PHEA arms analysis, CD spectroscopy, and DMD simulations (PDF)

AUTHOR INFORMATION

Corresponding Authors

*E-mail: john.f.quinn@monash.edu.
*E-mail: thomas.p.davis@monash.edu.

DOI: 10.1021/acs.biomac.7b01301
Biomacromolecules 2017, 18, 4249−4260

*E-mail: pu-chun.ke@monash.edu.

ORCID

Michael R. Whittaker: 0000-0001-5706-3932
Esteban N. Gurzov: 0000-0003-4642-0273
Feng Ding: 0000-0003-1850-6336
John F. Quinn: 0000-0002-4593-1170
Thomas P. Davis: 0000-0003-2581-4986
Pu Chun Ke: 0000-0003-2134-0859

Author Contributions

P.C.K. and T.P.D. conceived the project. M.L., M.R.W., and J.F.Q. designed and performed PHEA synthesis and characterization. E.H.P. performed TEM, ThT, CD, and in vitro viability assays and analysis. M.W., M.A.S., and A.K. performed TEM and CD data analysis. E.N.G. and W.J.S. conducted the ex vivo viability assay and analysis. X.G., B.W., and F.D. performed DMD simulations and data analysis. E.H.P., P.C.K., J.F.Q., and X.G. wrote the paper. All authors discussed the data and agreed on the manuscript.

Notes

The authors declare no competing financial interest.

■ ACKNOWLEDGMENTS

This work was supported by ARC Project CE140100036 (T.P.D.), NSF CAREER CBET-1553945 (F.D.), NIH MIRA R35GM119691 (F.D.), NHMRC project grant APP1071350 (E.N.G.), and the Monash Institute of Pharmaceutical Sciences (P.C.K.). T.P.D. is thankful for the award of an Australian Laureate Fellowship from the ARC. J.F.Q. acknowledges receipt of a Future Fellowship from the ARC. E.H.P. acknowledges the support of an Australian Government Research Training Program scholarship. E.N.G. is supported by a Juvenile Diabetes Research Foundation (JDRF) fellowship.

■ REFERENCES

(1) Mendis, S. *Global status report on noncommunicable diseases 2014*; World Health Organization: Geneva, Switzerland, 2014.
(2) Kahn, S. E. The Importance of the β-Cell in the Pathogenesis of Type 2 Diabetes Mellitus. *Am. J. Med.* **2000**, *108*, 2S−8S.
(3) Pillay, K.; Govender, P. Amylin Uncovered: A Review on the Polypeptide Responsible for Type II Diabetes. *BioMed Res. Int.* **2013**, *2013*, 1.
(4) Despa, S.; Margulies, K. B.; Chen, L.; Knowlton, A. A.; Havel, P. J.; Taegtmeyer, H.; Bers, D. M.; Despa, F. Hyperamylinemia Contributes to Cardiac Dysfunction in Obesity and Diabetes: A Study in Humans and Rats. *Circ. Res.* **2012**, *110*, 598−608.
(5) Srodulski, S.; Sharma, S.; Bachstetter, A. B.; Brelsford, J. M.; Pascual, C.; Xie, X. S.; Saatman, K. E.; Van Eldik, L. J.; Despa, F. Neuroinflammation and neurologic deficits in diabetes linked to brain accumulation of amylin. *Mol. Neurodegener.* **2014**, *9*, 30.
(6) Wang, M.; Käkinen, A.; Pilkington, E. H.; Davis, T. P.; Ke, P. C. Differential Effects of Silver and Iron Oxide Nanoparticles on IAPP Aggregation and Toxicity. *Biomater. Sci.* **2017**, *5*, 485−493.
(7) Govindan, P. N.; Gurzov, E. N.; Chen, P.; Pilkington, E. H.; Stanley, W. J.; Litwak, S. A.; Davis, T. P.; Ke, P. C.; Ding, F. Graphene Oxide Inhibits hIAPP Amyloid Fibrillation and Toxicity in Insulin-Producing NIT-1 Cells. *Phys. Chem. Chem. Phys.* **2016**, *18*, 94−100.
(8) Wang, B.; Pilkington, E. H.; Sun, Y.; Davis, T. P.; Ke, P. C.; Ding, F. Modulating protein amyloid aggregation with nanomaterials. *Environ. Sci.: Nano* **2017**, *4*, 1772−1783.
(9) Ke, P. C.; Sani, M.-A.; Ding, F.; Käkinen, A.; Javed, I.; Separovic, F.; Davis, T. P.; Mezzenga, R. Implications of peptide assemblies in amyloid diseases. *Chem. Soc. Rev.* **2017**, DOI: 10.1039/C7CS00372B.
(10) Cabaleiro-Lago, C.; Quinlan-Pluck, F.; Lynch, I.; Lindman, S.; Minogue, A. M.; Thulin, E.; Walsh, D. M.; Dawson, K. A.; Linse, S. Inhibition of Amyloid β Protein Fibrillation by Polymeric Nanoparticles. *J. Am. Chem. Soc.* **2008**, *130*, 15437−15443.
(11) Breydo, L.; Newland, B.; Zhang, H.; Rosser, A.; Werner, C.; Uversky, V. N.; Wang, W. A hyperbranched dopamine-containing PEG-based polymer for the inhibition of α-synuclein fibrillation. *Biochem. Biophys. Res. Commun.* **2016**, *469*, 830−835.
(12) Chowdhury, S. R.; Agarwal, M.; Meher, N.; Muthuraj, B.; Iyer, P. K. Modulation of Amyloid Aggregates into Nontoxic Coaggregates by Hydroxyquinoline Appended Polyfluorene. *ACS Appl. Mater. Interfaces* **2016**, *8*, 13309−13319.
(13) Debnath, K.; Shekhar, S.; Kumar, V.; Jana, N. R.; Jana, N. R. Efficient Inhibition of Protein Aggregation, Disintegration of Aggregates, and Lowering of Cytotoxicity by Green Tea Polyphenol-Based Self-Assembled Polymer Nanoparticles. *ACS Appl. Mater. Interfaces* **2016**, *8*, 20309−20318.
(14) McCarthy, J. M.; Appelhans, D.; Tatzelt, J.; Rogers, S. M. Nanomedicine for prion disease treatment. *Prion* **2013**, *7*, 198−202.
(15) Sorokina, S. A.; Stroylova, Y. Y.; Shifrina, Z. B.; Muronetz, V. I. Disruption of Amyloid Prion Protein Aggregates by Cationic Pyridylphenylene Dendrimers. *Macromol. Biosci.* **2016**, *16*, 266−275.
(16) Fischer, M.; Appelhans, D.; Schwarz, S.; Klajnert, B.; Bryszewska, M.; Voit, B.; Rogers, M. Influence of Surface Functionality of Poly(propylene imine) Dendrimers on Protease Resistance and Propagation of the Scrapie Prion Protein. *Biomacromolecules* **2010**, *11*, 1314−1325.
(17) Klajnert, B.; Appelhans, D.; Komber, H.; Morgner, N.; Schwarz, S.; Richter, S.; Brutschy, B.; Ionov, M.; Tonkikh, A. K.; Bryszewska, M.; Voit, B. The Influence of Densely Organized Maltose Shells on the Biological Properties of Poly(propylene imine) Dendrimers: New Effects Dependent on Hydrogen Bonding. *Chem. - Eur. J.* **2008**, *14*, 7030−7041.
(18) Solassol, J.; Crozet, C.; Perrier, V.; Leclaire, J.; Béranger, F.; Caminade, A.-M.; Meunier, B.; Dormont, D.; Majoral, J.-P.; Lehmann, S. Cationic phosphorus-containing dendrimers reduce prion replication both in cell culture and in mice infected with scrapie. *J. Gen. Virol.* **2004**, *85*, 1791−1799.
(19) Supattapone, S.; Nguyen, H.-O. B.; Cohen, F. E.; Prusiner, S. B.; Scott, M. R. Elimination of prions by branched polyamines and implications for therapeutics. *Proc. Natl. Acad. Sci. U. S. A.* **1999**, *96*, 14529−14534.
(20) Supattapone, S.; Wille, H.; Uyechi, L.; Safar, J.; Tremblay, P.; Szoka, F. C.; Cohen, F. E.; Prusiner, S. B.; Scott, M. R. Branched Polyamines Cure Prion-Infected Neuroblasoma Cells. *J. Virol.* **2001**, *75*, 3453−3461.
(21) Benseny-Cases, N.; Klementieva, O.; Cladera, J. Dendrimers antiamyloidogenic potential in neurodegenerative diseases. *New J. Chem.* **2012**, *36*, 211−216.
(22) Klementieva, O.; Aso, E.; Filippini, D.; Benseny-Cases, N.; Carmona, M.; Juvés, S.; Appelhans, D.; Cladera, J.; Ferrer, I. Effect of Poly(propylene imine) Glycodendrimers on β-Amyloid Aggregation in Vitro and in APP/PS1 Transgenic Mice, as a Model of Brain Amyloid Deposition and Alzheimer's Disease. *Biomacromolecules* **2013**, *14*, 3570−3580.
(23) Neelov, I. M.; Janaszewska, A.; Klajnert, B.; Bryszewska, M.; Makova, N. Z.; Hicks, D.; Pearson, H. A.; Vlaslov, G. P.; Ilyash, M. Y.; Dubrovskaya, N. M.; Tumanova, N. L.; Zhuravin, I. A.; Turner, A. J.; Nalivaeva, N. N. Molecular Properties of Lysine Dendrimers and their Interactions with Aβ-Peptides and Neuronal Cells. *Curr. Med. Chem.* **2013**, *20*, 134−143.
(24) Nguyen, P. T.; Sharma, R.; Rej, R.; De Carufel, C. A.; Roy, R.; Bourgault, S. Low generation anionic dendrimers modulate islet amyloid polypeptide self-assembly and inhibit pancreatic β-cell toxicity. *RSC Adv.* **2016**, *6*, 76360−76369.
(25) Nowacka, O.; Shcharbin, D.; Klajnert-Maculewicz, B.; Bryszewska, M. Stabilizing effect of small concentrations of PAMAM dendrimers at the insulin aggregation. *Colloids Surf., B* **2014**, *116*, 757−760.
(26) Gurzov, E. N.; Wang, B.; Pilkington, E. H.; Chen, P.; Käkinen, A.; Stanley, W. J.; Litwak, S. A.; Hanssen, E. G.; Davis, T. P.; Ding, F.;

Ke, P. C. Inhibition of hIAPP Amyloid Aggregation and Pancreatic β-Cell Toxicity by OH-Terminated PAMAM Dendrimer. *Small* **2016**, *12*, 1615−1626.
(27) Fowler, D. M.; Koulov, A. V.; Alory-Jost, C.; Marks, M. S.; Balch, W. E.; Kelly, J. W. Functional Amyloid Formation within Mammalian Tissue. *PLoS Biol.* **2006**, *4*, 0100−0107.
(28) Cheng, I. H.; Scearce-Levie, K.; Legleiter, J.; Palop, J. J.; Gerstein, H.; Bien-Ly, N.; Puoliväli, J.; Lesné, S.; Ashe, K. H.; Muchowski, P. J.; Mucke, L. Accelerating Amyloid-β Fibrillization Reduces Oligomer Levels and Functional Deficits in Alzheimer Disease Mouse Models. *J. Biol. Chem.* **2007**, *282*, 23818−23828.
(29) Chen, J.; Armstrong, A. H.; Koehler, A. N.; Hecht, M. H. Small Molecule Microarrays Enable the Discovery of Compounds that Bind the Alzheimer's Aβ Peptide and Reduce its Cytotoxicity. *J. Am. Chem. Soc.* **2010**, *132*, 17015−17022.
(30) Bieschke, J.; Herbst, M.; Wiglenda, M.; Friedrich, R. P.; Boeddrich, A.; Schiele, F.; Kleckers, D.; del Amo, J. M. L.; Grüning, B. A.; Wang, Q.; Schmidt, M. R.; Lurz, R.; Anwyl, R.; Schnoegl, S.; Fändrich, M.; Frank, R. F.; Reif, B.; Günther, S.; Walsh, D. M.; Wanker, E. E. Small-molecule conversion of toxic oligomers to nontoxic β-sheet−rich amyloid fibrils. *Nat. Chem. Biol.* **2011**, *8*, 93−101.
(31) Barrajón-Catalán, E.; Herranz-López, M.; Joven, J.; Segura-Carretero, A.; Alonso-Villaverde, C.; Menéndez, J. A.; Micol, V. Molecular Promiscuity of Plant Polyphenols in the Management of Age-Related Diseases: Far Beyond Their Antioxidant Properties. In *Oxidative Stress and Inflammation in Non-communicable Diseases - Molecular Mechanisms and Perspectives in Therapeutics*; Camps, J., Ed.; Springer International: Switzerland, 2014; pp 141−159.
(32) Ren, M.; McKenzie, T. G.; Fu, Q.; Wong, E. H. H.; Xu, J.; An, Z.; Shanmugam, S.; Davis, T. P.; Boyer, C.; Qiao, G. G. Star Polymers. *Chem. Rev.* **2016**, *116*, 6743−6836.
(33) Ferreira, J.; Syrett, J.; Whittaker, M. R.; Haddleton, D. M.; Davis, T. P.; Boyer, C. Optimizing the generation of narrow polydispersity 'arm-first' star polymers made using RAFT polymerization. *Polym. Chem.* **2011**, *2*, 1671−1677.
(34) Hu, J.; Qiao, R.; Whittaker, M. R.; Quinn, J. F.; Davis, T. P. Synthesis of Star Polymers by RAFT Polymerization as Versatile Nanoparticles for Biomedical Applications. *Aust. J. Chem.* **2017**, DOI: 10.1071/CH17391.
(35) Ding, F.; Tsao, D.; Nie, H.; Dokholyan, N. V. Ab initio folding of proteins with all-atom discrete molecular dynamics. *Structure* **2008**, *16*, 1010−1018.
(36) Usov, I.; Mezzenga, R. FiberApp: An Open-Source Software for Tracking and Analyzing Polymers, Filaments, Biomacromolecules, and Fibrous Objects. *Macromolecules* **2015**, *48*, 1269−1280.
(37) Adamcik, J.; Jung, J.-M.; Flakowski, J.; De Los Rios, P.; Dietler, G.; Mezzenga, R. Understanding amyloid aggregation by statistical analysis of atomic force microscopy images. *Nat. Nanotechnol.* **2010**, *5*, 423−428.
(38) Stanley, W. J.; Litwak, S. A.; Quah, H. S.; Tan, S. M.; Kay, T. W.; Tiganis, T.; de Haan, J. B.; Thomas, H. E.; Gurzov, E. N. Inactivation of Protein Tyrosine Phosphatases Enhances Interferon Signaling in Pancreatic Islets. *Diabetes* **2015**, *64*, 2489−2496.
(39) Hanwell, M. D.; Curtis, D. E.; Lonie, D. C.; Vandermeersch, T.; Zurek, E.; Hutchison, G. R. Avogadro: an advanced semantic chemical editor, visualization, and analysis platform. *J. Cheminf.* **2012**, *4*, 17.
(40) Halgren, T. A. MMFF VI. MMFF94s option for energy minimization studies. *J. Comput. Chem.* **1999**, *20*, 720−729.
(41) Yin, S.; Biedermannova, L.; Vondrasek, J.; Dokholyan, N. V. MedusaScore: An Accurate Force-Field Based Scoring Function for Virtual Drug Screening. *J. Chem. Inf. Model.* **2008**, *48*, 1656−1662.
(42) Ding, F.; Dokholyan, N. Emergence of Protein Fold Families through Rational Design. *PLoS Comput. Biol.* **2006**, *2*, e85.
(43) Ding, F.; Dokholyan, N. Incorporating Backbone Flexibility in MedusaDock Improves Ligand-Binding Pose Prediction in the CSAR2011 Docking Benchmark. *J. Chem. Inf. Model.* **2013**, *53*, 1871−1879.
(44) Govindan, P. N.; Jemec, D. B.; Ding, F. CSAR Benchmark of Flexible MedusaDock in Affinity Prediction and Nativelike Binding Pose Selection. *J. Chem. Inf. Model.* **2016**, *56*, 1042−1052.
(45) Jean, L.; Lee, C. F.; Hodder, P.; Hawkins, N.; Vaux, D. J. Dynamics of the formation of a hydrogel by a pathogenic amyloid peptide: islet amyloid polypeptide. *Sci. Rep.* **2016**, *6*, 32124.
(46) Govindan, P. N.; Käkinen, A.; Pilkington, E. H.; Davis, T. P.; Ke, P. C.; Ding, F. Stabilizing Off-pathway Oligomers by Polyphenol Nanoassemblies for IAPP Aggregation Inhibition. *Sci. Rep.* **2016**, *6*, 19463.
(47) Pilkington, E. H.; Gurzov, E. N.; Käkinen, A.; Litwak, S. A.; Stanley, W. J.; Davis, T. P.; Ke, P. C. Pancreatic β-Cell Membrane Fluidity and Toxicity Induced by Human Islet Amyloid Polypeptide Species. *Sci. Rep.* **2016**, *6*, 21274.
(48) Sparr, E.; Engel, M. F. M.; Sakharov, D. V.; Sprong, M.; Jacobs, J.; de Kruijff, B.; Höppener, J. W. M.; Killian, J. A. Islet amyloid polypeptide-induced membrane leakage involves uptake of lipids by forming amyloid fibres. *FEBS Lett.* **2004**, *577*, 117−120.
(49) Huang, B.; He, J.; Ren, J.; Yan, X.-Y.; Zeng, C.-M. Cellular Membrane Disruption by Amyloid Fibrils Involved Intermolecular Disulfide Cross-Linking. *Biochemistry* **2009**, *48*, 5794−5800.
(50) Friedrich, R. P.; Tepper, K.; Rönicke, R.; Soom, M.; Westermann, M.; Reymann, K.; Kaether, C.; Fändrich, M. Mechanism of amyloid plaque formation suggests an intracellular basis of Aβ pathogenicity. *Proc. Natl. Acad. Sci. U. S. A.* **2010**, *107*, 1942−1947.
(51) Klementieva, O.; Benseny-Cases, N.; Gella, A.; Appelhans, D.; Voit, B.; Cladera, J. Dense Shell Glycodendrimers as Potential Nontoxic Anti-amyloidogenic Agents in Alzheimer's Disease. Amyloid-Dendrimer Aggregates Morphology and Cell Toxicity. *Biomacromolecules* **2011**, *12*, 3903−3909.
(52) Cedervall, T.; Lynch, I.; Lindman, S.; Berggård, T.; Thulin, E.; Nilsson, H.; Dawson, K. A.; Linse, S. Understanding the nanoparticle-protein corona using methods to quantify exchange rates and affinities of proteins for nanoparticles. *Proc. Natl. Acad. Sci. U. S. A.* **2007**, *104*, 2050−2055.
(53) Pilkington, E. H.; Xing, Y.; Wang, B.; Käkinen, A.; Wang, M.; Davis, T. P.; Ding, F.; Ke, P. C. Effects of Protein Corona on IAPP Amyloid Aggregation, Fibril Remodelling, and Cytotoxicity. *Sci. Rep.* **2017**, *7*, 2455.
(54) Wang, B.; Geitner, N. K.; Davis, T. P.; Ke, P. C.; Ladner, D. L.; Ding, F. Deviation from the Unimolecular Micelle Paradigm of PAMAM Dendrimers Induced by Strong Interligand Interactions. *J. Phys. Chem. C* **2015**, *119*, 19475−19484.
(55) Radic, S.; Davis, T. P.; Ke, P. C.; Ding, F. Contrasting effects of nanoparticle-protein attraction on amyloid aggregation. *RSC Adv.* **2015**, *5*, 105489−105498.
(56) Peterson, S. A.; Klabunde, T.; Lashuel, H. A.; Purkey, H.; Sacchettini, J. C.; Kelly, J. W. Inhibiting transthyretin conformational changes that lead to amyloid fibril formation. *Proc. Natl. Acad. Sci. U. S. A.* **1998**, *95*, 12956−12960.

DOI: 10.1021/acs.biomac.7b01301
Biomacromolecules 2017, 18, 4249−4260

Chapter Five: Conclusions

Amyloidosis, with its associated dysfunction and damage elicited to cells and tissues, is a hallmark of a number of metabolic and neurodegenerative diseases.[1] IAPP represents an understudied amyloidogenic peptide, with regards to its role within the scope of pancreatic β-cell failure and T2D, and beyond, as circulating toxic amyloid species translocate throughout the body.[2] This thesis presented a streamlined biophysical, biochemical and toxicological investigation of IAPP amyloidosis, IAPP species and their biological interactions within a tightly controlled *in vitro* environment towards facilitating the design of effective anti-amyloidosis agents.

For assigning the associated toxicity of amyloidosis to specific pathway species, the 'oligomer hypothesis' has long been the reigning paradigm.[3] This theory was largely based on studies that pertained to well-characterized amyloid species such as Aβ and αSyn, whose slow fibrillization kinetics allow for more facile gating and consequent interrogation of discrete monomeric, oligomeric and fibrillar populations comparative to the more rapidly aggregating IAPP. Characterization of IAPP amyloid pathway species in **Chapter Two** of this thesis ultimately aligned with this hypothesis: through the effective *in vitro* isolation of intermediate populations sans foreign stabilizing agents, early intermediate species elicited significantly higher cytotoxicity in primary cells comparative to mature amyloid species. Additionally, in **Chapter Two**, the impact of model proteins, lipids and ultrasmall membranes on amyloidosis was explored *in vitro*, demonstrating that each biomolecule had the capacity to modulate IAPP fibrillization, yet was unable to ameliorate its intrinsic cytotoxicity. IAPP interfaced with these model interactors adopted novel morphologies, potentiating an array of native states of IAPP in a biological milieu, beyond the fibrillar structures prepared in absence of interacting factors *in vitro*. Notably, utilizing model proteins with analogous molecular weights and globular structures yet opposing charges further demonstrated that the charge of IAPP interactors is not a major factor impacting the cytotoxic behavior of the net positively charged IAPP fibrillating species. Consequently, targeting cationic anti-amyloid agents towards net negatively charged amyloids, such as Aβ and αSyn, may not be a strategy worth the cytotoxic trade-off of the cationic agents themselves.

Thus, two key findings in **Chapter Two** – the cytotoxicity of fibrillating IAPP species nullified upon reaching the mature amyloid state, and the charges of interactors of fibrillating IAPP having negligible impact on toxicity mitigation therein – advised the strategic approach utilized

for mitigation of IAPP-mediated cytotoxicity: firstly, enhancing the fibrillization of IAPP in order to reduce the half-life of toxic intermediate species through their incorporation into nontoxic mature amyloid morphologies, and, secondly, providing a neutral charge to the anti-amyloid agent utilized for superior biocompatibility. Consequently, the novel synthesis of 'PHEA' star polymers, designed with aromatic moieties and terminal hydroxyls to maximize amyloid contact, resulted in near-complete mitigation of IAPP-associated cytotoxicity in pancreatic β-cells *in vitro* and in mouse islets *ex vivo*. Indeed, cytotoxic IAPP intermediates were effectively scavenged from solution by PHEA stars, with the hydrophobic-hydrophobic IAPP-star binding interactions effectively facilitated by the rigid star polymer branches – further providing a scaffold for rapid fibril propagation to generate nontoxic 'stelliform' amyloids. Thus, the promotion of IAPP fibrillization presents an alternative approach to aggregation inhibition as the predominant anti-IAPP amyloidosis strategy currently employed. Moreover, star polymers represent an inexpensive and highly tunable class of nanomaterials to be further explored as anti-amyloidosis agents.

Though this thesis has established fibrillating IAPP species as the major cytotoxic species within the amyloid pathway, and thus through bypassing the toxic intermediate stage via a 'fibrillization promotion' strategy IAPP-associated toxicity can be effectively ameliorated, the role of the amyloid fibril in IAPP pathogenesis should not be so readily discarded. While the 'oligomer hypothesis' can be correlated to cell dysfunction and tissue damage in the short term, the research presented herein underscores a longer-term impact of amyloid plaques *in vivo*. The binding and remodeling of IAPP amyloid fibrils by model proteins in **Chapter Two** conferred a protective effect against low-level amyloid-associated cytotoxicity *in vitro* – again, regardless of charge – demonstrated, for the first time, the potential biological impact of an 'amyloid-protein corona.' Association of a single protein, from either a native or foreign source, has been demonstrated to significantly impact a nanomaterial's biological properties. For example, Aβ amyloid fibril association with human immunodeficiency virus envelope protein Tat highly enhances the neurotoxicity of the complex beyond the capacity of either ligand alone[4] – accordingly, endogenously available clusterin, upregulated in AD, has been found enriched in Aβ plaques *in vivo*, impacting both their localization and pathology.[5] Upon further interrogation within a complex biological milieu in **Chapter Three**, it was revealed through biophysical and proteomic analyses that IAPP amyloid forms extensive, nonuniform coronae of proteins involved in a number of biological niches, with fibrillar conformations and structural plasticity pertaining to the most favorable binders while no trends were observed in

the charge or hydrophobicity of coronal proteins, further supporting observations in **Chapter Two**. Remarkably, variation in coronal proteins was seen when amyloids were exposed to the same media under different biological conditions, implicating both a complex architecture of permanent-transient interactors, and, consequently, a unique biological identity conferred to plaques localized to different areas of the body.

The 'amyloid-protein corona' studies in **Chapters Two** and **Three** support *in vivo* observations of protein enrichment to amyloid plaques, giving detailed context to clinical profiles. Chaperone proteins and proteolytic species found highly localized to amyloid deposits, as observed in Liao and colleagues' proteomic analysis of plaque-enriched proteins within AD patient tissues,[6] could present a failed mechanism by the body to disaggregate amyloid fibrils, resulting instead in a highly proteolytic environment that likely impacts the local populations of circulating protein. Such 'downstream' effects would not be observed in short term studies, where the duration of experiments is within hours to days *in vitro*. Indeed, rodents, as the predominant animal model utilized in *in vivo* studies of amyloidosis, have a lifespan of a mere couple of years, whereas insoluble amyloid plaques in human tissues can exist for decades.[7] Thus, amyloid fibrils and plaques – and, by extension, the amyloid-protein corona – may facilitate long term pathologic effect, through disruption and destabilization of the local microenvironment rather than the short-term damage elicited by fibrillating species. Thus, **Chapter Four**'s landmark, comprehensive study into amyloid-protein corona formation in biological media provides new insights into potential amyloid interactors, illustrating a complex network of proteins with diverse functions that exemplify how pancreatic and extra-pancreatic amyloid plaques exposed to different environmental conditions and localized concentrations of circulating protein may impact numerous biological processes in the surrounding milieu. With further quantitative *in vitro* analyses complemented by isolation and characterization of plaques from different *in vivo* microenvironments, new pathologies of amyloid-associated disease could be revealed. For example, the role of the protein corona on the cross-seeding of amyloid proteins, and the metal hosting capacity of amyloid fibrils and plaques modulated by their dynamic protein corona, are two significant topics to be fully elucidated towards understanding the implications of amyloidogenesis in *in vivo* environments.

Lastly, in a follow-up study to elucidating the amyloid-protein corona in complex environs in **Chapter Three**, the candidate sought to characterize the protein corona of IAPP oligomers in biological media. Curiously, intermediate species of IAPP displayed very little binding to the oligomer-specific antibody A11 when exposure occurred under flow conditions. This data is

not presented herein as the results were inconclusive, but serve to underline a key point: that the breadth of conformations adopted by IAPP intermediate species, such as the novel biannular oligomer morphology identified herein, highlight challenges inherent in the application of (largely conformation-specific)[8] targeting antibodies against amyloidosis. The recent revival of Biogen's anti-amyloidosis drug towards FDA approval and commercialization has reinvigorated interest in the amyloid hypothesis of pathogenicity in neurodegenerative and metabolic disease: however, our understanding into amyloid-associated pathologies needs to continue to evolve in order for treatment strategies to effectively combat amyloid diseases.

5.1 References

(1) Chiti, F.; Dobson, C. M., Protein Misfolding, Functional Amyloid, and Human Disease. *Ann. Rev. Biochem.* **2006,** *75*, 333-366.

(2) Kahn, S. E.; Andrikopoulos, S.; Verchere, C. B., Islet amyloid: a long-recognized but underappreciated pathological feature of type 2 diabetes. *Diabetes* **1999,** *48*, 241-253.

(3) Zraika, S.; Hull, R. L.; Verchere, C. B.; Clark, A.; Potter, K. J.; Fraser, P. E.; Kahn, S. E., Toxic oligomers and islet beta cell death: guilty by association or convicted by circumstantial evidence? *Diabetologia* **2010,** *53*, 1046-1056.

(4) Hategan, A.; Bianchet, M. A.; Steiner, J.; Karnaukhova, E.; Masliah, E.; Fields, A.; Lee, M. H.; Dickens, A., M.; Haughey, N.; Dimitriadis, E. K.; Nath, A., HIV Tat protein and amyloid-β peptide form multifibrillar structures that cause neurotoxicity. *Nat. Struct. Mol. Biol.* **2017,** *24*, 379-386.

(5) Wojtas, A. M.; Kang, S. S.; Olley, B. M.; Gatherer, M.; Shinohara, M.; Loranzo, P. A.; Liu, C. C.; Kurti, A.; Baker, K. E.; Dickson, D. W.; Yue, M.; Petrucelli, L.; Bu, G.; Carare, R. O.; Fryer, J. D., Loss of clusterin shifts amyloid deposition to the cerebrovasculature via disruption of perivascular drainage pathways. *Proc. Natl. Acad. Sci. U.S.A.* **2017,** *114*, E6962-E6971.

(6) Liao, L.; Cheng, D.; Wang, J.; Duong, D. M.; Losik, T. G.; Gearing, M.; Rees, H. D.; Lah, J. J.; Levey, A. I.; Peng, J., Proteomic Characterization of Postmortem Amyloid Plaques Isolated by Laser Capture Microdissection. *J. Biol. Chem.* **2004,** *279*, 37061-37068.

(7) Drummond, E.; Wisniewski, T., Alzheimer's disease: experimental models and reality. *Acta Neuropathol.* **2017,** *133*, 155-175.

(8) Glabe, C. G., Structural Classification of Toxic Amyloid Oligomers. *J. Biol. Chem.* **2008,** *283*, 29639-29643.

Appendices

Supporting Information

Model Interactions of Amyloid Protein Species

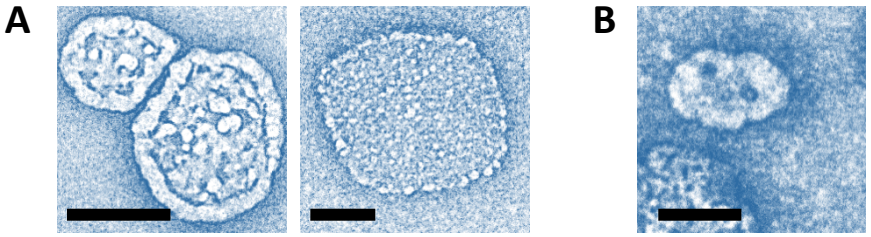

Figure S1: A. Two morphologies of off-pathway IAPP amyloid particulates identified during intermediate profiling study. Scale = 100 nm. B. Example of a biannular oligomer identified in oligomerized Aβ1-42 after incubation for 24 h at 4 °C in aqueous solution. Scale = 50 nm.

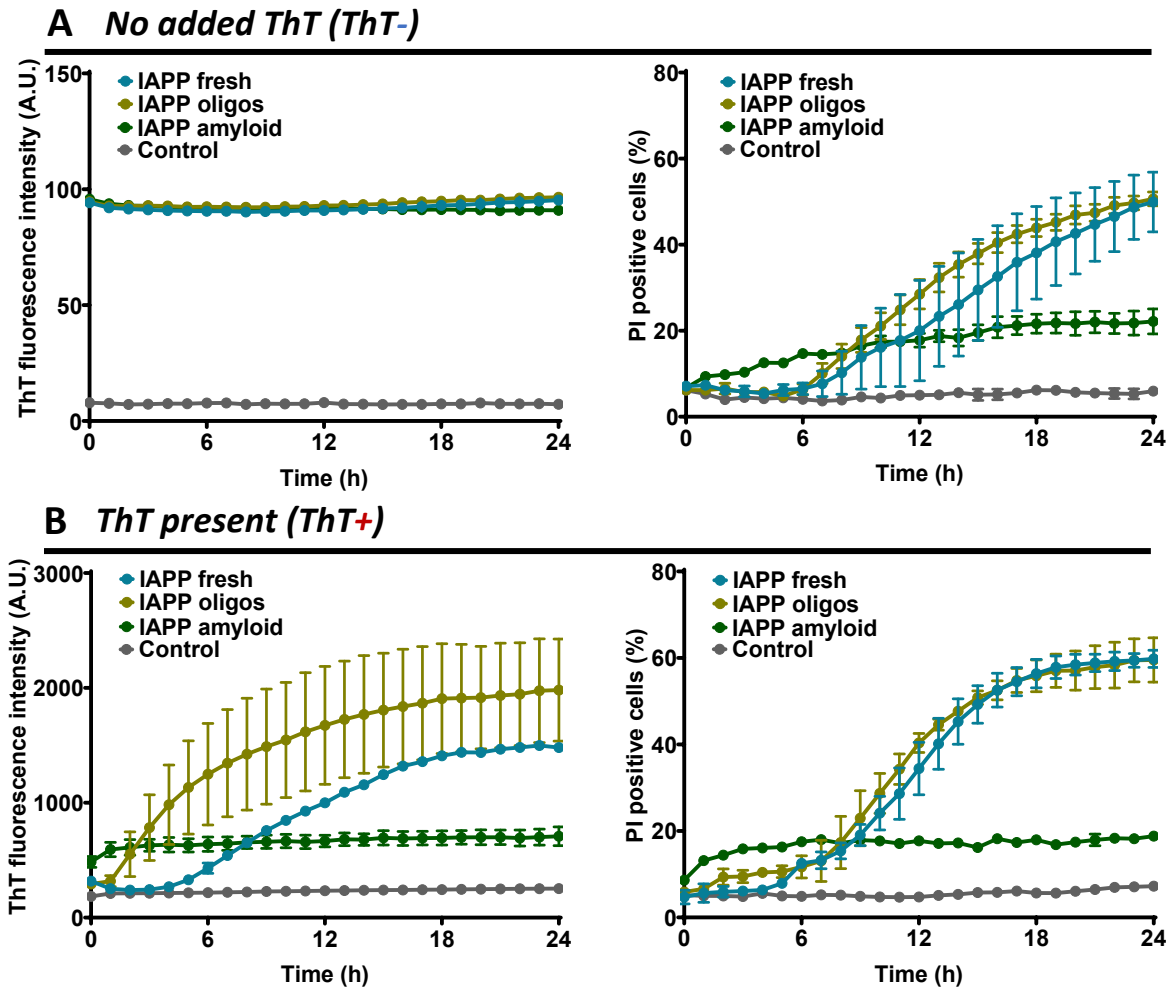

Figure S2: Cytotoxicity (as determined by PI positive cells) and ThT fluorescence intensity in the absence (A) and presence (B) of ThT dye in HUVECs treated with IAPP species (25 μM) over 24 h, n = 3. Unpaired t-tests using Holm-Sidak's method for multiple comparisons confirmed no significant difference in endpoint cytotoxicity between ThT+ and ThT- sets, and all ThT+ datasets were significantly differentiated from ThT- datasets by ThT fluorescence intensity.

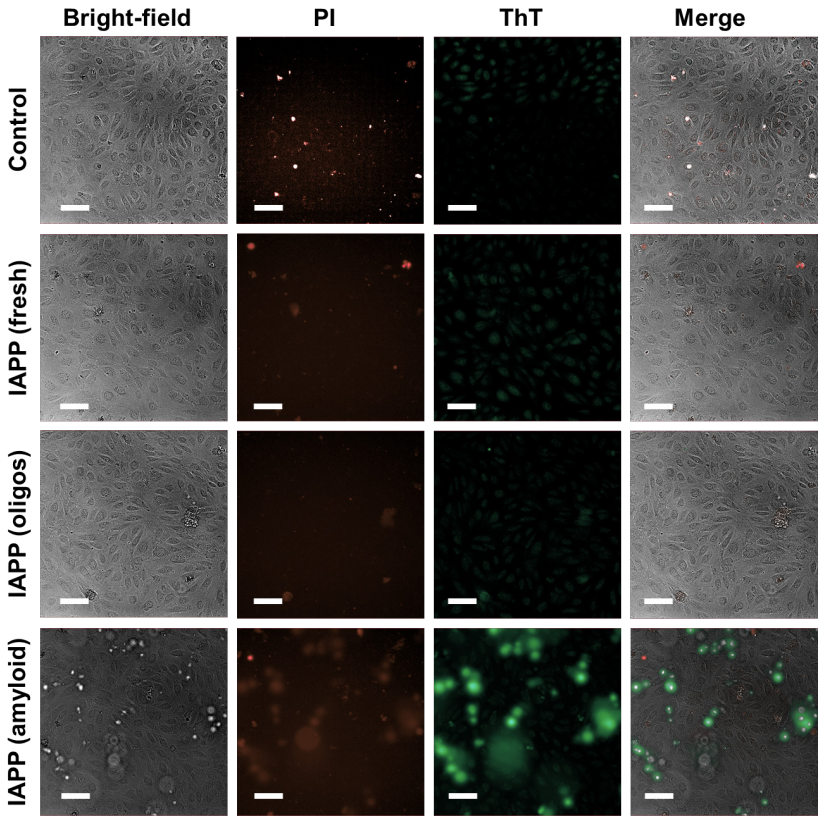

Figure S3: Fluorescence microscopy of IAPP species (25 μM), either fresh (lyophilized monomers), oligos (low order aggregates, pre-incubated for 4 h in aqueous at 4 °C) and amyloid (mature fibrils, pre-incubated for ~2 weeks in aqueous at room temperature) added to HUVECs and immediately imaged (T = 0 h). Propidium iodide (PI) indicates dead cell nuclei, and the formation of β-rich amyloid is probed by thioflavin T (ThT). Scale = 100 μm.

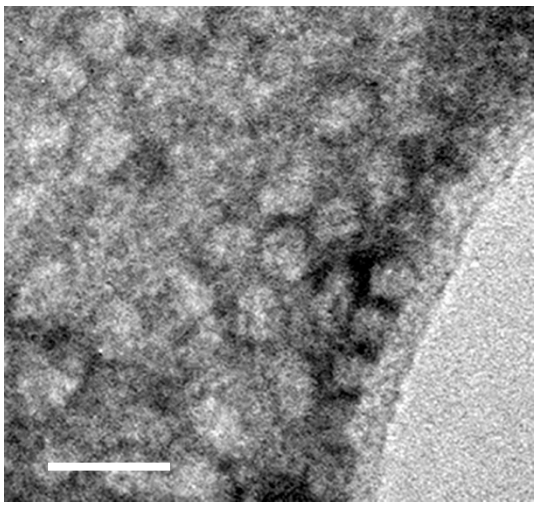

Figure S4: TEM image of LPC micelles at 2 mM (>CMC). Scale = 10 nm. Reproduced by permission of the PCCP Owner Societies from Xing, Y.; Pilkington, E. H.; Wang, M.; Nowell, C. J.; Käkinen, A.; Sun, Y.; Wang, B.; Davis, T. P.; Ding, F.; Ke, P. C., Lysophosphatidylcholine modulates the aggregation of human islet amyloid polypeptide. *Phys. Chem. Chem. Phys.* **2017,** *19*, 30627-30635.

Supporting Information

Profiling the Serum Protein Corona of Fibrillar Human Islet Amyloid Polypeptide

Emily H. Pilkington,[1,2] Ove J. R. Gustafsson,[3] Yanting Xing,[4] Juan Hernandez-Fernaud,[5] Cleidi Zampronio,[5] Aleksandr Kakinen,[1] Ava Faridi,[1] Feng Ding,[4] Paul Wilson,[1,2] Pu Chun Ke[1] and Thomas P. Davis[1,2*]*

[1]ARC Centre of Excellence in Convergent Bio-Nano Science and Technology, Monash Institute of Pharmaceutical Sciences, 381 Royal Parade, Parkville, VIC 3052, Australia

[2]Department of Chemistry, University of Warwick, Library Road, CV4 4AL, Coventry, UK

[3]ARC Centre of Excellence in Convergent Bio-Nano Science and Technology, Future Industries Institute, University of South Australia, University Boulevard, Mawson Lakes, SA 5095, Australia

[4]Department of Physics and Astronomy, Clemson University, Clemson, SC 29634, USA

[5]Warwick Proteomics Research Technology Platform, School of Life Sciences, Gibbet Hill Road, University of Warwick, CV4 7AL, Coventry, UK

Blue-Native polyacrylamide gel electrophoresis (PAGE) and analysis

Blue-Native PAGE allowed the examination of protein complex formation between IAPP amyloid fibrils (0.9 mg/mL) and FBS, which were pre-incubated (2% and 50%, in water) for 2 h. A 15 µL aliquot of each sample was mixed 1:1 with chilled Native PAGE sample buffer and then transferred to 4-15% gel (Mini-Protean TGX). Blue-Native PAGE was performed at 4 $^{\circ}$C, pH = 8.3, using sequential buffer steps: briefly, Tris/Glycine buffer was supplemented with Coomassie Brilliant Blue G-250 at either 0.02%, 0.002%, or omitted, with each buffer solution utilized in this order during the assay. For protein binding capacity a densitometry of lane and well band profiles, normalized against background intensity, was performed using ImageJ. The experiment was performed and analyzed in duplicate. All materials listed were sourced from BioRad.

Circular dichroism spectroscopy

Structural changes in bovine serum albumin (BSA), the most abundant protein species in FBS medium, were examined upon its interaction with IAPP fibrils. BSA (0.1 mg/mL) was exposed to IAPP amyloid fibrils (>1 week old, in water; 0.1 mg/mL) for 24 h, and CD spectra of BSA were obtained at different timepoints using an Aviv Model 410 CD spectrophotometer (Biomedical, Inc.). The spectra were recorded over a wavelength range of 190~260 nm, with a 1 nm step size and a scanning speed of 15 nm/min at room temperature. The final spectra were baseline-corrected and IAPP amyloid spectrum subtracted where applicable. The data were measured in mean residue ellipticity (θ) and converted to the standard units $deg \cdot cm^2\ dmol^{-1}$.

nLC-MS/MS queries, analysis and informatics

Analysis of nLC-MS/MS data utilizing custom R[1] scripts are as follows. Briefly, the combined summary files were used to plot peptide sequences identified, ratio of MS/MS identified: MS/MS submitted, the number of peaks and the mass standard deviation (ppm). Protein ID, protein name, gene name and sequence were extracted from the same uniprot reference proteome (*Bos taurus*) using *seqinr*[2] and primary sequence dependent characteristics (GRAVY, pI, MW) were calculated using *alakazam*.[3] Using protein ID as a key, the calculated values were extracted from the processed reference proteome for those proteins identified in the combined proteinGroup file to create a final data frame for plotting of identification overlaps and trends in GRAVY/pI/MW as well as amino acid composition of sequences for selected protein subsets (*seqinr, ggplot2, gridExtra, VennDiagram*).[4-6]

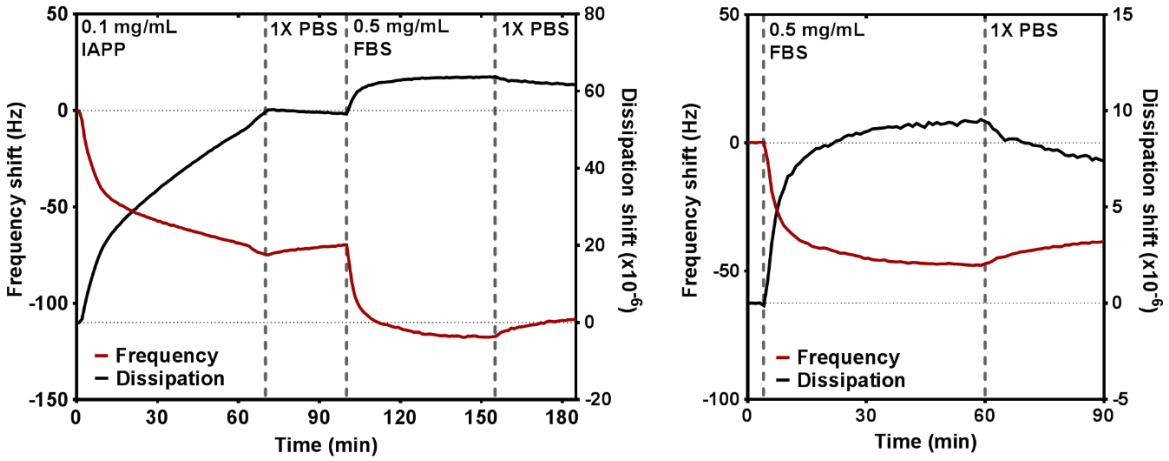

Figure S1. Protein deposition on IAPP-functionalized QCM sensors (n = 4), as illustrated by frequency and dissipation shift after sequential introduction of IAPP amyloid and FBS.

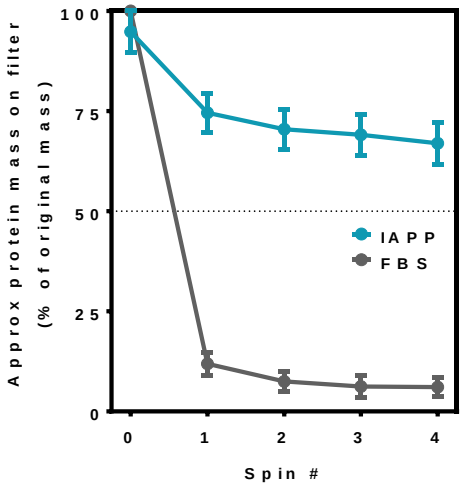

Figure S2. Optimization of centrifugal capture (CC) methodology, demonstrating retention of IAPP amyloid on high molecular weight filter surface (n = 6) with only low nonspecific binding of FBS proteins (n = 8) after four spin-wash cycles. Error is SEM.

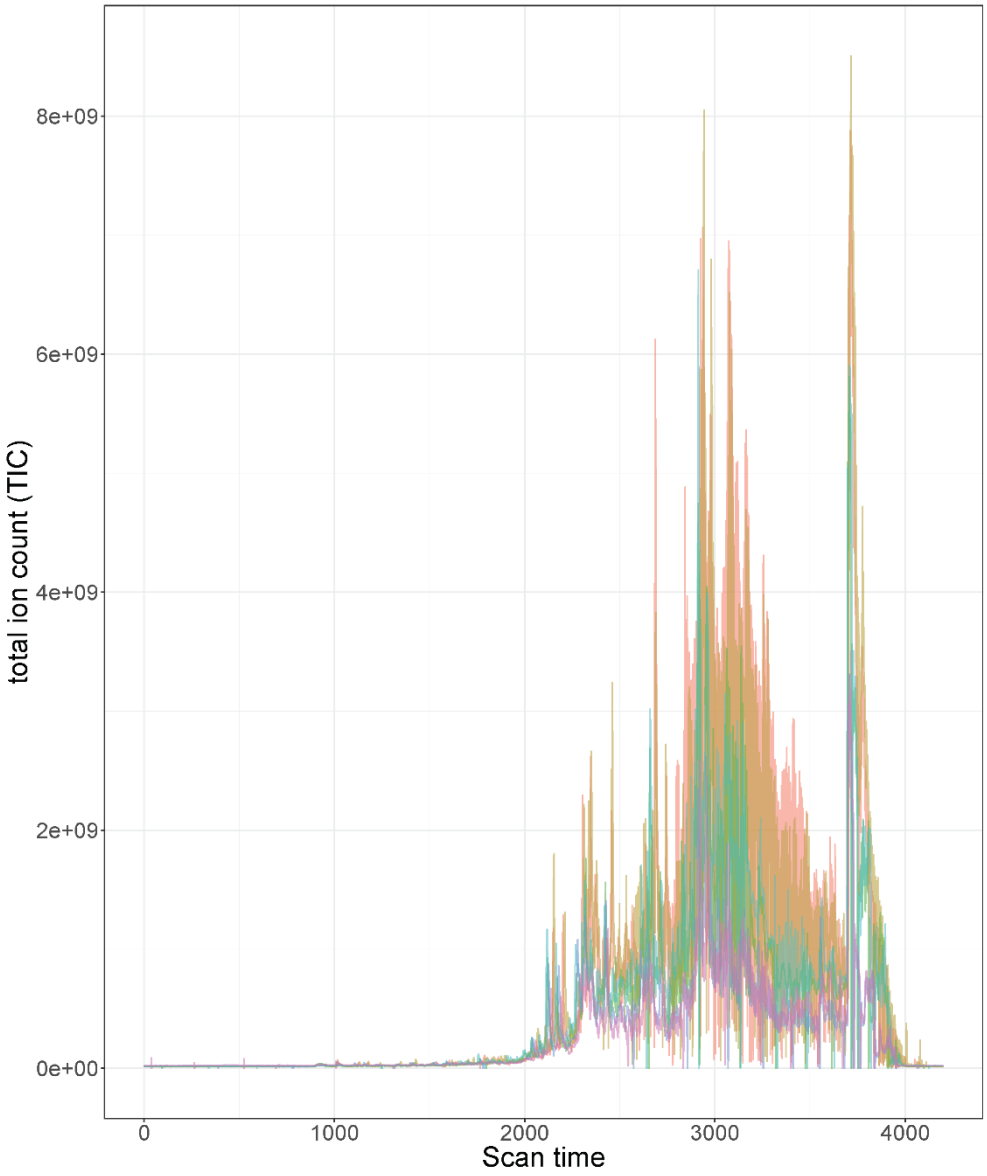

Figure S3a. LC-MS/MS chromatogram showing correlation between independent experiments of A (n = 6, overlaid).

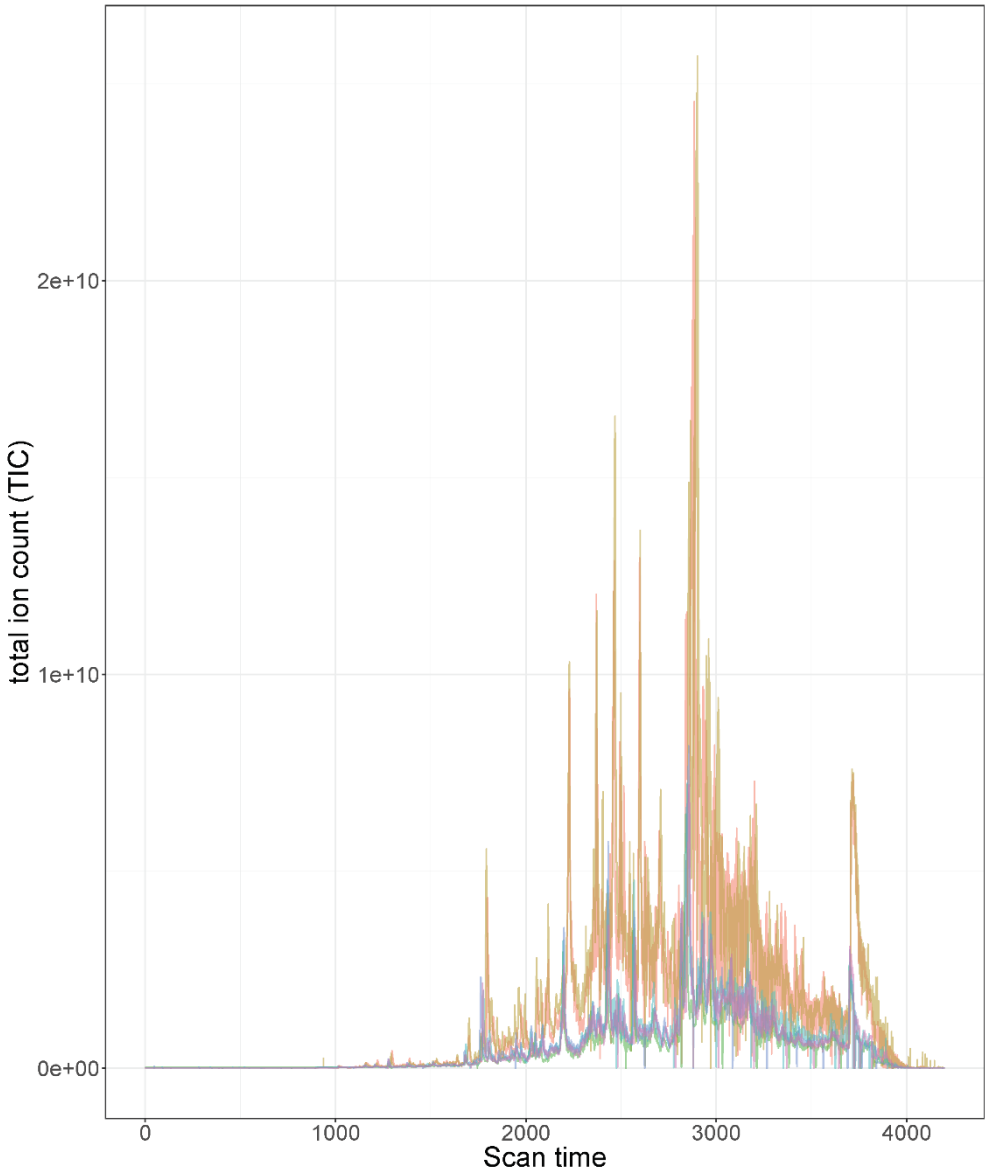

Figure S3b. LC-MS/MS chromatogram showing correlation between independent experiments of AF (n = 6, overlaid).

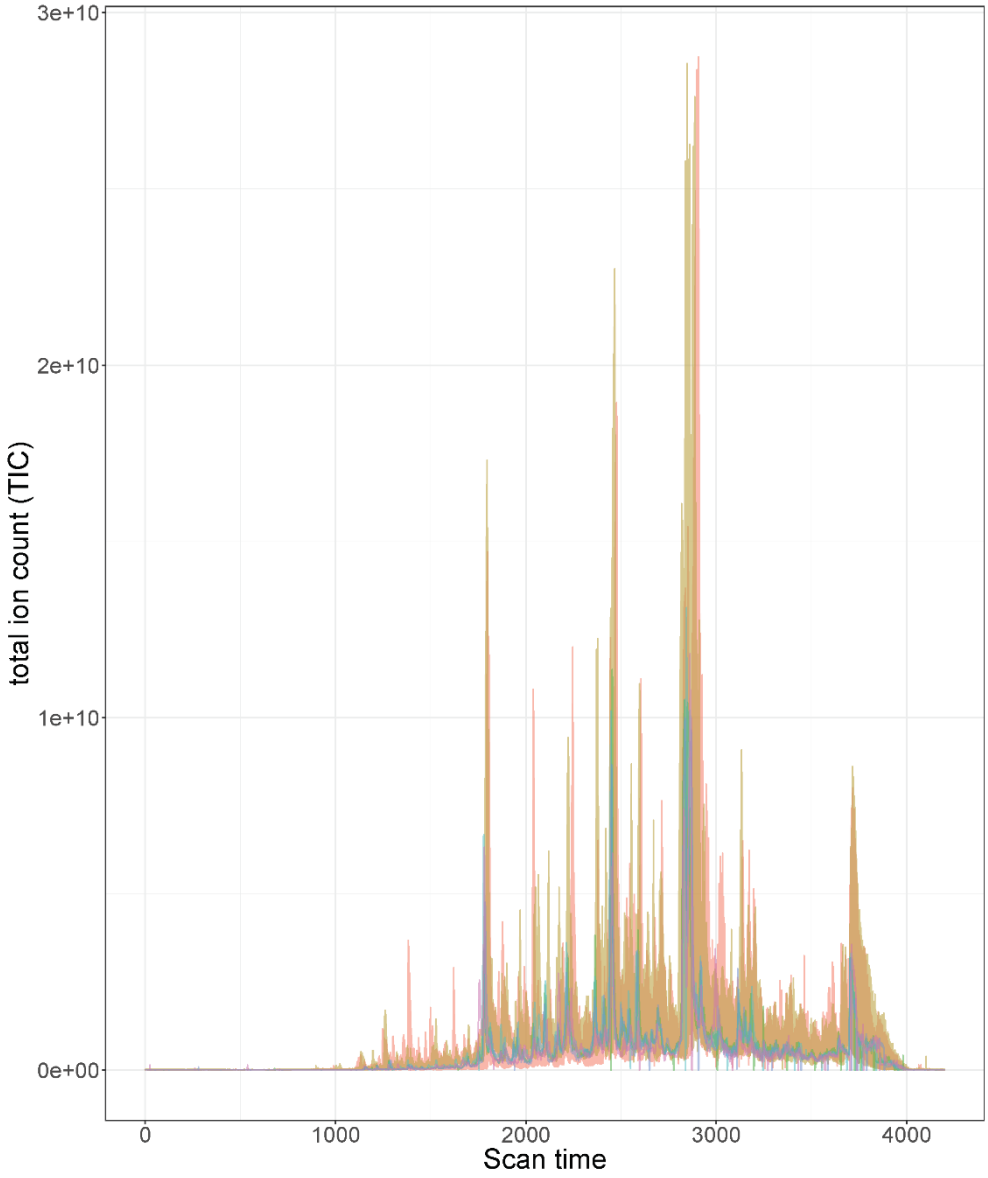

Figure S3c. LC-MS/MS chromatogram showing correlation between independent experiments of F (n = 12, overlaid).

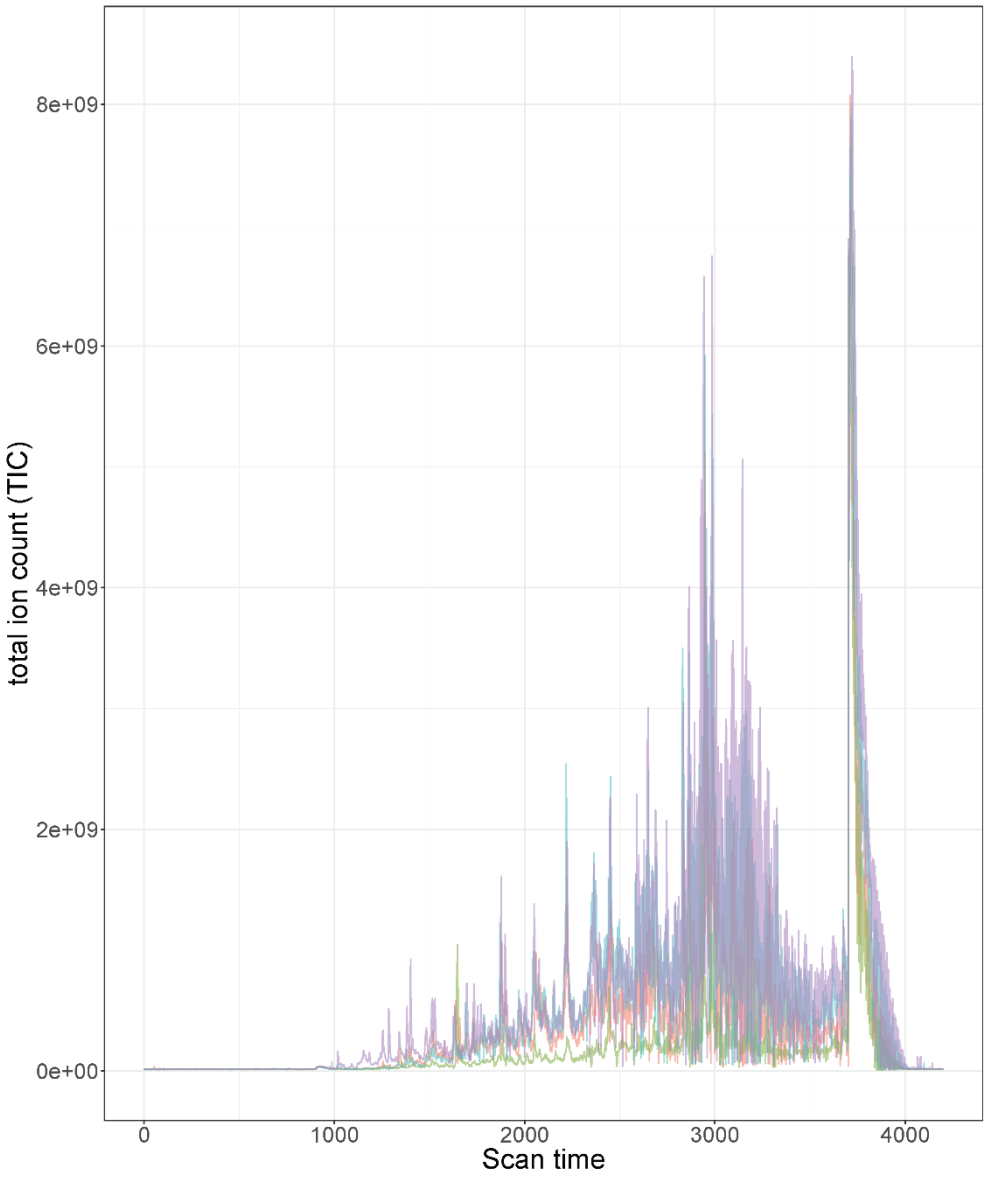

Figure S3d. LC-MS/MS chromatogram showing correlation between independent experiments of AE (n = 4, overlaid).

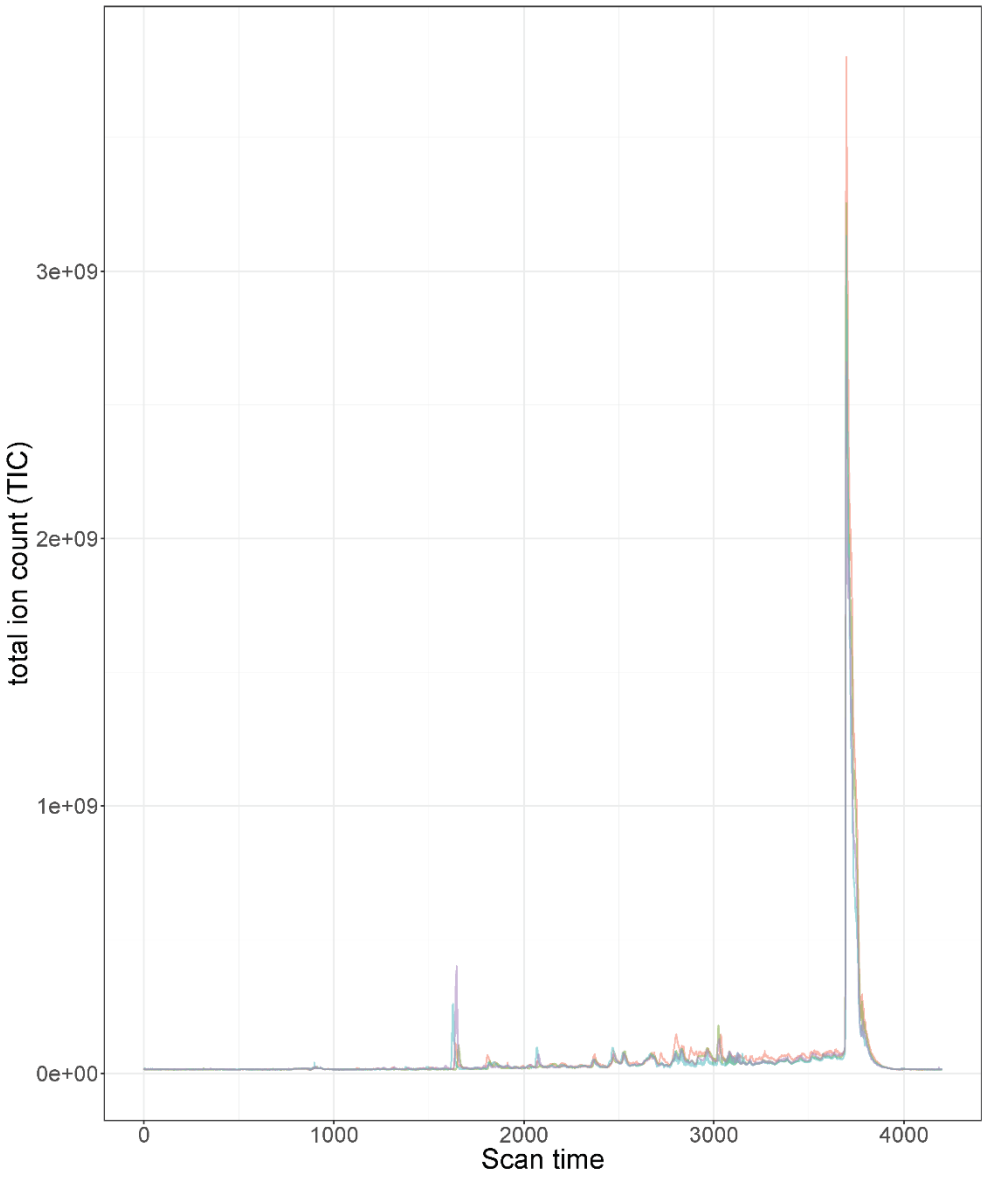

Figure S3e. LC-MS/MS chromatogram showing correlation between independent experiments of EF (n = 4, overlaid).

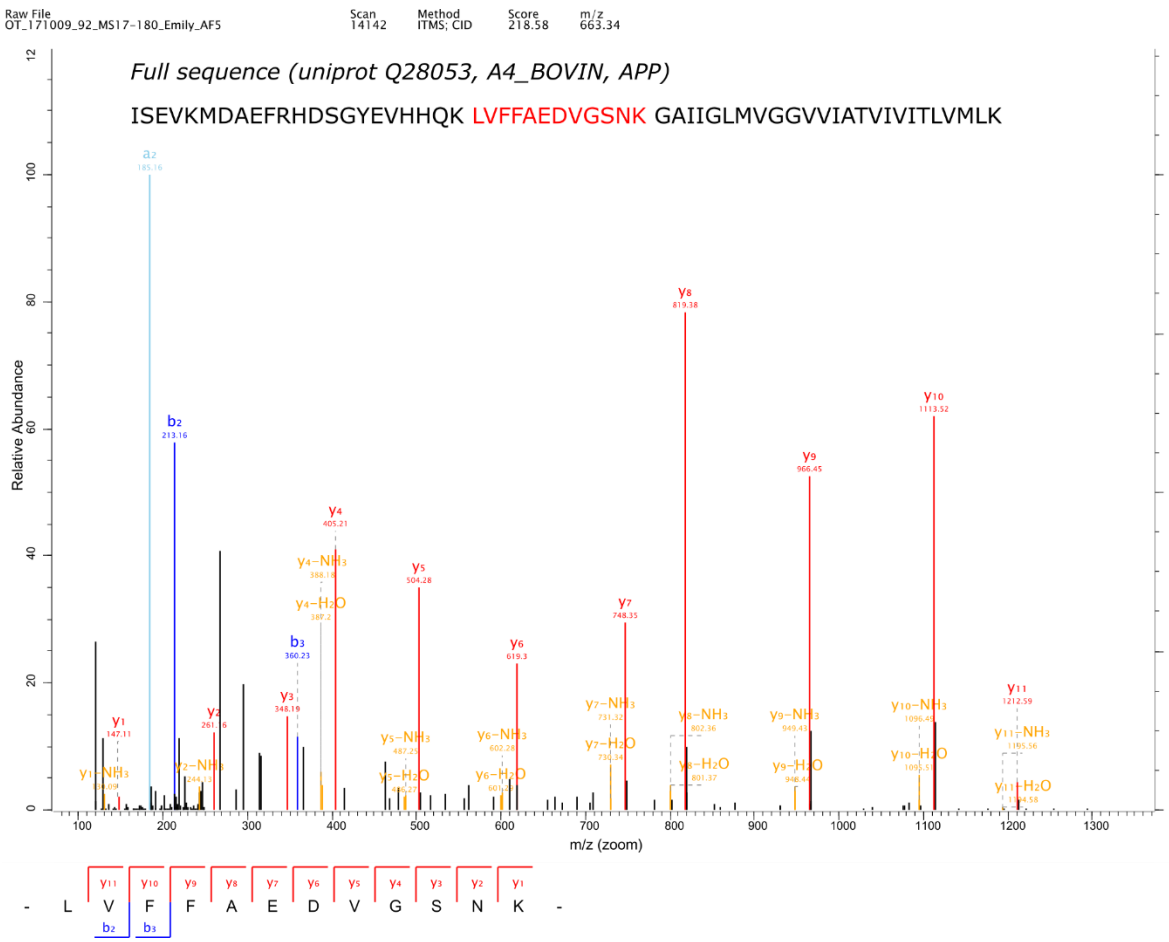

Figure S4. MS/MS spectrum identified by MaxQuant/Andromeda as a tryptic peptide of Amyloid Precursor Protein (*APP*, uniprot IDs Q28053, A4_BOVIN). Full sequence with identified peptide emphasized in red is overlaid onto the MaxQuant annotated MS/MS visualization, including matched fragments for the b and y ion series.

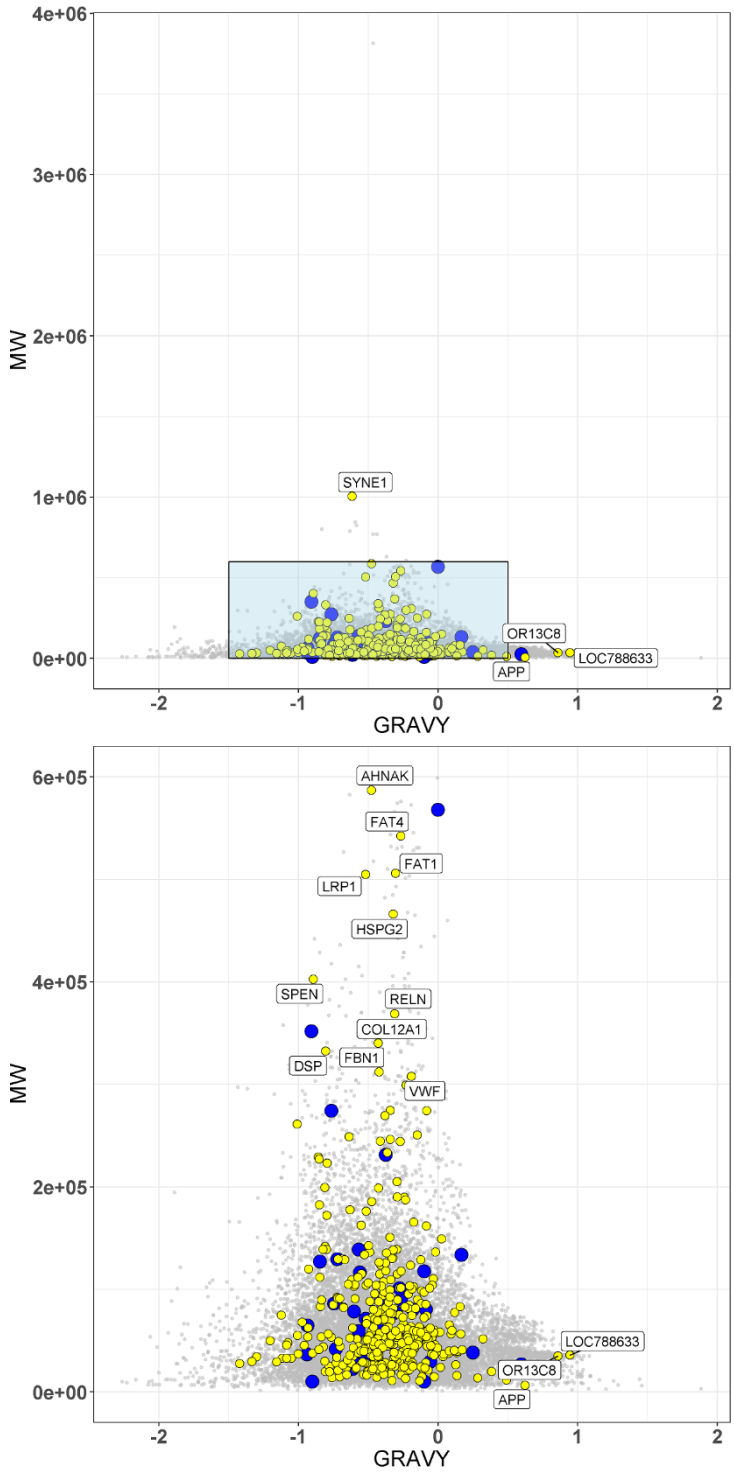

Figure S5a. The GRAVY/molecular weight (MW) relationships for unique amyloid-corona proteins (yellow markers, unique AF) and unique FBS-only proteins (blue markers, F) for CC experiments. All plots are overlaid onto the *Bos taurus* proteome background (gray). Top: points labelled are GRAVY $\leqslant$ -1.5 and $\geqslant$ 0.5, MW $\geqslant$ $6E^{+5}$. Bottom: points labelled are GRAVY (same as top) and MW $\geqslant$ $2E^{+5}$.

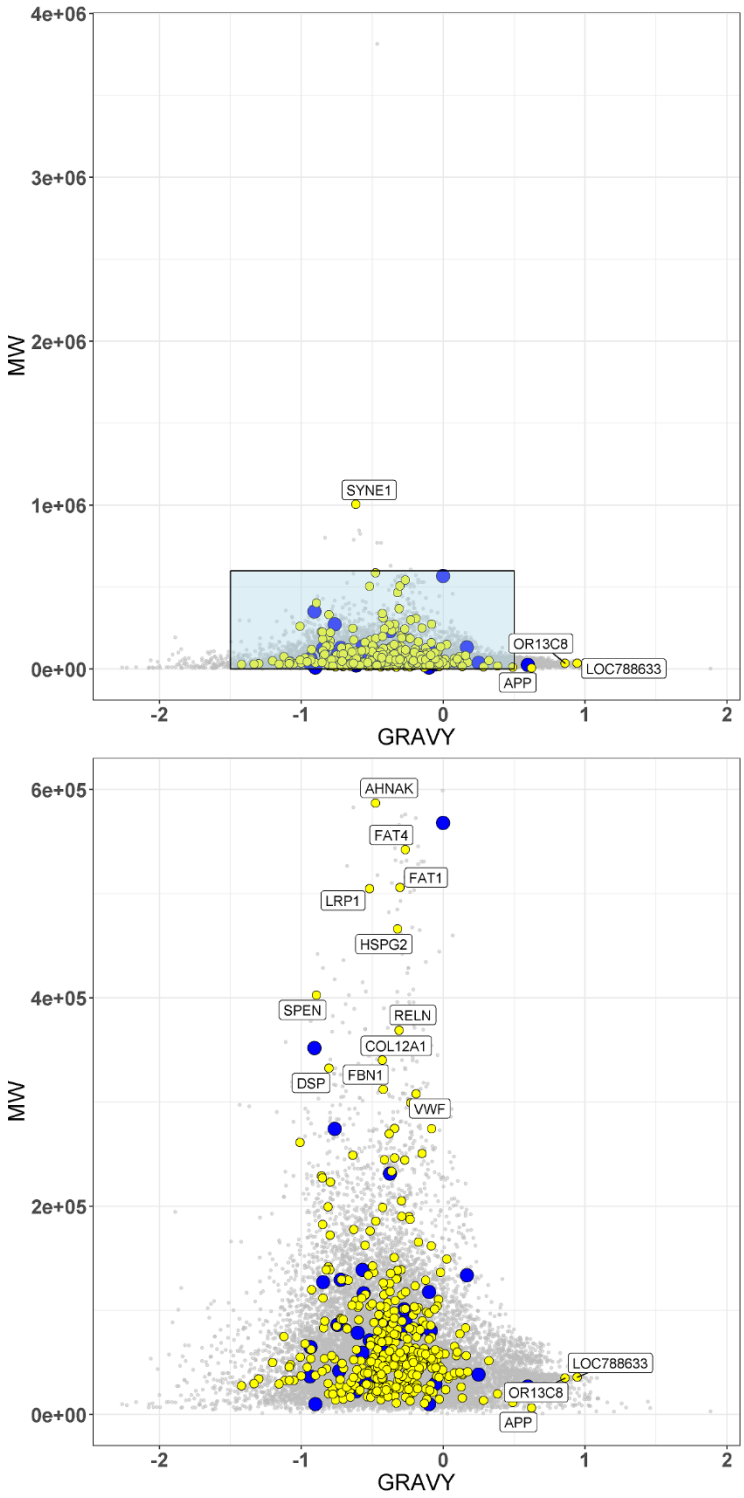

Figure S5b. The GRAVY/molecular weight (MW) relationships for unique amyloid-corona proteins (yellow markers, AE) and unique control proteins (blue markers, EF) for QCM experiments (AE/EF) are shown. Plots are overlaid onto the *Bos taurus* proteome background (gray). Top: points labelled are outside ranges GRAVY $\geqslant$ 0.5 and GRAVY $\leqslant$ -1.5, MW $\geqslant$ $6E^{+5}$. Bottom: points labelled are outside ranges GRAVY >= 0.5 and GRAVY <= -1.5, MW >= $3E^{+5}$.

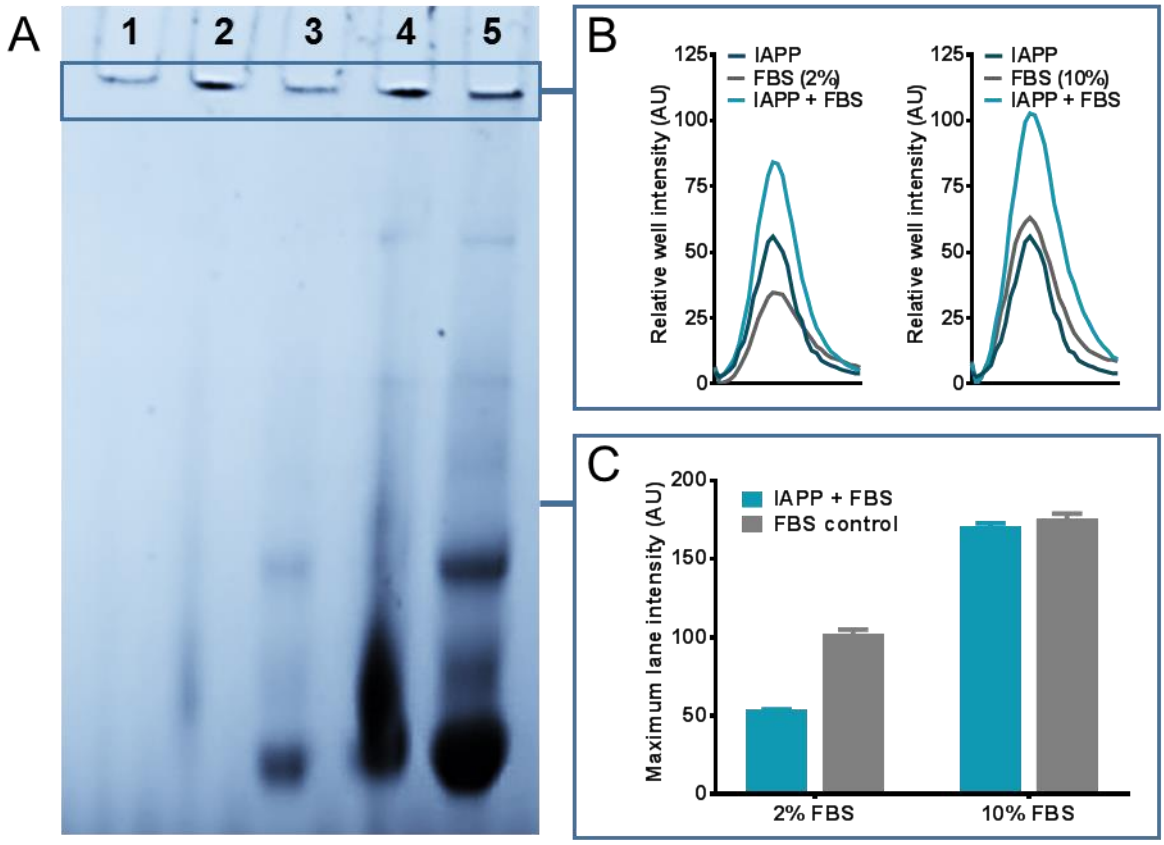

Figure S6: Blue-Native PAGE demonstrates sequestering of FBS proteins through corona formation on IAPP amyloids. A: Representative gel of n = 2 runs. Lanes are as follows: (**1**) IAPP amyloid (0.9 mg/mL); (**2**) IAPP amyloid + 2% FBS; (**3**) 2% FBS control; (**4**) IAPP amyloid + 10% FBS; (**5**) 10% FBS control. B: Intensity profile of sample wells. C: Comparison of maximum intensity measured within sample lanes (excluding well); error = SEM.

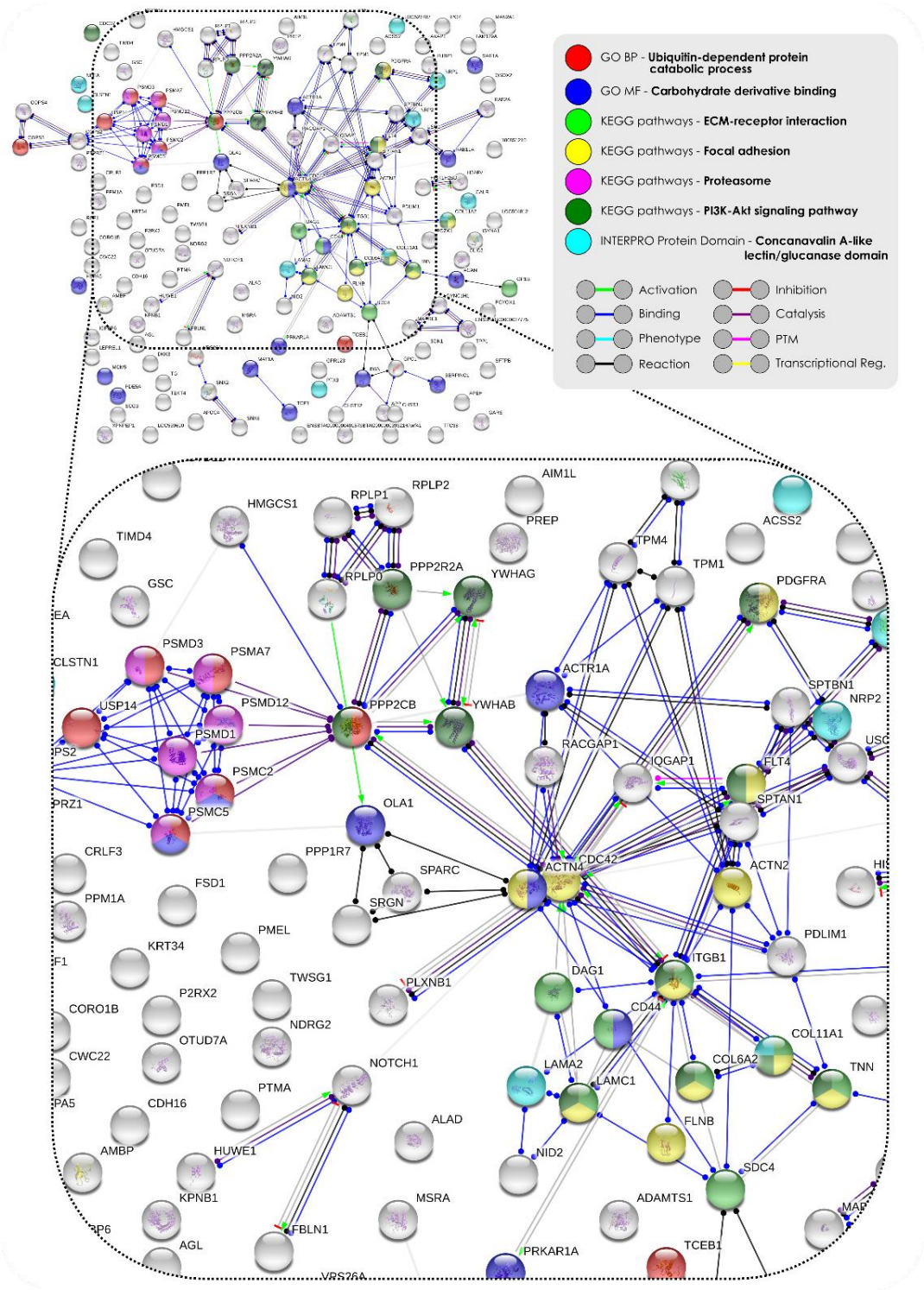

Figure S7. Centrifugal capture (CC) method amyloid and serum corona (AF) STRING (string-db.org)[7,8] protein network (molecular action) produced using *database* and *experimental* interactors, with a minimum interaction score of 0.400 and no additional interactors, against a whole *Bos taurus* genome background. Enrichment analysis and molecular action legends are included, in addition to predicted action effects – positive (arrowhead), negative (endpoint line), unspecified (endpoint circle).

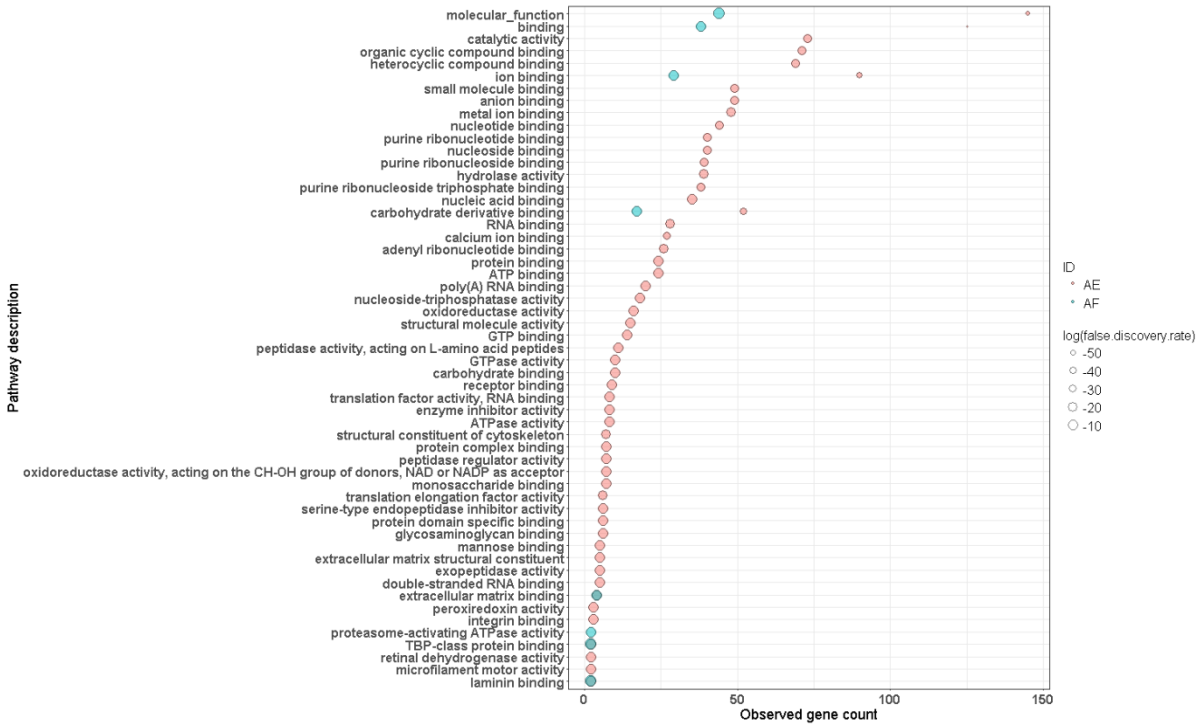

Figure S8a. Enriched gene ontology (GO) molecular function terms for proteins identified in AE (red) and AF (blue) experiments. Enrichment was performed using the STRING resource. Plot was generated in R using ggplot (see scatter plot code below). Point size is scaled to log(false.discovery.rate).

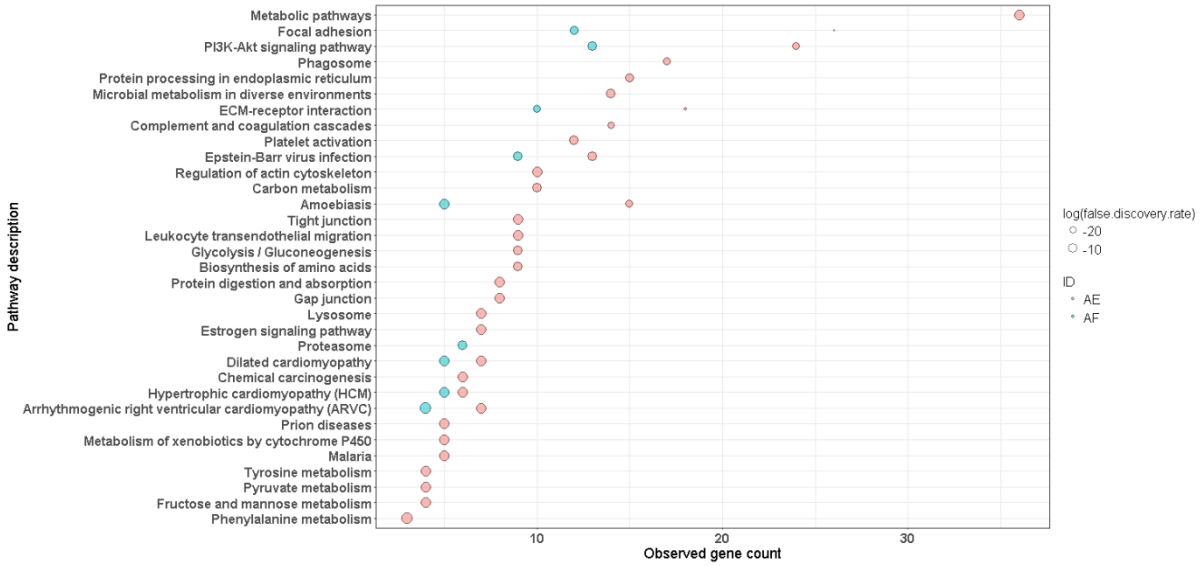

Figure S8b. Enriched gene ontology (GO) KEGG pathway terms for proteins identified in AE (red) and AF (blue) experiments. Enrichment was performed using the STRING resource. Plot was generated in R using ggplot (see scatter plot code below). Point size is scaled to log(false.discovery.rate).

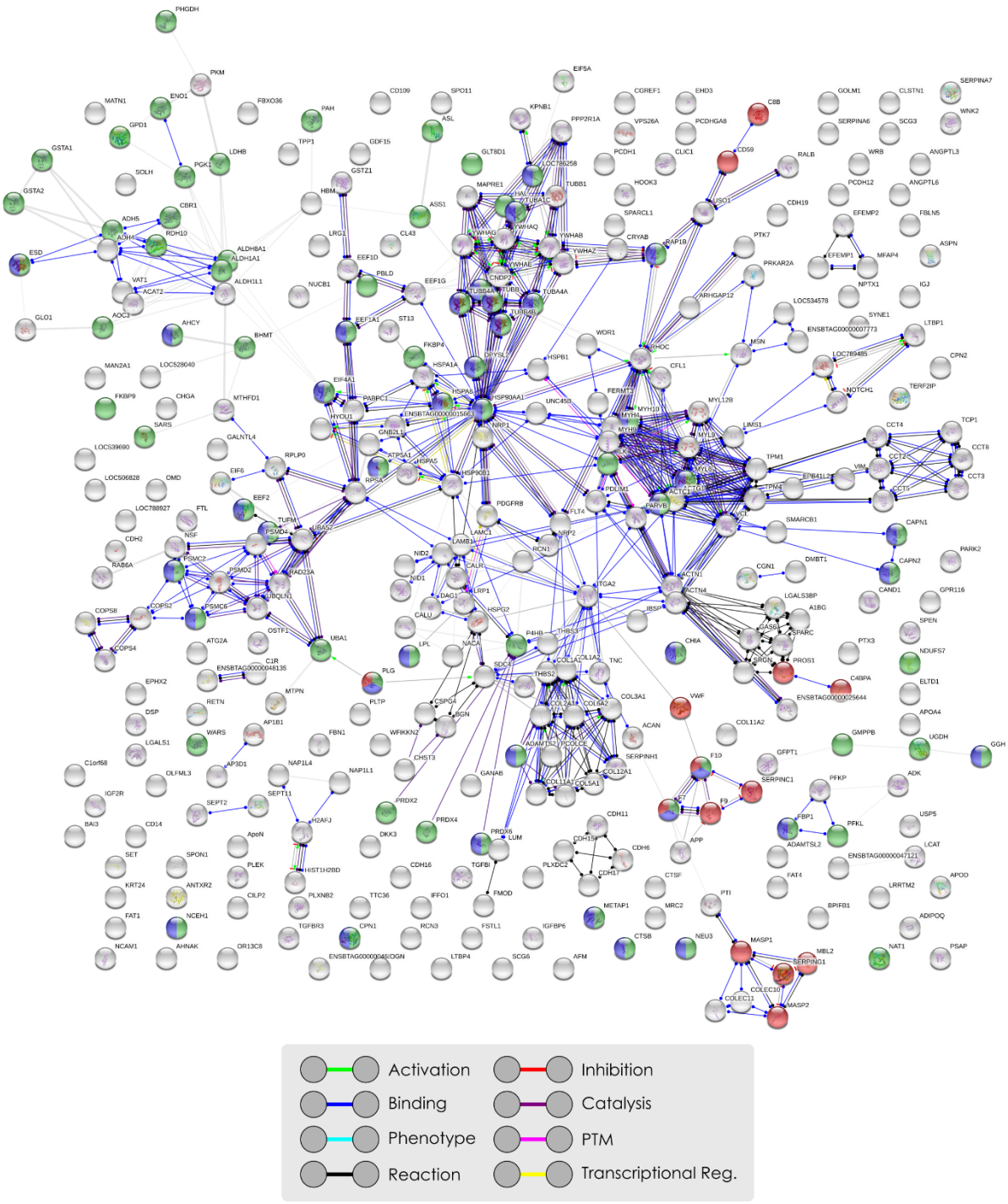

Figure S8c. Enriched gene ontology (GO) molecular functions for *Catalytic activity* (green) and *hydrolase activity* (blue), with the KEGG pathway for *Complement and coagulation cascades* also included (red). Enrichment was performed using the STRING resource. Enrichment analysis and molecular action legends are included, in addition to predicted action effects – positive (arrowhead), negative (endpoint line), unspecified (endpoint circle).

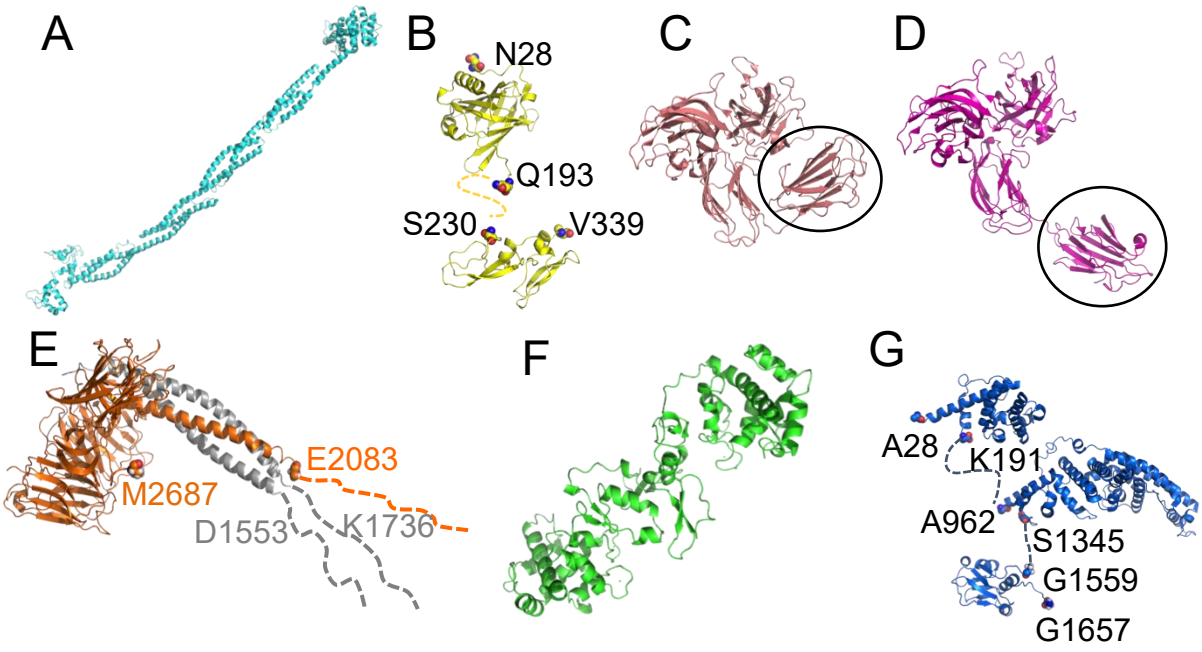

Figure S9. Structures of top AF proteins. Alpha-actinin-4 (a), protein AMBP (b), neuropilin in either close (c) or open state (d), laminin subunit alpha 2 (orange) (e), SPARC (f), and IQ motif containing GTPase activating protein 1 (g) are shown in cartoon representations. The missing structures are represented by dashed lines.

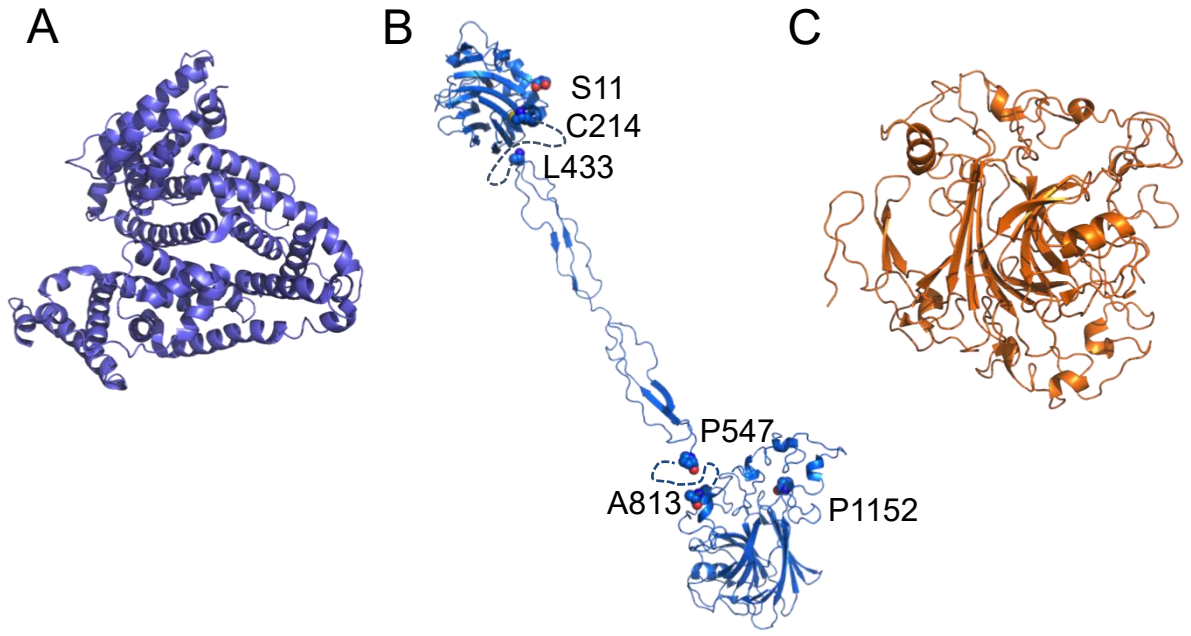

Figure S10. Structures of top AE proteins. Serum albumin (a), thrombospondin-1 (b), and cartilage oligomeric matrix protein (c) are shown in cartoon representations. The missing structures are represented by dashed lines.

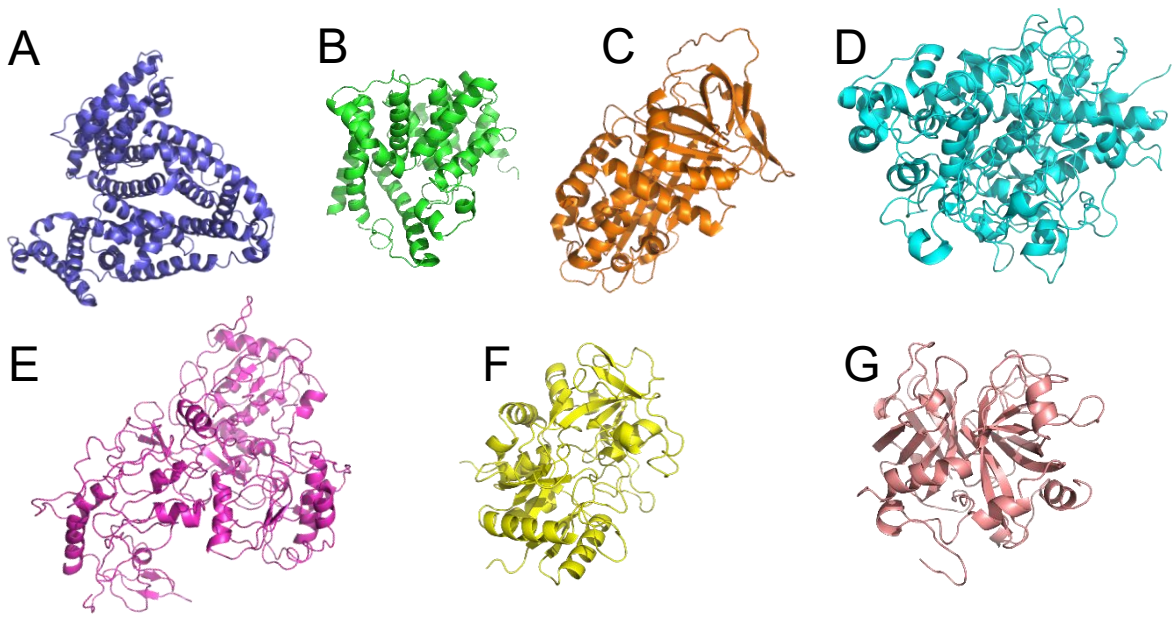

Figure S11. Structures of top FBS proteins. Serum albumin (a), cataytic domain of the Cone cGMP-specific 3′,5′-cyclic phosphodiesterase alpha-subunit (b), alpha-1-antiproteinase (c), Lactoperoxidase (d), NADH-ubiquinone oxido-reductase 75 from CroyEM (e), Hemiferrin (f), and thrombin domain of Prothrombin (g) are shown in cartoon representations.

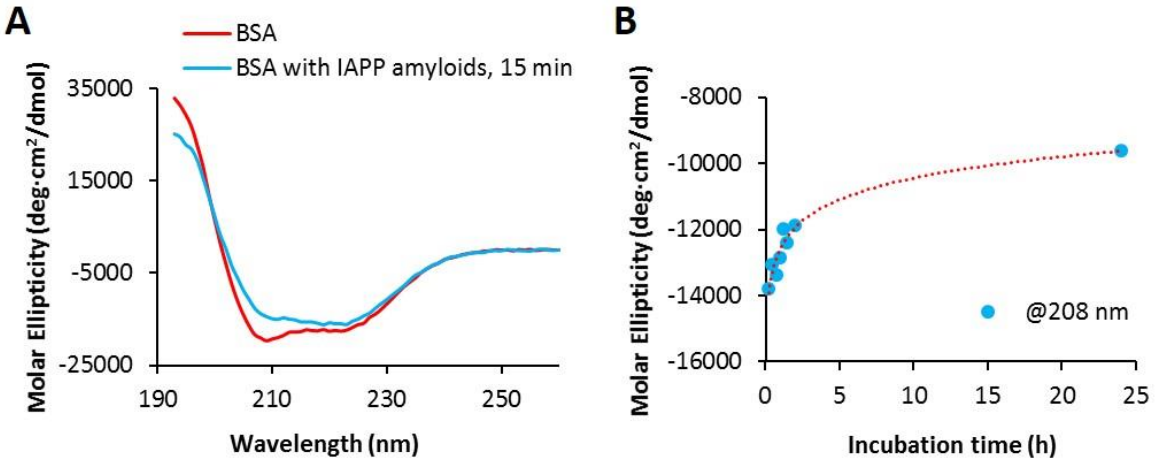

Fig S12. (A) CD spectra of BSA (0.1 mg/mL) upon its interaction with IAPP amyloid fibrils (0.1 mg/mL) after 15 min of incubation. (B) Changing intensity of CD spectra of BSA interacting with IAPP fibrils at 208 nm (one of two signature peaks of alpha helices) up to 24 h of interaction.

#	FBS protein name	PDB ID	# Residues	Net Charge
1	Serum albumin	5UJB	607	-13
2	Cone cGMP-specific 3′,5′-cyclic phosphodiesterase alpha-subunit	Catalytic domain: 3JWQ (536-855)	855	-23
3	Alpha-1-antiproteinase	1QLP (46-415) (human: 72%)	416	-9
4	Plasminogen	N/A	812	5
5	Lactoperoxidase	2IPS (118-712)	712	11
6	Kininogen, LMW II	N/A	619	-15
7	NADH-ubiquinone oxido-reductase 75	5O31 (24-727)	727	-9
8	Alpha-2-HS-glycoprotein	N/A	359	-13
9	Hemiferrin	1H76 (1-215) (rat: 70%)	216	2
10	Prothrombin	Thrombin domain: 1TBQ (318-366, 367-625)	625	-8
		Mean	594.8	-7.2

Table S1. Top 10 FBS proteins from a LC-MS method[9].

STRING scatter plot code:

```
###libraries required###
library(ggplot2)
library(ggrepel)

###theme###
#see https://rstudio-pubs-static.s3.amazonaws.com/3364_d1a578f521174152b46b19d0c83cbe7e.html
themeTIFF <- theme(legend.text = element_text(size = 16), legend.title=element_text(size=16),
axis.title=element_text(size=18),
        legend.key.size = unit(0.8, "cm"), axis.text.x = element_text(face = "bold", angle=0, vjust=0.5,
size=16),
        axis.text.y = element_text(face = "bold", size=16), title = element_text(size=18))

###molecular function###
AE <- read.csv("./input/string_input/2018_03_05_STRING_analysis/AE/enrichment.Function.tsv", sep="\t",
header=TRUE)
AF <- read.csv("./input/string_input/2018_03_05_STRING_analysis/AF/enrichment.Function.tsv", sep="\t",
header=TRUE)
###KEGG###
```

```
AE_kegg <- read.csv("./input/string_input/2018_03_05_STRING_analysis/AE/enrichment.KEGG.tsv", sep="\t",
header=TRUE)
AF_kegg <- read.csv("./input/string_input/2018_03_05_STRING_analysis/AF/enrichment.KEGG.tsv", sep="\t",
header=TRUE)

###select columns and add ID###
AE <- AE[,c(2,3,4)]
AF <- AF[,c(2,3,4)]
AE$ID <- "AE"
AF$ID <- "AF"
AE_kegg <- AE_kegg[,c(2,3,4)]
AF_kegg <- AF_kegg[,c(2,3,4)]
AE_kegg$ID <- "AE"
AF_kegg$ID <- "AF"

###combined dataframes###
COMB <- rbind(AE, AF)
COMB_kegg <- rbind(AE_kegg, AF_kegg)

###plots###
tiff("./output/molecular_function_figure.tiff", height=900, width=1500)
a <- ggplot(COMB)
a <- a + geom_point(aes(reorder(pathway.description, observed.gene.count), observed.gene.count,
                size = log(false.discovery.rate), fill=ID), pch=21, alpha=0.5)
a <- a + theme_bw() + themeTIFF + coord_flip()
a <- a + xlab("Pathway description") + ylab("Observed gene count")
plot(a)
dev.off()

tiff("./output/kegg_figure.tiff", height=700, width=1500)
a <- ggplot(COMB_kegg)
a <- a + geom_point(aes(reorder(pathway.description, observed.gene.count), observed.gene.count,
                size = log(false.discovery.rate), fill=ID), pch=21, alpha=0.5)
a <- a + theme_bw() + themeTIFF + coord_flip()
a <- a + xlab("Pathway description") + ylab("Observed gene count")
plot(a)
dev.off()
```

MaxQuant parameter set 1 (*Bos taurus*):

Parameter	Value
Version	1.6.0.16
User name	GUSTAFOJ
Machine name	IOR268965
Date of writing	02/19/2018 12:26:38
Fixed modifications	Carbamidomethyl (C)
Include contaminants	TRUE
PSM FDR	0.01
Protein FDR	0.01
Site FDR	0.01
Use Normalized Ratios For Occupancy	TRUE
Min. peptide Length	5

Min. score for unmodified peptides	0
Min. score for modified peptides	40
Min. delta score for unmodified peptides	0
Min. delta score for modified peptides	6
Min. unique peptides	0
Min. razor peptides	1
Min. peptides	1
Use only unmodified peptides and	TRUE
Modifications included in protein quantification	Oxidation (M);Acetyl (Protein N-term)
Peptides used for protein quantification	Razor
Discard unmodified counterpart peptides	TRUE
Label min. ratio count	2
Use delta score	FALSE
iBAQ	FALSE
iBAQ log fit	FALSE
Match between runs	FALSE
Find dependent peptides	FALSE
Fasta file	E:\MaxQuant\fasta_files\2018_02_19\UP000009136_9913.fasta
Decoy mode	revert
Include contaminants	TRUE
Advanced ratios	TRUE
Fixed andromeda index folder	
Temporary folder	
Combined folder location	
Second peptides	TRUE
Stabilize large LFQ ratios	TRUE
Separate LFQ in parameter groups	FALSE
Require MS/MS for LFQ comparisons	TRUE
Calculate peak properties	FALSE
Main search max. combinations	200
Advanced site intensities	TRUE
LFQ norm for sites and peptides	FALSE
Write msScans table	TRUE
Write msmsScans table	TRUE
Write ms3Scans table	TRUE
Write allPeptides table	TRUE
Write mzRange table	TRUE
Write pasefMsmsScans table	TRUE
Write accumulatedPasefMsmsScans table	TRUE
Max. peptide mass [Da]	4600
Min. peptide length for unspecific search	8
Max. peptide length for unspecific search	25
Razor protein FDR	TRUE
Disable MD5	FALSE
Max mods in site table	3
Match unidentified features	FALSE

MS/MS tol. (FTMS)	20 ppm
Top MS/MS peaks per Da interval. (FTMS)	12
Da interval. (FTMS)	100
MS/MS deisotoping (FTMS)	TRUE
MS/MS deisotoping tolerance (FTMS)	7
MS/MS deisotoping tolerance unit (FTMS)	ppm
MS/MS higher charges (FTMS)	TRUE
MS/MS water loss (FTMS)	TRUE
MS/MS ammonia loss (FTMS)	TRUE
MS/MS dependent losses (FTMS)	TRUE
MS/MS recalibration (FTMS)	FALSE
MS/MS tol. (ITMS)	0.5 Da
Top MS/MS peaks per Da interval. (ITMS)	8
Da interval. (ITMS)	100
MS/MS deisotoping (ITMS)	FALSE
MS/MS deisotoping tolerance (ITMS)	0.15
MS/MS deisotoping tolerance unit (ITMS)	Da
MS/MS higher charges (ITMS)	TRUE
MS/MS water loss (ITMS)	TRUE
MS/MS ammonia loss (ITMS)	TRUE
MS/MS dependent losses (ITMS)	TRUE
MS/MS recalibration (ITMS)	FALSE
MS/MS tol. (TOF)	40 ppm
Top MS/MS peaks per Da interval. (TOF)	10
Da interval. (TOF)	100
MS/MS deisotoping (TOF)	TRUE
MS/MS deisotoping tolerance (TOF)	0.01
MS/MS deisotoping tolerance unit (TOF)	Da
MS/MS higher charges (TOF)	TRUE
MS/MS water loss (TOF)	TRUE
MS/MS ammonia loss (TOF)	TRUE
MS/MS dependent losses (TOF)	TRUE
MS/MS recalibration (TOF)	FALSE
MS/MS tol. (Unknown)	0.5 Da
Top MS/MS peaks per Da interval. (Unknown)	8
Da interval. (Unknown)	100
MS/MS deisotoping (Unknown)	FALSE
MS/MS deisotoping tolerance (Unknown)	0.15
MS/MS deisotoping tolerance unit (Unknown)	Da
MS/MS higher charges (Unknown)	TRUE
MS/MS water loss (Unknown)	TRUE
MS/MS ammonia loss (Unknown)	TRUE
MS/MS dependent losses (Unknown)	TRUE
MS/MS recalibration (Unknown)	FALSE
Site tables	Oxidation (M)Sites.txt

MaxQuant parameter set 2 (*Homo sapiens*):

Parameter	Value
Version	1.6.0.16
User name	GUSTAFOJ
Machine name	IOR268965
Date of writing	02/27/2018 14:12:31
Fixed modifications	Carbamidomethyl (C)
Include contaminants	TRUE
PSM FDR	0.01
Protein FDR	0.01
Site FDR	0.01
Use Normalized Ratios For Occupancy	TRUE
Min. peptide Length	5
Min. score for unmodified peptides	0
Min. score for modified peptides	40
Min. delta score for unmodified peptides	0
Min. delta score for modified peptides	6
Min. unique peptides	0
Min. razor peptides	1
Min. peptides	1
Use only unmodified peptides and	TRUE
Modifications included in protein quantification	Oxidation (M);Acetyl (Protein N-term)
Peptides used for protein quantification	Razor
Discard unmodified counterpart peptides	TRUE
Label min. ratio count	2
Use delta score	FALSE
iBAQ	FALSE
iBAQ log fit	FALSE
Match between runs	FALSE
Find dependent peptides	FALSE
Fasta file	E:\MaxQuant\fasta_files\2018_02_23\UP000005640_9606.fasta
Decoy mode	revert
Include contaminants	TRUE
Advanced ratios	TRUE
Fixed andromeda index folder	
Temporary folder	
Combined folder location	
Second peptides	TRUE
Stabilize large LFQ ratios	TRUE
Separate LFQ in parameter groups	FALSE
Require MS/MS for LFQ comparisons	TRUE

Calculate peak properties	FALSE
Main search max. combinations	200
Advanced site intensities	TRUE
LFQ norm for sites and peptides	FALSE
Write msScans table	TRUE
Write msmsScans table	TRUE
Write ms3Scans table	TRUE
Write allPeptides table	TRUE
Write mzRange table	TRUE
Write pasefMsmsScans table	TRUE
Write accumulatedPasefMsmsScans table	TRUE
Max. peptide mass [Da]	4600
Min. peptide length for unspecific search	8
Max. peptide length for unspecific search	25
Razor protein FDR	TRUE
Disable MD5	FALSE
Max mods in site table	3
Match unidentified features	FALSE
MS/MS tol. (FTMS)	20 ppm
Top MS/MS peaks per Da interval. (FTMS)	12
Da interval. (FTMS)	100
MS/MS deisotoping (FTMS)	TRUE
MS/MS deisotoping tolerance (FTMS)	7
MS/MS deisotoping tolerance unit (FTMS)	ppm
MS/MS higher charges (FTMS)	TRUE
MS/MS water loss (FTMS)	TRUE
MS/MS ammonia loss (FTMS)	TRUE
MS/MS dependent losses (FTMS)	TRUE
MS/MS recalibration (FTMS)	FALSE
MS/MS tol. (ITMS)	0.5 Da
Top MS/MS peaks per Da interval. (ITMS)	8
Da interval. (ITMS)	100
MS/MS deisotoping (ITMS)	FALSE
MS/MS deisotoping tolerance (ITMS)	0.15
MS/MS deisotoping tolerance unit (ITMS)	Da
MS/MS higher charges (ITMS)	TRUE
MS/MS water loss (ITMS)	TRUE
MS/MS ammonia loss (ITMS)	TRUE
MS/MS dependent losses (ITMS)	TRUE
MS/MS recalibration (ITMS)	FALSE
MS/MS tol. (TOF)	40 ppm
Top MS/MS peaks per Da interval. (TOF)	10
Da interval. (TOF)	100
MS/MS deisotoping (TOF)	TRUE
MS/MS deisotoping tolerance (TOF)	0.01
MS/MS deisotoping tolerance unit (TOF)	Da

MS/MS higher charges (TOF)	TRUE
MS/MS water loss (TOF)	TRUE
MS/MS ammonia loss (TOF)	TRUE
MS/MS dependent losses (TOF)	TRUE
MS/MS recalibration (TOF)	FALSE
MS/MS tol. (Unknown)	0.5 Da
Top MS/MS peaks per Da interval. (Unknown)	8
Da interval. (Unknown)	100
MS/MS deisotoping (Unknown)	FALSE
MS/MS deisotoping tolerance (Unknown)	0.15
MS/MS deisotoping tolerance unit (Unknown)	Da
MS/MS higher charges (Unknown)	TRUE
MS/MS water loss (Unknown)	TRUE
MS/MS ammonia loss (Unknown)	TRUE
MS/MS dependent losses (Unknown)	TRUE
MS/MS recalibration (Unknown)	FALSE
Site tables	Oxidation (M)Sites.txt

Complete script used to generate Rmarkdown html report:

```
---
title: "Supplementary data analysis methods - Profiling the Serum Protein Corona of Human IAPP Amyloid"
output:
  html_document:
    toc: true
    toc_depth: 2
    toc_float: TRUE
    self_contained: no
    number_sections: TRUE
---

<style type="text/css">
#TOC {
width: 900px;
overflow:auto;
color:blue;
font-family:Helvetica;
}
body{
font-family:Helvetica;
font-size: 12px;
max-width: 2000px;
margin: auto;
margin-left:50px;
line-height: 20px;
}
h1.title{font-size: 26px}
h1{font-size: 22px}
h2{font-size: 20px}
h3{font-size: 20px}
h4{font-size: 18px}
code.r{font-size: 11px;}
```

pre{font-size: 11px;}
</style>

***

```{r setup, include=FALSE}
###global settings###
knitr::opts_chunk$set(echo = TRUE, cache=TRUE, autodep=TRUE)
###installs###
#install.packages(c("ggplot2", "gridExtra",
#                   "seqinr", "alakazam",
#                   "sqldf", "stringr",
#                   "ggrepel", "VennDiagram",
#                   "rmarkdown", "knitr"))
###libraries###
library(gridExtra)
library(ggplot2)
library(seqinr)
library(alakazam)
library(sqldf)
library(stringr)
library(ggrepel)
library(VennDiagram)
library(reshape2)
#update.packages()
```

***

Introduction

The specific research questions addressed in this document include:

1. Which proteins can be identified in IAPP amyloid-coronae formed in-solution (CC method)?
2. Which proteins can be identified in IAPP amyloid-coronae formed under micro-flow conditions (QCM method)?
3. What is the difference in protein corona composition for CC and QCM methods?
4. What proteins are identified for IAPP amyloid-only experiments?

This document details the combination, processing and presentation of summary and proteinGroup text files resulting from MaxQuant Andromeda database queries, where each experiment type was pooled to maximise identifications (e.g. A1+A2+A3....).
Independent searches were performed for selected experiment types (e.g. AF, F).

***

Analysis notes

General information

- MaxQuant peptide identifications used a fasta file containing all reviewed and unreviewed Bos taurus entries available as a reference proteome @ ftp://ftp.uniprot.org/pub/databases/uniprot/current_release/knowledgebase/reference_proteomes/Eukaryota/.
- Reviewed + unreviewed entries included to maximise identifications.
- Database 1: UP000009136_9913.fasta dated 21/12/2017.
- Database 2: UP000005640_9606.fasta dated 21/12/2017.
- Whole proteome of Bos taurus as plotting background (same fasta as above, 9136_9913).
- nLC-MS chromatograms imported from a separate R script (provided at the end of this document).
- Protein network analysis images were imported from a manual analysis using the online resource STRING (v10.5).
- STRING resource link - see https://string-db.org/cgi/input.pl

Plotting theme

```{r}
###set theme###
#see https://rstudio-pubs-static.s3.amazonaws.com/3364_d1a578f521174152b46b19d0c83cbe7e.html
```

```
themeTIFF <- theme(legend.text = element_text(size = 16), legend.title=element_text(size=16),
axis.title=element_text(size=18),
              legend.key.size = unit(0.8, "cm"), axis.text.x = element_text(face = "bold", angle=0, vjust=0.5, size=16),
              axis.text.y = element_text(face = "bold", size=16), title = element_text(size=18))
```

***

Experiment key

ID	Method	Meaning
A	CC	Control - Amyloid only
F	CC	Control - FBS only
AF	CC	Amyloid + FBS
EF	QCM	Control - FBS only
AE	QCM	Amyloid + FBS

***

Combined MaxQuant files

Summary files

Function to combine MaxQuant summary files for analysis of the nLC-MS/MS data.

This analysis includes:

- Peptide sequences identified,
- Ratio of MS/MS identified : MS/MS submitted,
- The number of peaks, and
- The mass standard deviation (ppm)

```{r sum}
###set path###
path = "./input/IAPP"

###GETsummaries###
GETsummaries <- function(x){
  #see https://stackoverflow.com/questions/4876813/using-r-to-list-all-files-with-a-specified-extension
  sum_files <- list.files(path = x, pattern = "summary.txt", recursive=TRUE, include.dirs=TRUE, ignore.case =
TRUE)
  complete_summary <- data.frame()
  for (i in sum_files){
    #see https://stackoverflow.com/questions/8996134/extract-vectors-from-strsplit-list-without-using-a-loop
    Experiment <- rapply(strsplit(i, "/"), function(a) a[1])
    summary <- read.csv(paste(x, "/", i, sep=""), sep="\t", header=TRUE)
    summary <- summary[summary$Raw.file!="Total",]
    summary$Experiment <- Experiment
    id <- rapply(strsplit(as.character(summary$Raw.file), "_"), function(a) a[4])
    exp <- rapply(strsplit(as.character(summary$Raw.file), "_"), function(a) a[6])
    ID_EXP <- paste(id, exp, sep="-")
    summary$ID_EXP <- ID_EXP
    complete_summary <- rbind(summary, complete_summary)
    }
  return(complete_summary)
}
summaries <- GETsummaries(path)
```

Summary file plot

```{r sumplot}
tiff(file=paste("./output/summary_plots.tiff", sep=""), width=600, height=1000)
#see https://www.statmethods.net/advgraphs/layout.html
a <- ggplot(summaries)
b <- a + geom_bar(stat="identity", aes(ID_EXP, Peptide.Sequences.Identified, fill=Experiment))
```

```
b <- b + expand_limits(y=0) + coord_flip() + xlab("Experimental ID") + theme_bw()
#see http://www.cookbook-r.com/Graphs/Legends_(ggplot2)/
b <- b + guides(fill=FALSE)
c <- a + geom_bar(stat="identity", aes(ID_EXP, MS.MS.Identified..../MS.MS.Submitted, fill=Experiment))
c <- c + expand_limits(y=0) + coord_flip() + xlab("Experimental ID") + theme_bw() + guides(fill=FALSE)
d <- a + geom_bar(stat="identity", aes(ID_EXP, Mass.Standard.Deviation..ppm., fill=Experiment))
d <- d + expand_limits(y=0) + coord_flip() + xlab("Experimental ID") + theme_bw()
e <- a + geom_bar(stat="identity", aes(ID_EXP, Peaks, fill=Experiment))
e <- e + expand_limits(y=0) + coord_flip() + xlab("Experimental ID") + theme_bw() + guides(fill=FALSE)
grid.arrange(b, c, e, d, ncol=2, nrow=2)
dev.off()
```

The number of peptide sequences identified (top left), ratio of MS/MS identified : MS/MS submitted (top right), the number of peaks (bottom left) and the mass standard deviation (ppm, bottom right) for the indicated shotgun nLC-MS/MS experiments.

proteinGroup files
Function to combine MaxQuant outputs for subsequent analyses.
The Experiment ID (see Experiment key) is added to the dataframe here to allow subsetting of the data.

```{r group}
GETgroups <- function(x){
  #see https://stackoverflow.com/questions/4876813/using-r-to-list-all-files-with-a-specified-extension
  prot_files <- list.files(path = x, pattern = "proteinGroups.txt", recursive=TRUE, include.dirs=TRUE,
ignore.case=TRUE)
  complete_group <- data.frame()
  count <- 0
  for (i in prot_files){
    #see https://stackoverflow.com/questions/8996134/extract-vectors-from-strsplit-list-without-using-a-loop
    Experiment <- rapply(strsplit(i, "/"), function(a) a[1])
    prot_group <- read.csv(paste(x, "/", i, sep=""), sep="\t", header=TRUE)
    prot_group$Experiment <- Experiment
    count <- count + nrow(prot_group)
    print(paste("Experiment ", Experiment, " identified ", count, " proteins", sep=""))
    count <- 0
    complete_group <- rbind(prot_group, complete_group)
  }
  return(complete_group)
}
protgroups <- GETgroups(path)
```

The unique Experiments included in the final proteinGroups data frame are `r unique(protgroups$Experiment)`.
The total identifications for each appear in the table below.

```{r}
###count Experiment-specific ID###
table(protgroups$Experiment)
```

Uniprot database

Load database

Here, the Bos taurus uniprot database file "UP000009136_9913.fasta"" is loaded and the protein ID, protein name, gene name and sequence are extracted.

```{r up}
###read uniprot fasta file using seqinr function read.fasta###
UP <- read.fasta(file="./input/fasta/UP000009136_9913.fasta", seqtype="AA", as.string=TRUE)

###function to extract sequences and annotations from fasta files###
```

```
GetAnnotSeqFASTA <- function(x){
  UP_sequence <- unlist(getSequence(x, as.string=TRUE))
  UP_annotations <- unlist(getAnnot(x, as.string=TRUE))
  ProtName <- rapply(strsplit(UP_annotations, "IN ", fixed=TRUE), function(a) a[2])
  UP_prot_name <- rapply(strsplit(ProtName, " OS", fixed=TRUE), function(a) a[1])
  Gene <- rapply(strsplit(UP_annotations, "GN=", fixed=TRUE), function(a) a[2])
  UP_gene <- rapply(strsplit(Gene, " ", fixed=TRUE), function(a) a[1])
  UP_prot_ID <- rapply(strsplit(UP_annotations, "|", fixed=TRUE), function(a) a[2])
  return(data.frame(UP_prot_ID, UP_prot_name, UP_gene, UP_sequence))
}

###apply function to extract sequences and annotations###
dataUP <- GetAnnotSeqFASTA(UP)

str(dataUP)
```

This uniprot Bos taurus reference proteome contains `r nrow(dataUP)` proteins.

Filter database
These are the amino acid counts across the proteome:

```{r upfilter}
#see https://stackoverflow.com/questions/19476210/counting-the-number-of-each-letter-in-a-vector-of-strings
table(unlist(strsplit(as.character(dataUP$UP_sequence), ""), use.names=FALSE))
```

To allow the package functions to work properly when calculating sequence dependent values - isoelectric point (pI), molecular weight (MW) and Grand Average of Hydropathy (GRAVY) - U, B and X residues need to be removed.

```{r}
###remove U, B and X containing sequences###
#see https://stackoverflow.com/questions/6650510/remove-rows-from-data-frame-where-a-row-match-a-string
dataUP <- dataUP[!(str_count(as.character(dataUP$UP_sequence), "U")>=1),]
dataUP <- dataUP[!(str_count(as.character(dataUP$UP_sequence), "B")>=1),]
dataUP <- dataUP[!(str_count(as.character(dataUP$UP_sequence), "X")>=1),]
```

Following removal of U, B and X containing sequences the Uniprot database contains `r nrow(dataUP)` proteins.

Calculate protein characteristics
Now the pI, MW and GRAVY can be calculated.

```{r}
###string split uniprot sequences and calculate GRAVY, pI and MW###
split_SEQ <- strsplit(as.character(dataUP$UP_sequence), "")
dataUP$pI <- unlist(lapply(split_SEQ, computePI))
dataUP$MW <- unlist(lapply(split_SEQ, pmw))
dataUP$GRAVY <- gravy(dataUP$UP_sequence)
```

Protein filtering and ID matching
Here, entries with greater than, or equal to, 1 unique peptide are retained. In addition, the first protein ID in the "Protein.IDs"" column is extracted and used from here on.

```{r extract}
###Proteins with >= 1 unique peptide retained###
protgroupsMOD <- protgroups[protgroups$Unique.peptides >= 1,]
###Multiple entries for protein IDs removed - first entry retained###
protgroupsMOD$Prot_ID <- rapply(strsplit(as.character(protgroupsMOD$Protein.IDs),";"), function(a) a[1])
```

The extracted protein ID in the combined MaxQuant protein groups summary is then used to match to the uniprot dataframe protein ID and extract the GRAVY, pI and MW values for these entries.

```{r}
###EXTRACT by matching Prot_ID in "protgroupsMOD" dataframe to UP_prot_ID from "dataUP"###
#see https://www.r-bloggers.com/manipulating-data-frames-using-sqldf-a-brief-overview/
extract <- sqldf("select * from dataUP inner join protgroupsMOD on protgroupsMOD.Prot_ID =
dataUP.UP_prot_ID")
```

Final count of protein IDs:

```{r}
###count Experiment-specific ID###
table(extract$Experiment)
```

Data subsets
These data subsets are used for the plots generated by this script.

```{r subsets}
###combined experiment subsets###
Q_AF_F <- extract[extract$Exp=="AF" | extract$Exp=="F",]
Q_AE_EF <- extract[extract$Experiment=="AE" | extract$Experiment=="EF",]
Q_AF_AE <- extract[extract$Exp=="AF" | extract$Exp=="AE",]
Q_AF_AE_EF_F <- extract[extract$Experiment=="AF" | extract$Experiment=="AE" | extract$Experiment=="EF" |
extract$Experiment=="F",]

###single experiment subsets###
Q_A <- extract[extract$Experiment=="A",]
Q_F <- extract[extract$Experiment=="F",]
Q_AF <- extract[extract$Experiment=="AF",]
Q_EF <- extract[extract$Experiment=="EF",]
Q_AE <- extract[extract$Experiment=="AE",]

###venn subsets###
vA <- Q_A[,"UP_prot_ID"]
vF <- Q_F[,"UP_prot_ID"]
vAF <- Q_AF[,"UP_prot_ID"]
vAE <- Q_AE[,"UP_prot_ID"]
vEF <- Q_EF[,"UP_prot_ID"]
```

***

General considerations

Count across samples

```{r}
counts <- data.frame(table(extract$Prot_ID))
colnames(counts) <- c("Entry", "Count")
nrow(extract)
str(counts)
```

```{r}
tiff("./output/all_sample_count_prot_ID.tiff", height=300, width=300)
a = ggplot(counts, aes(Count)) + geom_histogram(binwidth=1, col="black", fill="blue", alpha=0.5)
a = a + geom_hline(yintercept=c(10,50,100,200,300,400), col="red", linetype="dashed")
a = a + theme_bw() + themeTIFF + xlab("Protein ID") + ylab("Count")
plot(a)
dev.off()
```

The total count of protein IDs across all the experiment types appears below.

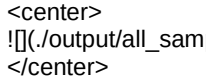

Overrepresented proteins across samples

```{r}
###find proteins across all experiments###
##list these proteins for 4/5 occurrences###
overlap <- rbind(counts[counts$Count==4,],counts[counts$Count==5,])
overlap_match <- data.frame()
for(i in overlap$Entry){
  data <- extract[extract$Prot_ID==i,]
  data <- cbind(data, rep(i, nrow(data)))
  overlap_match <- rbind(data, overlap_match)
}
ID_count <- data.frame(table(overlap_match$Prot_ID))
ID_count <- ID_count[ID_count$Freq>=1,]
ID_count <- ID_count[ order(-ID_count$Freq), ]
colnames(ID_count) <- c("Protein_ID", "Count")
```

There were `r nrow(ID_count)` proteins that were identified across 4 or more experiment types (N = 5 total).

```{r}
IDs <- ID_count[ID_count$Count==5,]
IDmatch <- data.frame()

for(i in IDs$Protein_ID){
  data <- dataUP[dataUP$UP_prot_ID==i,]
  data$Protein_ID <- i
  IDmatch <- rbind(data, IDmatch)
}

COUNT5 <- data.frame(IDmatch$UP_prot_ID, IDmatch$Protein_ID, IDmatch$UP_prot_name)
colnames(COUNT5) <- c("UP_prot_ID", "Protein_ID", "UP_prot_name")
COUNT5

```

Count (independent AF searches)

```{r}
path <- "./input/IAPP_independent_searches/"

###function to extract proteinGroup files from independent Andromeda searches###
GETindependent <- function(x){
#see https://stackoverflow.com/questions/4876813/using-r-to-list-all-files-with-a-specified-extension
  files_IND <- list.files(path = x, pattern = "proteinGroups.txt", recursive=TRUE, include.dirs=TRUE,
ignore.case=TRUE)
  complete_group <- data.frame()
  for (i in files_IND){
#see https://stackoverflow.com/questions/8996134/extract-vectors-from-strsplit-list-without-using-a-loop
    Experiment <- rapply(strsplit(i, "/"), function(a) a[1])
    prot_group <- read.csv(paste(x, "/", i, sep=""), sep="\t", header=TRUE)
    prot_group$Experiment <- Experiment
    complete_group <- rbind(prot_group, complete_group)
  }
  return(complete_group)
}

###modify data frame###
protgroups_IND <- GETindependent(path)
protgroups_IND$Prot_ID <- rapply(strsplit(as.character(protgroups_IND$Protein.IDs),";"), function(a) a[1])

###check experiments included###
table(protgroups_IND$Experiment)

###subset based on experiment###
AF1 <- protgroups_IND[protgroups_IND$Experiment == "AF_1",]
```

```
AF2 <- protgroups_IND[protgroups_IND$Experiment == "AF_2",]
AF3 <- protgroups_IND[protgroups_IND$Experiment == "AF_3",]
AF4 <- protgroups_IND[protgroups_IND$Experiment == "AF_4",]
AF5 <- protgroups_IND[protgroups_IND$Experiment == "AF_5",]
AF6 <- protgroups_IND[protgroups_IND$Experiment == "AF_6",]

F1 <- protgroups_IND[protgroups_IND$Experiment == "F_1_156",]
F2 <- protgroups_IND[protgroups_IND$Experiment == "F_1_164",]
F3 <- protgroups_IND[protgroups_IND$Experiment == "F_1_170",]
F4 <- protgroups_IND[protgroups_IND$Experiment == "F_2_156",]
F5 <- protgroups_IND[protgroups_IND$Experiment == "F_2_170",]
F6 <- protgroups_IND[protgroups_IND$Experiment == "F_3_180",]
F7 <- protgroups_IND[protgroups_IND$Experiment == "F_4_180",]
F8 <- protgroups_IND[protgroups_IND$Experiment == "F_5_180",]
F9 <- protgroups_IND[protgroups_IND$Experiment == "F_6_180",]

###AF venn subsets###
vAF1 <- AF1[,"Prot_ID"]
vAF2 <- AF2[,"Prot_ID"]
vAF3 <- AF3[,"Prot_ID"]
vAF4 <- AF4[,"Prot_ID"]
vAF5 <- AF5[,"Prot_ID"]
vAF6 <- AF6[,"Prot_ID"]

###F venn subsets###
vF1 <- F1[,"Prot_ID"]
vF2 <- F2[,"Prot_ID"]
vF3 <- F3[,"Prot_ID"]
vF4 <- F4[,"Prot_ID"]
vF5 <- F5[,"Prot_ID"]
vF6 <- F6[,"Prot_ID"]
vF7 <- F7[,"Prot_ID"]
vF8 <- F8[,"Prot_ID"]
vF9 <- F9[,"Prot_ID"]

#see https://stackoverflow.com/questions/25019794/venn-diagram-with-item-labels
venn <- venn.diagram(list(AF1 = vAF1, AF2 = vAF2, AF3 = vAF3, AF4 = vAF4, AF5 = vAF5),
                     fill = c("red", "blue", "green", "yellow", "purple"),
                     alpha = 0.4, lwd = 1, cex = 1, cat.cex = 1, filename = NULL)

tiff("./output/venn_AF_independent.tiff", height=300, width=300)
grid.newpage()
grid.draw(venn)
dev.off()

venn <- venn.diagram(list(AF2 = vAF2, AF3 = vAF3, AF4 = vAF4, AF5 = vAF5, AF6= vAF6),
                     fill = c("blue", "green", "yellow", "purple", "brown"),
                     alpha = 0.4, lwd = 1, cex = 1, cat.cex = 1, filename = NULL)

tiff("./output/venn_AF_independent_2.tiff", height=300, width=300)
grid.newpage()
grid.draw(venn)
dev.off()

venn <- venn.diagram(list(F1 = vF1, F2 = vF2, F3 = vF3, F4 = vF4, F5 = vF5),
                     fill = c("blue", "green", "yellow", "purple", "orange"),
                     alpha = 0.4, lwd = 1, cex = 1, cat.cex = 1, filename = NULL)

tiff("./output/venn_F_independent.tiff", height=300, width=300)
grid.newpage()
grid.draw(venn)
dev.off()

venn <- venn.diagram(list(F3 = vF3, F4 = vF4, F5 = vF5, F6 = vF6, F7 = vF7),
                     fill = c("yellow", "purple", "orange", "brown", "pink"),
                     alpha = 0.4, lwd = 1, cex = 1, cat.cex = 1, filename = NULL)
```

```
tiff("./output/venn_F_independent_2.tiff", height=300, width=300)
grid.newpage()
grid.draw(venn)
dev.off()

venn <- venn.diagram(list(F5 = vF5, F6 = vF6, F7 = vF7, F8 = vF8, F9 = vF9),
                     fill = c("orange", "brown", "pink", "gray", "darkblue"),
                     alpha = 0.4, lwd = 1, cex = 1, cat.cex = 1, filename = NULL)

tiff("./output/venn_F_independent_3.tiff", height=300, width=300)
grid.newpage()
grid.draw(venn)
dev.off()

```

Global faceted analysis of variables

Unique peptides vs peptides
```{r}
#see http://ggplot2.tidyverse.org/reference/facet_grid.html
b <- ggplot(extract)
b <- b + geom_point(aes(Unique.peptides, Peptides), alpha=0.7, pch=21, fill="gray")
b <- b + facet_grid(. ~ Experiment)
b <- b + theme_bw() + theme(axis.text.x = element_text(angle=90, vjust=0.5))
plot(b)
```

GRAVY vs pI
```{r}
c <- ggplot(extract)
c <- c + geom_point(aes(GRAVY, pI), alpha=0.7, pch=21, fill="gray")
c <- c + facet_grid(. ~ Experiment)
c <- c + theme_bw()
plot(c)
```

GRAVY vs MW
```{r}
d <- ggplot(extract)
d <- d + geom_point(aes(GRAVY, MW), alpha=0.7, pch=21, fill="gray")
d <- d + facet_grid(. ~ Experiment)
d <- d + theme_bw() + scale_y_continuous(limits=c(0,1E+6))
plot(d)
```

Question 1 - CC coronae

Overlap of AF/F protein IDs

Comparing FBS only (F), with IAPP amyloids exposed to FBS (AF). These samples were prepared with 1 MDa molecular weight cut-off (MWCO) spin columns (CC method).

The identification overlap was as follows:
```{r}
#see https://stackoverflow.com/questions/25019794/venn-diagram-with-item-labels
venn <- venn.diagram(list(F = vF, AF = vAF), fill = c("red", "blue"),
                     alpha = 0.4, lwd = 1, cex = 1.5, cat.cex = 1.5, filename = NULL)
```

```
tiff("./output/venn_F_AF.tiff", height=300, width=300)
grid.newpage()
grid.draw(venn)
dev.off()
```

Unique AF proteins

Here, plots are created that summarise the physico-chemical properties of proteins unique to the AF samples, highlighting some potentially interesting amyloid binding proteins that could be investigated in future.

Extracting unique entries from combined AF/F data:
```{r}
#see https://stackoverflow.com/questions/16905425/find-duplicate-values-in-r
AF_F_ID_count <- data.frame(table(Q_AF_F$Prot_ID))
AF_F_ID_count <- AF_F_ID_count[AF_F_ID_count$Freq==1,]

###extract unique entries for AF and F###
AF_F_unique <- data.frame()
for(i in AF_F_ID_count$Var1){
  data <- Q_AF_F[Q_AF_F$Prot_ID==i,]
  data <- cbind(data, i)
  AF_F_unique <- rbind(data, AF_F_unique)
}
###check dataframe###
#head(AF_F_unique)
```

Confirming Venn diagram counts:
```{r}
AF_F_unique_count <- data.frame(table(AF_F_unique$Experiment))
colnames(AF_F_unique_count) <- c("Prot_ID", "Count")
AF_F_unique_count
```

Extract unique AF proteins and export these for STRING network analysis:
```{r}
###create subset dataframe###
AF <- AF_F_unique[AF_F_unique$Experiment=="AF",]
F <- AF_F_unique[AF_F_unique$Experiment=="F",]

#see http://r.789695.n4.nabble.com/write-text-file-as-output-without-quotes-td888020.html
write.table(AF$Prot_ID, "./output/exp_AF_protlist.txt", sep="\t", quote=FALSE, row.names = FALSE, col.names = FALSE)
```

The top 12 unique AF proteins, based on unique peptide count were:
```{r}
#see https://stackoverflow.com/questions/1296646/how-to-sort-a-dataframe-by-columns
uniqueAF_sort <- AF[ order(-AF$Unique.peptides), ]
uniqueAF_sort <- data.frame(uniqueAF_sort$Prot_ID, uniqueAF_sort$UP_prot_name, uniqueAF_sort$Unique.peptides)
colnames(uniqueAF_sort) <- c("Protein ID", "Protein name", "Unique peptides")
uniqueAF_sort[1:12,]
```

Unique AF/F amino acid composition

Concept inspired by a table in the following reference -> DOI:10.1039/C7EN00466D (see http://pubs.rsc.org/en/content/articlehtml/2017/en/c7en00466d)

```{r}
###experimental###
```

```
propAF <- data.frame()
for (i in AF_F_unique$UP_sequence){
  seq_vec <- unlist(strsplit(as.character(i), ""))
  info <- AAstat(seq_vec, plot=FALSE)
  all <- AF_F_unique[AF_F_unique$UP_sequence==i,]
  summary <- cbind(all, info$Prop$Aliphatic, info$Prop$Aromatic, info$Prop$Non.polar,
                   info$Prop$Polar, info$Prop$Charged, info$Prop$Basic, info$Prop$Acidic)
  propAF <- rbind(summary, propAF)
}

###uniprot###
propUP <- data.frame()
for (i in dataUP$UP_sequence){
  seq_vec <- unlist(strsplit(as.character(i), ""))
  info <- AAstat(seq_vec, plot=FALSE)
  all <- dataUP[dataUP$UP_sequence==i,]
  summary <- cbind(all, info$Prop$Aliphatic, info$Prop$Aromatic, info$Prop$Non.polar,
                   info$Prop$Polar, info$Prop$Charged, info$Prop$Basic, info$Prop$Acidic)
  propUP <- rbind(summary, propUP)
}

###subset based on specific columns###
propAF <- propAF[,c(1,2,3,40,41,43,44,45,46,47,48,49)]
###check colnames###
colnames(propAF)
colnames(propUP)

###update column names###
colnames(propAF) <- c("UP_prot_ID", "UP_prot_name", "UP_gene", "Experiment", "Prot_ID", "Aliphatic",
                      "Aromatic", "NonPolar", "Polar", "Charged", "Basic", "Acidic")

colnames(propUP) <- c("UP_prot_ID", "UP_prot_name", "UP_gene", "UP_sequence", "pI", "MW", "GRAVY",
"Aliphatic",
                      "Aromatic", "NonPolar", "Polar", "Charged", "Basic", "Acidic")

###plots###
a <- ggplot(propUP) + geom_point(aes(NonPolar, Acidic), col="gray", alpha=0.4)
a <- a + geom_point(data=propAF[propAF$Experiment=="F",], aes(NonPolar, Acidic), fill = "blue", pch=21)
a <- a + geom_point(data=propAF[propAF$Experiment=="AF",], aes(NonPolar, Acidic), fill = "yellow", pch=21)
a <- a + theme_bw() + coord_fixed()
plot(a)
```

Unique AF proteins (GRAVY/pI + proteome)

Here, the Bos taurus proteome (gray) is overlaid with all unique FBS only proteins (F, blue), as well as those proteins unique to amyloid + FBS (AF, yellow). Labels are gene names, outside the box indicated on the plot. The top panel labels unique AF proteins outside the boundaries indicated by the highlighted blue box. The bottom panel labels unique AF proteins (GRAVY <=-1 and GRAVY >=0 and pI <= 4.5 and pI >= 7).

```{r}
###plot###
tiff("./output/AF_unique_GRAVY_pI_BosT.tiff", width=2500, height=5000, res=300)
#themes, see #http://ggplot2.tidyverse.org/reference/theme.html
#geom_rect, see - https://stackoverflow.com/questions/4733182/how-to-highlight-time-ranges-on-a-plot
a <- ggplot(dataUP)
a <- a + geom_point(data=dataUP, aes(GRAVY, pI), col="gray", alpha=0.1)
a <- a + geom_point(data=F, aes(GRAVY, pI), pch=21, size=5, fill="blue")
a <- a + geom_point(data=AF, aes(GRAVY, pI), pch=21, size=3, fill="yellow")
a <- a + theme_bw() + themeTIFF + xlab("GRAVY") + ylab("pI")
b <- a + geom_rect(data=data.frame(xmin=-1.5, xmax=0.5, ymin=4, ymax=10),
                   aes(xmin=xmin, xmax=xmax, ymin=ymin, ymax=ymax),
                   fill="lightblue", col="black", alpha=0.4,
                   inherit.aes = FALSE)
b <- b + geom_label_repel(data=AF[AF$GRAVY<=-1.5 | AF$GRAVY>=0.5 | AF$pI<=4 | AF$pI>=10,],
                          aes(GRAVY, pI, label=UP_gene), size=4)
```

```
c <- a + scale_y_continuous(limits=c(4,10)) + scale_x_continuous(limits=c(-1.5,0.5))
c <- c + geom_rect(data=data.frame(xmin=-1, xmax=0, ymin=4.5, ymax=7),
                   aes(xmin=xmin, xmax=xmax, ymin=ymin, ymax=ymax),
                   fill="lightblue", col="black", alpha=0.4,
                   inherit.aes = FALSE)
c <- c + geom_label_repel(data=AF[AF$GRAVY<=-1 | AF$GRAVY>=0 | AF$pI<=4.5 | AF$pI>=7,],
                          aes(GRAVY, pI, label=UP_gene), size=4)
c <- c + guides(fill=FALSE)
grid.arrange(b, c, nrow=2)
dev.off()
```

The following figure includes all AF and unique AF proteins, with the scatter markers size based on number of unique peptides. Unique AF proteins with >= 10 unique peptides (yellow) and all AF proteins with >= 20 unique peptides (white) are labelled.

```{r}
###plot###
tiff("./output/AF_unique_GRAVY_pI_all_AF_unique_pep.tiff", width=700, height=700)
d <- ggplot(Q_AF) + geom_point(aes(GRAVY, pI, size=Unique.peptides), col="blue")
d <- d + geom_point(data=AF, aes(GRAVY, pI, size=Unique.peptides), col="yellow")
d <- d + scale_x_continuous(limits=c(-1,0)) + scale_y_continuous(limits=c(4,7.5))
d <- d + geom_label_repel(data=Q_AF[Q_AF$Unique.peptides>=20,], aes(GRAVY, pI, label=UP_gene), size=3)
d <- d + geom_label_repel(data=AF[AF$Unique.peptides>=10,], aes(GRAVY, pI, label=UP_gene), fill="yellow",
size=3)
d <- d + theme_bw() + themeTIFF + xlab("GRAVY") + ylab("pI")
d <- d + theme(panel.background = element_rect(fill="gray"), panel.grid.minor = element_line(colour="gray"),
               panel.grid.major = element_line(colour="gray"))
plot(d)
dev.off()
```

Unique AF proteins (GRAVY/MW + proteome)

A matching overlay of unique F (blue) and unique AF (yellow) proteins against the Bos taurus proteome (gray) is shown below - plotting GRAVY and MW. Labels are gene names, with unique AF proteins labelled in both the top (>= 600 kDa) and bottom (>= 200 kDa) panel. GRAVY ranges for labelling are identical for both panels (GRAVY >= 0.5 & <= -1.5)

```{r}
###plot###
tiff("./output/AF_unique_GRAVY_MW_BosT.tiff", width=2500, height=5000, res=300)
a <- ggplot(dataUP)
a <- a + geom_point(data=dataUP, aes(GRAVY, MW), col="gray", alpha=0.1)
a <- a + geom_point(data=F, aes(GRAVY, MW), pch=21, size=5, fill="blue")
a <- a + geom_point(data=AF, aes(GRAVY, MW), pch=21, size=3, fill="yellow", col="blue")
a <- a + theme_bw() + themeTIFF + xlab("GRAVY") + ylab("MW")
b <- a + geom_rect(data=data.frame(xmin=-1.5, xmax=0.5, ymin=0, ymax=6E+5),
                   aes(xmin=xmin, xmax=xmax, ymin=ymin, ymax=ymax),
                   fill="lightblue", col="black", alpha=0.4, inherit.aes = FALSE)
b <- b + geom_label_repel(data=AF[AF$GRAVY<=-1.5 | AF$GRAVY>=0.5 | AF$MW>=6E+5,],
                          aes(GRAVY, MW, label=UP_gene), size=4)
c <- a + scale_y_continuous(limits=c(0,6E+5)) + scale_x_continuous(limits=c(-1.5,0.5))
c <- c + geom_label_repel(data=AF[AF$GRAVY<=-1.5 | AF$GRAVY>=0.5 | AF$MW>=2E+5,],
                          aes(GRAVY, MW, label=UP_gene), size=4)
c <- c + guides(fill=FALSE)
grid.arrange(b, c, nrow=2)
dev.off()
```

Question 2 - QCM coronae

Overlap of AE/EF protein IDs

The identification overlap was as follows:
```{r}
#see https://stackoverflow.com/questions/25019794/venn-diagram-with-item-labels
venn <- venn.diagram(list(AE = vAE, EF = vEF), fill = c("yellow", "blue"),
                     alpha = 0.4, lwd = 1, cex = 1.5, cat.cex = 1.5, filename = NULL)

tiff("./output/venn_AE_EF.tiff", width=2500, height=2500, res=300)
grid.newpage()
grid.draw(venn)
dev.off()
```

Overlay of unique AE/EF proteins
```{r}
#see https://stackoverflow.com/questions/16905425/find-duplicate-values-in-r
AE_EF_ID_count <- data.frame(table(Q_AE_EF$Prot_ID))
AE_EF_ID_count <- AE_EF_ID_count[AE_EF_ID_count$Freq==1,]

AE_EF_unique <- data.frame()
for(i in AE_EF_ID_count$Var1){
  data <- Q_AE_EF[Q_AE_EF$Prot_ID==i,]
  data <- cbind(data, i)
  AE_EF_unique <- rbind(data, AE_EF_unique)
}

AE_EF <- data.frame(table(AE_EF_unique$Experiment))
AE_EF <- AE_EF[AE_EF$Freq>0,]
colnames(AE_EF) <- c("Prot_ID", "Count")
Q2_AE <- AE_EF_unique[AE_EF_unique$Experiment=="AE",]
Q2_EF <- AE_EF_unique[AE_EF_unique$Experiment=="EF",]
```

There were a total of `r nrow(Q_EF)` and `r nrow(Q_AE)` IDs for experiments EF and AE, respectively. Of these there were `r nrow(Q2_EF)` and `r nrow(Q2_AE)` unique protein identifications for EF and AE, respectively.

The top 12 unique AE proteins, based on unique peptide count were:
```{r}
uniqueAE_sort <- Q2_AE[ order(-Q2_AE$Unique.peptides), ]
uniqueAE_sort <- data.frame(uniqueAE_sort$Prot_ID, uniqueAE_sort$UP_prot_name,
uniqueAE_sort$Unique.peptides)
colnames(uniqueAE_sort) <- c("Protein ID", "Protein name", "Unique peptides")
uniqueAE_sort[1:12,]
```

Here, the protein list for unique AE proteins was exported for STRING DB analysis.
```{r export_AE}
#see http://r.789695.n4.nabble.com/write-text-file-as-output-without-quotes-td888020.html
write.table(Q2_AE$Prot_ID, "./output/exp_AE_protlist.txt", sep="\t", quote=FALSE, row.names = FALSE,
col.names = FALSE)
```

The unique EF proteins were:
```{r}
```

```
uniqueEF_sort <- Q2_EF[ order(-Q2_EF$Unique.peptides), ]
uniqueEF_sort <- data.frame(uniqueEF_sort$Prot_ID, uniqueEF_sort$UP_prot_name,
uniqueEF_sort$Unique.peptides)
colnames(uniqueEF_sort) <- c("Protein ID", "Protein name", "Unique peptides")
uniqueEF_sort
```

Unique AE/EF amino acid composition

Concept inspired by a table in the following reference -> DOI:10.1039/C7EN00466D (see http://pubs.rsc.org/en/content/articlehtml/2017/en/c7en00466d)

```{r}
propAE <- data.frame()
for (i in AE_EF_unique$UP_sequence){
  seq_vec <- unlist(strsplit(as.character(i), ""))
  info <- AAstat(seq_vec, plot=FALSE)
  all <- AE_EF_unique[AE_EF_unique$UP_sequence==i,]
  summary <- cbind(all, info$Prop$Aliphatic, info$Prop$Aromatic, info$Prop$Non.polar,
                   info$Prop$Polar, info$Prop$Charged, info$Prop$Basic, info$Prop$Acidic)
  propAE <- rbind(summary, propAE)
}

###subset and rename columns###
propAE <- propAE[,c(1,2,3,40,41,43,44,45,46,47,48,49)]
###check column names###
colnames(propAE)
###update column names###
colnames(propAE) <- c("UP_prot_ID", "UP_prot_name", "UP_gene", "Experiment", "Prot_ID", "Aliphatic",
                      "Aromatic", "NonPolar", "Polar", "Charged", "Basic", "Acidic")

###plots###
a <- ggplot(propUP) + geom_point(aes(NonPolar, Acidic), col="gray", alpha=0.4)
a <- a + geom_point(data=propAE[propAE$Experiment=="AE",], aes(NonPolar, Acidic), fill = "yellow", pch=21)
a <- a + geom_point(data=propAE[propAE$Experiment=="EF",], aes(NonPolar, Acidic), fill = "blue", pch=21)
a <- a + theme_bw() + coord_fixed()
plot(a)

```

Unique AE/EF proteins (GRAVY/pI/MW + proteome)
Here, the Bos taurus proteome (gray) is overlaid with unique AE (yellow) and unique EF (blue) proteins - plotting GRAVY/pI and GRAVY/MW.
```{r}
tiff("./output/AE_EF_unique_GRAVY_pI_BosT.tiff", width=2500, height=5000, res=300)
#themes, see #http://ggplot2.tidyverse.org/reference/theme.html
d <- ggplot(dataUP)
d <- d + geom_point(aes(GRAVY, pI), size=1, col="gray", alpha=0.5)
d <- d + geom_point(data=Q2_EF, aes(GRAVY, pI), pch=21, fill="blue", size=5)
d <- d + geom_point(data=Q2_AE, aes(GRAVY, pI), pch=21, fill="yellow", size=3)
d <- d + xlab("GRAVY") + ylab("pI") + theme_bw() + themeTIFF
#geom_rect, see - https://stackoverflow.com/questions/4733182/how-to-highlight-time-ranges-on-a-plot
e <- d + geom_rect(data=data.frame(xmin=-1.5, xmax=0.5, ymin=4, ymax=10),
                   aes(xmin=xmin, xmax=xmax, ymin=ymin, ymax=ymax),
                   fill="lightblue", col="black", alpha=0.4, inherit.aes = FALSE)
e <- e + geom_label_repel(data=Q2_AE[Q2_AE$pI>=10 | Q2_AE$pI<=4 | Q2_AE$GRAVY>=0.5 |
Q2_AE$GRAVY<=-1.5,],
                          aes(GRAVY, pI, label=UP_gene), size=4)
f <- d + scale_x_continuous(limits=c(-1.5,1)) + scale_y_continuous(limits=c(4,10))
f <- f + geom_rect(data=data.frame(xmin=-1, xmax=0, ymin=4.5, ymax=8.5),
                   aes(xmin=xmin, xmax=xmax, ymin=ymin, ymax=ymax),
                   fill="lightblue", col="black", alpha=0.4, inherit.aes = FALSE)
f <- f + geom_label_repel(data=Q2_AE[Q2_AE$pI>=8.5 | Q2_AE$pI<=4.5 | Q2_AE$GRAVY>=0 |
Q2_AE$GRAVY<=-1,],
                          aes(GRAVY, pI, label=UP_gene), size=4)
grid.arrange(e, f, nrow=2)
dev.off()
```

```

<center>
![](./output/AE_EF_unique_GRAVY_pI_BosT.tiff)
</center>

```{r}
tiff("./output/AE_EF_unique_GRAVY_MW_BosT.tiff", width=2500, height=5000, res=300)
#themes, see #http://ggplot2.tidyverse.org/reference/theme.html
d <- ggplot(dataUP)
d <- d + geom_point(aes(GRAVY, MW), size=1, col="gray", alpha=0.5)
d <- d + geom_point(data=Q2_EF, aes(GRAVY, MW), pch=21, fill="blue", size=5)
d <- d + geom_point(data=Q2_AE, aes(GRAVY, MW), pch=21, fill="yellow", size=3)
d <- d + xlab("GRAVY") + ylab("MW") + theme_bw() + themeTIFF
#geom_rect, see - https://stackoverflow.com/questions/4733182/how-to-highlight-time-ranges-on-a-plot
e <- d + geom_rect(data=data.frame(xmin=-1.5, xmax=0.5, ymin=0, ymax=600000),
                   aes(xmin=xmin, xmax=xmax, ymin=ymin, ymax=ymax),
                   fill="lightblue", col="black", alpha=0.4, inherit.aes = FALSE)
e <- e + geom_label_repel(data=Q2_AE[Q2_AE$MW>=6E+5 | Q2_AE$GRAVY>=0.5 | Q2_AE$GRAVY<=-1.5,],
                          aes(GRAVY, MW, label=UP_gene), size=4)
f <- d + scale_y_continuous(limits=c(0,600000))
f <- f + geom_label_repel(data=Q2_AE[Q2_AE$MW>=3E+5 | Q2_AE$GRAVY>=0.5 | Q2_AE$GRAVY<=-1.5,],
                          aes(GRAVY, MW, label=UP_gene), size=4)
grid.arrange(e, f, nrow=2)
dev.off()
```

<center>

</center>

***

Question 3 - CC vs QCM

Overlap of AF/AE protein IDs
The next comparison of interest was to consider the difference, if any, between the amyloids + FBS prepared by either the CC method (AF) or the QCM method (AE).

The identification overlap for these experiments was as follows:
```{r}
#see https://stackoverflow.com/questions/25019794/venn-diagram-with-item-labels
venn <- venn.diagram(list(AF = vAF, AE = vAE), fill = c("red", "blue"),
                     alpha = 0.4, lwd = 1, cex = 2.5, cat.cex = 2.5, filename = NULL)

tiff("./output/venn_AF_AE.tiff", width=2500, height=2500, res=300)
grid.newpage()
grid.draw(venn)
dev.off()
```

<center>

</center>

There were a total of `r nrow(Q_AF)` and `r nrow(Q_AE)` IDs for experiments AF and AE, respectively.

If we consider the Venn diagram showing the four experiments F/AF/AE/EF, we can identify those proteins unique to AF/AE.

```{r}
#see https://stackoverflow.com/questions/25019794/venn-diagram-with-item-labels
venn <- venn.diagram(list(AF = vAF, AE = vAE, F=vF, EF=vEF), fill = c("red", "blue", "green", "yellow"),
                     alpha = 0.4, lwd = 1, cex = 1.5, cat.cex = 1.5, filename = NULL)

tiff("./output/venn_AF_AE_F_EF.tiff", height=300, width=300)
grid.newpage()
```
```

```
grid.draw(venn)
dev.off()
```

***

Question 4 - Control nLC-MS/MS
A

Amyloid only control for CC method.

Sample A nLC-MS/MS analyses identified a total of `r nrow(Q_A)` proteins.

These proteins were:
```{r}
Q_A_sort <- Q_A[ order(-Q_A$Unique.peptides), ]
A_list <- data.frame(Q_A_sort$Prot_ID, Q_A_sort$UP_prot_name, Q_A_sort$Unique.peptides)
colnames(A_list) <- c("Protein ID", "Protein name", "Unique peptides")
A_list[1:12,]
```

The identification overlap for A/F/AF was:
```{r}
#see https://stackoverflow.com/questions/25019794/venn-diagra♣m-with-item-labels
venn <- venn.diagram(list(A = vA, F = vF, AF=vAF), fill = c("green", "blue", "yellow"),
                     alpha = 0.4, lwd = 1, cex = 2.5, cat.cex = 2.5, filename = NULL)

tiff("./output/venn_A_F_AF.tiff", width=2500, height=2500, res=300)
grid.newpage()
grid.draw(venn)
dev.off()

```

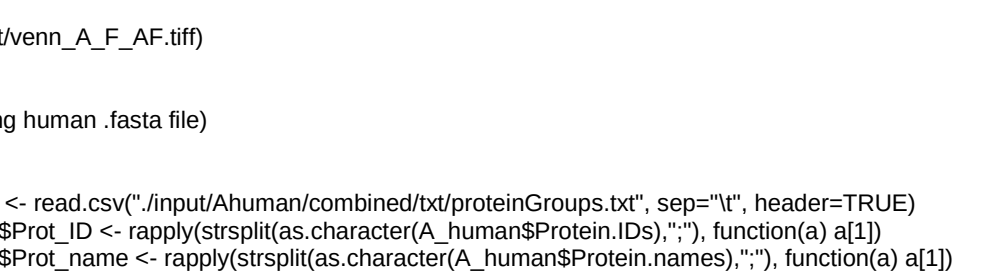

A (using human .fasta file)

```{r}
A_human <- read.csv("./input/Ahuman/combined/txt/proteinGroups.txt", sep="\t", header=TRUE)
A_human$Prot_ID <- rapply(strsplit(as.character(A_human$Protein.IDs),";"), function(a) a[1])
A_human$Prot_name <- rapply(strsplit(as.character(A_human$Protein.names),";"), function(a) a[1])
```

Sample A nLC-MS/MS analyses using a human fasta file for the Andromeda search identified a total of `r nrow(A_human)` proteins.

The top 12 proteins in this list, based on unique peptides counts, were:
```{r}
A_human_sort <- A_human[ order(-A_human$Unique.peptides), ]
A_human_sort <- data.frame(A_human_sort$Prot_ID, A_human_sort$Prot_name,
A_human_sort$Unique.peptides)
colnames(A_human_sort) <- c("Protein ID", "Protein name", "Unique peptides")
A_human_sort[1:12,]
```

***

Extract data consistency check

Random subset of 30 rows from extract dataframe checked to make sure that IDs, names and sequences align correctly.

```{r}
# see https://stackoverflow.com/questions/8273313/sample-random-rows-in-dataframe
CHECK <- extract[sample(nrow(extract), 30), ]
write.table(CHECK, "./output/extract_consistency_check.txt", sep="\t")
```

***

Check of MaxQuant parameters
This section checks the consistency of the parameters used for MaxQuant.

```{r}
path <- "./input/IAPP"
GETparameters <- function(x){
  #see https://stackoverflow.com/questions/4876813/using-r-to-list-all-files-with-a-specified-extension
  parameter_files <- list.files(path = x, pattern = "parameters.txt", recursive=TRUE, include.dirs=TRUE,
ignore.case = TRUE)
  complete_parameters <- data.frame()
  complete_parameters <- read.csv(paste(x, "/", parameter_files[[1]], sep=""), sep="\t", header=TRUE)$Parameter
  for (i in parameter_files){
    #see https://stackoverflow.com/questions/8996134/extract-vectors-from-strsplit-list-without-using-a-loop
    Experiment <- rapply(strsplit(i, "/"), function(a) a[1])
    parameters <- read.csv(paste(x, "/", i, sep=""), sep="\t", header=TRUE)
    colnames(parameters) <- c("Parameter", Experiment)
    # see http://www.r-tutor.com/r-introduction/data-frame/data-frame-column-slice
    complete_parameters <- cbind(complete_parameters, parameters[2])
  }
  return(complete_parameters)
}

parameters <- GETparameters(path)

#see https://stackoverflow.com/questions/28628384/count-number-of-unique-values-per-row
apply(parameters[,2:6], 1, function(x)length(unique(x)))
```

Row four contains multiple unique entries. This row contains reports the following variable:

```{r}
parameters[4,1]
```

***

Chromatogram plotting script

Package xcms license is GPL (>= 2) + a file LICENSE available @
https://bioconductor.org/packages/release/bioc/licenses/xcms/LICENSE.

```{r}
#source("https://bioconductor.org/biocLite.R")
#biocLite("xcms")

#########################
###libraries required###
#########################
#library(xcms)
#library(ggplot2)
#library(gridExtra)
#library(stringr)
#library(plyr)

###############
###citations###
```

```
###############
#citation("xcms")
#citation("ggplot2")
#citation("gridExtra")
#citation("stringr")

###########
###notes###
###########
#see https://bioconductor.org/packages/3.7/bioc/vignettes/xcms/inst/doc/new_functionality.html
#see https://bioconductor.org/packages/release/bioc/vignettes/xcms/inst/doc/xcms.html
#see https://www.rdocumentation.org/packages/xcms/versions/1.48.0/topics/xcmsRaw
#these vignettes, documentation and examples were used in writing of the code provided below.

#########################################################################
###############set data directory and file_type#####################
###mzR can load many file types - this code was written for mzML###
#########################################################################
#path <- "./Converted_RAW_files/"
#file_type <- ".mzML"

#####################################################
###################lcms_vis#########################
###FUNCTION TO CREATE TIC CHROMATOGRAM OUTPUTS###
#####################################################

#lcms_vis <- function(x){
#  #see https://stackoverflow.com/questions/4876813/using-r-to-list-all-files-with-a-specified-extension
#  files <- list.files(path = x, pattern= paste("\\", file_type, sep=""))
#  complete_TIC_data <- data.frame()
#  for (i in files){
#    #see https://stackoverflow.com/questions/8996134/extract-vectors-from-strsplit-list-without-using-a-loop
#    id <- rapply(strsplit(i, "_"), function(a) a[6])
#    ID <- rapply(strsplit(id, ".m"), function(a) a[1])
#    #see https://stackoverflow.com/questions/18115550/how-to-combine-two-or-more-columns-in-a-dataframe-
into-a-new-column-with-a-new-n
#    uniqueID <- paste(rapply(strsplit(i,"_"), function(a) a[4]),"_", ID, sep="")
#    #see https://stackoverflow.com/questions/9756360/r-split-character-data-into-numbers-and-letters
#    replicate <- as.numeric(str_extract(ID, "[0-9]+"))
#    experiment <- (str_extract(ID, "[aA-zZ]+"))
#    #see https://www.rdocumentation.org/packages/xcms/versions/1.48.0/topics/xcmsRaw
#    data <- xcmsRaw(paste(path, i, sep=""), profstep = 1, profmethod = "bin", profparam = list(),
#                    includeMSn=FALSE, mslevel=NULL, scanrange=NULL)
#    tiff(file=paste("./chromatograms/", uniqueID, "_combined_chromatograms.tiff", sep=""), width=1500,
height=750)
#    #see https://www.statmethods.net/advgraphs/layout.html
#    par(mfrow=c(1,2))
#    plotChrom(data, base=TRUE)
#    plotChrom(data, base=FALSE)
#    dev.off()
#    TIC <- data.frame(uniqueID, ID, experiment, replicate, data@scantime, data@tic)
#    complete_TIC_data <- rbind(complete_TIC_data, TIC)
#  }
#  return(complete_TIC_data)
#}

#################################
###Process selected directory###
#################################
#DATA <- lcms_vis(path)
#write.table(DATA, "./complete_TIC_data.txt", sep="\t")

###################################
###Create combined chromatograms###
###################################

#for (i in unique(DATA$experiment)){
```

```
#  plotDATA <- subset(DATA, DATA$experiment==i)
#  pdf(paste("./chromatogram_overlays/chromatograms_",i,".pdf",sep=""), width=15, height=15)
#  #see http://ggplot2.tidyverse.org/reference/scale_brewer.html
#  a = ggplot(plotDATA, aes(data.scantime, data.tic)) + geom_line(alpha=0.5, aes(col=as.character(replicate)))
#  #see https://stackoverflow.com/questions/14622421/how-to-change-legend-title-in-ggplot
#  a = a + ggtitle(paste("LC-MS/MS chromatograms for ", i, " experiments", sep=""))
#  a = a + xlab("Scan time") + ylab("total ion count (TIC)") + labs(color="Experiment No.")
#  #see http://ggplot2.tidyverse.org/reference/theme.html
#  a = a + theme_bw() + theme(legend.text = element_text(size = 20), legend.title=element_text(size=25),
#                         axis.title=element_text(size=25), legend.key.size = unit(0.8, "cm"),
#                         axis.text.x = element_text(size=20), axis.text.y = element_text(size=20),
#                         plot.title = element_text(size=25))
#  plot(a)
#  dev.off()
#}

###session info###
#sessionInfo()
```

***

Attributions

General attributions

Description	Link
Rmarkdown basics	http://rmarkdown.rstudio.com/authoring_basics.html
Rmarkdown format	http://rmarkdown.rstudio.com/markdown_document_format.html
In-line R code	http://rmarkdown.rstudio.com/lesson-4.html
Degree symbol	https://stackoverflow.com/questions/26234119/how-can-i-write-a-degree-symbol-in-rmarkdown2-for-html-and-pdf-output
Tables	https://stackoverflow.com/questions/19997242/simple-manual-rmarkdown-tables-that-look-good-in-html-pdf-and-docx
Tables	https://www.rstudio.com/wp-content/uploads/2015/03/rmarkdown-reference.pdf
Table dimensions	https://stackoverflow.com/questions/27219629/how-to-control-cell-width-in-pandoc-markdown-table
Rmarkdown themes	http://rmarkdown.rstudio.com/html_document_format.html
Rmarkdown image formatting	https://stackoverflow.com/questions/15625990/how-to-set-size-for-local-image-using-knitr-for-markdown
Image formatting	https://stackoverflow.com/questions/24677642/centering-image-and-text-in-r-markdown-for-a-pdf-report
css fonts	https://stackoverflow.com/questions/29274501/r-markdown-changing-font-size-and-font-type-in-html-output
css style	https://stackoverflow.com/questions/30446905/rmarkdown-font-size-and-header
css body/TOC modifications	https://rpubs.com/stevepowell99/floating-css
TOC	https://stackoverflow.com/questions/42546001/how-to-change-colors-and-attributes-of-table-of-contents-in-r-markdown-html-docu?rq=1
reshape	https://www.statmethods.net/management/reshape.html
ggrepel	https://cran.r-project.org/web/packages/ggrepel/vignettes/ggrepel.html
themes	http://ggplot2.tidyverse.org/reference/theme.html
geom_rect	https://stackoverflow.com/questions/4733182/how-to-highlight-time-ranges-on-a-plot
ggplot theme	https://rstudio-pubs-static.s3.amazonaws.com/3364_d1a578f521174152b46b19d0c83cbe7e.html
Stand alone error	https://github.com/rstudio/rmarkdown/issues/228

|Subsetting |http://adv-r.had.co.nz/Subsetting.html
|
|TIFF resolution |https://www.r-bloggers.com/high-resolution-figures-in-r/ & https://stat.ethz.ch/pipermail/r-help/2010-August/250893.html |

Additional attributions appear throughout this document. Citations, session information and package links appear below.

Session info
```{r sessioninfo}
sessionInfo()
```
Package links
Name	URL
gridExtra	https://CRAN.R-project.org/package=gridExtra
ggplot2	http://ggplot2.org
seqinr	https://cran.r-project.org/web/packages/seqinr/
alakazam	http://doi.org/10.1126/scitranslmed.3008879
sqldf	https://CRAN.R-project.org/package=sqldf
ggrepel	https://CRAN.R-project.org/package=ggrepel
VennDiagram	https://cran.r-project.org/web/packages/VennDiagram/index.html
stringr	https://cran.r-project.org/web/packages/stringr/index.html
reshape2	https://cran.r-project.org/web/packages/reshape2/
xcms	https://bioconductor.org/packages/release/bioc/html/xcms.html
Package citations
```{r citations}
citation("gridExtra")
citation("ggplot2")
citation("seqinr")
citation("alakazam")
citation("sqldf")
citation("ggrepel")
citation("VennDiagram")
citation("stringr")
citation("reshape2")
#citation("xcms")
```

References

1. R Core Team, R: A Language and Environment for Statistical Computing. R Foundation for Statistical Computing, Vienna, Austria. [Online] **2014**, http://www.R-project.org/ (accessed Feb 19, 2018).
2. Charif, D.; J. R. Lobry, SeqinR 1.0-2: A Contributed Package to the R Project for Statistical Computing Devoted to Biological Sequences Retrieval and Analysis. In *Structural Approaches to Sequence Evolution: Molecules, Networks, Populations*; Bastolla, U., Porto, M., Roman, H. E., Vendruscolo, M., Eds.; Springer: Berlin, Heildelberg, 2007; pp 207-232.

3. Gupta, N. T.; Vander Heiden, J. A.; Uduman, M.; Gadala-Maria, D.; Yaari, G.; Kleinstein, S. H., Change-O: A Toolkit for Analyzing Large-scale B Cell Immunoglobulin Repertoire Sequencing Data. *Bioinformatics* **2015**, *31*, 3356-3358.
4. Baptiste, A. gridExtra: Miscellaneous Functions for "Grid" Graphics. [Online] **2017**, https://CRAN.R-project.org/package=gridExtra, R-project (accessed Feb 19, 2018).
5. Chen, H. VennDiagram: Generate High-Resolution Venn and Euler Plots. [Online] **2017**, https://CRAN.R-project.org/package=VennDiagram, R-project (accessed Feb 19, 2018).
6. Wickham, H. ggplot2: Elegant Graphics for Data Analysis. [Online] **2009**, http://ggplot2.org, Springer-Verlag New York (accessed Feb 19, 2018).
7. Szklarczyk, D.; Franceschini, A.; Wyder, S.; Forslund, K.; Heller, D.; Huerta-Cepas, J.; Simonovic, M.; Roth, A.; Santos, A.; Tsafou, K. P.; Kuhn, M.; Bork, P.; Jensen, L. J.; von Mering, C., STRING v10: Protein-Protein Interaction Networks, Integrated over the Tree of Life. *Nucleic Acids Res.* **2015**, *45*, D447-D452.
8. Szklarczyk, D.; Morris, J. H.; Cook, H.; Kuhn, M.; Wyder, S.; Simonovic, M.; Santos, A.; Doncheva, N. T.; Roth, A.; Bork, P.; Jensen, L. J.; von Mering, C., The STRING Database in 2017: Quality-Controlled Protein–Protein Association Networks, Made Broadly Accessible. *Nucleic Acids Res.* **2017,** *43*, D362-D368.
9. Zheng, X.; Baker, H.; Hancock, W. S.; Fawaz, F.; McCaman, M.; Pungor, E., Jr., Proteomic Analysis for the Assessment of Different Lots of Fetal Bovine Serum as a Raw Material for Cell Culture. Part IV. Application of Proteomics to the Manufacture of Biological Drugs. *Biotechnol. Prog.* **2006,** *22,* 1294-1300.

Supporting Information

Star Polymers Reduce IAPP Toxicity via Accelerated Amyloid Aggregation

Emily H. Pilkington,[†] May Lai,[†] Xinwei Ge,[‡] William J. Stanley,[¶§] Bo Wang,[‡] Miaoyi Wang,[†] Aleksandr Kakinen,[†] Marc-Antonie Sani,[#] Michael R. Whittaker,[†] Esteban N. Gurzov,[¶§] Feng Ding,[‡] John F. Quinn,[†] Thomas P. Davis,[†∥*] and Pu Chun Ke[†*]*

[†]ARC Centre of Excellence in Convergent Bio-Nano Science and Technology, Monash Institute of Pharmaceutical Sciences, Monash University, 381 Royal Parade, Parkville, VIC 3052, Australia

[‡]Department of Physics and Astronomy, Clemson University, Clemson, SC 29634, USA

[¶]St Vincent's Institute of Medical Research, 9 Princes Street, Fitzroy, VIC 3065, Australia

[§]Department of Medicine, St. Vincent's Hospital, The University of Melbourne, Melbourne, Australia

[#]School of Chemistry, Bio21 Institute, The University of Melbourne, 30 Flemington Rd, Parkville, VIC 3010, Australia

[∥]Department of Chemistry, University of Warwick, Gibbet Hill, Coventry, CV4 7AL, United Kingdom

Table S1. Summary of PHEA homopolymers of various lengths.

Arm	[M]:[RAFT]:[I]	Conversion[a] (%)	M_n[b] (NMR)	M_n[c](th)	M_n (GPC)	PDI
PHEA 1	38:1:0.1	88	4373	4141	8276	1.30
PHEA 2	75:1:0.1	85	7728	7716	14688	1.18
PHEA 3	144:1:0.1	91	15961	15553	26676	1.24

[a] Conversion % was calculated using the following equation: $X = [1 - [(I_{5.9})/(I_{4.6\text{-}4.9})]] \times 100\%$

[b] M_n determined by NMR were calculated by the equation: $M_n = MW_{DBTC} + (N_{HEA} \times MW_{HEA})$ where repeating units of HEA (N_{HEA}) was calculated from the integrals of the two peak areas from 7.1-7.4 ppm and 4.6-4.9 ppm. $N_{HEA} = (I_{4.6\text{-}4.8} \times 5)/(I_{7.1\text{-}7.4})$

[c] Theoretical M_w was determine by the equation: $MW_{DBTC} + (\text{conversion}/100) \times (n_{HEA} / n_{DBTC}) \times MW_{HEA}$

Table S2. Summary of PHEA star formation of varying lengths of homopolymer and XL ratios with time points taken at 2, 6 12 and 24 h.

Entry	M_n homopolymer (^{1}H NMR)	M_n homopolymer β (GPC)	[P]:[M]:[X]	Time (h)	M_n Star β	PDI	Arm number 2* M_n star/M_n homopolymer
1	4373	8300	1:6:4	0		1.30	
1-4-2	4373	8300	1:6:4	2	11500	1.34	3
1-4-6	4373	8300	1:6:4	6	11500	1.34	3
1-4-12	4373	8300	1:6:4	12	13400	1.45	3
1-4-24	4373	8300	1:6:4	24	14800	1.49	4
1-4-24*	4373	8300	1:6:4	24	15600	1.51	4
1	4373	8300	1:6:8	0		1.30	
1-8-2	4373	8300	1:6:8	2	10200	1.28	2
1-8-6	4373	8300	1:6:8	6	18200	1.65	4
1-8-12	4373	8300	1:6:8	12	26500	1.70	6
1-8-24	4373	8300	1:6:8	24	31200	1.75	8
1-8-24*	4373	8300	1:6:8	24	40100	1.60	10
1	4373	8300	1:6:16	0		1.30	
1-16-2[†]	4373	8300	1:6:16	2	48300	1.92	12
2	7728	14700	1:12:4	0		1.24	
2-4-2	7728	14700	1:12:4	2	17400	1.32	2
2-4-6	7728	14700	1:12:4	6	17700	1.44	2
2-4-12	7728	14700	1:12:4	12	18600	1.46	3
2-4-24	7728	14700	1:12:4	24	18600	1.47	3
2-4-24*	7728	14700	1:12:4	24	18400	1.49	3
2	7728	14700	1:12:8	0		1.24	
2-8-2	7728	14700	1:12:8	2	23000	1.37	3
2-8-6	7728	14700	1:12:8	6	30400	1.53	4
2-8-12	7728	14700	1:12:8	12	33000	1.54	4
2-8-24	7728	14700	1:12:8	24	34200	1.56	5
2-8-24*	7728	14700	1:12:8	24	33738	1.54	5
2	7728	14700	1:12:16	0		1.24	

2-16-2	7728	14700	1:12:16	2	50200	1.69	7
2-16-6	7728	14700	1:12:16	6	70300	1.91	10
2-16-12	7728	14700	1:12:16	12	78400	1.92	11
2-16-24	**7728**	**14700**	**1:12:16**	**24**	**82200**	**1.94**	**11**
2-16-24*	7728	14700	1:12:16	24	82800	1.98	11
3	15961	26700	1:14:16	0		1.24	
3-16-2	15961	26700	1:14:16	2	52000	1.53	4
3-16-6	15961	26700	1:14:16	6	66000	1.62	5
3-16-12	15961	26700	1:14:16	12	66800	1.67	5
3-16-24	15961	26700	1:14:16	24	71500	1.65	5
3-16-24*	15961	26700	1:14:16	24	66800	1.67	5
3	15961	26700	1:14:24	0		1.24	
3-24-2	15961	26700	1:14:24	2	69700	1.78	5
3-24-6	15961	26700	1:14:24	6	102600	2.07	8
3-24-12	15961	26700	1:14:24	12	106000	2.16	8
3-24-24	15961	26700	1:14:24	24	116600	2.13	9
3-24-24*	15961	26700	1:14:24	24	110000	2.26	8
3	15961	26700	1:14:32	0		1.24	
3-32-2	15961	26700	1:14:32	2	123000	3.07	9
3-32-6	15961	26700	1:14:32	6	143600	3.73	11
3-32-12	15961	26700	1:14:32	12	160000	3.89	12
3-32-24	15961	26700	1:14:32	24	172000	3.88	13
3-32-24*	15961	26700	1:14:32	24	177900	4.24	13

* indicates an addition of 1.7, 0.86 and 0.45 mg of AIBN in 4373, 7728 and 15961 homopolymer reaction mixtures respectively after 12 h of polymerization.

† After 2h of polymerization mixture formed a gel.

β Value reported to nearest hundred

Entry **2-16-24** conditions were implemented on a larger scale.

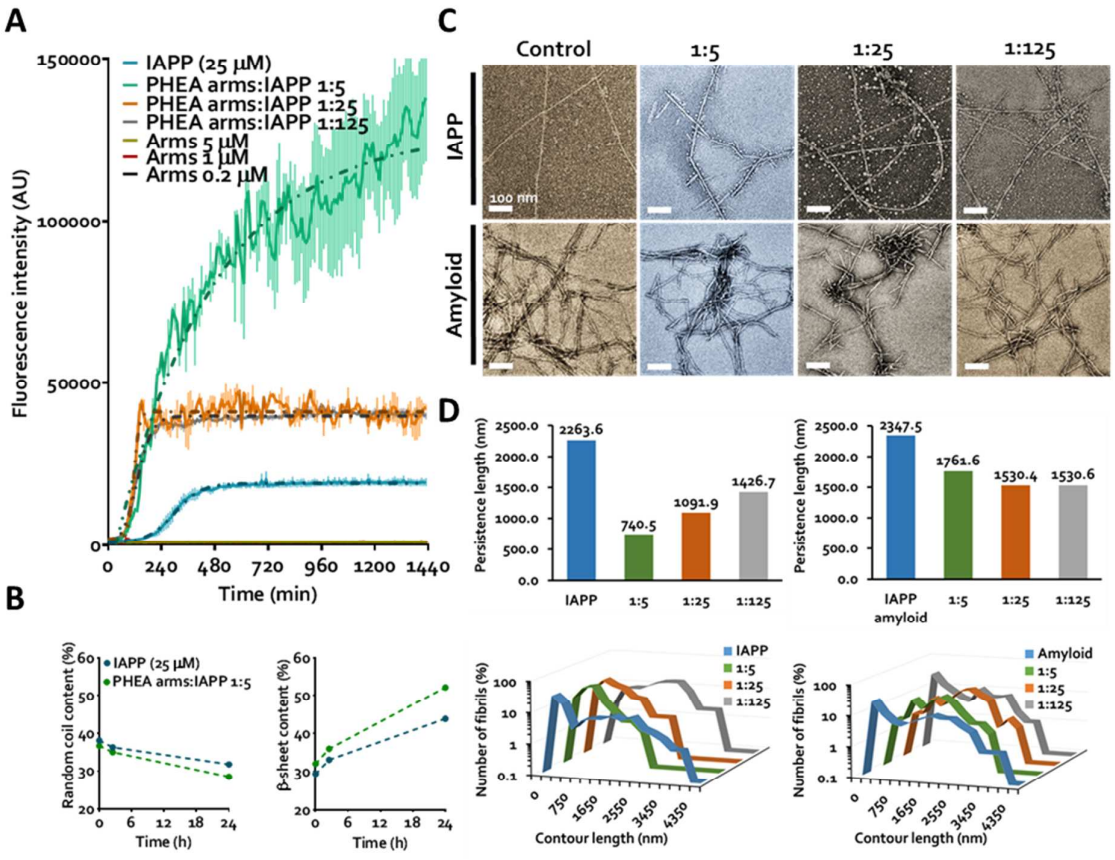

Figure S1. Promotion of IAPP fibrillization and remodeling of IAPP amyloids by PHEA arms. Concentration of IAPP in all experiments is 25 µM. (A) ThT fluorescence of IAPP in the presence of PHEA arms over 24 h. Dotted lines represent sigmoidal curve fitting (least squares fit), error is SEM. (B) Secondary structure transitions in IAPP mapped by CD spectroscopy at 0, 2.5 and 24 h time points. Lines are intended to guide the eye. (C) TEM imaging of fibrillating IAPP (IAPP) and mature IAPP amyloids (Amyloid) in the presence and absence of PHEA arms after 24 h incubation. Scale = 100 nm. (D) Structural analysis of amyloid fibrils visualized in (C).

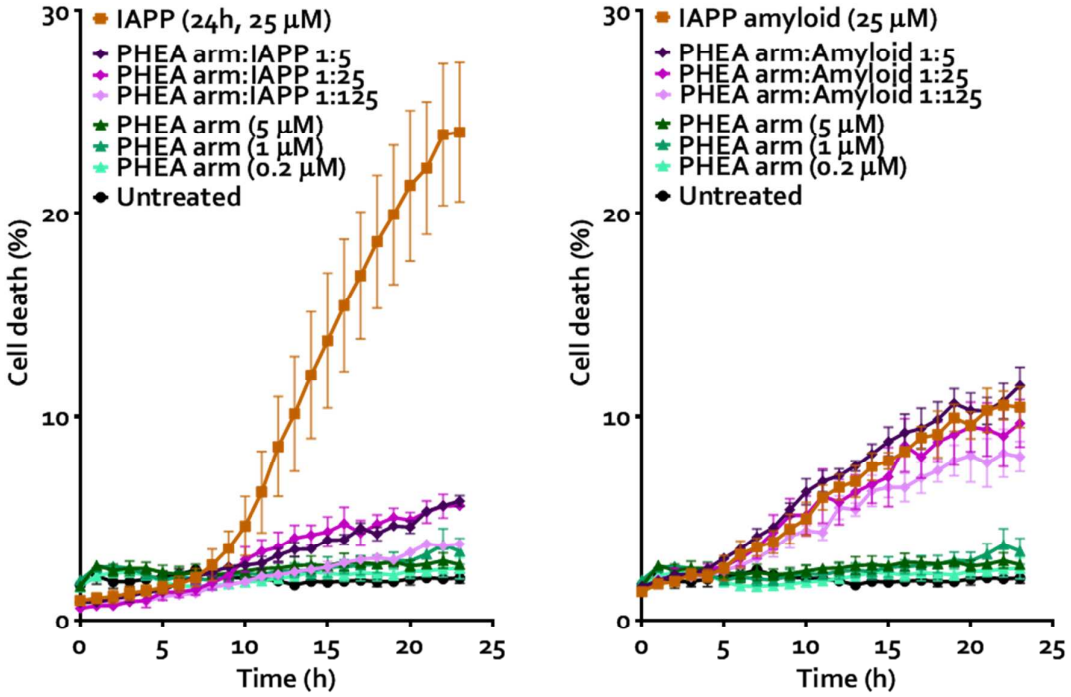

Figure S2. Protective effect of PHEA arms against IAPP-mediated cytotoxicity in βTC6 pancreatic β-cells.

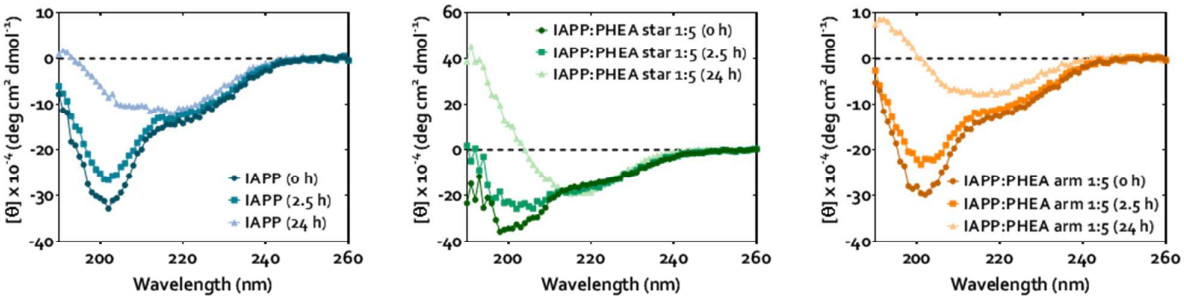

Figure S3. Normalized circular dichroism spectra of IAPP (25 µM) alone and in the presence of PHEA stars and arms after incubation in Milli-Q water at 0, 2.5 and 24 h.

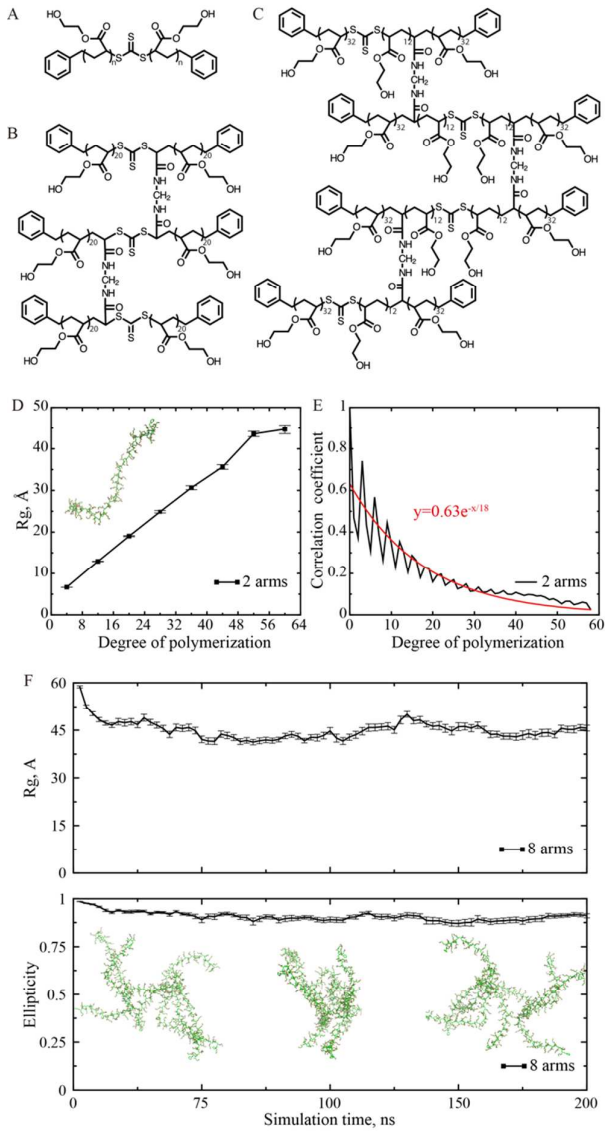

Figure S4. Simulations of various PHEA stars. (A-C) Chemical structures of the 2-arm, 6-arm, and 8-arm PHEA modelled in simulations. (D) The radius of gyration (*Rg*) of 2-arm PHEA increased approximately linearly with the degree of polymerization *n* (up to ~ 40), suggesting the polymers are rather rigid. (E) Autocorrelation analysis of 2-arm PHEAs. The exponential fitting returned a persistence length of n~18 (i.e., corresponding to a Kuhn length of ~36), which confirmed the rigidity of PHEA polymers. (F) Time evolution of Rg and ellipticity of an 8-arm PHEA model depicted in panel (C). The equilibrated *Rg* of ~ 45Å is consistent with the experimentally measured hydrodynamic diameter of ~ 9.8 nm in Fig. 1C. A high ellipticity value suggests that the 8-arm PHEA adopted a non-spherical conformation (e.g., an equilibrated snapshot with three different views in the inset). Error bars indicate s.e.

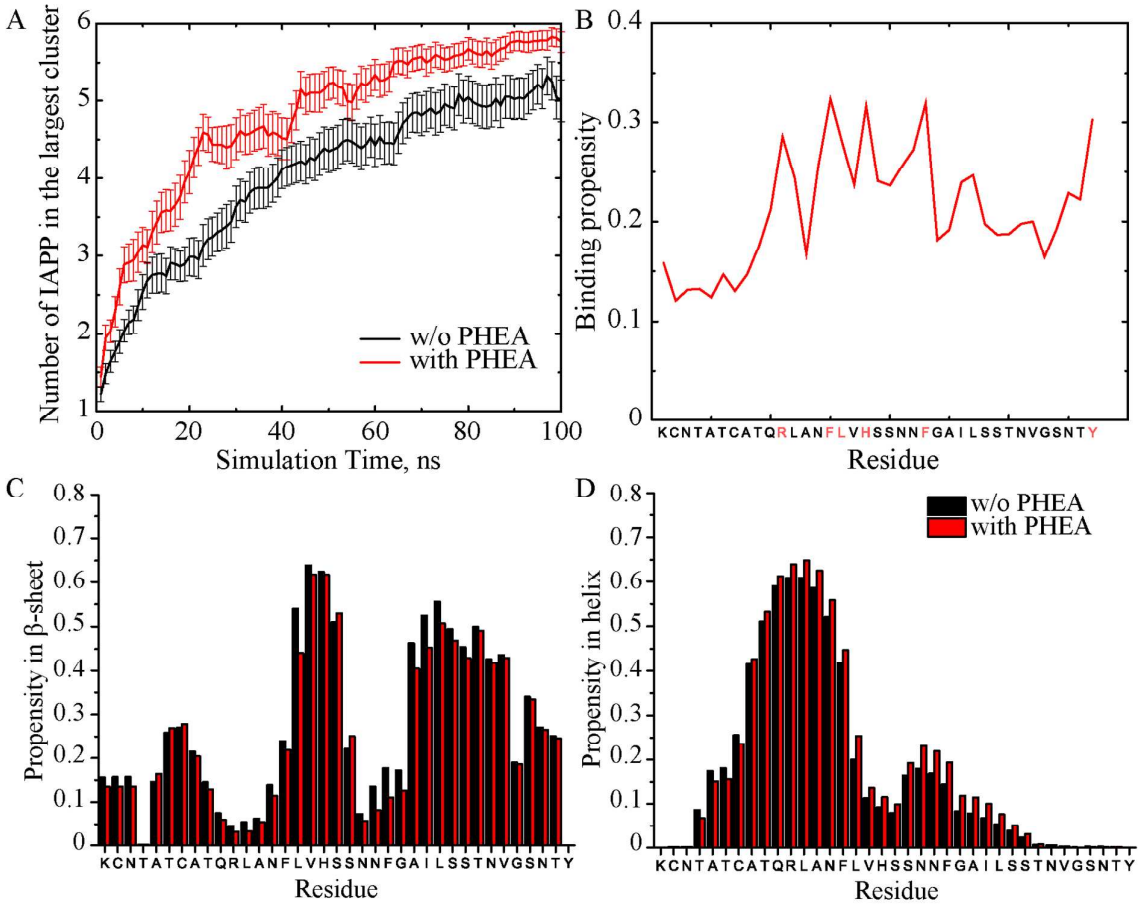

Figure S5. Binding of IAPP with a PHEA star in simulations. (A) Time evolution of the size of the largest IAPP aggregates in DMD simulations of 6 IAPPs with and w/o the presence of a 6-arm PHEA. Error bars indicate s.e. (B) Binding probability of each IAPP residue with PHEA. Residues with the highest binding probabilities are highlighted in red. (C&D) The secondary structure contents in terms of β-sheets and helices of the equilibrated IAPP residues, averaged for the last 25 ns of the DMD simulations.

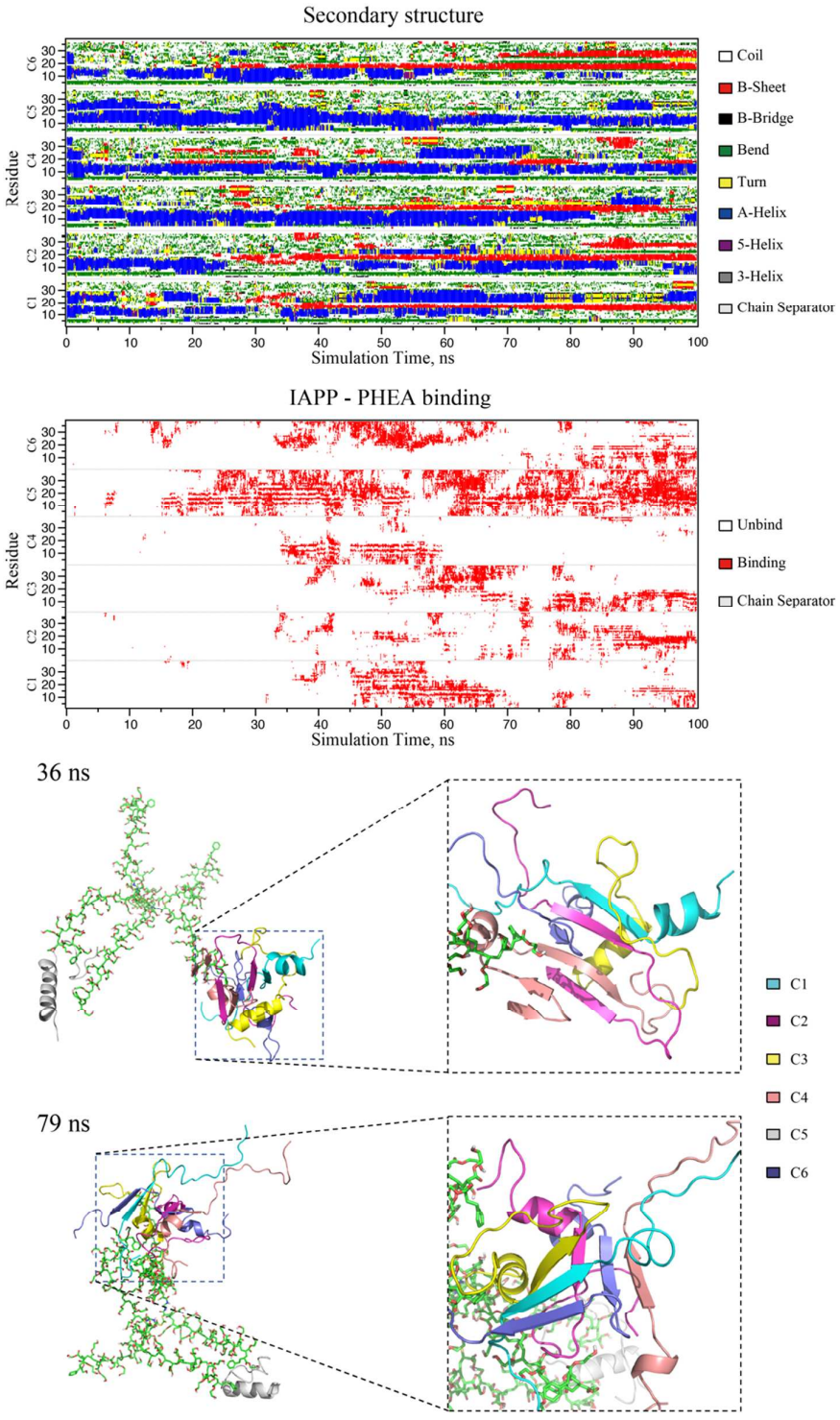

Figure S6. β-sheet formation in IAPP aggregates is correlated with their binding with PHEA. Secondary structure change of IAPP peptides (C1 ~ C6) is shown in the upper panel, while the PHEA-binding of each peptide is illustrated as red pixels in the bottom panel accordingly. Snapshots at the 36 ns and 79 ns are used to display the structure of the modeled system. It's noticeable that one of the peptides (C5) is not clustered in the IAPP aggregate.

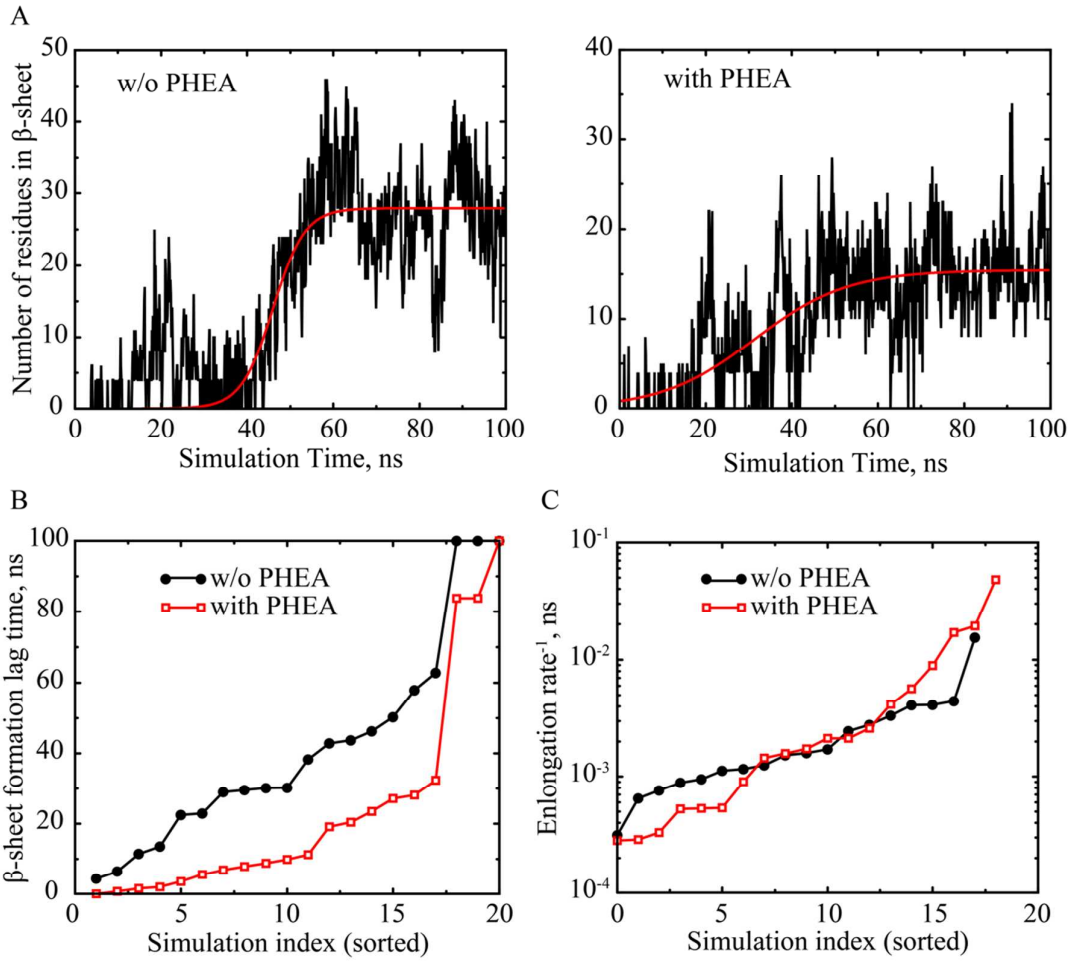

Figure S7. Binding with PHEA star reduced the aggregation lag time and induced the heterogeneity in the fibril elongation rate of IAPP self-association. (A) Time evolution of the total number of IAPP residues in β-sheet content with and w/o the presence of a 6-arm PHEA. (B-C) Distributions of the lag time and elongation rate of 20 independent simulations.

6.2. Complete Bibliography

Pertaining to a complete list of references cited in this thesis, ordered alphabetically. References herein are numbered only as a visual and navigational aid – as such, citation numbers in this bibliography do not correspond to in-text citations in thesis chapters.

(1) Abbott, A.; Dolgin, E., Leading Alzheimer's Theory Survives Drug Failure. *Nature* **2016,** *540*, 15-16.

(2) Abedini, A.; Cao, P.; Plesner, A.; He, M.; Derk, J.; Patil, S. A.; Rosario, R.; Lonier, J.; Song, F.; Koh, H.; Li, H.; Raleigh, D. P.; Schmidt, A. M., RAGE binds preamyloid IAPP intermediates and mediates pancreatic β cell proteotoxicity. *J. Clin. Invest.* **2018,** *128*, 682-698.

(3) Abedini, A.; Raleigh, D. P., The Role of His-18 in Amyloid Formation by Human Islet Amyloid Polypeptide. *Biochemistry* **2005,** *44*, 16284-16291.

(4) Adamcik, J.; Jung, J.-M.; Flakowski, J.; De Los Rios, P.; Dietler, G.; Mezzenga, R., Understanding amyloid aggregation by statistical analysis of atomic force microscopy images. *Nat. Nanotechnol.,* **2010,** 5, 423-428.

(5) Adamcik, J.; Mezzenga, R., Amyloid Polymorphism in the Protein Folding and Aggregation Energy Landscape. *Angew. Chem., Int. Ed. Engl.* **2018,** *57*, 8370-8382.

(6) Adler-Abramovich, L.; Vaks, L.; Carny, O.; Trudler, D.; Magno, A.; Caflisch, A.; Frenkel, D.; Gazit, E., Phenylalanine assembly into toxic fibrils suggests amyloid etiology in phenylketonuria. *Nat. Chem. Biol.* **2012,** *8*, 701-706.

(7) Aguilera, P.; Marcoleta, A.; Lobos-Ruiz, P.; Arranz, R.; Valpuesta, J. M.; Monasterio, O.; Lagos, R., Identification of Key Amino Acid Residues Modulating Intracellular and *In vitro* Microcin E492 Amyloid Formation. *Front. Microbiol.* **2016,** *7*, 35.

(8) Ahlschwede, K. M.; Curran, G. L.; Rosenberg, J. T.; Grant, S. C.; Sarkar, G.; Jenkins, R. B.; Ramakrishnan, S.; Poduslo, J. F.; Kandimalla, K. K., Cationic carrier peptide enhances cerebrovascular targeting of nanoparticles in Alzheimer's disease brain. *Nanomedicine* **2019,** *16*, 258-266.

(9) Akhavan, O.; Ghaderi, E.; Akhavan, A., Size-Dependent Genotoxicity of Graphene Nanoplatelets in Human Stem Cells. *Biomaterials* **2012,** *33*, 8017-8025.

(10) Akhavan, O.; Ghaderi, E.; Hashemi, E.; Akbari, E., Dose-Dependent Effects of Nanoscale Graphene Oxide on Reproduction Capability of Mammals. *Carbon* **2015,** *95*, 309-317.

(11) Alexandrescu, A. T., Amide Proton Solvent Protection in Amylin Fibrils Probed by Quenched Hydrogen Exchange NMR. *PLoS ONE* **2013,** *8*, No. e56467.

(12) Alexis, F.; Pridgen, E.; Molnar, L. K.; Farokhzad, O. C., Factors Affecting the Clearance and Biodistribution of Polymeric Nanoparticles. *Mol. Pharmaceutics* **2008,** *5*, 505-515.

(13) Al-Garawi, Z. S.; McIntosh, B. A.; Neill-Hall, D.; Hatimy, A. A.; Sweet, S. M.; Bagley, M. C.; Serpell, L. C., The Amyloid Architecture Provides a Scaffold for Enzyme-Like Catalysts. *Nanoscale* **2017,** *9*, 10773-10783.

(14) Allaire, J. J.; Xie, Y.; McPherson, J.; Luraschi, J.; Ushey, K.; Atkins, A.; Wickham, H.; Cheng, J.; Chang, W. Rmarkdown: Dynamic Documents for R. https://CRAN.R-project.org/package=rmarkdown (accessed Feb 19, 2018).

(15) Altieri, F.; Di Stadio, C. S.; Severino, V.; Sandomenico, A.; Minopoli, G.; Miselli, G.; Di Maro, A.; Ruvo, M.; Chambery, A.; Quagliariello, V.; Masullo, M.; Rippa, E.; Arcari, P., Anti-amyloidogenic property of human gastrokine 1. *Biochimie* **2014,** *106*, 91-100.

(16) Andreetto, E.; Yan, L.-M.; Tatarek-Nossol, M.; Velkova, A.; Frank, R.; Kapurniotu, A., Identification of Hot Regions of the Aβ–IAPP Interaction Interface as High-Affinity Binding Sites in both Cross- and Self-Association. *Angew. Chem. Int. Ed., Engl.* **2010,** *49*, 3081-3085.

(17) Arimon, M.; Grimminger, V.; Sanz, F.; Lashuel, H. A., Hsp104 Targets Multiple Intermediates on the Amyloid Pathway and Suppresses the Seeding Capacity of Aβ Fibrils and Protofibrils. *J. Mol. Biol.* **2008,** *384*, 1157-1173.

(18) Arya, S.; Kumari, A.; Dalal, V.; Bhattacharya, M.; Mukhopadhyay, S., Appearance of annular ring-like intermediates during amyloid fibril formation from human serum albumin. *Phys. Chem. Chem. Phys.* **2015,** *17*, 22862-22871.

(19) Aso, E.; Martinsson, I.; Appelhans, D.; Effenberg, C.; Benseny-Cases, N.; Cladera, J. C.; Gouras, G.; Ferrer, I.; Klementieva, O., Poly(propylene imine) dendrimers with histidine-maltose shell as novel type of nanoparticles for synapse and memory protection. *Nanomedicine* **2019,** *17*, 198-209.

(20) Audas, T. E.; Audas, D. E.; Jacob, M. D.; Ho, J. J. D.; Khacho, M.; Wang, M.; Perera, J. K.; Gardiner, C.; Bennett, C. A.; Head, T.; Kryvenko, O. N.; Jorda, M.; Daunert, S.; Malhotra, A.; Trinkle-Mulcahy, L.; Gonzalgo, M. L.; Lee, S., Adaptation to Stressors by Systemic Protein Amyloidogenesis. *Dev. Cell* **2016,** *39*, 155-168.

(21) Auluck, P. K.; Chan, H. Y. E.; Trojanowski, J. Q.; Lee, V. M. Y.; Bonini, N. M., Chaperone Suppression of α-Synuclein Toxicity in a Drosophila Model for Parkinson's Disease. *Science* **2002,** *295*, 865-868.

(22) Avramovich-Tirosh, Y.; Amit, T.; Bar-Am, O.; Weinreb, O.; Youdim, M. B. H., Physiological and pathological aspects of Abeta in iron homeostasis via 5'UTR in the APP mRNA and the therapeutic use of iron-chelators. *BMC Neurosci.* **2008,** *9 (Suppl 2)*, S2.

(23) Babych, M.; Bertheau-Mailhot, G.; Zottig, X.; Dion, J.; Gauthier, L.; Archambault, D.; Bourgault, S., Engineering and evaluation of amyloid assemblies as a nanovaccine against the Chikungunya virus. *Nanoscale* **2018,** *10*, 19547-19556.

(24) Badman, M. K.; Pryce, R. A.; Chargé, S. B. P.; Morris, J. F.; Clark, A., Fibrillar islet amyloid polypeptide (amylin) is internalised by macrophages but resists proteolytic degradation. *Cell Tissue Res.* **1998,** *291*, 285-294.

(25) Bag, N.; Ali, A.; Chauhan, V. S.; Wohland, T.; Mishra, A., Membrane destabilisation by monomeric hIAPP observed by imaging fluorescence correlation spectroscopy. *Chem. Commun.* **2013,** *49*, 9155-9157.

(26) Ban, D. K.; Paul, S., Nano Zinc Oxide Inhibits Fibrillar Growth and Suppresses Cellular Toxicity of Lysozyme Amyloid. *ACS Appl. Mater. Interfaces* **2016,** *8*, 31587-31601.

(27) Baptiste, A. gridExtra: Miscellaneous Functions for "Grid" Graphics. https://CRAN.R-project.org/package=gridExtra.

(28) Barrajón-Catalán, E.; Herranz-López, M.; Joven, J.; Segura-Carretero, A.; Alonso-Villaverde, C.; Menéndez, J. A.; Micol, V., Molecular Promiscuity of Plant Polyphenols in the Management of Age-Related Diseases: Far Beyond Their Antioxidant Properties. *Adv. Exp. Med. Biol.* **2014,** *824*, 141-159.

(29) Bartlett, A. I.; Radford, S. E., An expanding arsenal of experimental methods yields an explosion of insights into protein folding mechanisms. *Nat. Struc. Mol. Biol.* **2009,** *16*, 582-588.

(30) Barton, S. M.; Janve, V. A.; McClure, R.; Anderson, A.; Matsubara, J. A.; Gore, J. C.; Pham, W., Lipopolysaccharide Induced Opening of the Blood Brain Barrier on Aging 5XFAD Mouse Model. *J. Alzheimers Dis.* **2019,** *67*, 503-513.

(31) Bauer, P. O.; Goswami, A.; Wong, H. K.; Kurosawa, M.; Yamada, M.; Miyazaki, H.; Matsumoto, G.; Kino, Y.; Nagai, Y.; Nukina, N., Harnessing chaperone-mediated autophagy for the selective degradation of mutant huntingtin protein. *Nat. Biotechnol.* **2010,** *28*, 256-263.

(32) Bellomo, G.; Bologna, S.; Gonnelli, L.; Ravera, E.; Fragai, M.; Lelli, M.; Luchinat, C., Aggregation kinetics of the Aβ1–40 peptide monitored by NMR. *Chem. Commun.* **2018,** *54*, 7601-7604.

(33) Benseny-Cases, N.; Klementieva, O.; Cladera, J., Dendrimers antiamyloidogenic potential in neurodegenerative diseases. *New J. Chem.* **2012,** 36, 211-216.

(34) Bergmann, S. R.; Ferguson, T. B.; Sobel, B. E., Effects of amphiphiles on erythrocytes, coronary arteries, and perfused hearts. *Am. J. Physiol.* **1981,** *240*, H229-H237.

(35) Bertrand, N.; Grenier, P.; Mahmoudi, M.; Lima, E. M.; Appel, E. A.; Dormont, F.; Lim, J.-M.; Karnik, R.; Langer, R.; Farokhzad, O. C., Mechanistic Understanding of *In Vivo* Protein Corona Formation on Polymeric Nanoparticles and Impact on Pharmacokinetics. *Nat. Commun.* **2017,** *8*, No. 777.

(36) Betsholtz, C.; Christmansson, L.; Engström, U.; Rorsman, F.; Svensson, V.; Johnson, K. H.; Westermark, P., Sequence divergence in a specific region of islet amyloid polypeptide (IAPP) explains differences in islet amyloid formation between species. *FEBS Lett.* **1989,** *251*, 261-264.

(37) Bieschke, J.; Herbst, M.; Wiglenda, M.; Friedrich, R. P.; Boeddrich, A.; Schiele, F.; Kleckers, D.; del Amo, J. M. L.; Grüning, B. A.; Wang, Q.; Schmidt, M. R.; Lurz, R.; Anwyl, R.; Schnoegl, S.; Fändrich, M.; Frank, R. F.; Reif, B.; Günther, S.; Walsh, D. M.; Wanker, E. E., Small-molecule conversion of toxic oligomers to nontoxic β-sheet–rich amyloid fibrils. *Nat. Chem. Biol.* **2011,** *8*, 93-101.

(38) Bieschke, J.; Russ, J.; Friedrich, R. P.; Ehrnhoefer, D. E.; Wobst, H.; Neugebauer, K.; Wanker, E. E., EGCG remodels mature α-synuclein and amyloid-β fibrils and reduces cellular toxicity. *Proc. Natl. Acad. Sci. U.S.A.* **2010,** *107*, 7710-7715.

(39) Bilia, A. R.; Nardiello, P.; Piazzini, V.; Leri, M.; Bergonzi, M. C.; Bucciantini, M.; Casamenti, F., Successful Brain Delivery of Andrographolide Loaded in Human Albumin Nanoparticles to TgCRND8 Mice, an Alzheimer's Disease Mouse Model. *Front. Pharmacol.* **2019,** *10*, 910.

(40) Birol, M.; Kumar, S.; Rhoades, E.; Miranker, A. D., Conformational switching within dynamic oligomers underpins toxic gain-of-function by diabetes-associated amyloid. *Nat. Commun.* **2018,** *9*, 1312.

(41) Blanco, L. P.; Evans, M. L.; Smith, D. R.; Badtke, M. P.; Chapman, M. R., Diversity, Biogenesis and Function of Microbial Amyloids. *Trends Microbiol.* **2012,** *20*, 66-73.

(42) Bobylev, A. G.; Kraevaya, O. A.; Bobyleva, L. G.; Khakina, E. A.; Fadeev, R. S.; Zhilenkov, A. V.; Mishchenko, D. V.; Penkov, N. V.; Teplov, I. Y.; Yakupova, E. I.; Vikhlyantsev, I. M.; Troshin, P. A., Anti-amyloid activities of three different types of water-soluble fullerene derivatives. *Colloids Surf. B Biointerfaces* **2019,** *183*, 110426.

(43) Bolisetty, S.; Harnau, L.; Jung, J.; Mezzenga, R., Gelation, Phase Behavior, and Dynamics of *β*-Lactoglobulin Amyloid Fibrils at Varying Concentrations and Ionic Strengths. *Biomacromolecules* **2012,** *13*, 3241-3252.

(44) Bolisetty, S.; Mezzenga, R., Amyloid-carbon hybrid membranes for universal water purification. *Nat. Nanotechnol.* **2016,** *11*, 365-372.

(45) Bongiovanni, M. N.; Aprile, F. A.; Sormanni, P.; Vendruscolo, M., A Rationally Designed Hsp70 Variant Rescues the Aggregation-Associated Toxicity of Human IAPP in Cultured Pancreatic Islet β-Cells. *Int. J. Mol. Sci.* **2018,** *19*, 1443.

(46) Borchi, E.; Bargelli, V.; Guidotti, V.; Berti, A.; Stefani, M.; Nediani, C.; Rigacci, S., Mild exposure of RIN-5F β-cells to human islet amyloid polypeptide aggregates upregulates antioxidant enzymes via NADPH oxidase-RAGE: An hormetic stimulus. *Redox Biol.* **2014,** *2*, 114-122.

(47) Brender, J. R.; Hartman, K.; Nanga, R. P. R.; Popovych, N.; de la Salud Bea, R.; Vivekanandan, S.; Marsh, E. N. G.; Ramamoorthy, A., Role of Zinc in Human Islet Amyloid Polypeptide Aggregation. *J. Am. Chem. Soc.* **2010,** *132*, 8973-8983.

(48) Breydo, L.; Newland, B.; Zhang, H.; Rosser, A.; Werner, C.; Uversky, V. N.; Wang, W., A hyperbranched dopamine-containing PEG-based polymer for the inhibition of α-synuclein fibrillation. *Biochem. Biophys. Res. Commun.* **2016,** *469*, 830-835.

(49) Bruno, E.; Pereira, C.; Roman, K. P.; Takiguchi, M.; Kao, P.-Y.; Nogaj, L. A.; Moffet, D. A., IAPP aggregation and cellular toxicity are inhibited by 1,2,3,4,6-penta-O-galloyl-β-$_D$-glucose. *Amyloid* **2013,** *20*, 34-38.

(50) Cabaleiro-Lago, C.; Lynch, I.; Dawson, K. A.; Linse, S., Inhibition of IAPP and IAPP$_{(20-29)}$ Fibrillation by Polymeric Nanoparticles. *Langmuir* **2009,** *26*, 3453-3461.

(51) Cabaleiro-Lago, C.; Quinlan-Pluck, F.; Lynch, I.; Lindman, S.; Minogue, A. M.; Thulin, E.; Walsh, D. M.; Dawson, K. A.; Linse, S., Inhibition of Amyloid β Protein Fibrillation by Polymeric Nanoparticles. *J. Am. Chem. Soc.* **2008,** *130*, 15437-15443.

(52) Cadavez, L.; Montane, J.; Alzarraz-Vizán, G.; Visa, M.; Vidal-Fàbrega, L.; Servitja, M.; Novials, A., Chaperones Ameliorate Beta Cell Dysfunction Associated with Human Islet Amyloid Polypeptide Overexpression. *PLoS ONE* **2014,** *9*, e101797.

(53) Camargo, D. C. R.; Garg, D.; Buday, K.; Franko, A.; Camargo, A. R.; Schmidt, F.; Cox, S. J.; Suladze, S.; Haslbeck, M.; Mideksa, Y. G.; Gemmecker, G.; Aichler, M.; Mettenleiter, G.; Schulz, M.; Walch, A. K.; de Angelis, M. H.; Feige, M. J.; Sierra, C. A.; Conrad, M.; Tripsianes, K.; Ramamoorthy, A.; Reif, B., hIAPP forms toxic oligomers in plasma. *Chem. Commun.* **2018,** *54*, 5426-5429.

(54) Cano, A.; Ettcheto, M.; Chang, J.-H.; Barroso, E.; Espina, M.; Kühne, B. A.; Barenys, M.; Auladell, C.; Folch, J.; Souto, E. B.; Camins, A.; Turowski, P.; García, M. L., Dual-drug loaded nanoparticles of Epigallocatechin-3-gallate (EGCG)/Ascorbic acid enhance therapeutic efficacy of EGCG in a APPswe/PS1dE9 Alzheimer's disease mice model. *J. Control. Release* **2019,** *301*, 62-75.

(55) Cao, P.; Abedini, A.; Wang, H.; Tu, L.-T.; Zhang, X.; Schmidt, A. M.; Raleigh, D. P., Islet amyloid polypeptide toxicity and membrane interactions. *Proc. Natl. Acad. Sci. USA* **2013,** *110*, 19279-19284.

(56) Cao, P.; Raleigh, D. P., Analysis of the Inhibition and Remodeling of Islet Amyloid Polypeptide Amyloid Fibers by Flavanols. *Biochemistry* **2012,** *51*, 2670-2683.

(57) Carrotta, R.; Canale, C.; Diaspro, A.; Trapani, A.; Biagio, P. L. S.; Bulone, D., Inhibiting effect of α(s1)-casein on Aβ(1-40) fibrillogenesis. *Biochim. Biophys. Acta* **2012,** *1820*, 124-132.

(58) Casas, S.; Gomis, R.; Gribble, F. M.; Altirriba, J.; Knuutila, S.; Novials, A., Impairment of the Ubiquitin-Proteasome Pathway is a Downstream Endoplasmic Reticulum Stress Response Induced by Extracellular Human Islet Amyloid Polypeptide and Contributes to Pancreatic β-cell Apoptosis. *Diabetes* **2007,** *56*, 2284-2294.

(59) Cedervall, T.; Lynch, I.; Lindman, S.; Berggård, T.; Thulin, E.; Nilsson, H.; Dawson, K. A.; Linse, S., Understanding the Nanoparticle-Protein Corona Using Methods to Quantify Exchange Rates and Affinities of Proteins for Nanoparticles. *Proc. Natl. Acad. Sci. U.S.A.* **2007,** *104*, 2050-2055.

(60) Chargé, S. B. P.; Esiri, M. M.; Bethune, C. A.; Hansen, B. C.; Clark, A., Apolipoprotein E is Associated With Islet Amyloid and Other Amyloidoses: Implications for Alzheimer's Disease. *J. Pathol.* **1996,** *179*, 443-447.

(61) Charif, D.; Lobry, J. R., SeqinR 1.0-2: a contributed package to the R project for statistical computing devoted to biological sequences retrieval and analysis. In *Structural approaches to sequence evolution: Molecules, networks, populations*, Bastolla, U.; Porto, M.; Roman, H. E.; Vendruscolo, M., Eds. Springer Verlag: New York, 2007.

(62) Chen, H. VennDiagram: Generate High-Resolution Venn and Euler Plots. https://CRAN.R-project.org/package=VennDiagram.

(63) Chen, J.; Armstrong, A. H.; Koehler, A. N.; Hecht, M. H., Small Molecule Microarrays Enable the Discovery of Compounds that Bind the Alzheimer's Aβ Peptide and Reduce its Cytotoxicity. *J. Am. Chem. Soc.* **2010,** *132*, 17015-17022.

(64) Chen, L.; Wei, Y.; Wang, X.; He, R., d-Ribosylated Tau forms globular aggregates with high cytotoxicity. *Cell. Mol. Life Sci.* **2009,** *66*, 2559-2571.

(65) Chen, L.; Wei, Y.; Wang, X.; He, R., Ribosylation Rapidly Induces α-Synuclein to Form Highly Cytotoxic Molten Globules of Advanced Glycation End Products. *PLoS ONE* **2010,** *5*, e9052.

(66) Chen, S. W.; Drakulic, S.; Deas, E.; Ouberai, M.; Aprile, F. A.; Arranz, R.; Ness, S.; Roodveldt, C.; Guilliams, T.; De-Genst, E. J.; Klenerman, D.; Wood, N. W.; Knowles, T. P. J.; Alfonso, C.; Ricas, G.; Abramov, A. Y.; Valpuesta, J. M.; Dobson, C. M.; Cremades, N., Structural characterization of toxic oligomers that are kinetically trapped during α-synuclein fibril formation. *Proc. Natl. Acad. Sci. U.S.A.* **2015,** *112*, E1194-E2003.

(67) Cheng, C.-H.; Lin, K.-J.; Hong, C.-T.; Wu, D.; Chang, H.-M.; Liu, C.-H.; Hsiao, I.-T.; Yang, C.-P.; Liu, Y.-C.; Hu, C.-J., Plasmon-Activated Water Reduces Amyloid Burden and Improves Memory in Animals with Alzheimer's Disease. *Sci. Rep.* **2019,** *9*, 13252.

(68) Cheng, I. H.; Scearce-Levie, K.; Legleiter, J.; Palop, J. J.; Gerstein, H.; Bien-Ly, N.; Puoliväli, J.; Lesné, S.; Ashe, K. H.; Muchowski, P. J.; Mucke, L., Accelerating Amyloid-β Fibrillization Reduces Oligomer Levels and Functional Deficits in Alzheimer Disease Mouse Models. *J. Biol. Chem.* **2007,** 282, 23818-23828.

(69) Chien, V.; Aitken, J. F.; Zhang, S.; Buchanan, C. E.; Hickey, A.; Brittain, T.; Cooper, G. J.; Loomes, K. M., The chaperone proteins HSP70, HSP40/DnaJ and GRP78/BiP suppress misfolding and formation of β-sheet-containing aggregates by human amylin: a potential role for defective chaperone biology in Type 2 diabetes. *Biochem. J.* **2010,** *432*, 113-121.

(70) Chimienti, F.; Favier, A.; Seve, M., ZnT-8, a pancreatic beta-cell-specific zinc transporter. *BioMetals* **2005,** *18*, 313-317.

(71) Chiti, F.; Calamai, M.; Taddei, N.; Stefani, M.; Ramponi, G.; Dobson, C. M., Studies of the aggregation of mutant proteins *in vitro* provide insights into the genetics of amyloid diseases. *Proc. Natl. Acad. Sci. U.S.A.* **2002,** *99*, 16419-16426.

(72) Chiti, F.; Dobson, C. M., Protein Misfolding, Functional Amyloid, and Human Disease. *Annu. Rev. Biochem.* **2006,** *75*, 333-366.

(73) Choi, S. H.; Kim, Y. H.; Hebisch, M.; Sliwinski, C.; Lee, S.; D'Avanzo, C.; Chen, H.; Hooli, B.; Asselin, C.; Muffat, J.; Klee, J. B.; Zhang, C.; Wainger, B. J.; Peitz, M.; Kovacs, D. M.; Woolf, C. J.; Wagner, S. L.; Tanzi, R. E.; Kim, D. Y., A three-dimensional human neural cell culture model of Alzheimer's disease. *Nature* **2014,** *515*, 274-278.

(74) Choi, S. H.; Kim, Y. H.; Quinti, L.; Tanzi, R. E.; Kim, D. Y., 3D culture models of Alzheimer's disease: a road map to a "cure-in-a-dish". *Mol. Neurodegener.* **2016,** *11*, 75.

(75) Chowdhury, S. R.; Agarwal, M.; Meher, N.; Muthuraj, B.; Iyer, P. K., Modulation of Amyloid Aggregates into Nontoxic Coaggregates by Hydroxyquinoline Appended Polyfluorene. *ACS Appl. Mater. Interfaces* **2016,** *8*, 13309-13319.

(76) Clinton, L. K.; Blurton-Jones, M.; Myczek, K.; Trojanowski, J. Q.; LaFerla, F. M., Synergistic Interactions between Aβ, Tau, and α-Synuclein: Acceleration of Neuropathology and Cognitive Decline. *J. Neurosci.* **2010,** *30*, 7281-7289.

(77) Cox, D.; Selig, E.; Griffin, M. D. W.; Carver, J. A.; Ecroyd, H., Small Heat-shock Proteins Prevent α-Synuclein Aggregation via Transient Interactions and Their Efficacy Is Affected by the Rate of Aggregation. *J. Biol. Chem.* **2016,** *291*, 22618-22629.

(78) Cox, J.; Mann, M., MaxQuant Enables High Peptide Identification Rates, Individualized P.P.B.-Range Mass Accuracies and Proteome-Wide Protein Quantification. *Nat. Biotechnol.* **2008,** *26*, 1367-1372.

(79) De Baets, G.; Reumers, J.; Blanco, J. D.; Dopazo, J.; Schymkowitz, J.; Rousseau, F., An Evolutionary Trade-Off between Protein Turnover Rate and Protein Aggregation Favors a Higher Aggregation Propensity in Fast Degrading Proteins. *PLoS Comput. Biol.* **2011,** *7*, e1002090.

(80) De Baets, G.; Van Doorn, L.; Rousseau, F.; Shymkowitz, J., Increased Aggregation Is More Frequently Associated to Human Disease-Associated Mutations Than to Neutral Polymorphisms. *PLoS Comput. Biol.* **2015,** *11*, e1004374.

(81) Debnath, K.; Shekhar, S.; Kumar, V.; Jana, N. R.; Jana, N. R., Efficient Inhibition of Protein Aggregation, Disintegration of Aggregates, and Lowering of Cytotoxicity by Green Tea Polyphenol-Based Self-Assembled Polymer Nanoparticles. *ACS Appl. Mater. Interfaces* **2016,** *8*, 20309-20318.

(82) Despa, S.; Margulies, K. B.; Chen, L.; Knowlton, A. A.; Havel, P. J.; Taegtmeyer, H.; Bers, D. M.; Despa, F., Hyperamylinemia Contributes to Cardiac Dysfunction in Obesity and Diabetes: A Study in Humans and Rats. *Circ. Res.* **2012,** *110*, 598-608.

(83) Despa, S.; Margulies, K. B.; Chen, L.; Knowlton, A. A.; Havel, P. J.; Taegtmeyer, H.; Bers, D. M.; Despa, F., Hyperamylinemia Contributes to Cardiac Dysfunction in Obesity and Diabetes: A Study in Humans and Rats. *Circ. Res.* **2012,** *110*, 598-608.

(84) D'Este, L.; Wimalawansa, S. J.; Renda, T. G., Distribution of Amylin-Immunoreactive Neurons in the Monkey Hypothalamus and their Relationships with the Histaminergic System. *Arch. Histol. Cytol.* **2001,** *64*, 295-303.

(85) DeToma, A. S.; Salamekh, S.; Ramamoorthy, A.; Lim, M. H., Misfolded Proteins in Alzheimer's Disease and Type II Diabetes. *Chem. Soc. Rev.* **2012,** *41*, 608-621.

(86) Dikic, I.; Elazar, Z., Mechanism and medical implications of mammalian autophagy. *Nat. Rev. Mol. Cell Biol.* **2018,** *19*, 349-364.

(87) Ding, F.; Dokholyan, N., Emergence of Protein Fold Families through Rational Design. *PLoS Comput. Biol.,* **2006,** 2, e85.

(88) Ding, F.; Dokholyan, N., Incorporating Backbone Flexibility in MedusaDock Improves Ligand-Binding Pose Prediction in the CSAR2011 Docking Benchmark. *J. Chem. Inf. Model.,* **2013,** 53, 1871-1879.

(89) Ding, F.; Radic, S.; Chen, R.; Chen, P.; Geitner, N. K.; Brown, J. M.; Ke, P. C., Direct observation of a single nanoparticle-ubiquitin corona formation. *Nanoscale* **2013,** *5*, 9162-9169.

(90) Ding, F.; Tsao, D.; Nie, H.; Dokholyan, N. V., Ab initio folding of proteins with all-atom discrete molecular dynamics. *Structure*, **2008,** 16, 1010-1018.

(91) Dobson, C. M., Principles of protein folding, misfolding and aggregation. *Semin. Cell Dev. Biol.* **2004,** *15*, 3-16.

(92) Docter, D.; Westmeier, D.; Markiewicz, M.; Stolte, S.; Knauer, S. K.; Stauber, R. H., The Nanoparticle Biomolecule Corona: Lessons Learned – Challenge Accepted? *Chem. Soc. Rev.* **2015,** *44*, 6094-6121.

(93) Dodart, J.-C.; Bales, K. R.; Paul, S. M., Immunotherapy for Alzheimer's disease: will vaccination work? *Trends Mol. Med.* **2003,** *9*, 85-87.

(94) Dominy, S. S.; Lynch, C.; Ermini, F.; Benedyk, M.; Marczyk, A.; Konradi, A.; Nguyen, M.; Haditsch, U.; Raha, D.; Griffin, C.; Holsinger, L. J.; Arastu-Kapur, S.; Kaba, S.; Lee, A.; Ryder, M. I.; Potempa, B.; Mydel, P.; Hellvard, A.; Adamowicz, K.; Hasturk, H.; Walker, G. D.; Reynolds, E. C.; Faull, R. L. M.; Curtis, M. A.; Dragunow, M.; Potempa, J., *Porphyromonas gingivalis* in Alzheimer's disease brains: Evidence for disease causation and treatment with small-molecule inhibitors. *Sci. Adv.* **2019,** *5*, eaau3333.

(95) Dong, X.; Svantesson, T.; Sholts, S. B.; Wallin, C.; Jarvet, J.; Gräslund, A.; Wärmländer, S. K. T. S., Copper ions induce dityrosine-linked dimers in human but not in murine islet amyloid polypeptide (IAPP/amylin). *Biochem. Biophys. Res. Communs.* **2019,** *510*, 520-524.

(96) Dowding, J. M.; Song, W.; Bossy, K.; Karakoti, A.; Kumar, A.; Kim, A.; Bossy, B.; Seal, S.; Ellisman, M. H.; Perkins, G.; Self, W. T.; Bossy-Wetzel, E., Cerium oxide nanoparticles protect against Aβ-induced mitochondrial fragmentation and neuronal cell death. *Cell Death Differ.* **2014,** *21*, 1622-1632.

(97) Drummond, E.; Wisniewski, T., Alzheimer's disease: experimental models and reality. *Acta Neuropathol.* **2017,** *133*, 155-175.

(98) Du, Z.; Gao, N.; Guan, Y.; Ding, C.; Sun, Y.; Ren, J.; Qu, X., Rational Design of a "Sense and Treat" System to Target Amyloid Aggregates Related to Alzheimer's Disease. *Nano Res.* **2018,** *11*, 1987-1997.

(99) Duan, M.; Fan, J.; Huo, S., Conformations of islet amyloid polypeptide monomers in a membrane environment: implications for fibril formation. *PLoS ONE* **2012,** *7*, e47150.

(100) Dzwolak, W., Chirality and Chiroptical Properties of Amyloid Fibrils. *Chirality* **2014,** *26*, 580-587.

(101) Eisenberg, D.; Jucker, M., The amyloid state of proteins in human diseases. *Cell* **2012,** *148*, 1188-1203.

(102) Engel, M. F. M.; Khemtémourian, L.; Kleijer, C. C.; Meeldijk, H. J. D.; Jacobs, J.; Verkleij, A. J.; de Kruijff, B.; Killian, J. A.; Höppener, J. W. M., Membrane Damage by Human Islet Amyloid Polypeptide Through Fibril Growth at the Membrane. *Proc. Natl. Acad. Sci. U.S.A.* **2008,** *105*, 6033-6038.

(103) Evgrafova, Z.; Voigt, B.; Roos, A. H.; Hause, G.; Hinderberger, D.; Balbach, J.; Binder, W. H., Modulation of amyloid β peptide aggregation by hydrophilic polymers. *Phys. Chem. Chem. Phys.* **2019,** *21*, 20999-21006.

(104) Ezzat, K.; Pernemalm, M.; Palsson, S.; Roberts, T. C.; Jarver, P.; Dondalska, A.; Bestas, B.; Sobkowiak, M. J.; Levanen, B.; Skold, M.; Thompson, E. A.; Saher, O.; Kari, O. K.; Lajunen, T.; Ekström, E. S.; Nilsson, C.; Ischenko, Y.; Malm, T.; Wood, M. J. A.; Power, U. F.; Masich, S.; Linden, A.; Sandberg, J. K.; Lehtio, J.; Spetz, A.-L.; Andaloussi, S. E. L., The viral protein corona directs viral pathogenesis and amyloid aggregation. *Nat. Commun.* **2018,** *10*, 2331.

(105) Faridi, A.; Sun, Y.; Okazaki, Y.; Peng, G.; Gao, J.; Käkinen, A.; Faridi, P.; Zhao, M.; Javed, I.; Purcell, A. W.; Davis, T. P.; Lin, S.; Oda, R.; Ding, F.; Ke, P. C., Mitigating Human IAPP Amyloidogenesis In Vivo with Chiral Silica Nanoribbons. *Small* **2018,** *14*, 1802825.

(106) Ferreira, J.; Syrett, J.; Whittaker, M. R.; Haddleton, D. M.; Davis, T. P.; Boyer, C., Optimizing the generation of narrow polydispersity 'arm-first' star polymers made using RAFT polymerization. *Polym. Chem.*, **2011,** 2, 1671-1677.

(107) Ferrier, G. J. M.; Pierson, A. M.; Bloom, S. R.; Girgis, S. I.; Legon, S., Expression of the rat amylin (IAPP/DAP) gene. *J. Mol. Endocrinol.* **1989,** *3*, R1-4.

(108) Filipek, S.; Krzysko, K. A.; Fotiadis, D.; Liang, Y.; Saperstein, D. A.; Engel, A.; Palczewski, K., A concept for G protein activation by G protein-coupled receptor dimers: the transducin/rhodopsin interface. *Photochem. Photobiol. Sci.* **2004,** *3*, 628-638.

(109) Fischer, M.; Appelhans, D.; Schwarz, S.; Klajnert, B.; Bryszewska, M.; Voit, B.; Rogers, M., Influence of Surface Functionality of Poly(propylene imine) Dendrimers on Protease Resistance and Propagation of the Scrapie Prion Protein. *Biomacromolecules* **2010,** 11, 1314-1325.

(110) Flanagan, P.; Lionetti, F., Lysozyme Distribution in Blood. *Blood* **1955,** *10*, 497-501.

(111) Foote, M.; Zhou, Y., 14-3-3 proteins in neurological disorders. *Int. J. Biochem. Mol. Biol.* **2012,** *3*, 152-164.

(112) Fowler, D. M.; Koulov, A. V.; Alory-Jost, C.; Marks, M. S.; Balch, W. E.; Kelly, J. W., Functional Amyloid Formation within Mammalian Tissue. *PLoS Biol.* **2006,** *4*, 0100-0107.

(113) Fox, N.; Schrementi, J.; Nishi, M.; Ohagi, S.; Chan, S. J.; Heisserman, J. A.; Westermark, G. T.; Leckström, A.; Westermark, P.; Steiner, D. F., Human islet amyloid polypeptide transgenic mice as a model of non-insulin-dependent diabetes mellitus (NIDDM). *FEBS Lett.* **1993,** *323*, 40-44.

(114) Friedlich, A. L.; Tanzi, R. E.; Rogers, J. T., The 5'-untranslated region of Parkinson's disease α-synuclein messengerRNA contains a predicted iron responsive element. *Mol. Psychiatry* **2007,** *12*, 222-223.

(115) Friedrich, R. P.; Tepper, K.; Rönicke, R.; Soom, M.; Westermann, M.; Reymann, K.; Kaether, C.; Fändrich, M., Mechanism of amyloid plaque formation suggests an intracellular basis of Aβ pathogenicity. *Proc. Natl. Acad. Sci. U.S.A.* **2009,** 107, 1942-1947.

(116) Galvagnion, C.; Buell, A. K.; Meisl, G.; Michaels, T. C. T.; Vendruscolo, M.; Knowles, T. P. J.; Dobson, C. M., Lipid vesicles trigger α-synuclein aggregation by stimulating primary nucleation. *Nat. Chem. Biol.* **2015,** *11*, 229-234.

(117) Gao, M.; Estel, K.; Seeliger, J.; Friedrich, R. P.; Dogan, S.; Wanker, E. E.; Winter, R.; Ebbinghaus, S., Modulation of human IAPP fibrillation: cosolutes, crowders and chaperones. *Phys. Chem. Chem. Phys.* **2015,** *17*, 8338-8348.

(118) Gao, M.; Winter, R., The Effects of Lipid Membranes, Crowding and Osmolytes on the Aggregation, and Fibrillation Propensity of Human IAPP. *J. Diabetes Res.* **2015,** *2015*, 849017.

(119) Gao, N.; Sun, H.; Dong, K.; Ren, J.; Duan, T.; Xu, C.; Qu, X., Transition-metal-substituted polyoxometalate derivatives as functional anti-amyloid agents for Alzheimer's disease. *Nat. Commun.* **2014,** *5*, 3422.

(120) Ge, X.; Kakinen, A.; Gurzov, E. N.; Pang, L.; Pilkington, E. H.; Separovic, F.; Davis, T. P.; Ke, P. C.; Ding, F., Zinc-coordination and C-peptide complexation: a potential mechanism for the endogenous inhibition of IAPP aggregation. *Chem. Commun.* **2017,** *53*, 9394-9397.

(121) Geng, J.; Li, M.; Ren, J.; Wang, E.; Qu, X., Polyoxometalates as Inhibitors of the Aggregation of Amyloid β Peptides Associated with Alzheimer's Disease. *Angew. Chem. Int Ed., Engl.* **2011,** *50*, 4184-4188.

(122) Ghavami, M.; Rezaei, M.; Ejtehadi, R.; Lofti, M.; Shokrgozar, M. A.; Emamy, B. A.; Raush, J.; Mahmoudi, M., Physiological Temperature Has a Crucial Role in Amyloid Beta in the Absence and Presence of Hydrophobic and Hydrophilic Nanoparticles. *ACS Chem. Neurosci.* **2013,** *4*, 375-378.

(123) Gianneli, M.; Yan, Y.; Polo, E.; Peiris, D.; Aastrup, T.; Dawson, K. A., Novel QCM-Based Method to Predict *In Vivo* behaviour of nanoparticles. *Proc. Technol.* **2017,** *27*, 197-200.

(124) Glabe, C. G., Structural Classification of Toxic Amyloid Oligomers. *J. Biol. Chem.* **2008,** *283*, 29639-29643.

(125) Gladytz, A.; Abel, B.; Risselada, H. J., Gold-Induced Fibril Growth: The Mechanism of Surface-Facilitated Amyloid Aggregation. *Angew. Chem. Int. Ed., Engl.* **2016,** *55*, 11242-11246.

(126) Glickman, M. H.; Ciechanover, A., The Ubiquitin-Proteasome Proteolytic Pathway: Destruction for the Sake of Construction. *Physiol. Rev.* **2001,** *82*, 373-428.

(127) Gong, W.; Liu, Z. H.; Zeng, C. H.; Peng, A.; Chen, H. P.; Zhou, H.; Li, L. S., Amylin Deposition in the Kidney of Patients With Diabetic Nephropathy. *Kidney Int.* **2007,** *72*, 213-218.

(128) Govers, S. K.; Mortier, J.; Adam, A.; Aertsen, A., Protein aggregates encode epigenetic memory of stressful encounters in individual *Escherichia coli* cells. *PLoS Biol.* **2018,** *16*, e2003853.

(129) Govindan, P. N.; Gurzov, E. N.; Chen, P.; Pilkington, E. H.; Stanley, W. J.; Litwak, S. A.; Davis, T. P.; Ke, P. C.; Ding, F., Graphene Oxide Inhibits hIAPP Amyloid Fibrillation and Toxicity in Insulin-Producing NIT-1 Cells. *Phys. Chem. Chem. Phys.* **2015,** *18*, 94-100.

(130) Govindan, P. N.; Jemec, D. B.; Ding, F., CSAR Benchmark of Flexible MedusaDock in Affinity Prediction and Nativelike Binding Pose Selection. *J. Chem. Inf. Model.,* **2016,** 56, 1042-1052.

(131) Govindan, P. N.; Käkinen, A.; Pilkington, E. H.; Davis, T. P.; Ke, P. C.; Ding, F., Stabilizing Off-pathway Oligomers by Polyphenol Nanoassemblies for IAPP Aggregation Inhibition. *Sci. Rep.* **2016,** *6*, 19463.

(132) Grey, M.; Linse, S.; Nilsson, H.; Brundin, P.; Sparr, E., Membrane Interaction of α-Synuclein in Different Aggregation States. *J. Parkinsons Dis.* **2011,** *1*, 359-371.

(133) Gsponer, J.; Babu, M. M., Cellular Strategies for Regulating Functional and Nonfunctional Protein Aggregation. *Cell Reports* **2012,** *2*, 1425-1437.

(134) Guariguata, L.; Whiting, D. R.; Hambleton, I.; Beagley, J.; Linnenkamp, U.; Shaw, J. E., Global estimates of diabetes prevalence for 2013 and projections for 2035. *Diabetes Res. Clin. Pract.* **2014,** *103*, 137-149.

(135) Guerreiro, L. H.; Da Silva, D.; Ricci-Junior, E.; Girard-Dias, W.; Mascarenhas, C. M.; Sola-Penna, M.; Miranda, K.; Lima, L. M. T. R., Polymeric particles for the controlled release of human amylin. *Colloids Surf. B Biointerfaces* **2012,** *94*, 101-106.

(136) Guivernau, B.; Bonet, J.; Valls-Comamala, V.; Bosch-Morató, M.; Godoy, J. A.; Inestrosa, N. C.; Perálvarez-Martin, A.; Fernández-Busquets, X.; Andreu, D.; Oliva, B.; Muñoz, F. J., Amyloid-β Peptide Nitrotyrosination Stabilizes Oligomers and Enhances NMDAR-Mediated Toxicity. *J. Neurosci.* **2016,** *36*, 11693-11703.

(137) Guo, C.; Côté, S.; Mousseau, N.; Wei, G., Distinct Helix Propensities and Membrane Interactions of Human and Rat IAPP1–19 Monomers in Anionic Lipid Bilayers. *J. Phys. Chem. B* **2015,** *119*, 3366-3376.

(138) Gupta, N. T.; Vander Heiden, J. A.; Uduman, M.; Gadala-Maria, D.; Yaari, G.; Kleinstein, S. H., Change-O: a toolkit for analyzing large-scale B cell immunoglobulin repertoire sequencing data. *Bioinformatics* **2015,** *31*, 3356-3358.

(139) Gursky, O., *Lipids in Protein Misfolding*. Springer: Cham, Switzerland, 2015; Vol. 855.

(140) Gurzov, E. N.; Wang, B.; Pilkington, E. H.; Chen, P.; Käkinen, A.; Stanley, W. J.; Litwak, S. A.; Hanssen, E. G.; Davis, T. P.; Ding, F.; Ke, P. C., Inhibition of hIAPP Amyloid Aggregation and Pancreatic β-Cell Toxicity by OH-Terminated PAMAM Dendrimer. *Small* **2016,** *12*, 1615-1626.

(141) Gustafsson, M.; Thyberg, J.; Näslund, J.; Eliasson, E.; Johansson, J., Amyloid fibril formation by pulmonary surfactant protein C. *FEBS Lett.* **1999,** *464*, 138-142.

(142) Haataja, L.; Gurlo, T.; Huang, C. J.; Butler, P. C., Islet Amyloid in Type 2 Diabetes, and the Toxic Oligomer Hypothesis. *Endocrine Rev.* **2008,** *29*, 303-316.

(143) Hadjidemetriou, M.; Al-Ahmady, Z.; Mazza, M.; Collins, R. F.; Dawson, K.; Kostarelos, K., *In Vivo* Biomolecule Corona Around Blood-Circulating, Clinically Used and Antibody-Targeted Lipid Bilayer Nanoscale Vesicles. *ACS Nano* **2015,** *9*, 8142-8156.

(144) Halgren, T. A., MMFF VI. MMFF94s option for energy minimization studies. *J. Comput. Chem.,* **1999,** 20, 720-729.

(145) Hanwell, M. D.; Curtis, D. E.; Lonie, D. C.; Vandermeersch, T.; Zurek, E.; Hutchison, G. R., Avogadro: an advanced semantic chemical editor, visualization, and analysis platform. *J. Cheminf.*, **2012,** 4, 17.

(146) Haque, E.; Kamil, M.; Hasan, A.; Irfan, S.; Sheikh, S.; Khatoon, A.; Nazir, A.; Mir, S. S., Advanced Glycation End Products (AGEs), Protein Aggregation and their Crosstalk: New Insight in Tumorigenesis. *Glycobiology* **2019**, cwz073.

(147) Hartl, F. U.; Bracher, A.; Hayer-Hartl, M., Molecular chaperones in protein folding and proteostasis. *Nature* **2011,** *475*, 324-332.

(148) Hartter, E.; Svoboda, T.; Ludvik, B.; Schuller, M.; Lell, B.; Kuenburg, E.; Brunnbauer, M.; Woloszczuk, W.; Prager, R., Basal and Stimulated Plasma Levels of Pancreatic Amylin Indicate Its Co-Secretion With Insulin in Humans. *Diabetologia* **1991,** *34*, 52-54.

(149) Hatami, A.; Monjazeb, S.; Milton, S.; Glabe, C. G., Familial Alzheimer's Disease Mutations within the Amyloid Precursor Protein Alter the Aggregation and Conformation of the Amyloid-β Peptide. *J. Biol. Chem.* **2017,** *292*, 3172-3185.

(150) Hategan, A.; Bianchet, M. A.; Steiner, J.; Karnaukhova, E.; Masliah, E.; Fields, A.; Lee, M. H.; Dickens, A., M.; Haughey, N.; Dimitriadis, E. K.; Nath, A., HIV Tat Protein and Amyloid-β Peptide Form Multifibrillar Structures That Cause Neurotoxicity. *Nat. Struct. Mol. Biol.* **2017,** *24*, 379-386.

(151) Hatters, D. M.; Minton, A. P.; Howlett, G. J., Macromolecular Crowding Accelerates Amyloid Formation by Human Apolipoprotein C-II. *J. Biol. Chem.* **2002,** *277*, 7824-7830.

(152) He, X.-P.; Deng, Q.; Cai, L.; Wang, C.-Z.; Zang, Y.; Li, J.; Chen, G.-R.; Tian, H., Fluorogenic Resveratrol-Confined Graphene Oxide For Economic and Rapid Detection Of Alzheimer's Disease. *ACS Appl. Mater. Interfaces* **2014,** *6*, 5379-5382.

(153) Hernández, M. G.; Aguilar, A. G.; Burillo, J.; Oca, R. G.; Manca, A. M.; Novials, A.; Alcarraz-Vizan, G.; Guillén, C.; Benito, M., Pancreatic β cells overexpressing hIAPP impaired mitophagy and unbalanced mitochondrial dynamics. *Cell Death Dis.* **2018,** *9*, 481.

(154) Hickey, A. J. R.; Bradley, J. W. I.; Skea, G. L.; Middleditch, M. J.; Buchanan, C. M.; Phillips, A. R. J.; Cooper, G. J. S., Proteins Associated with Immunopurified Granules from a Model Pancreatic Islet β-Cell System: Proteomic Snapshot of an Endocrine Secretory Granule. *J. Proteome Res.* **2009,** *8*, 178-186.

(155) Hinault, M.-P.; Cuendet, A. F. H.; Mattoo, R. U. H.; Mensi, M.; Dietler, G.; Lashuel, H. A.; Goloubinoff, P., Stable α-Synuclein Oligomers Strongly Inhibit Chaperone Activity of the Hsp70 System by Weak Interactions with J-domain Co-chaperones. *J. Biol. Chem.* **2010,** *285*.

(156) Hirakura, Y.; Yiu, W. W.; Yamamoto, A.; Kagan, B. L., Amyloid peptide channels: blockade by zinc and inhibition by Congo red (amyloid channel block). *Amyloid* **2000,** *7*, 194-199.

(157) Hong, L.; Huang, H.-C.; Jiang, Z.-F., Relationship between amyloid-beta and the ubiquitin–proteasome system in Alzheimer's disease. *Neurol. Res.* **2014,** *36*, 276-282.

(158) Hsu, Y.-H.; Chen, Y.-W.; Wu, M.-H.; Tu, L.-H., Protein Glycation by Glyoxal Promotes Amyloid Formation by Islet Amyloid Polypeptide. *Biophys. J.* **2019,** *116*, 2304-2313.

(159) Hu, J.; Qiao, R.; Whittaker, M. R.; Quinn, J. F.; Davis, T. P., Synthesis of Star Polymers by RAFT Polymerization as Versatile Nanoparticles for Biomedical Applications. *Aust. J. Chem.,* **2017,** doi: 10.1071/CH17391

(160) Huang, B.; He, J.; Ren, J.; Yan, X.-Y.; Zeng, C.-M., Cellular Membrane Disruption by Amyloid Fibrils Involved Intermolecular Disulfide Cross-Linking. *Biochemistry* **2009,** 48, 5794-5800.

(161) Huang, C. C.; Faber, P. W.; Persichetti, F.; Mittal, V.; Vonsattel, J.-P.; MacDonald, M. E.; Gusella, J. F., Amyloid Formation by Mutant Huntingtin: Threshold, Progressivity and Recruitment of Normal Polyglutamine Proteins. *Somatic Cell Mol. Genet.* **1998,** *24*, 217-233.

(162) Huang, C. J.; Haataja, L.; Gurlo, T.; Butler, A. E.; Wu, X.; Soeller, W. C.; Butler, P. C., Induction of endoplasmic reticulum stress-induced beta-cell apoptosis and accumulation of polyubiquitinated proteins by human islet amyloid polypeptide. *Am. J. Physiol. Endocrinol. Metab.* **2007,** *293*, E1656-E1662.

(163) Huang, C.-J.; Lin, C.-Y.; Haataja, L.; Gurlo, T.; Butler, A. E.; Rizza, R. A.; Butler, P. C., High Expression Rates of Human Islet Amyloid Polypeptide Induce Endoplasmic Reticulum Stress–Mediated β-Cell Apoptosis, a Characteristic of Humans With Type 2 but Not Type 1 Diabetes. *Diabetes* **2007,** *56*, 2016-2027.

(164) Huang, H.; Li, P.; Zhang, M.; Yu, Y.; Huang, Y.; Gu, H.; Wang, C.; Yang, Y., Graphene quantum dots for detecting monomeric amyloid peptides. *Nanoscale* **2017,** *9*, 5044-5048.

(165) Huang, J.; Liu, S.; Zhang, C.; Wang, X.; Pu, J.; Ba, F.; Xue, S.; Ye, H.; Zhao, T.; Li, K.; Wang, Y.; Zhang, J.; Wang, L.; Fan, C.; Lu, T. K.; Zhong, C., Programmable and printable *Bacillus subtilis* biofilms as engineered living materials. *Nat. Chem. Biol.* **2019,** *15*, 34-41.

(166) Ittner, A.; Chua, S. W.; Bertz, J.; Volkerling, A.; van der Hoven, J.; Gladbach, A.; Przybyla, M.; Bi, M.; van Hummel, A.; Stevens, C. H.; Ippati, S.; Suh, L. S.; Macmillan, A.; Sutherland, G.; Kril, J. J.; Silva, A. P. G.; Mackay, J. P.; Poljak, A.; Delerue, F.; Ke, Y. D.; Ittner, L. M., Site-specific phosphorylation of tau inhibits amyloid-β toxicity in Alzheimer's mice. *Science* **2016,** *354*, 904-908.

(167) Jackson, K.; Barisone, G. A.; Diaz, E.; Jin, L.-W.; DeCarli, C.; Despa, F., Amylin Deposition in the Brain: A Second Amyloid in Alzheimer Disease? *Ann. Neurol.* **2013,** *74*, 517-526.

(168) Jacob, R. S.; Das, S.; Singh, N.; Patel, K.; Datta, D.; Sen, S.; Maji, S. K., Amyloids Are Novel Cell-Adhesive Matrices. In *Biochemical and Biophysical Roles of Cell Surface Molecules*, Chattopadhyay, K.; Basu, S., Eds. Springer: Singapore, 2018.

(169) Jaikaran, E. T. A. S.; Nilsson, M. R.; Clark, A., Pancreatic *β*-cell granule peptides form heteromolecular complexes which inhibit islet amyloid polypeptide fibril formation. *Biochem. J.* **2004,** *377*, 709-716.

(170) Jain, R.; Khandelwal, G.; Roy, S., Unraveling the Design Rules in Ultrashort Amyloid-Based Peptide Assemblies toward Shape-Controlled Synthesis of Gold Nanoparticles. *Langmuir* **2019,** *35*, 5878-5889.

(171) Jang, H. H., Regulation of Protein Degradation by Proteasomes in Cancer. *J. Cancer Prev.* **2018,** *23*, 153-161.

(172) Jansen, W. J.; Ossenkoppele, R.; Knol, D. L.; Tijms, B. M.; Scheltens, P.; Verhey, F. R. J.; Visser, P. J.; The Amyloid Biomarker Study Group, Prevalence of Cerebral Amyloid Pathology in Persons Without Dementia: A Meta-Analysis. *J. Am. Med. Assoc.* **2015,** *313*, 1924-1938.

(173) Javed, I.; Peng, G.; Xing, Y.; Yu, T.; Zhao, M.; Käkinen, A.; Faridi, A.; Parish, C. L.; Ding, F.; Davis, T. P.; Ke, P. C.; Lin, S., Inhibition of amyloid beta toxicity in zebrafish with a chaperone-gold nanoparticle dual strategy. *Nat. Commun.* **2019,** *10*, 3780.

(174) Javed, I.; Sun, Y.; Adamcik, J.; Wang, B.; Käkinen, A.; Pilkington, E. H.; Ding, F.; Mezzenga, R.; Davis, T. P.; Ke, P. C., Cofibrillization of Pathogenic and Functional Amyloid Proteins with Gold Nanoparticles against Amyloidogenesis. *Biomacromolecules* **2017,** *18*, 4316-4322.

(175) Javed, I.; Yu, T.; Peng, G.; Sánchez-Ferrer, A.; Faridi, A.; Käkinen, A.; Zhao, M.; Mezzenga, R.; Davis, T. P.; Lin, S.; Ke, P. C., In Vivo Mitigation of Amyloidogenesis through Functional−Pathogenic Double-Protein Coronae. *Nano Lett.* **2018,** *18*, 5797-5804.

(176) Jean, L.; Lee, C. F.; Hodder, P.; Hawkins, N.; Vaux, D. J., Dynamics of the formation of a hydrogel by a pathogenic amyloid peptide: islet amyloid polypeptide. *Sci. Rep.* **2016,** *6*, 32124.

(177) Jha, S.; Patil, S. M.; Gibson, J.; Nelson, C. E.; Alder, N. N.; Alexandrescu, A. T., Mechanism of Amylin Fibrillization Enhancement by Heparin. *J. Biol. Chem.* **2011,** *286*, 22894-22904.

(178) Jo, Y. H.; Jang, I. J.; Nemeno, J. G.; Lee, S.; Kim, B. Y.; Nam, B. M.; Yang, W.; Lee, K. M. K., H.; Takebe, T.; Kim, Y. S.; Lee, J. I., Artificial Islets From Hybrid Spheroids of Three Pancreatic Cell Lines. *Transplant. Proc.* **2014,** *46*, 1156-1160.

(179) John, T.; Gladytz, A.; Kubeil, C.; Martin, L. L.; Risselada, H. J.; Abel, B., Impact of nanoparticles on amyloid peptide and protein aggregation: a review with a focus on gold nanoparticles. *Nanoscale* **2018,** *10*, 20894-20913.

(180) Jollès, J.; Jollès, P., Lysozymes' esterase activity. *FEBS Lett.* **1983,** *162*, 120-121.

(181) Jurgens, C. A.; Toukatly, M. N.; Fligner, C. L.; Udayasankar, J.; Subramanian, S. L.; Zraika, S.; Aston-Mourney, K.; Carr, D. B.; Westermark, P.; Westermark, G. T., β-Cell Loss and β-Cell

Apoptosis in Human Type 2 Diabetes Are Related to Islet Amyloid Deposition. *Am. J. Pathol.* **2011,** *178*, 2632-2640.

(182) Kahn, S. E., The Importance of the β-Cell in the Pathogenesis of Type 2 Diabetes Mellitus. *Am. J. Med.* **2000,** *108*, 2S-8S.

(183) Kahn, S. E.; Andrikopoulos, S.; Verchere, C. B., Islet Amyloid: A Long-Recognized But Underappreciated Pathological Feature of Type 2 Diabetes. *Diabetes* **1999,** *48*, 241-253.

(184) Kahn, S. E.; Zraika, S.; Utzschneider, K. M.; Hull, R. L., The beta cell lesion in type 2 diabetes: there has to be a primary functional abnormality. *Diabetologia* **2009,** *52*, 1003-1012.

(185) Käkinen, A.; Adamcik, J.; Wang, B.; Ge, X.; Mezzenga, R.; Davis, T. P.; Ding, F.; Ke, P. C., Nanoscale inhibition of polymorphic and ambidextrous IAPP amyloid aggregation with small molecules. *Nano Res.* **2017,** *11*, 3636-3647.

(186) Käkinen, A.; Javed, I.; Faridi, A.; Davis, T. P.; Ke, P. C., Serum albumin impedes the amyloid aggregation and hemolysis of human islet amyloid polypeptide and alpha synuclein. *Biochim. Biophys. Acta, Biomembranes* **2018,** *1860*, 1803-1809.

(187) Kamata, K.; Mizukami, H.; Inaba, W.; Tsuboi, K.; Tateishi, Y.; Yoshida, T.; Yagihashi, S., Islet amyloid with macrophage migration correlates with augmented β-cell deficits in type 2 diabetic patients. *Amyloid* **2014,** *21*, 191-201.

(188) Kawahara, M.; Kuroda, Y.; Arispe, N.; Rojas, E., Alzheimer's β-Amyloid, Human Islet Amylin, and Prion Protein Fragment Evoke Intracellular Free Calcium Elevations by a Common Mechanism in a Hypothalamic GnRH Neuronal Cell Line. *J. Biol. Chem.* **2000,** *275*, 14077-14083.

(189) Kayed, R.; Pensalfini, A.; Margol, L.; Sokolov, Y.; Sarsoza, F.; Head, E.; Hall, J.; Glabe, C., Annular Protofibrils Are a Structurally and Functionally Distinct Type of Amyloid Oligomer. *J. Biol. Chem.* **2009,** *284*, 4230-4237.

(190) Kayed, R.; Sokolov, Y.; Edmonds, B.; McIntire, T. M.; Milton, S. C.; Hall, J. E.; Glabe, C. G., Permeabilization of Lipid Bilayers Is a Common Conformation-dependent Activity of Soluble Amyloid Oligomers in Protein Misfolding Diseases. *J. Biol. Chem.* **2004,** *279*, 46363-46366.

(191) Ke, P. C.; Lin, S.; Parak, W. J.; Davis, T. P.; Caruso, F., A Decade of the Protein Corona. *ACS Nano* **2017,** *11*, 11773-11776.

(192) Ke, P. C.; Pilkington, E. H.; Sun, Y.; Javed, I.; Käkinen, A.; Peng, G.; Ding, F.; Davis, T. P., Mitigation of Amyloidosis with Nanomaterials. *Adv. Mater.* **2019**, 1901690.

(193) Ke, P. C.; Qiao, R., Carbon nanomaterials in biological systems. *J. Phys. Condens. Matter* **2007,** *19*, 373101.

(194) Ke, P. C.; Sani, M.-A.; Ding, F.; Käkinen, A.; Javed, I.; Separovic, F.; Davis, T. P.; Mezzenga, R., Implications of peptide assemblies in amyloid diseases. *Chem. Soc. Rev.* **2017,** *46*, 6492-6531.

(195) Ke, P. C.; Sani, M.-A.; Ding, F.; Käkinen, A.; Javed, I.; Separovic, F.; Davis, T. P.; Mezzenga, R., Implications of Peptide Assemblies in Amyloid Diseases. *Chem. Soc. Rev.* **2017,** *46*, 6492-6531.

(196) Keller, A.; Fritzsche, M.; Yu, Y.-P.; Liu, Q.; Li, Y.-M.; Dong, M.; Besenbacher, F., Influence of Hydrophobicity on the Surface-Catalyzed Assembly of the Islet Amyloid Polypeptide. *ACS Nano* **2011,** *5*, 2770-2778.

(197) Khemtémourian, L.; Doménech, E.; Doux, J. P. F.; Koorengevel, M. C.; Killian, J. A., Low pH Acts as Inhibitor of Membrane Damage Induced by Human Islet Amyloid Polypeptide. *J. Am. Chem. Soc.* **2011,** *133*, 15598-15604.

(198) Kim, D.; Kwon, H. J.; Hyeon, T., Magnetite/Ceria Nanoparticle Assemblies for Extracorporeal Cleansing of Amyloid-β in Alzheimer's Disease. *Adv. Mater.* **2019,** *31*, e1807965.

(199) Kim, H. S.; Lee, S. H.; Choi, I., On-chip plasmonic immunoassay based on targeted assembly of gold nanoplasmonic particles. *Analyst* **2019,** *144*, 2820-2826.

(200) Kim, H. Y.; Kim, H. V.; Jo, S.; Lee, J.; Choi, S. Y.; Kim, D. J.; Kim, Y., EPPS rescues hippocampus-dependent cognitive deficits in APP/PS1 mice by disaggregation of amyloid-β oligomers and plaques. *Nat. Commun.* **2015,** *6*, 8997.

(201) Kim, Y. S.; Liu, L.; Axelsen, P. H.; Hochstrasser, R. M., 2D IR Provides Evidence for Mobile Water Molecules in β-Amyloid Fibrils. *Proc. Natl. Acad. Sci. U.S.A.* **2009,** *106*, 17751-17756.

(202) Kishimoto, T.; Soda, Y.; Matsuyama, Y.; Mizuno, K., An enzymatic assay for lysophosphatidylcholine concentration in human serum and plasma. *Clin. Biochem.* **2002,** *35*, 411-416.

(203) Klajnert, B.; Appelhans, D.; Komber, H.; Morgner, N.; Schwarz, S.; Richter, S.; Brutschy, B.; Ionov, M.; Tonkikh, A. K.; Bryszewska, M.; Voit, B., The Influence of Densely Organized Maltose Shells on the Biological Properties of Poly(propylene imine) Dendrimers: New Effects Dependent on Hydrogen Bonding. *Chem. Eur. J.* **2008,** 14, 7030-7041.

(204) Kleinberg, D. L., Human α-Lactalbumin: Measurement in Serum and in Breast Cancer Organ Cultures by Radioimmunoassay. *Science* **1975,** *190*, 276-278.

(205) Klementieva, O.; Aso, E.; Filippini, D.; Benseny-Cases, N.; Carmona, M.; Juvés, S.; Appelhans, D.; Cladera, J.; Ferrer, I., Effect of Poly(propylene imine) Glycodendrimers on β‑Amyloid Aggregation in Vitro and in APP/PS1 Transgenic Mice, as a Model of Brain Amyloid Deposition and Alzheimer's Disease. *Biomacromolecules* **2013,** 14, 3570-3580.

(206) Klementieva, O.; Benseny-Cases, N.; Gella, A.; Appelhans, D.; Voit, B.; Cladera, J., Dense Shell Glycodendrimers as Potential Nontoxic Anti-amyloidogenic Agents in Alzheimer's Disease. Amyloid-Dendrimer Aggregates Morphology and Cell Toxicity. *Biomacromolecules* **2011,** 12, 3903-3909.

(207) Knowles, T. P. J.; Vendruscolo, M.; Dobson, C. M., The amyloid state and its association with protein misfolding diseases. *Nat. Rev. Mol. Cell Biol.* **2014,** *15*, 384-396.

(208) Koh, A.; Molinaro, A.; Ståhlman, M.; Khan, M. T.; Schmidt, C.; Mannerås-Holm, L.; Wu, H.; Carreras, A.; Jeong, H.; Olofsson, L. E.; Bergh, P.-O.; Gerdes, V.; Hartstra, A.; de Brauw, M.; Perkins,

R.; Nieuwdorp, M.; Bergström, G.; Bäckhed, F., Microbially Produced Imidazole Propionate Impairs Insulin Signaling through mTORC1. *Cell* **2018,** *175*, 947-961.

(209) Kopito, R. R., Aggresomes, inclusion bodies and protein aggregation. *Trends Cell Biol.* **2000,** *10*, 524-530.

(210) Kostarelos, K., The long and short of carbon nanotube toxicity. *Nat. Biotechnol.* **2008,** *26*, 774-776.

(211) Kuhn, D. M.; Sykes, C. E.; Geddes, T. J.; Jaunarajs, K. L. E.; Bishop, C., Tryptophan hydroxylase 2 aggregates through disulfide cross-linking upon oxidation: possible link to serotonin deficits and non-motor symptoms in Parkinson's disease. *J. Neurochem.* **2011,** *116*, 426-437.

(212) Kumar, D. K. V.; Choi, S. H.; Washicosky, K. J.; Eimer, W. A.; Tucker, S.; Ghofrani, J.; Lefkowitz, A.; McColl, G.; Goldstein, L. E.; Tanzi, R. E.; Moir, R. D., Amyloid-β peptide protects against microbial infection in mouse and worm models of Alzheimer's disease. *Sci. Transl. Med.* **2016,** *8*, 340ra72.

(213) Kumar, S. T.; Meinhardt, J.; Fuchs, A.-K.; Aumüller, T.; Leppert, J.; Büchele, B.; Knüpfer, U.; Ramachandran, R.; Yadav, J. K.; Prell, E.; Morgado, I.; Ohlenschläger, O.; Horn, U.; Simmet, T.; Görlach, M.; Fändrich, M., Structure and Biomedical Applications of Amyloid Oligomer Nanoparticles. *ACS Nano* **2014,** *8*, 11042-11052.

(214) Kumar, S.; Walter, J., Phosphorylation of amyloid beta (Aβ) peptides - a trigger for formation of toxic aggregates in Alzheimer's disease. *Aging* **2011,** *3*, 803-812.

(215) Kumar, S.; Wirths, O.; Stüber, K.; Wunderlich, P.; Koch, P.; Theil, S.; Rezaei-Ghaleh, N.; Zweckstetter, M.; Bayer, T. A.; Brüstle, O.; Thal, D. R.; Walter, J., Phosphorylation of the amyloid β-peptide at Ser26 stabilizes oligomeric assembly and increases neurotoxicity. *Acta Neuropathol.* **2016,** *131*, 525-537.

(216) Larson, J. L.; Miranker, A. D., The Mechanism of Insulin Action on Islet Amyloid Polypeptide Fiber Formation. *J. Mol. Biol.* **2004,** *335*, 221-231.

(217) Leahy, J. L., Pathogenesis of Type 2 Diabetes Mellitus. *Arch. Med. Res.* **2005,** *36*, 197-209.

(218) Lee, M.; Wang, T.; Makhlynets, O. V.; Wu, Y.; Polizzi, N. F.; Wu, H.; Gosavi, P. M.; Stöhr, J.; Korendovych, I. V.; DeGrado, W. F.; Hong, M., Zinc-Binding Structure of a Catalytic Amyloid From Solid-State NMR. *Proc. Natl. Acad. Sci. U.S.A.* **2017,** *114*, 6191-6196.

(219) Lee, M.-C.; Yu, W.-C.; Shih, Y.-H.; Chen, C.-Y.; Guo, Z.-H.; Huang, S.-J.; Chan, J. C. C.; Chen, Y.-R., Zinc ion rapidly induces toxic, off-pathway amyloid-β oligomers distinct from amyloid-β derived diffusible ligands in Alzheimer's disease. *Sci. Rep.* **2018,** *8*, 4772.

(220) Lee, S.; Lee, D.; Hong, C.-S.; Yang, J. E.; Kang, J. S.; Sung, Y.-E.; Paik, S. R., Alternative Assembly of α-Synuclein Leading to Protein Film Formation and Its Application for Developing Polydiacetylene-Based Sensing Materials. *Langmuir* **2019,** *35*, 11923-11931.

(221) Lemaire, K.; Ravier, M. A.; Schraenen, A.; Creemers, J. W. M.; Van de Plas, R.; Granvik, M.; Van Lommel, L.; Waelkens, E.; Chimienti, F.; Rutter, G. A.; in't Veld, P. A.; Schuit, F. C., Insulin

crystallization depends on zinc transporter ZnT8 expression, but is not required for normal glucose homeostasis in mice. *Proc. Natl. Acad. Sci. U.S.A.* **2009,** *106*, 14872-14877.

(222) Li, C.; Mezzenga, R., The interplay between carbon nanomaterials and amyloid fibrils in bio-nanotechnology. *Nanoscale* **2013,** *5*, 6207-6218.

(223) Li, M.; Zhao, A.; Dong, K.; Li, W.; Ren, J.; Qu, X., Chemically exfoliated WS_2 nanosheets efficiently inhibit amyloid β-peptide aggregation and can be used for photothermal treatment of Alzheimer's disease. *Nano Res.* **2015,** *8*, 3216-3227.

(224) Li, N.; Luo, H.-C.; Yang, C.; Deng, J.-J.; Ren, M.; Xie, X.-Y.; Lin, D.-Z.; Yan, L.; Zhang, L.-M., Cationic star-shaped polymer as an siRNA carrier for reducing MMP-9 expression in skin fibroblast cells and promoting wound healing in diabetic rats. *Int. J. Nanomedicine* **2014,** *9*, 3377-3387.

(225) Li, X.-H.; Du, L.-L.; Cheng, X.-S.; Jiang, X.; Zhang, Y.; Lv, B.-L.; Liu, R.; Wang, J.-Z.; Zhou, X.-W., Glycation exacerbates the neuronal toxicity of β-amyloid. *Cell Death Dis.* **2013,** *4*, e673.

(226) Li, Y.; Wang, L.; Lu, T.; Wei, Y.; Li, F., The Effects of Chondroitin Sulfate and Serum Albumin on the Fibrillation of Human Islet Amyloid Polypeptide at the Phospholipid Membranes. *Phys. Chem. Chem. Phys.* **2016,** *18*, 12000-12008.

(227) Li, Z.; Wang, C.; Wang, Z.; Zhu, C.; Li, J.; Sha, T.; Ma, L.; Gao, C.; Yang, Y.; Sun, Y.; Wang, J.; Sun, X.; Lu, C.; Difiglia, D.; Mei, Y.; Ding, C.; Luo, S.; Dang, Y.; Ding, Y.; Fei, Y.; Lu, B., Allele-selective lowering of mutant HTT protein by HTT–LC3 linker compounds. *Nature* **2019,** *575*, 203-209.

(228) Liao, L.; Cheng, D.; Wang, J.; Duong, D. M.; Losik, T. G.; Gearing, M.; Rees, H. D.; Lah, J. J.; Levey, A. I.; Peng, J., Proteomic Characterization of Postmortem Amyloid Plaques Isolated by Laser Capture Microdissection. *J. Biol. Chem.* **2004,** *279*, 37061-37068.

(229) Liberek, K.; Lewandowska, A.; Zietkiewicz, S., Chaperones in control of protein disaggregation. *EMBO J.* **2008,** *27*, 328-335.

(230) Librizzi, F.; Carrotta, R.; Spigolon, D.; Bulone, D.; Biagio, P. L. S., α-Casein Inhibits Insulin Amyloid Formation by Preventing the Onset of Secondary Nucleation Processes. *J. Phys. Chem. Lett.* **2014,** *5*, 3043-3048.

(231) Limbocker, R.; Chia, S.; Ruggeri, F. S.; Perni, M.; Cascella, R.; Heller, G. T.; Meisl, G.; Mannini, B.; Habchi, J.; Michaels, T. C. T.; Challa, P. K.; Ahn, M.; Casford, S. T.; Fernando, N.; Xu, C. K.; Kloss, N. D.; Cohen, S. I. A.; Kumita, J. R.; Cecchi, F.; Zasloff, M.; Linse, S.; Knowles, T. P. J.; Chiti, F.; Vendruscolo, M.; Dobson, C. M., Trodusquemine enhances Aβ42 aggregation but suppresses its toxicity by displacing oligomers from cell membranes. *Nat. Commun.* **2019,** *10*, 225.

(232) Little, W. C.; Schwartlander, R.; Smith, M. L.; Gourdon, D.; Vogel, V., Stretched Extracellular Matrix Proteins Turn Fouling and Are Functionally Rescued by the Chaperones Albumin and Casein. *Nano Lett.* **2009,** *9*, 4158-4167.

(233) Liu, C.; Zhang, Y., Nucleic acid-mediated protein aggregation and assembly. *Adv. Protein Chem. Struct. Biol.* **2011,** *84*, 1-40.

(234) Liu, J.; Li, L., Targeting Autophagy for the Treatment of Alzheimer's Disease: Challenges and Opportunities. *Front. Mol. Neurosci.* **2019,** *12*, 203.

(235) Liu, P.; Zhang, S.; Chen, M.-S.; Liu, Q.; Wang, C.; Wang, C.; Li, Y.-M.; Besenbacher, F.; Dong, M., Co-Assembly of Human Islet Amyloid Polypeptide (hIAPP)/Insulin. *Chem. Commun.* **2012,** *48*, 191-193.

(236) Liu, X. G.; Lu, S.; Liu, D. Q.; Zhang, L.; Zhang, L. X.; Yu, X. L.; Liu, R. T., ScFv-conjugated superparamagnetic iron oxide nanoparticles for MRI-based diagnosis in transgenic mouse models of Parkinson's and Huntington's diseases. *Brain Res.* **2019,** *1707*, 141-153.

(237) Liu, Y.; Xu, L.-P.; Dai, W.; Dong, H.; Wen, Y.; Zhang, X., Graphene quantum dots for the inhibition of β amyloid aggregation. *Nanoscale* **2015,** *7*, 19060-19065.

(238) Liu, Y.; Zhou, H.; Yin, T.; Gong, Y.; Yang, G.; Chen, L.; Liu, J., Quercetin-modified gold-palladium nanoparticles as a potential autophagy inducer for the treatment of Alzheimer's disease. *J. Colloid Interface Sci.* **2019,** *552*, 388-400.

(239) Lopes, D. H. J.; Attar, A.; Nair, G.; Hayden, E. Y.; Du, Z.; McDaniel, K.; Dutt, S.; Bandmann, H.; Bravo-Rodriguez, K.; Mittal, S.; Klärner, F.-G.; Wang, C.; Sanchez-Garcia, E.; Schrader, T.; Bitan, G., Molecular Tweezers Inhibit Islet Amyloid Polypeptide Assembly and Toxicity by a New Mechanism. *ACS Chem. Biol.* **2015,** *10*, 1555-1569.

(240) Lopes, D. H. J.; Meister, A.; Gohlke, A.; Hauser, A.; Blume, A.; Winter, R., Mechanism of Islet Amyloid Polypeptide Fibrillation at Lipid Interfaces Studied by Infrared Reflection Absorption Spectroscopy. *Biophys. J.* **2007,** *93*, 3132-3141.

(241) Lorenzo, A.; Razzaboni, B.; Weir, G. C.; Yankner, B. A., Pancreatic islet cell toxicity of amylin associated with type-2 diabetes mellitus. *Nature* **1994,** *368*, 756-760.

(242) Lu, M.; Williamson, N.; Mishra, A.; Michel, C. H.; Kaminski, C. F.; Tunnacliffe, A.; Schierle, G. S. K., Structural progression of amyloid-β Arctic mutant aggregation in cells revealed by multiparametric imaging. *J. Biol. Chem.* **2018,** *294*, 1478-1487.

(243) Luca, S.; Yau, W.-M.; Leapman, R.; Tycko, R., Peptide Conformation and Supramolecular Organization in Amylin Fibrils: Constraints From Solid-State NMR. *Biochemistry* **2007,** *46*, 13505-13522.

(244) Lundqvist, M.; Stigler, J.; Elia, G.; Lynch, I.; Cedervall, T.; Dawson, K. A., Nanoparticle Size and Surface Properties Determine the Protein Corona With Possible Implications for Biological Impacts. *Proc. Natl. Acad. Sci. U.S.A.* **2008,** *105*, 14265-14270.

(245) Luo, J.; Wärmländer, S. K. T. S.; Gräslund, A.; Abrahams, J. P., Human lysozyme inhibits the *in vitro* aggregation of Aβ peptides, which *in vivo* are associated with Alzheimer's disease. *Chem. Commun.* **2013,** *49*, 6507-6509.

(246) Luo, J.; Wärmländer, S. K. T. S.; Gräslund, A.; Abrahams, J. P., Non-chaperone Proteins Can Inhibit Aggregation and Cytotoxicity of Alzheimer Amyloid *β* Peptide. *J. Biol. Chem.* **2014,** *289*, 27766-27775.

(247) Luo, Q.; Lin, Y.-X.; Yang, P.-P.; Wang, Y.; Qi, G.-B.; Qiao, Z.-Y.; Li, B.-N.; Zhang, K.; Zhang, J.-P.; Wang, L.; Wang, H., A self-destructive nanosweeper that captures and clears amyloid β-peptides. *Nat. Commun.* **2018,** *9*, 1802.

(248) Ly, H.; Despa, F., Hyperamylinemia as a Risk Factor for Accelerated Cognitive Decline in Diabetes. *Expert Rev. Proteomics* **2015,** *12*, 575-577.

(249) Ma, X.; Zhou, P.; Kugelmass, A.; Toskic, D.; Warner, M.; Lee, L.; Fogaren, T.; Godara, A.; Wang, M.; Li, Y.; Yang, L.; Xu, Q.; Comenzo, R. L., A novel xenograft mouse model for testing approaches targeting human kappa light-chain diseases. *Gene Ther.* **2019,** *26*, 187-197.

(250) MacDonald, M. J.; Ade, L.; Ntambi, J. M.; Ansari, I.-U. H.; Stoker, S. W., Characterization of Phospholipids in Insulin Secretory Granules and Mitochondria in Pancreatic Beta Cells and Their Changes with Glucose Stimulation. *J. Biol. Chem.* **2015,** *290*, 11075-11092.

(251) Mahmoudi, M.; Akhavan, O.; Ghavami, M.; Rezaee, F.; Ghiasi, S. M. A., Graphene Oxide Strongly Inhibits Amyloid Beta Fibrillation. *Nanoscale* **2012,** *4*, 7322-7325.

(252) Mäkimattila, S.; Fineman, M. S.; Yki-Järvinen, H., Deficiency of Total and Nonglycosylated Amylin in Plasma Characterizes Subjects with Impaired Glucose Tolerance and Type 2 Diabetes. *J. Clin. Endocrinol. Metab.* **2000,** *85*, 2822-2827.

(253) Malishev, R.; Arad, E.; Bhunia, S. K.; Shaham-Niv, S.; Kolusheva, S.; Gazit, E.; Jelinek, R., Chiral modulation of amyloid beta fibrillation and cytotoxicity by enantiomeric carbon dots. *Chem. Commun.* **2018,** *54*, 7762-7765.

(254) Mansson, C.; Arosio, P.; Hussein, R.; Kampinga, H. H.; Hashem, R. M.; Boelens, W. C.; Dobson, C. M.; Knowles, T. P. J.; Linse, S.; Emanuelsson, C., Interaction of the molecular chaperone DNAJB6 with growing amyloid-beta 42 (Aβ42) aggregates leads to sub-stoichiometric inhibition of amyloid formation. *J. Biol. Chem.* **2014,** *289*, 31066-31076.

(255) Masliah, E.; Rockenstein, E.; Veinbergs, I.; Sagara, Y.; Mallory, M.; Hashimoto, M.; Mucke, L., β-Amyloid peptides enhance α-synuclein accumulation and neuronal deficits in a transgenic mouse model linking Alzheimer's disease and Parkinson's disease. *Proc. Natl. Acad. Sci. U.S.A.* **2001,** *98*, 12245-12250.

(256) Mathers, C. D.; Loncar, D., Projections of Global Mortality and Burden of Disease from 2002 to 2030. *PLoS Med.* **2006,** *3*, 2011-2030.

(257) Matveyenko, A. V.; Butler, P. C., Islet Amyloid Polypeptide (IAPP) Transgenic Rodents as Models for Type 2 Diabetes. *ILAR J.* **2006,** *47*, 225-233.

(258) Mayer, E. A.; Knight, R.; K., M. S.; Cryan, J. F.; Tillisch, K., Gut Microbes and the Brain: Paradigm Shift in Neuroscience. *J. Neurosci.* **2014,** *34*, 15490-15496.

(259) McCarthy, J. M.; Appelhans, D.; Tarzelt, J.; Rogers, S. M., Nanomedicine for prion disease treatment. *Prion* **2013,** 7, 198-202.

(260) McGlinchey, R. P.; Shewmaker, F.; McPhie, P.; Monterroso, B.; Thurber, K.; Wickner, R. B., The repeat domain of the melanosome fibril protein Pmel17 forms the amyloid core promoting melanin synthesis. *Proc. Natl. Acad. Sci. U.S.A.* **2009,** *106*, 13731-13736.

(261) Meier, J. J.; Kayed, R.; Lin, C.-Y.; Gurlo, T.; Haataja, L.; Jajasinghe, S.; Langen, R.; Glabe, C. G.; Butler, P. C., Inhibition of human IAPP fibril formation does not prevent β-cell death: evidence for distinct actions of oligomers and fibrils of human IAPP. *Am. J. Physiol. Endocrinol. Metab.* **2006,** *291*, E1317-E1324.

(262) Meijnikman, A. S.; Gerdes, V. E.; Nieuwdorp, M.; Herrema, H., Evaluating Causality of Gut Microbiota in Obesity and Diabetes in Humans. *Endocr. Rev.* **2018,** *39*, 133-153.

(263) Mendis, S. *Global status report on noncommunicable diseases 2014*; World Health Organisation: Geneva, **2014.**

(264) Meng, F.; Abedini, A.; Song, B.; Raleigh, D. P., Amyloid Formation by Pro-Islet Amyloid Polypeptide Processing Intermediates: Examination of the Role of Protein Heparan Sulfate Interactions and Implications for Islet Amyloid Formation in Type 2 Diabetes. *Biochemistry* **2007,** *46*, 12091-12099.

(265) Meng, F.; Marek, P.; Potter, K. J.; Verchere, C. B.; Raleigh, D. P., Rifampicin Does Not Prevent Amyloid Fibril Formation by Human Islet Amyloid Polypeptide but Does Inhibit Thioflavin-T Interactions: Implications for Mechanistic Studies of *β*-cell Death. *Biochemistry* **2008,** *47*, 6016-6024.

(266) Mi, W.; Pawlik, M.; Sastre, M.; Jung, S. S.; Radvinsky, D. S.; Klein, A. M.; Sommer, J.; Schmidt, S. D.; Nixon, R. A.; Mathews, P. M.; Levy, E., Cystatin C inhibits amyloid-β deposition in Alzheimer's disease mouse models. *Nat. Genet.* **2007,** *39*, 1440-1442.

(267) Mietlick-Baase, E. G., Amylin-mediated control of glycemia, energy balance, and cognition. *Physiol. Behav.* **2016,** *162*, 130-140.

(268) Mirzabekov, T. A.; Lin, M.-C.; Kagan, B. L., Pore Formation by the Cytotoxic Islet Amyloid Peptide Amylin. *J. Biol. Chem.* **1996,** *271*, 1988-1992.

(269) Moghimi, S. M.; Hunter, A. C.; Murray, J. C., Long-Circulating and Target-Specific Nanoparticles: Theory to Practice. *Pharmacol. Rev.* **2001,** *53*, 283-318.

(270) Moir, R. D.; Lathe, R.; Tanzi, R. E., The antimicrobial protection hypothesis of Alzheimer's disease. *Alzheimers Dement.* **2018,** *14*, 1602-1614.

(271) Moores, B.; Drolle, E.; Attwood, S. J.; Simons, J.; Leonenko, Z., Effect of Surfaces on Amyloid Fibril Formation. *PLoS ONE* **2011,** *6*, e25954.

(272) Moreno-Gonzalez, I.; Soto, C., Misfolded Protein Aggregates: Mechanisms, Structures and Potential for Disease Transmission. *Semin. Cell Dev. Biol.* **2011,** *22*, 482-487.

(273) Nakae, T.; Ishii, J.; Tokunaga, M., Subunit Structure of Functional Porin Oligomers That Form Permeability Channels in the Outer Membrane of *Escherichia coli*. *J. Biol. Chem.* **1978,** *254*, 1457-1461.

(274) Nanga, R. P. R.; Brender, J. R.; Vivekanandan, S.; Ramamoorthy, A., Structure and membrane orientation of IAPP in its natively amidated form at physiological pH in a membrane environment. *Biochim. Biophys. Acta* **2011,** *2011*, 2337-2342.

(275) Neelov, I. M.; Janaszewska, A.; Klajnert, B.; Bryszewska, M.; Makova, N. Z.; Hicks, D.; Pearson, H. A.; Vlaslov, G. P.; Ilyash, M. Y.; Dubrovskaya, N. M.; Tumanova, N. L.; Zhuravin, I. A.; Turner, A. J.; Nalivaeva, N. N., Molecular Properties of Lysine Dendrimers and their Interactions with Aβ-Peptides and Neuronal Cells. *Curr. Med. Chem.* **2013,** 20, 134-143.

(276) Nerelius, C.; Gustafsson, M.; Nordling, K.; Larsson, A.; Johansson, J., Anti-Amyloid Activity of the C-Terminal Domain of proSP-C against Amyloid β-Peptide and Medin. *Biochemistry* **2009,** *48*, 3778-3786.

(277) Neuhauser, N.; Michalski, A.; Scheltema, R. A.; Olsen, J. V.; Mann, M., Andromeda: A Peptide Search Engine Integrated Into the MaxQuant Environment. *J. Proteome Res.* **2011,** *10*, 1794-1805.

(278) Nguyen, P. T.; Sharma, R.; Rej, R.; De Carufel, C. A.; Roy, R.; Bourgault, S., Low generation anionic dendrimers modulate islet amyloid polypeptide self-assembly and inhibit pancreatic β-cell toxicity. *RSC Adv.* **2016,** *6*, 76360-76369.

(279) Noble, W.; Hanger, D. P.; Miller, C. C. J.; Lovestone, S., The Importance of Tau Phosphorylation for Neurodegenerative Diseases. *Front. Neurol.* **2013,** *4*, 83.

(280) Nowacka, O.; Shcharbin, D.; Klajnert-Maculewicz, B.; Bryszewska, M., Stabilizing effect of small concentrations of PAMAM dendrimers at the insulin aggregation. *Colloids Surf. B Biointerfaces* **2014,** 116, 757-760.

(281) O'Nuallain, B.; Williams, A. D.; Westermark, P.; Wetzel, R., Seeding Specificity in Amyloid Growth Induced by Heterologous Fibrils. *J. Biol. Chem.* **2004,** *279*, 17490-17499.

(282) Ookoshi, T.; Hasegawa, K.; Ohhashi, Y.; Kimura, H.; Takahashi, N.; Yoshida, H.; Miyazaki, R.; Goto, Y.; Naiki, H., Lysophospholipids induce the nucleation and extension of beta2-microglobulin-related amyloid fibrils at a neutral pH. *Nephrol. Dial. Transplant.* **2008,** *23*, 3247-3255.

(283) Oskarsson, M. E.; Paulsson, J. F.; Schultz, S. W.; Ingelsson, M.; Westermark, P.; Westermark, G. T., *In Vivo* Seeding and Cross-Seeding of Localized Amyloidosis. *Am. J. Pathol.* **2015,** *185*, 834-846.

(284) Oskarsson, M. E.; Singh, K.; Wang, J.; Vlodavsky, I.; Li, J.-P.; Westermark, G. T., Heparan Sulfate Proteoglycans are important for Islet Amyloid Formation and Islet Amyloid Polypeptide-Induced Apoptosis. *J. Biol. Chem.* **2015,** *290*, 15121-15132.

(285) Oslakovic, C.; Cedervall, T.; Linse, S.; Dahlbäck, B., Polystyrene Nanoparticles Affecting Blood Coagulation. *Nanomedicine* **2012,** *8*, 981-986.

(286) Owen, M. C.; Gnutt, D.; Gao, M.; Wärmländer, S. K. T. S.; Jarvet, J.; Gräslund, A.; Winter, R.; Ebbinghaus, S.; Strodel, B., Effects of *in vivo* conditions on amyloid aggregation. *Chem. Soc. Rev.* **2019,** *48,* 3946-3996.

(287) Padrick, S. B.; Miranker, A. D., Islet amyloid: phase partitioning and secondary nucleation are central to the mechanism of fibrillogenesis. *Biochemistry* **2002,** *41*, 4694-4703.

(288) Pansierei, J.; Gerstenmayer, M.; Lux, F.; Mériaux, S.; Tillement, O.; Forge, V.; Larrat, B.; Marquette, C., Magnetic Nanoparticles Applications for Amyloidosis Study and Detection: A Review. *Nanomaterials* **2018,** *8*, 740.

(289) Pansierei, J.; Plissonneau, M.; Stransky-Heilkron, N.; Dumoulin, M.; Heinrich-Balard, L.; Rivory, P.; Morfin, J.-F.; Toth, E.; Saraiva, M. J.; Allémann, E.; Tillement, O.; Forge, V.; Lux, F.; Marquette, C., Multimodal imaging Gd-nanoparticles functionalized with Pittsburgh compound B or a nanobody for amyloid plaques targeting. *Nanomedicine* **2017,** *12*, 1675-1687.

(290) Park, H.; Oh, J.; Shim, G.; Cho, B.; Chang, Y.; Kim, S.; Baek, S.; Kim, H. S.; Shin, J.; Choi, H.; Yoo, J.; Kim, J.; Jun, W.; Lee, M.; Lengner, C.; Oh, Y.-K.; Kim, J., In vivo neuronal gene editing via CRISPR-Cas9 amphiphilic nanocomplexes alleviates deficits in mouse models of Alzheimer's disease. *Nat. Neurosci.* **2019,** *22*, 524-528.

(291) Park, J.-S.; Kim, D.-H.; Yoon, S.-Y., Regulation of amyloid precursor protein processing by its KFERQ motif. *BMB Rep.* **2016,** *49*, 337-342.

(292) Park, Y. J.; Woo, M., Pancreatic β cells: Gatekeepers of type 2 diabetes. *J. Cell Biol.* **2019,** *218,* 1094.

(293) Patil, S. M.; Xu, S.; Sheftic, S. R.; Alexandrescu, A. T., Dynamic α-Helix Structure of Micelle-bound Human Amylin. *J. Biol. Chem.* **2009,** *284*, 11982-11991.

(294) Peinado, J. R.; Sami, F.; Rajpurohit, N.; Lindberg, I., Blockade of islet amyloid polypeptide fibrillation and cytotoxicity by the secretory chaperones 7B2 and proSAAS. *FEBS Lett.* **2013,** *587*, 3406-3411.

(295) Peng, S.; Fitzen, M.; Jörnvall, H.; Johansson, J., The extracellular domain of Bri2 (ITM2B) binds the ABri peptide (1–23) and amyloid β-peptide (Aβ1–40): Implications for Bri2 effects on processing of amyloid precursor protein and Aβ aggregation. *Biochem. Biophys. Res. Commun.* **2010,** *393*, 356-361.

(296) Peng, S.; Glennert, J.; Westermark, P., Medin-amyloid: A recently characterized age-associated arterial amyloid form affects mainly arteries in the upper part of the body. *Amyloid* **2005,** *12*, 96-102.

(297) Peters, T. W.; Rardin, M. J.; Czerwieniec, G.; Evani, U. S.; Reis-Rodrigues, P.; Lithgow, G. J.; Mooney, S. D.; Gibson, B. W.; Hughes, R. E., Tor1 regulates protein solubility in *Saccharomyces cerevisiae*. *Mol. Biol. Cell* **2012,** *23*, 4679-4688.

(298) Peterson, S. A.; Klabunde, T.; Lashuel, H. A.; Purkey, H.; Sacchettini, J. C.; Kelly, J. W., Inhibiting transthyretin conformational changes that lead to amyloid fibril formation. *Proc. Natl. Acad. Sci. U.S.A.* **1998,** 95, 12956-12960.

(299) Pilkington, E. H.; Gurzov, E. N.; Käkinen, A.; Litwak, S. A.; Stanley, W. J.; Davis, T. P.; Ke, P. C., Pancreatic β-Cell Membrane Fluidity and Toxicity Induced by Human Islet Amyloid Polypeptide Species. *Sci. Rep.* **2016,** *6,* 21274.

(300) Pilkington, E. H.; Gustafsson, O. J. R.; Xing, Y.; Hernandez-Fernaud, J.; Zampronio, C.; Käkinen, A.; Faridi, A.; Ding, F.; Wilson, P.; Ke, P. C.; Davis, T. P., Profiling the Serum Protein Corona of Fibrillar Human Islet Amyloid Polypeptide. *ACS Nano* **2018,** *12*, 6066-6078.

(301) Pilkington, E. H.; Lai, M.; Ge, X.; Stanley, W. J.; Wang, B.; Wang, M.; Käkinen, A.; Sani, M.-A.; Whittaker, M. R.; Gurzov, E. N.; Ding, F.; Quinn, J. F.; Davis, T. P.; Ke, P. C., Star Polymers Reduce Islet Amyloid Polypeptide Toxicity via Accelerated Amyloid Aggregation. *Biomacromolecules* **2017,** *18*, 4249-4260.

(302) Pilkington, E. H.; Xing, Y.; Wang, B.; Käkinen, A.; Wang, M.; Davis, T. P.; Ding, F.; Ke, P. C., Effects of Protein Corona on IAPP Amyloid Aggregation, Fibril Remodelling, and Cytotoxicity. *Sci. Rep.* **2017,** *7*, 2455.

(303) Pillay, K.; Govender, P., Amylin Uncovered: A Review on the Polypeptide Responsible for Type II Diabetes. *Biomed Res. Int.* **2013,** *2013*, 826706.

(304) Pisani, C.; Gaillard, J.-C.; Odorico, M.; Nyalosaso, J. L.; Charnay, C.; Guari, Y.; Chopineau, J.; Devoisselle, J.-M.; Armengaud, J.; Prat, O., The Timeline of Corona Formation Around Silica Nanocarriers Highlights the Role of the Protein Interactome. *Nanoscale* **2017,** *9*, 1840-1851.

(305) Poduslo, J. F.; Hultman, K. L.; Curran, G. L.; Preboske, G. M.; Chamberlain, R.; Marjanska, M.; Garwood, M.; Jack Jr., C. R.; Wengenack, T. M., Targeting vascular amyloid in arterioles of Alzheimer disease transgenic mice with amyloid β protein antibody-coated nanoparticles. *J. Neuropathol. Exp. Neurol.* **2011,** *70*, 653-661.

(306) Ponomarenko, E. A.; Poverennaya, E. V.; Ilgisonis, E. V.; Pyatnitskiy, M. A.; Kopylov, A. T.; Zgoda, V. G.; Lisitsa, A. V.; Archakov, A. I., The Size of the Human Proteome: The Width and Depth. *Int. J. Anal. Chem.* **2016,** *2016*, 7436849.

(307) Porat, Y.; Kolusheva, S.; Jelinek, R.; Gazit, E., The Human Islet Amyloid Polypeptide Forms Transient Membrane-Active Prefibrillar Assemblies. *Biochemistry* **2003,** *42*, 10971-10977.

(308) Press, M.; Jung, T.; König, J.; Grune, T.; Höne, A., Protein aggregates and proteostasis in aging: Amylin and β-cell function. *Mech. Ageing Dev.* **2019,** *177*, 46-54.

(309) Pyle, E.; Kalli, A. C.; Amillis, S.; Hall, Z.; Lau, A. M.; Hanyaloglu, A. C.; Diallinas, G.; Byrne, B.; Politis, A., Structural Lipids Enable the Formation of Functional Oligomers of the Eukaryotic Purine Symporter UapA. *Cell Chem. Biol.* **2018,** *25*, 840-848.

(310) Qiao, R.; Ke, P. C., Lipid-Carbon Nanotube Self-Assembly in Aqueous Solution. *J. Am. Chem. Soc.* **2006,** *128*, 13656-13657.

(311) Qin, J.; Cho, M.; Lee, Y., Ultrasensitive Detection of Amyloid-β Using Cellular Prion Protein on the Highly Conductive Au Nanoparticles–Poly(3,4-ethylene dioxythiophene)–Poly(thiophene-3-acetic acid) Composite Electrode. *Anal. Chem.* **2019,** *91*, 11259-11265.

(312) Qiu, W. Q.; Wallack, M.; Dean, M.; Liebson, E.; Mwamburi, M.; Zhu, H., Association between Amylin and Amyloid-β Peptides in Plasma in the Context of Apolipoprotein E4 Allele. *PLoS ONE* **2014,** *9*, e88063.

(313) Quist, A.; Doudevski, I.; Lin, H.; Azimova, R.; Ng, D.; Frangione, B.; Kagan, B.; Ghiso, J.; Lal, R., Amyloid ion channels: A common structural link for protein-misfolding disease. *Proc. Natl. Acad. Sci. U.S.A.* **2005,** *102*, 10427-10432.

(314) R Core Team, R: A Language and Environment for Statistical Computing. https://www.R-project.org/ (accessed Feb 19, 2018).

(315) Radic, S.; Davis, T. P.; Ke, P. C.; Ding, F., Contrasting effects of nanoparticle-protein attraction on amyloid aggregation. *RSC Adv.*, **2015,** 5, 105489-105498 (2015)

(316) Rahman, M.; Zetterberg, H.; Lendel, C.; Härd, T., Binding of Human Proteins to Amyloid-β Protofibrils. *ACS Chem. Biol.* **2015,** *10*, 766-774.

(317) Raleigh, D.; Zhang, X.; Hastoy, B.; Clark, A., The β-Cell Assassin: IAPP Cytotoxicity. *J. Mol. Endocrinol.* **2017,** *59*, R121-R140.

(318) Raman, B.; Ban, T.; Sakai, M.; Pasta, S. Y.; Ramakrishna, T.; Naiki, H.; Goto, Y.; Rao, C. M., αB-crystallin, a small heat-shock protein, prevents the amyloid fibril growth of an amyloid β-peptide and β2-microglobulin. *Biochem. J.* **2005,** *392*, 573-581.

(319) Rappsilber, J.; Mann, M.; Ishihama, Y., Protocol for Micro-Purification, Enrichment, Pre-Fractionation and Storage of Peptides for Proteomics Using StageTips. *Nat. Protoc.* **2007,** *8*, 1896-1906.

(320) Rawat, A.; Maity, B. K.; Chandra, B.; Maiti, S., Aggregation-induced conformation changes dictate islet amyloid polypeptide (IAPP) membrane affinity. *Biochim. Biophys. Acta* **2018,** *1860*, 1734-1740.

(321) Reches, M.; Gazit, E., Casting metal nanowires within discrete self-assembled peptide nanotubes. *Science* **2003,** *300*, 625-627.

(322) Ren, J. M.; McKenzie, T. G.; Fu, Q.; Wong, E. H. H.; Xu, J.; An, Z.; Shanmugam, S.; Davis, T. P.; Boyer, C.; Qiao, G. C., Star Polymers. *Chem. Rev.* **2016,** *116*, 6743-6836.

(323) Reumers, J.; Maurer-Stroh, S.; Schymkowitz, J.; Rousseau, F., Protein sequences encode safeguards against aggregation. *Hum. Mutat.* **2009,** *30*, 431-437.

(324) Rezaei-Ghaleh, N.; Amininasab, M.; Kumar, S.; Walter, J.; Zweckstetter, M., Phosphorylation modifies the molecular stability of β-amyloid deposits. *Nat. Commun.* **2016,** *7*, 11359.

(325) Ritzel, R. A.; Meier, J. J.; Lin, C.-Y.; Veldhuis, J. D.; Butler, P. C., Human Islet Amyloid Polypeptide Oligomers Disrupt Cell Coupling, Induce Apoptosis, and Impair Insulin Secretion in Isolated Human Islets. *Diabetes* **2007,** *56*, 65-71.

(326) Rogers, J. T.; Randall, J. D.; Cahill, C. M.; Eder, P. S.; Huang, X.; Gunshin, H.; Leiter, L.; McPhee, J.; Sarang, S. S.; Utsuki, T.; Greig, N. H.; Lahiri, D. K.; Tanzi, R. E.; Bush, A. I.; Giordani, T.; Gullans, S. R., An iron-responsive element type II in the 5'-untranslated region of the Alzheimer's amyloid precursor protein transcript. *J. Biol. Chem.* **2002,** *277*, 45518-45528.

(327) Romero, D.; Kolter, R., Functional amyloids in bacteria. *Int. Microbiol.* **2014,** *17*, 65-73.

(328) Rosas, P. C.; Nagaraja, G. M.; Kaur, P.; Panossia, A.; Wickman, G.; Garcia, L. R.; Al-Khamis, F. A.; Asea, A. A. A., Hsp72 (HSPA1A) Prevents Human Islet Amyloid Polypeptide Aggregation and Toxicity: A New Approach for Type 2 Diabetes Treatment. *PLoS ONE* **2016,** *11*, e0149409.

(329) Rothe, S.; Prakash, A.; Tyedmers, J., The Insoluble Protein Deposit (IPOD) in Yeast. *Front. Mol. Neurosci.* **2018,** *11*, 237.

(330) Rousseau, F.; Schymkowitz, J.; Serrano, L., Protein aggregation and amyloidosis: confusion of the kinds? *Curr. Opin. Struct. Biol.* **2006,** *16*, 118-126.

(331) Sade, D.; Shaham-Niv, S.; Arnon, Z. A.; Tavassoly, O.; Gazit, E., Seeding of proteins into amyloid structures by metabolite assemblies may clarify certain unexplained epidemiological associations. *Open Biol.* **2018,** *8*, 170229.

(332) Sadik, G.; Tanaka, T.; Kato, K.; Yamamori, H.; Nessa, B. N.; Morihara, T.; Takeda, M., Phosphorylation of tau at Ser214 mediates its interaction with 14-3-3 protein: implications for the mechanism of tau aggregation. *J. Neurochem.* **2009,** *108*, 33-43.

(333) Sakagashira, S.; Hiddinga, H. J.; Tateishi, K.; Sanke, T.; Hanabusa, T.; Nanjo, K.; Eberhardt, N. L., S20G Mutant Amylin Exhibits Increased *in Vitro* Amyloidogenicity and Increased Intracellular Cytotoxicity Compared to Wild-Type Amylin. *Am. J. Pathol.* **2000,** *157*, 2101-2109.

(334) Sanati, M.; Khodagholi, F.; Ghasemi, F.; Gholami, M.; Kebriaeezadeh, A.; Sabzevari, O.; Hajipour, M. J.; Imani, M.; Mahmoudi, M.; Sharifzadeh, M., Impact of Gold Nanoparticles on Amyloid β-Induced Alzheimer's Disease in a Rat Animal Model: Involvement of STIM Proteins. *ACS Chem. Neurosci.* **2019,** *10*, 2299-2309.

(335) Sanke, T.; Hanabusa, T.; Nakano, Y.; Oki, C.; Okai, K.; Nishimura, S.; Kondo, M.; Nanjo, K., Plasma Islet Amyloid Polypeptide (Amylin) Levels and Their Responses to Oral Glucose in Type 2 (Non-Insulin-Dependent) Diabetic Patients. *Diabetologia* **1991,** *34*, 129-132.

(336) Saptarshi, S. R.; Duschi, A.; Lopata, A. L., Interaction of nanoparticles with proteins: relation to bio-reactivity of the nanoparticle. *J. Nanobiotechnol.* **2013,** *11,* No. 26.

(337) Sasahara, K.; Morigaki, K.; Shinya, K., Amyloid aggregation and deposition of human islet amyloid polypeptide at membrane interfaces. *FEBS J.* **2014,** *281*, 2597-2612.

(338) Scherbaum, W. A., The role of amylin in the physiology of glycemic control. *Exp. Clin. Endocrinol. Diabetes* **1998,** *106*, 97-102.

(339) Schmitz, O.; Brock, B.; Rungby, J., Amylin Agonists: A Novel Approach in the Treatment of Diabetes. *Diabetes* **2004,** *53*, S233-S238.

(340) Schubert, D.; Behl, C.; Lesley, R.; Brack, A.; Dargusch, R.; Sagara, Y.; Kimura, H., Amyloid peptides are toxic via a common oxidative mechanism. *Proc. Natl. Acad. Sci. U.S.A.* **1995,** *92*, 1989-1993.

(341) Sciacca, M. F. M.; Milardi, D.; Messina, G. M. L.; Marletta, G.; Brender, J. R.; Ramamoorthy, A.; La Rosa, C., Cations as Switches of Amyloid-Mediated Membrane Disruption Mechanisms: Calcium and IAPP. *Biophys. J.* **2013,** *104*, 173-184.

(342) Seeliger, J.; Weise, K.; Opitz, N.; Winter, R., The effect of Aβ on IAPP aggregation in the presence of an isolated β-cell membrane. *J. Mol. Biol.* **2012,** *421*, 348-363.

(343) Seino, S.; Study Group of Comprehensive Analysis of Genetic Factors in Diabetes Mellitus, T., S20G mutation of the amylin gene is associated with Type II diabetes in Japanese. *Diabetologia* **2001,** *44*, 906-909.

(344) Serebryany, E.; Woodard, J. C.; Adkar, B. V.; Shabab, M.; King, J. A.; Shakhnovich, E. I., An Internal Disulfide Locks a Misfolded Aggregation-prone Intermediate in Cataract-linked Mutants of Human γD-Crystallin. *J. Biol. Chem.* **2016,** *291*, 19172-19183.

(345) Serpooshan, V.; Mahmoudi, M.; Zhao, M.; Wei, K.; Sivanesan, S.; Motamedchaboki, K.; Malkovskiy, A. V.; Goldstone, A. B.; Cohen, J. E.; Yang, P. C.; Rajadas, J.; Bernstein, D.; Woo, Y. J.; Ruiz-Lozano, P., Protein Corona Influences Cell–Biomaterial Interactions in Nanostructured Tissue Engineering Scaffolds. *Adv. Funct. Mater.* **2015,** *25*, 4379-4389.

(346) Sheikh, A. M.; Michikawa, M.; Kim, S. U.; Nagai, A., Lysophosphatidylcholine increases the neurotoxicity of Alzheimer's amyloid β1-42 peptide: Role of oligomer formation. *Neuroscience* **2015,** *292*, 159-169.

(347) Sheikh, A. M.; Nagai, A., Lysophosphatidylcholine modulates fibril formation of amyloid beta peptide. *FEBS J.* **2011,** *278*, 634-642.

(348) Shen, Y.; Posavec, L.; Bolisetty, S.; Hilty, F. M.; Nyström, G.; Kohlbrecher, J.; Hilbe, M.; Rossi, A.; Baumgartner, J.; Zimmermann, M. B.; Mezzenga, R., Amyloid fibril systems reduce, stabilize and deliver bioavailable nanosized iron. *Nat. Nanotechnol.* **2017,** *12*, 642-647.

(349) Shtilerman, M. D.; Ding, T. D.; Lansbury, P. T., Molecular Crowding Accelerates Fibrillization of α-Synuclein: Could an Increase in the Cytoplasmic Protein Concentration Induce Parkinson's Disease? *Biochemistry* **2002,** *41*, 3855-3860.

(350) Siekierska, A.; De Baets, G.; Reumers, J.; Gallardo, R.; Rudyak, S.; Broersen, K.; Couceiro, J.; Van Durme, J.; Schymkowitz, J.; Rousseau, F., α-Galactosidase Aggregation Is a Determinant of Pharmacological Chaperone Efficacy on Fabry Disease Mutants. *J. Biol. Chem.* **2012,** *287*, 28386-28397.

(351) Sipe, J. D.; Benson, M. D.; Buxbaum, J. N.; Ikeda, S.-I.; Merlini, G.; Saraiva, M. J. M.; Westermark, P., Nomenclature 2014: Amyloid fibril proteins and clinical classification of the amyloidosis. *Amyloid* **2014,** *21*, 221-224.

(352) Smith, C. A.; Want, E. J.; O'Maille, G.; Abagyan, R.; Siuzdak, G., XCMS: Processing Mass Spectrometry Data for Metabolite Profiling Using Nonlinear Peak Alignment, Matching, and Identification. *Anal. Chem.* **2006,** *78*, 779-787.

(353) Smith, D. P.; Ciccotosto, G. D.; Tew, D. J.; Fodero-Tavoletti, M. T.; Johanssen, T.; Masters, C. L.; Barnham, K. J.; Cappai, R., Concentration Dependent Cu^{2+} Induced Aggregation and Dityrosine Formation of the Alzheimer's Disease Amyloid-β Peptide. *Biochemistry* **2007,** *46*, 2881-2891.

(354) Solassol, J.; Crozet, C.; Perrier, V.; Leclaire, J.; Béranger, F.; Caminade, A.-M.; Meunier, B.; Dormont, D.; Majoral, J.-P.; Lehmann, S., Cationic phosphorus-containing dendrimers reduce prion replication both in cell culture and in mice infected with scrapie. *J. Gen. Virol.* **2004,** 85, 1791-1799.

(355) Soldi, G.; Bemporad, F.; Torrassa, S.; Relini, A.; Ramazzotti, M.; Taddei, N.; Chiti, F., Amyloid Formation of a Protein in the Absence of Initial Unfolding and Destabilization of the Native State. *Biophys. J.* **2005,** *89*, 4234-4244.

(356) Sonawane, S. K.; Ahmad, A.; Chinnathambi, S., Protein-Capped Metal Nanoparticles Inhibit Tau Aggregation in Alzheimer's Disease. *ACS Omega* **2019,** *4*, 12833-12840.

(357) Song, Q.; Huang, M.; Yao, L.; Wang, X.; Gu, X.; Chen, J.; Chen, J.; Huang, J.; Hu, Q.; Kang, T.; Rong, Z.; Qi, H.; Zheng, G.; Chen, H.; Gao, X., Lipoprotein-Based Nanoparticles Rescue the Memory Loss of Mice with Alzheimer's Disease by Accelerating the Clearance of Amyloid-Beta. *ACS Nano* **2014,** *8*, 2345-2359.

(358) Sörgjerd, K. M.; Zako, T.; Sakono, M.; Stirling, P. C.; Leroux, M. R.; Saito, T.; Nilsson, P.; Sekimoto, M.; Saido, T. C.; Maeda, M., Human Prefoldin Inhibits Amyloid-β (Aβ) Fibrillation and Contributes to Formation of Nontoxic Aβ Aggregates. *Biochemistry* **2013,** *52*, 3532-3542.

(359) Sorokina, S. A.; Stroylova, Y. Y.; Shifrina, Z. B.; Muronetz, V. I., Disruption of Amyloid Prion Protein Aggregates by Cationic Pyridylphenylene Dendrimers. *Macromol. Biosci.* **2016,** 16, 266-275.

(360) Sorrentino, V.; Romani, M.; Mouchiroud, L.; Beck, J. S.; Zhang, H.; D'Amico, D.; Moullan, N.; Potenza, F.; Schmid, A. W.; Rietsch, S.; Counts, S. E.; Auwerx, J., Enhancing mitochondrial proteostasis reduces amyloid-β proteotoxicity. *Nature* **2017,** *552*, 187-193.

(361) Sparr, E.; Engel, M. F. M.; Sakharov, D. V.; Sprong, M.; Jacobs, J.; de Kruijff, B.; Höppener, J. W. M.; Killian, J. A., Islet Amyloid Polypeptide-Induced Membrane Leakage Involves Uptake of Lipids by Forming Amyloid Fibres. *FEBS Lett.* **2004,** *577*, 117-120.

(362) Srodulski, S.; Sharma, S.; Bachstetter, A. B.; Brelsford, J. M.; Pascual, C.; Xie, X. S.; Saatman, K. E.; Van Eldik, L. J.; Despa, F., Neuroinflammation and neurologic deficits in diabetes linked to brain accumulation of amylin. *Mol. Neurodegener.* **2014,** *9,* 30.

(363) Stanley, W. J.; Litwak, S. A.; Quah, H. S.; Tan, S. M.; Kay, T. W.; Tiganis, T.; de Haan, J. B.; Thomas, H. E.; Gurzov, E. N., Inactivation of Protein Tyrosine Phosphatases Enhances Interferon Signaling in Pancreatic Islets. *Diabetes*, **2015,** *64,* 2489-2496.

(364) Stanyon, H. F.; Viles, J. H., Human Serum Albumin Can Regulate Amyloid-β Peptide Fiber Growth in the Brain Interstitium. *J. Biol. Chem.* **2012,** *2012*, 28163-28168.

(365) Stine, W. B.; Dahlgren, K. N.; Krafft, G. A.; LaDu, M. J., *In Vitro* Characterization of Conditions for Amyloid-β Peptide Oligomerization and Fibrillogenesis. *J. Biol. Chem.* **2003,** *278*, 11612-11622.

(366) Stine, W. B.; Jungbauer, L.; Yu, C.; LaDu, M. J., Preparing Synthetic Aβ in Different Aggregation States. *Methods Mol. Biol.* **2011,** *670*, 13-32.

(367) Sun, Y.; Käkinen, A.; Xing, Y.; Pilkington, E. H.; Davis, T. P.; Ke, P. C.; Ding, F., Nucleation of β-rich oligomers and β-barrels in the early aggregation of human islet amyloid polypeptide. *Biochim. Biophys. Mol. Basis Dis.* **2019,** *1865*, 434-444.

(368) Supattapone, S.; Nguyen, H.-O. B.; Cohen, F. E.; Prusiner, S. B.; Scott, M. R., Elimination of prions by branched polyamines and implications for therapeutics. *Proc. Natl. Acad. Sci. U.S.A.* **1999,** 96, 14529-14534.

(369) Supattapone, S.; Wille, H.; Uyechi, L.; Sarfar, J.; Tremblay, P.; Szoka, F. C.; Cohen, F. E.; Prusiner, S. B.; Scott, M. R., Branched Polyamines Cure Prion-Infected Neuroblasoma Cells. *J. Virol.* **2001,** 75, 3453-3461.

(370) Szklarczyk, D.; Franceschini, A.; Wyder, S.; Forslund, K.; Heller, D.; Huerta-Cepas, J.; Simonovic, M.; Roth, A.; Santos, A.; Tsafou, K. P.; Kuhn, M.; Bork, P.; Jensen, L. J.; von Mering, C., STRING v10: Protein-Protein Interaction Networks, Integrated Over the Tree of Life. *Nucleic Acids Res.* **2015,** *43*, D447-D452.

(371) Szklarczyk, D.; Morris, J. H.; Cook, H.; Kuhn, M.; Wyder, S.; Simonovic, M.; Santos, A.; Doncheva, N. T.; Roth, A.; Bork, P.; Jensen, L. J.; von Mering, C., The STRING Database in 2017: Quality-Controlled Protein–Protein Association Networks, Made Broadly Accessible. *Nucleic Acids Res.* **2017,** *45*, D362-D368.

(372) Tamamis, P.; Adler-Abramovich, L.; Reches, M.; Marshall, K.; Sikorski, P.; Serpell, L.; Gazit, E.; Archontis, G., Self-Assembly of Phenylalanine Oligopeptides: Insights from Experiments and Simulations. *Biophys. J.* **2009,** *96*, 5020-5029.

(373) Tang, F.; Li, L.; Chen, D., Mesoporous Silica Nanoparticles: Synthesis, Biocompatibility and Drug Delivery. *Adv. Mater.* **2012,** *24*, 1504-1534.

(374) Teo, J.; McCarroll, J. A.; Boyer, C.; Youkhana, J.; Sagnella, S. M.; Duong, H. T. T.; Liu, J.; Sharbeen, G.; Goldstein, D.; Davis, T. P.; Kavallaris, M.; Phillips, A. P., A Rationally Optimized Nanoparticle System for the Delivery of RNA Interference Therapeutics into Pancreatic Tumors in Vivo. *Biomacromolecules* **2016,** *17*, 2337-2351.

(375) Törnquist, M.; Michaels, T. C. T.; Sanagavarapu, K.; Yang, X.; Meisl, G.; Cohen, S. I. A.; Knowles, T. P. J.; Linse, S., Secondary nucleation in amyloid formation. *Chem. Commun.* **2018,** *54*, 8667-8684.

(376) Trigo, D.; Nadais, A.; da Cruz e Silva, O. A. B., Unravelling protein aggregation as an ageing related process or a neuropathological response. *Ageing Res. Rev.* **2019,** *51*, 67-77.

(377) Tuttle, M. D.; Comellas, G.; Nieuwkoop, A. J.; Covell, D. J.; Berthold, D. A.; Kloepper, K. D.; Courtney, J. M.; Kim, J. K.; Barclay, A. M.; Kendall, A.; Wan, W.; Stubbs, G.; Schwieters, C. D.; Lee, V. M. Y.; George, J. M.; Rienstra, C. M., Solid-State NMR Structure of a Pathogenic Fibril of Full-Length Human α-Synuclein. *Nat. Struc. Mol. Biol.* **2016,** *23*, 409-415.

(378) Umahara, T.; Uchihara, T.; Tsuchiya, K.; Nakamura, A.; Iwamoto, T.; Ikeda, K.; Takasaki, M., 14-3-3 proteins and zeta isoform containing neurofibrillary tangles in patients with Alzheimer's disease. *Acta Neuropathol.* **2004,** *108*, 279-286.

(379) Usov, I.; Mezzenga, R., FiberApp: An Open-Source Software for Tracking and Analyzing Polymers, Filaments, Biomacromolecules and Fibrous Objects. *Macromolecules* **2015,** *48*, 1269-1280.

(380) Uversky, V. N.; Cooper, M. E.; Bower, K. S.; Li, J.; Fink, A. L., Accelerated α-synuclein fibrillation in crowded milieu. *FEBS Lett.* **2002,** *515*, 99-103.

(381) Vaiana, S. M.; Ghirlando, R.; Yau, W.-M.; Eaton, W. A.; Hofrichter, J., Sedimentation Studies on Human Amylin Fail to Detect Low-Molecular-Weight Oligomers. *Biophys. J.* **2008,** *94*, L45-L47.

(382) Van der Munnik, N. P.; Moss, M. A.; Uline, M. J., Obstacles to translating the promise of nanoparticles into viable amyloid disease therapeutics. *Phys. Biol.* **2019,** *16*, 021002.

(383) van Diggelen, F.; Tepper, A. W. J. W.; Apetri, M. M.; Otzen, D. E., α-Synuclein Oligomers: A Study in Diversity. *Isr. J. Chem.* **2016,** *57*, 699-723.

(384) Vetri, V.; Foderà, V., The route to protein aggregate superstructures: Particulates and amyloid-like spherulites. *FEBS Lett.* **2015,** *589*, 2448-2463.

(385) Vidal, J.; Verchere, C. B.; Andrikopoulos, S.; Wang, F.; Hull, R. L.; Cnop, M.; Olin, K. L.; LeBoeuf, R. C.; O'Brien, K. D.; Chait, A.; Kahn, S. E., The Effect of Apolipoprotein E Deficiency on Islet Amyloid Deposition in Human Islet Amyloid Polypeptide Transgenic Mice. *Diabetologia* **2003,** *46*, 71-79.

(386) Viles, J. H., Metal ions and amyloid fiber formation in neurodegenerative diseases. Copper, zinc and iron in Alzheimer's, Parkinson's and prion diseases. *Coord. Chem. Rev.* **2012,** *256*, 2271-2284.

(387) Vogiatzi, T.; Xilouri, M.; Vekrellis, K.; Stefanis, L., Wild Type α-Synuclein Is Degraded by Chaperone-mediated Autophagy and Macroautophagy in Neuronal Cells. *J. Biol. Chem.* **2008,** *283*, 23542-23556.

(388) Wadghiri, Y. Z.; Sigurdsson, E. M.; Sadowski, M.; Elliott, J. I.; Li, Y.; Scholtzova, H.; Tang, C. Y.; Aguinaldo, G.; Pappolla, M.; Duff, K.; Wisniewski, T.; Turnbull, D. H., Detection of Alzheimer's amyloid in transgenic mice using magnetic resonance microimaging. *Magn. Res. Med.* **2003,** *50*, 293-302.

(389) Wadman, M.; Servick, K., Alzheimer's drug resurrected, as company claims clinical benefits. *Science* **2019**.

(390) Walkey, C. D.; Chan, C. W., Understanding and Controlling the Interaction of Nanomaterials With Proteins in a Physiological Environment. *Chem. Soc. Rev.* **2012,** *41*, 2780-2799.

(391) Walsh, D. M.; Selkoe, D. J., Aβ Oligomers - a decade of discovery. *J. Neurochem.* **2007,** *101*, 1172-1184.

(392) Wang, B.; Geitner, N. K.; Davis, T. P.; Ke, P. C.; Ladner, D. L.; Ding, F., Deviation from the Unimolecular Micelle Paradigm of PAMAM Dendrimers Induced by Strong Interligand Interactions *J. Phys. Chem. C,* **2015,** 119, 19475-19484.

(393) Wang, B.; Pilkington, E. H.; Sun, Y.; Davis, T. P.; Ke, P. C.; Ding, F., Modulating protein amyloid aggregation with nanomaterials. *Environ. Sci. Nano*, **2017,** 4, 1772-1783.

(394) Wang, J.; Liu, L.; Ge, D.; Zhang, H.; Feng, Y.; Zhang, Y.; Chen, M.; Dong, M., Differential Modulating Effect of MoS_2 on Amyloid Peptide Assemblies. *Chem. Eur. J.* **2018,** *24*, 3397-3402.

(395) Wang, M.; Käkinen, A.; Pilkington, E. H.; Davis, T. P.; Ke, P. C., Differential Effects of Silver and Iron Oxide Nanoparticles on IAPP Aggregation and Toxicity. *Biomater. Sci.* **2017,** *5*, 485-493.

(396) Wang, M.; Sun, Y.; Cao, X.; Peng, G.; Javed, I.; Käkinen, A.; Davis, T. P.; Lin, S.; Liu, J.; Ding, F.; Ke, P. C., Graphene quantum dots against human IAPP aggregation and toxicity *in vivo*. *Nanoscale* **2018,** *10*, 19995-20006.

(397) Wang, X.; Zhou, Y.; Ren, J.-J.; Hammer, N. D.; Chapman, M. R., Gatekeeper residues in the major curlin subunit modulate bacterial amyloid fiber biogenesis. *Proc. Natl. Acad. Sci. U.S.A.* **2010,** *107*, 163-168.

(398) Wang, Y.; Mandelkow, E., Degradation of tau protein by autophagy and proteasomal pathways. *Biochem. Soc. Trans.* **2012,** *40*, 644-652.

(399) Weids, A. J.; Ibstedt, S.; Tamás, M. J.; Grant, C. M., Distinct stress conditions result in aggregation of proteins with similar properties. *Sci. Rep.* **2016,** *6*, 24554.

(400) Westermark, P.; Andersson, A.; Westermark, G. T., Islet Amyloid Polypeptide, Islet Amyloid, and Diabetes Mellitus. *Physiol. Rev.* **2011,** *91*, 795-826.

(401) Westermark, P.; Li, Z.-C.; Westermark, G. T.; Leckström, A.; Steiner, D. F., Effects of beta cell granule components on human islet amyloid polypeptide fibril formation. *FEBS Lett.* **1996,** *379*, 203-206.

(402) Westermark, P.; Skinner, M.; Cohen, A. S., The P-Component of Amyloid of Human Islets of Langerhans. *Scand. J. Immunol.* **1975,** *4*, 95-97.

(403) Wickham, H. ggplot2: Elegant Graphics for Data Analysis. http://ggplot2.org.

(404) Wilhelmus, M. M. M.; Boelens, W. C.; Otte-Höller, I.; Kamps, B.; de Waal, R. M. W.; Verbeek, M. M., Small heat shock proteins inhibit amyloid-β protein aggregation and cerebrovascular amyloid-β protein toxicity. *Brain Res.* **2006,** *1089*, 67-78.

(405) Willander, H.; Presto, J.; Askarieh, G.; Biverstal, H.; Frohm, B.; Knight, S. D.; Johansson, J.; Linse, S., BRICHOS domains efficiently delay fibrillation of amyloid β-peptide. *J. Biol. Chem.* **2012,** *287*, 31608-31617.

(406) Wojtas, A. M.; Kang, S. S.; Olley, B. M.; Gatherer, M.; Shinohara, M.; Loranzo, P. A.; Liu, C. C.; Kurti, A.; Baker, K. E.; Dickson, D. W.; Yue, M.; Petrucelli, L.; Bu, G.; Carare, R. O.; Fryer, J. D., Loss of Clusterin Shifts Amyloid Deposition to the Cerebrovasculature *via* Disruption of Perivascular Drainage Pathways. *Proc. Natl. Acad. Sci. U.S.A.* **2017,** *114*, E6962-E6971.

(407) Woodruff, J. B.; Hyman, A. A.; Boke, E., Organization and Function of Non-dynamic Biomolecular Condensates. *Trends Biochem. Sci.* **2018,** *43*, 81-94.

(408) Wördehoff, M. M.; Bannach, O.; Shaykhalishahi, H.; Kulawik, A.; Schiefer, S.; Willbold, D.; Hoyer, W.; Birkmann, E., Single Fibril Growth Kinetics of α-Synuclein. *J. Mol. Biol.* **2015,** *427*, 1428-1435.

(409) Wu, Y.; Hudson, J. S.; Lu, Q.; Moore, J. M.; Mount, A. S.; Rao, A. M.; Alexov, E.; Ke, P. C., Coating Single-Walled Carbon Nanotubes with Phospholipids. *J. Phys. Chem. B* **2006,** *110*, 2475-2478.

(410) Xing, Y.; Pilkington, E. H.; Wang, M.; Nowell, C. J.; Käkinen, A.; Sun, Y.; Wang, B.; Davis, T. P.; Ding, F.; Ke, P. C., Lysophosphatidylcholine modulates the aggregation of human islet amyloid polypeptide. *Phys. Chem. Chem. Phys.* **2017,** *19*, 30627-30635.

(411) Xu, J.; Reumers, J.; Couceiro, J. R.; De Smet, F.; Gallardo, R.; Rudyak, S.; Cornelis, A.; Rozenski, J.; Zwolinska, A.; Marine, J.-C.; Lambrechts, D.; Suh, Y.-A.; Rousseau, F.; Schymkowitz, J., Gain of function of mutant p53 by coaggregation with multiple tumor suppressors. *Nat. Chem. Biol.* **2011,** *7*, 285-295.

(412) Yamamoto, S.; Hasegawa, K.; Yamaguchi, I.; Tsutsumi, S.; Kardos, J.; Goto, Y.; Gejyo, F.; Naiki, H., Low Concentrations of Sodium Dodecyl Sulfate Induce the Extension of β2-Microglobulin-Related Amyloid Fibrils at a Neutral pH. *Biochemistry* **2004,** *43*, 11075-11082.

(413) Yan, P.; Bero, A. W.; Cirrito, J. R.; Xiao, Q.; Hu, X.; Wang, Y.; Gonzales, E.; Holtzman, D. M.; Lee, J.-M., Characterizing the Appearance and Growth of Amyloid Plaques in APP/PS1 Mice. *J. Neurosci.* **2009,** *29*, 10706-10714.

(414) Yerbury, J. J.; Kumita, J. R.; Meehan, S.; Dobson, C. M.; Wilson, M. R., α2-Macroglobulin and Haptoglobin Suppress Amyloid Formation by Interacting with Prefibrillar Protein Species. *J. Biol. Chem.* **2009,** *284*, 4246-4254.

(415) Yerbury, J. J.; Poon, S.; Meehan, S.; Thompson, B.; Kumita, J. R.; Dobson, C. M.; Wilson, M. R., The extracellular chaperone clusterin influences amyloid formation and toxicity by interacting with prefibrillar structures. *FASEB J.* **2007,** *21*, 2312-2322.

(416) Yin, S.; Biedermannova, L.; Vondrasek, J.; Dokholyan, N. V., MedusaScore: An Accurate Force-Field Based Scoring Function for Virtual Drug Screening. *J. Chem. Inf. Model.* **2008,** 48, 1656-1662.

(417) Yoo, B. K.; Xiao, Y.; McElheny, D.; Ishii, Y., E22G Pathogenic Mutation of *β*-Amyloid (A*β*) Enhances Misfolding of A*β*40 by Unexpected Prion-like Cross Talk between A*β*42 and A*β*40. *J. Am. Chem. Soc.* **2018,** *140*, 2781-2784.

(418) Yoo, S. I.; Yang, M.; Brender, J. R.; Subramanian, V.; Sun, K.; Joo, N. E.; Jeong, S.-H.; Ramamoorthy, A.; Kotov, N. A., Inhibition of Amyloid Peptide Fibrillation by Inorganic Nanoparticles: Functional Similarities with Protein. *Angew. Chem. Int. Ed., Engl.* **2011,** *50*, 5110-5115.

(419) Yoshimura, Y.; Lin, Y.; Yagi, H.; Lee, Y.-H.; Kitayama, H.; Sakurai, K.; Masatomo, S.; Ogi, H.; Naiki, H.; Goto, Y., Distinguishing crystal-like amyloid fibrils and glass-like amorphous aggregates from their kinetics of formation. *Proc. Natl. Acad. Sci. U.S.A.* **2012,** *109*, 14446-14451.

(420) Young, I. D.; Ailles, L.; Narindrasorasak, S.; Tan, R.; Kisilevsky, R., Localization of the Basement Membrane Heparan Sulfate Proteoglycan in Islet Amyloid Deposits in Type II Diabetes Mellitus. *Arch. Pathol. Lab. Med.* **1992,** *116*, 951-954.

(421) Young, L. M.; Cao, P.; Raleigh, D. P.; Ashcroft, A. E.; Radford, S. E., Ion Mobility Spectrometry-Mass Spectrometry Defines the Oligomeric Intermediates in Amylin Amyloid Formation and the Mode of Action of Inhibitors. *J. Am. Chem. Soc.* **2014,** *136*, 660-670.

(422) Young, L. M.; Mahood, R. A.; Saunders, J. C.; Tu, L.-H.; Raleigh, D. P.; Radford, S. E.; Ashcroft, A. E., Insights Into the Consequences of Co-Polymerisation in the Early Stages of IAPP and Aβ Peptide Assembly From Mass Spectrometry. *Analyst* **2015,** *140*, 6990-6999.

(423) Yu, Y.-P.; Zhang, S.; Liu, Q.; Li, Y.-M.; Wang, C.; Besenbacher, F.; Dong, M., 2D Amyloid Aggregation of Human Islet Amyloid Polypeptide at the Solid-Liquid Interface. *Soft Matter* **2012,** *8*, 1616-1622.

(424) Zhang, C.; Wan, X.; Zheng, X.; Shao, X.; Liu, Q.; Zhang, Q.; Qian, Y., Dual-functional nanoparticles targeting amyloid plaques in the brains of Alzheimer's disease mice. *Biomaterials* **2014,** *35*, 456-465.

(425) Zhang, Q.; Bolisetty, S.; Cao, Y.; Handschin, S.; Adamcik, J.; Peng, Q.; Mezzenga, R., Selective and Efficient Removal of Fluoride from Water: In Situ Engineered Amyloid Fibril/ZrO2 Hybrid Membranes. *Angew. Chem. Int. Ed., Engl.* **2019,** *58*, 6012-6016.

(426) Zhang, S.; Andreasen, M.; Nielson, J. T.; Liu, L.; Nielson, E. H.; Song, J.; Ji, G.; Sun, F.; Skrydstrup, T.; Besenbacher, F.; Nielson, N. C.; Otzen, D. E.; Dong, M., Coexistence of ribbon and helical fibrils originating from $hIAPP_{20-29}$ revealed by quantitative nanomechanical atomic force microscopy. *Proc. Natl. Acad. Sci. U.S.A.* **2013,** *110*, 2798-2803.

(427) Zhang, S.; Liu, H.; Chuang, C. L.; Li, X.; Au, M.; Zhang, L.; Phillips, A. R. J.; Scott, D. W.; Cooper, G. J. S., The pathogenic mechanism of diabetes varies with the degree of overexpression and oligomerization of human amylin in the pancreatic islet β cells. *FASEB J.* **2014,** *28*, 5083-5096.

(428) Zhang, W.; Christofferson, A. J.; Besford, Q. A.; Richardson, J. J.; Guo, J.; Ju, Y.; Kempe, K.; Yarovsky, I.; Caruso, F., Metal-dependent inhibition of amyloid fibril formation: synergistic effects of cobalt–tannic acid networks. *Nanoscale* **2019,** *11*, 1921-1928.

(429) Zhang, Y.-J.; Gendron, T. F.; Xu, Y.-F.; Ko, L.-W.; Yen, S.-H.; Petrucelli, L., Phosphorylation regulates proteasomal-mediated degradation and solubility of TAR DNA binding protein-43 C-terminal fragments. *Mol. Neurodegener.* **2010,** *5*, 33.

(430) Zhao, J.; Gao, W.; Yang, Z.; Li, H.; Gao, Z., Nitration of amyloid-β peptide (1–42) as a protective mechanism for the amyloid-β peptide (1–42) against copper ion toxicity. *J. Inorg. Biochem.* **2019,** *190*, 15-23.

(431) Zheng, X.; Baker, H.; Hancock, W. S.; Fawaz, F.; McCaman, M.; Pungor Jr., E., Proteomic analysis for the assessment of different lots of fetal bovine serum as a raw material for cell culture. Part

IV. Application of proteomics to the manufacture of biological drugs. *Biotechnol. Progr.* **2006,** *22*, 1294-1300.

(432) Zhou, L.; Chen, Z.; Dong, K.; Yin, M.; Ren, J.; Qu, X., DNA-Mediated Construction of Hollow Upconversion Nanoparticles for Protein Harvesting and Near-Infrared Light Triggered Release. *Adv. Mater.* **2014,** *26*, 2424-2430.

(433) Zhu, B.; Jiang, L.; Huang, T.; Zhao, Y.; Liu, T.; Li, X.; Campos, A.; Pomeroy, K.; Masliah, E.; Zhang, D.; Xu, H., ER-associated degradation regulates Alzheimer's amyloid pathology and memory function by modulating γ-secretase activity. *Nat. Commun.* **2017,** *8*, 1472.

(434) Zhu, X.; Wen, Y.; Zhao, Y.; Liu, Y.; Sun, J.; Liu, J.; Chen, L., Functionalized chitosan-modified defect-related luminescent mesoporous silica nanoparticles as new inhibitors for hIAPP aggregation. *Nanotechnology* **2019,** *30*, 315705.

(435) Zimmerman, S. B.; Trach, S. O., Estimation of macromolecule concentrations and excluded volume effects for the cytoplasm of *Escherichia coli*. *J. Mol. Biol.* **1991,** *222*, 599-620.

(436) Zraika, S.; Hull, R. L.; Verchere, C. B.; Clark, A.; Potter, K. J.; Fraser, P. E.; Kahn, S. E., Toxic oligomers and islet beta cell death: guilty by association or convicted by circumstantial evidence? *Diabetologia* **2010,** *53*, 1046-1056.